

INITIATING OXIDATIVE EVENTS INDUCED BY PARTICULATE MATTER COMPONENT  
1,2-NAPHTHOQUINONE IN HUMAN AIRWAY CELLS

Katelyn Susan Lavrich

A dissertation submitted to the faculty at the University of North Carolina at Chapel Hill in partial fulfillment of the requirements for the degree of Doctor of Philosophy in the Curriculum in Toxicology in the School of Medicine.

Chapel Hill  
2018

Approved by:

James Samet

Rebecca Fry

Avram Gold

Steven Simmons

Mirek Styblo

Zhenfa Zhang

© 2018  
Katelyn Susan Lavrich  
ALL RIGHTS RESERVED

## ABSTRACT

Katelyn Susan Lavrich: Initiating Oxidative Events Induced by Particulate Matter Component 1,2-Naphthoquinone in Human Airway Cells  
(Under the direction of James M. Samet)

Over three million premature deaths are caused by ambient Particulate Matter (PM) worldwide each year, rendering it one of the deadliest environmental public health problems. Oxidative stress has been frequently cited as an initiating mechanism of PM-induced health effects, but has not been well-characterized. There is a growing awareness that oxidative events, particularly those resulting in perturbation of mitochondrial function and hydrogen peroxide levels, play a vital role in cellular health and function. Here, we sought to investigate the effect of the ubiquitous PM component, 1,2-naphthoquinone (1,2-NQ), on specific oxidative events in human airway cells. First, I show that 1,2-NQ increases hydrogen peroxide production through both non-mitochondrial redox cycling and inhibition of mitochondrial processes in human bronchial epithelial cells. This was the first time PM-associated quinones have been shown to disrupt mitochondrial substrate oxidation processes. I next expanded our model to characterize bioenergetics in primary human lung macrophages. 1,2-NQ caused similar mitochondrial dysfunction in human lung macrophages. This is the first report utilizing extracellular flux analysis in primary human lung macrophages, allowing us to identify distinct subpopulations of macrophages based on anatomical location in the lung. We also observed novel mechanisms of inflammatory activation that did not require metabolic reprogramming. Lastly, I showed that 1,2-NQ induced glycolytic inhibition through peroxide-mediated mechanisms, the first time that an environmentally relevant exposure has been shown to modify protein function through sulfenylation. I adapted novel technology developed originally in the redox biology field, bridging the gap to make these technologies accessible to toxicologists. Ultimately, the work here highlights the central role of bioenergetic function both as an initiator and target of oxidative stress mechanisms and provides a basis

to utilize bioenergetic measurements in a translational setting as a biomarker of PM-induced adverse cellular responses. In summary, this work identifies novel molecular mechanisms of PM-induced health effects to better our understanding and ideally improve public health through effective policy.

*I have no special talents. I am only passionately curious.*

-Albert Einstein

## ACKNOWLEDGMENTS

This work would not have been possible without the outstanding guidance by my mentor, Dr. James M. Samet. His training and mentoring was crucial in my development as a scientist and thinker, and I am deeply grateful for the numerous ways he has prepared me for the next step. To my current and former lab mates, Dr. Phillip Wages, Elizabeth Corteselli, Robert Silbajoris, and Dr. Eugene Gibbs-Flourney. I am also fortunate for the mentorship from Dr. Philip Bromberg, whom constantly sparked my curiosity with his endless insight and translational moments. I am appreciative of the guidance and support of Dr. Neil Alexis, who helped me spearhead a translational project and expand my perspective. I am also thankful to my thesis committee members for their commitment to my doctoral training.

I am sincerely appreciative of Dr. Emma Bowers and Dr. Shaun McCullough, who made working here a hilarious yet transforming experience. I am grateful for Lisa Dailey as the rock of CRB. I am thankful to the rest of the EPA family for helping me throughout and letting me be a co-investigator in the clinical studies. I would like to thank Dr. Ilona Jaspers and Julie Cannefax for their tireless work to keep our program and students thriving. To the incredible TiBBs staff and fellow members of the Science Policy Advocacy Group, who helped me always keep the bigger picture in mind and provided outstanding “real-world” training.

I would like to thank my parents for their love and support since day one and the rest of my family for nodding politely when I explained what my research is on. I am extremely lucky to have been surrounded by a fabulous cohort, Liz Mutter-Rottmayer, Kim Stratford, Phillip Clapp, Adam Speen, and Mimi Huang, every step of the way. They are killer competition, but also the most genuine, hard-working, and supportive group I have met and I know we will change the world. I would like to thank all my friends who provided the wine, food, laughs, and patient ears for the last five years, especially Claire Trincot, Rachel Dee, Carrie Wilczewski, Kate Geisen, Sravya Kattula, Nicole Corbin, and Adam Morgan. And I hold a special gratitude to Tyler for saying yes to adventures and being a patient partner-in-crime.

## PREFACE

Although I was the lead on the research presented in this dissertation, the work was done in collaboration with other talented scientists. For all work, Dr. James Samet was the principal investigator and provided guidance in experimental design and writing.

For Chapter 2, Elizabeth Corteselli, Phillip Wages, and Eugene Gibbs-Flournoy assisted with imaging intracellular H<sub>2</sub>O<sub>2</sub> production. Dr. Bromberg provided experimental and hypothesis guidance. Dr. Simmons provided advice and access to running Seahorse assay. I also express gratitude to Danielle Suarez for Seahorse instrument training and support. I also thank Claire Trincot and Dr. Kathleen Caron for providing the mouse hearts used in the isolated mitochondria experiments. I am also grateful to Dr. Haiyan Tong for her assistance with mitochondrial isolation. Chapter 2 was recently published as:

Lavrich, K.S., Corteselli, E., Wages, P., Bromberg, P., Simmons, S., Gibbs-Flournoy, E., Samet, J.M. (2018). Investigating Mitochondrial Dysfunction in Human Lung Cells Exposed to Redox-Active PM Components. *Toxicology and Applied Pharmacology*, 342, 99-107.

For Chapter 3, Adam Speen ran ELISAs for cytokine production. Dr. Ghio performed the bronchoscopies. Dr. Bromberg guided project design and editing. Dr. Alexis was a co-principal investigator with Dr. Samet, provided the induced sputum samples, and contributed to the experimental design and writing. I want to also thank the clinical staff at the Environmental Public Health Division of the U.S. Environmental Protection Agency, specifically Tracey Montilla, RN, Julie Wood, RN, Claudia Salazar, CCRC, Joleen Soukup, MSPH, and Lisa Dailey, MSPH. I am grateful to the clinical staff of the Center for Environmental Medicine, Asthma, and Lung Biology, including Heather Wells, Sha 'Leema Jenkins, and Carole Robinette. Chapter 3 was recently submitted for publication:

Lavrich, K.S., Speen, A.M., Ghio, A.J., Bromberg, P.A., Samet, J.M., Alexis, N.E. (2018). Characterizing the Bioenergetic Profiles of Human Lung Macrophages from Healthy Volunteers. *Submitted*.

For Chapter 4, numerous sulfenylation experiments were conducted in collaboration with Dr. Phillip Wages. Chapter 4 contains some data previously published in the following publication and has been reproduced in part with permission:

Wages, P. A., Lavrich, K. S., Zhang, Z., Cheng, W. Y., Corteselli, E., Gold, A., Bromberg, P.A., Simmons, S.O., & Samet, J. M. (2015). Protein Sulfenylation: A Novel Readout of Environmental Oxidant Stress. *Chemical Research in Toxicology*, 28(12), 2411-2418. Copyright 2015. American Chemical Society.

I was funded the EPA-UNC Toxicology Training Agreement [CR-83591401-0] and NIEHS [NRSA T32 ES007126] to complete this work. All copyrighted material presented in this dissertation is used with permission from the relevant copyright holders.

## TABLE OF CONTENTS

LIST OF TABLES .....	XI
LIST OF FIGURES.....	XII
LIST OF ABBREVIATIONS.....	XIV
CHAPTER 1: INTRODUCTION .....	1
Fine Particulate Matter – A Global Public Health Issue.....	1
Toxicologic Investigation of Human Airways .....	8
Defining Oxidative Stress .....	12
Bioenergetics: Needed for Life, Runs on Redox Signaling .....	19
Scope of the Dissertation .....	26
CHAPTER 2: INVESTIGATING MITOCHONDRIAL DYSFUNCTION IN HUMAN LUNG CELLS EXPOSED TO REDOX-ACTIVE PM COMPONENTS.....	28
Introduction .....	28
Methods .....	30
Results.....	36
Discussion .....	51
Summary .....	54
CHAPTER 3: CHARACTERIZING THE BIOENERGETIC PROFILE OF HUMAN LUNG MACROPHAGES FROM HEALTHY VOLUNTEERS.....	55
Introduction .....	55
Methods .....	56
Results.....	63
Discussion .....	76
Summary .....	78
CHAPTER 4: GLYCOLYSIS IS INHIBITED THROUGH PEROXIDE-MEDIATED INACTIVATION OF GLYCERALDEHYDE-3-PHOSPHATE DEHYDROGENASE.....	80
Introduction .....	80

Methods .....	82
Results .....	87
Discussion .....	98
Summary .....	101
CHAPTER 5: ADDITIONAL EXPERIMENTS .....	102
Normalization of Seahorse Results .....	102
Influence of Lung MAC Donor Characteristics on Bioenergetics .....	114
CHAPTER 6: CONCLUSIONS, PERSPECTIVES, AND FUTURE DIRECTIONS .....	121
The Oxygen Paradox: Linking Redox and Bioenergetics.....	121
Defining Redox Toxicology Mechanisms Using Bioenergetics .....	123
Role of Quinones in PM-Induced Health Effects.....	127
Translating bioenergetics as a marker of redox disruption .....	129
Conclusions & Public Health Policy Implications of Elucidating Cellular Mechanisms .....	131
REFERENCES.....	132

## LIST OF TABLES

Table 3-1. Characteristics of healthy subjects who underwent bronchoscopy (BAL, BF) or induced sputum (IS).....	58
Table 3-2. Differential Cell Count Percentages.....	59

## LIST OF FIGURES

Figure 1-1. Ambient PM-associated quinones have different mechanisms of toxicity. ....	7
Figure 1-2. GAPDH acts a redox switch .....	22
Figure 1-4. Overview of this dissertation.....	27
Figure 2-1. 1,2-NQ redox cycles to produce ROS .....	30
Figure 2-2. 1,2-NQ increases basal Oxygen Consumption Rate (OCR, pmol/min). ....	37
Figure 2-3. 1,2-NQ alters bioenergetic parameters as measured by the Cell Mito Stress Test.....	38
Figure 2-4. 1,2-NQ-induced OCR increases are independent of mitochondrial electron transport. ....	39
Figure 2-5. Exposure to environmentally relevant redox-cycling quinones increases OCR.....	41
Figure 2-6. Redox cycling quinones increase OCR and alter the bioenergetic profile in BEAS cells.....	42
Figure 2-7 Exposure to environmentally relevant redox-cycling quinones increases OCR.....	42
Figure 2-8. Glucose starvation does not alter quinone-induced cytotoxicity .....	43
Figure 2-9. Exposure to redox cycling quinones induces H <sub>2</sub> O <sub>2</sub> production .....	44
Figure 2-10. Permeabilization by XF PMP leaves mitochondria intact.....	45
Figure 2-11. Mitochondrial preparations show a diminished 1,2-NQ-induced OCR increase.....	45
Figure 2-12. 1,2-NQ impairs Complex I-linked respiration in permeabilized cells.....	47
Figure 2-13. Redox cycling quinones increase OCR in permeabilized cells .....	48
Figure 2-14. 1,2-NQ decreases pyruvate-driven substrate oxidation in isolated mitochondria. ....	49
Figure 2-15. DPI decreases basal OCR within 30 min. of exposure .....	50
Figure 3-1. Bioenergetic Profiles of Macrophages Sampled from Different Regions of the Human Lung. ....	64
Figure 3-2 Bronchoalveolar Macrophages Are Highly Dependent on Mitochondrial Respiration for Energy Production. ....	65
Figure 3-3. Induced Sputum Macrophages Rely on Glycolysis .....	68
Figure 3-4. Neutrophil content does not significantly correlate with bioenergetic parameters .....	69
Figure 3-5. Bioenergetic profile of BF MAC resemble that of BAL MAC .....	70

Figure 3-6. Acute LPS Challenge Does Not Alter BAL Macrophage Bioenergetics .....	71
Figure 3-7 Acute LPS Challenge Does Not Alter the Bioenergetics of Human Lung Macrophages.....	72
Figure 3-8. Activation of Protein Kinase C Induces Bronchoalveolar and Bronchial Fraction Macrophage OCR and ECAR.....	74
Figure 3-9. Exposure to 1,2-Naphthoquinone Impairs Mitochondrial Respiration in Human Bronchoalveolar Macrophages. ....	75
Figure 4-1. 1,2-NQ decreases glycolytic function and glycolytic capacity in a dose-dependent manner .....	88
Figure 4-2. Even in the presence of glucose, 1,2-NQ decreases glycolytic function and glycolytic capacity in a dose-dependent manner .....	89
Figure 4-3. Catalase overexpression partially rescues 1,2-NQ and 1,4-NQ-induced glycolytic inhibition .....	90
Figure 4-4. 1,2-NQ and 1,4-NQ impair GAPDH activity in BEAS-2B cells .....	91
Figure 4-5. 1,2-NQ produces H <sub>2</sub> O <sub>2</sub> <i>in vitro</i> to sulfenylate recombinant GAPDH .....	92
Figure 4-6. Sulfenylation of recombinant GAPDH peaks at 5 min. with 1,2-NQ, but increases adduction over time <i>in vitro</i> .....	93
Figure 4-7. Pretreatment of recombinant GAPDH with 1,2-NQ reduces sulfenylation by H <sub>2</sub> O <sub>2</sub> , but prior sulfenylation does not reduce 1,2-NQ adduction <i>in vitro</i> .....	95
Figure 4-8. 1,2-naphthoquinone induces intracellular protein sulfenylation .....	96
Figure 4-9. 1,2-NQ, 1,4-NQ, and 9,10-PQ increase global sulfenylation in BEAS-2B. ....	97
Figure 5-1. In-plate BCA-based protein assay measures protein linearly over cell density .....	107
Figure 5-2. CyQuant provides consistent linear DNA content over cell density .....	108
Figure 5-3. CyQuant consistently has the highest signal-to-noise ratio .....	109
Figure 5-4. Comparison between BCA protein and CyQuant DNA assays using BAL cells.....	110
Figure 5-5. Protein content of IS cells is consistent.....	111
Figure 5-6. IS cells from same subject have similar bioenergetic profile.....	116
Figure 5-7. Race may affect the bioenergetics of MAC from central airways.....	117
Figure 5-8. BAL MAC Bioenergetic Outcomes and donor characteristics.....	118
Figure 5-9. BF MAC Bioenergetic Outcomes and Donor Characteristics.....	119
Figure 6-1. Inherent link between metabolism and redox signaling .....	123

## LIST OF ABBREVIATIONS

1,2-NQ	1,2-Naphthoquinone
1,4-NQ	1,4-Naphthoquinone
2-DG	2-Deoxy-D-glucose
9,10-PQ	9,10-Phenanthrenequinone
Ant. A	Antimycin A
ATP	Adenosine triphosphate
BAL	Bronchoalveolar lavage
BF	Bronchial fraction
BHI	Bioenergetic Health Index
BQ	1,4-Benzoquinone
BSA	Bovine serum albumin
CO <sub>2</sub>	Carbon dioxide
COPD	Chronic obstructive pulmonary disease
DMD	Dimedone
DMNQ	1,4-dimethoxynaphthoquinone
DMSO	Dimethyl sulfoxide
DTT	Dithiothreitol
ECAR	Extracellular acidification rate
EGFR	Epidermal Growth Factor Receptor
EGTA	Ethylene glycol-bis (β-aminoethyl ether)-N,N,N',N'-tetra-acetic acid
FCCP	Carbonyl cyanide-p-trifluoromethoxyphenylhydrazone
GAPDH	Glyceraldehyde 3-phosphate dehydrogenase
GP6D	Glucose-6-phosphate dehydrogenase
GPx	Glutathione Peroxidase
GSH	Glutathione (reduced)
GSSG	Glutathione (oxidized)

GSTMI	Glutathione-S-transferase mu 1
H <sub>2</sub> O <sub>2</sub>	Hydrogen peroxide
HEPES	4-(2-hydroxyethyl)-1-piperazineethanesulfonic acid
HO-1	Heme oxygenase 1
IS	Induced sputum
KBM	Keratinocyte basal media
KGM	Keratinocyte growth media
KH <sub>2</sub> PO <sub>4</sub>	Monopotassium phosphate
MAC	Macrophage
MAS	Mitochondrial assay solution
MgCl <sub>2</sub>	Magnesium chloride
mRNA	Messenger RNA
NADH	Nicotinamide adenine dinucleotide
NADPH	Nicotinamide adenine dinucleotide phosphate
O <sub>2</sub>	Molecular oxygen
O <sub>2</sub> <sup>•-</sup>	Superoxide
OCR	Oxygen consumption rate
Oligo	Oligomycin A
PAH	Polyaromatic hydrocarbon
PM	Particulate Matter
PM <sub>10</sub>	Coarse particulate matter, 2.5-10 µm in diameter
PM <sub>2.5</sub>	Fine particulate matter, <2.5 µm in diameter
PMN	Polymorphonucleated cells, i.e. neutrophils
PTP	Protein tyrosine phosphatase
RNS	Reactive nitrogen species
ROS	Reactive oxygen species
Rot.	Rotenone
SOD	Superoxide dismutase

TNF- $\alpha$       Tumor necrosis factor alpha  
U.S. EPA      United States Environmental Protection Agency

## CHAPTER 1: INTRODUCTION

### **Fine Particulate Matter – A Global Public Health Issue**

Air pollution exposure is a global contributor to cardiopulmonary morbidity and mortality. The World Health Organization linked air pollution exposure to 1 in 8 premature deaths globally in 2012 and it is the leading environmental cause of death worldwide (World Health Organization, 2014; Health Effects Institute, 2017). Particulate matter (PM) alone was responsible for roughly 3 million premature deaths in 2012, up to 4.2 million in 2015, and was the fifth ranking risk factor worldwide for premature death in 2015 (World Health Organization, 2014; Cohen *et al.*, 2017; Health Effects Institute, 2017). Though the health implications of air pollution have been recognized for decades, it remains a global health problem linked to cardiovascular and respiratory diseases. Air pollution is also a social equality issue, as 87% of global ambient air pollution mortality occur in low- and middle- income countries (World Health Organization, 2014).

#### ***Formation and Historical Trends***

Ambient air pollution is a complex mixture of particles and gases which varies in composition over time and space. The U.S. Environmental Protection Agency (EPA) regulates six different pollutants defined in the National Ambient Air Quality Standards (NAAQS) – ozone, nitric oxides, sulfur oxides, carbon monoxide, lead, and PM (Environmental Protection Agency, 2013). Of these, ambient PM is one of the most frequent to exceed air pollution standards, typically in urban environments (Laumbach and Kipen, 2010).

PM is an intricate mix of small particles, liquid droplets of acids, organics, metals, and soil/dust particles. Both natural and anthropogenic sources contribute to PM. Natural processes include fires, volcanoes, and wind-blown dust. Anthropogenic sources are primarily combustion in mechanical and industrial processes, vehicle emissions, and tobacco smoke (Anderson *et al.*, 2012). In China, the country with the highest number of deaths from PM, coal burning was the top contributor to ambient PM (Health

Effects Institute, 2017). Primary PM is defined when PM is directly emitted into the air, and largely contains carbon, emitted from forest fires, motor vehicles, heavy equipment and burning waste. Primary PM can also contain crustal material from construction sites, unpaved roads, and stone crushing. In contrast, secondary PM forms from reactions of gases in the atmosphere, some of which are catalyzed by sunlight and require water vapor. Common secondary PM components are: 1) sulfates, formed from sulfur dioxide emitted from power plants and industrial processes, 2) nitrates, formed from nitrogen oxide emitted by motor vehicles and power plants, and 3) carbon, formed from reactive organic emissions from motor vehicles, industrial processes, and forest fires (US EPA, 2004). As the sources vary spatially and temporally, the PM composition does as well.

Particle size is a critical determinant for where particles deposit in the airway and therefore PM is typically defined by size. Larger particles deposit higher in the airway whereas smaller particles travel deeper in the respiratory tract, even reaching alveoli (Brown *et al.*, 1950). PM is currently regulated by particle size – coarse (PM<sub>10</sub>, diameter 10 µm – 2.5 µm) and fine (PM<sub>2.5</sub>, diameter < 2.5 µm). PM<sub>10</sub> is produced primarily from uncontrolled burning and mechanical processes, such as dust (resuspended by wind and cars), wildfires, demolitions, construction, and industrial processes. PM<sub>2.5</sub> is formed largely from combustion processes, including coal power plants, gas and diesel engines, and other industrial processes (Environmental Protection Agency, 2013). While not currently regulated, particles smaller than 0.1 µm are classified as ultrafine and may cross epithelial barrier in the airways, directly entering the circulatory system, though more investigation is needed. Fine and ultrafine PM often make up only 1-8% of the total mass of suspended PM, but they have high surface area and have a porous surface that can retain other chemicals. More than 96% of particles deposited in the lung were found to be PM<sub>2.5</sub> (Churg and Brauer, 1997). To date, PM<sub>2.5</sub> has been most strongly associated with adverse health effects, though more recent evidence suggests that ultrafine particles can cause potent adverse health effects (Li *et al.*, 2003; Schwarze *et al.*, 2006).

Negative health impacts of air pollution were first recognized during the Industrial Revolution in the mid-1900s. Several major air pollution incidents occurred across the world, including in Donora Valley, Pennsylvania in 1948 when smog built up from industrial coal-burning furnaces lasted five days, killing at least 20 people, while thousands more became sick (Schrenk *et al.*, 1949). In December 1952 in

London, a dense fog formed during an inversion weather situation, lasting for four days and leading to an estimated 4,000 deaths, primarily in the elderly with heart and lung diseases (Logan, 1953). These episodes were key catalysts for many developed countries to adopt environmental protection laws. The Clean Air Act of 1970 was the first major American regulatory effort to both control and limit air pollution and emissions. This act was administered by the newly established EPA to define and enforce the National Ambient Air Quality Standards (NAAQS), regulating six air pollutants (U.S. EPA, 2017). The NAAQS are periodically reviewed using the latest scientific data, and have become more stringent since their start. The World Health Organization published similar air quality guidelines in 1987 that are periodically updated, though these do not carry regulatory enforcement (World Health Organization and UNAIDS, 2006).

PM is still a global health concern despite introduction of better technology that has reduced combustion from traditional fossil fuels, such as coal, wood, biomass, and diesel that have a high sulfur content. There has been a steep increase in motor vehicle use worldwide, leading to increased PM<sub>2.5</sub> and ultrafine PM, primarily in big cities, but in small towns as well (Health Effects Institute, 2017). Indoor air pollution also has a significant negative effect on human health, mainly from the household burning of solid fuels, such as coal, wood, and dung (Health Effects Institute, 2017).

Developing countries tend to have higher air pollution, due to fewer regulations. In 2015, the highest PM<sub>2.5</sub> concentrations due to combustion sources were found in South/SE Asia, China, and Central/Western sub-Saharan Africa (Health Effects Institute, 2017). Approximately 92% of the world's population lived in areas exceeding the 10 µg/m<sup>3</sup> guideline set by the World Health Organization, primarily in China, India, Pakistan and Bangladesh (Health Effects Institute, 2017). Although declining in the U.S., globally the population-weighted PM<sub>2.5</sub> has increased 11.2% from 1990 to 2015 (Health Effects Institute, 2017). Many developed countries have made significant improvements in air quality through stricter regulations and improved technology.

### **Global Public Health Burden**

There is strong evidence that both short term and chronic adverse health effects are linked to air pollution exposure (Anderson *et al.*, 2012). Numerous large scale epidemiologic studies have positively correlated overall, cardiovascular, respiratory mortality with PM exposure. Hospital admissions for

cardiovascular (ischemic heart disease, congestive heart failure, acute myocardial infarction) and respiratory (lung cancer, COPD, pneumonia) diseases are positively associated with PM concentrations (Pope *et al.*, 1995; Samet *et al.*, 2000; Pope *et al.*, 2004). On a shorter time-scale, increases in respiratory symptoms and medication usage have been correlated with increase PM levels (Rabinovitch *et al.*, 2006; Zanobetti *et al.*, 2009). Epidemiological studies have found that even relatively low concentrations of PM have measurable human health effects (Pope and Dockery, 2006).

The vast epidemiologic data connecting PM exposure with cardiopulmonary outcomes is supported by numerous studies in animal models, controlled human exposure studies, and panel studies (Riediker *et al.*, 2004; Samet *et al.*, 2009; Kodavanti *et al.*, 2011). For example, a 2 hr exposure to concentrated ambient particles led to mild pulmonary inflammation and increased blood fibrinogen in healthy human volunteers (Ghio *et al.*, 2000). Controlled human exposure studies have shown adverse pulmonary health effects in response to PM exposure, including decreased lung function, increased neutrophil infiltration by bronchoalveolar lavage, and increased responsiveness to methacholine (Nordenhäll *et al.*, 2001; Pietropaoli *et al.*, 2004). Though pulmonary markers have been variable, there is a relatively consistent link between PM exposure and adverse cardiac events (e.g. increased heart rate variability, impaired vasodilation) (Brook *et al.*, 2010).

In addition to cardiopulmonary outcomes, associations have been made between PM<sub>2.5</sub> and other diseases including asthma, cerebrovascular disease, adverse birth outcomes and, diabetes (Lin *et al.*, 2002; Dominici *et al.*, 2006; Pearson *et al.*, 2010; Shah *et al.*, 2011). However more mechanistic and epidemiological evidence is needed to causally link PM exposure to these outcomes and they are not regularly included in global morbidity and mortality calculations (Ritz and Wilhelm, 2008; Health Effects Institute, 2017).

Certain populations are more susceptible to the effects of PM<sub>2.5</sub> (Sacks *et al.*, 2011). Older and younger people are more vulnerable. Those with prior respiratory (e.g. asthma, COPD) or cardiovascular disease (e.g. ischemic heart disease, atherosclerosis) are more susceptible (Pope 3rd, 2000). Additionally, certain genetic polymorphisms have been associated with increased susceptibility to PM (Yang *et al.*, 2009). For example, approximately 40% of the global population is null in glutathione S-transferase mu 1 (GSTM1) gene, and this polymorphism has been epidemiologically associated with

increased adverse health effects to acute exposure to PM and other air pollutants (Chahine *et al.*, 2007; Montero *et al.*, 2007; Curjuric *et al.*, 2010; Devlin *et al.*, 2014).

### ***Mechanisms of PM Toxicity***

PM exposure has been linked to systemic inflammation and many of the resulting adverse health outcomes have an inflammatory phenotype (Brook *et al.*, 2010). Oxidative stress is thought to initiate pro-inflammatory responses. These overarching mechanisms of PM-induced health effects have been investigated in human, animal, and *in vitro* experiments and provide plausibility for the epidemiologic data.

Both animal and human studies have shown that chronic PM exposure increases systemic inflammation, as primarily measured by inflammatory cytokines IL-6, TNF- $\alpha$ , and C-reactive protein (Sun *et al.*, 2005; Ruckerl *et al.*, 2006; Chuang *et al.*, 2007). Increased systemic inflammation is thought to play a role in atherosclerosis, acute myocardial infarction, and numerous other diseases. PM exposure has been linked to increases in pro-coagulant factors such as fibrinogen and plasminogen activator fibrinogen inhibitor-1 (PAI-1) in humans, which are precursors to coronary artery disease (Chuang *et al.*, 2007; Schicker *et al.*, 2009). Animal models have shown increased thrombosis formation and translocation of small particles into the bloodstream (Nemmar *et al.*, 2002; Snow *et al.*, 2014).

PM exposure has been shown to induce pulmonary oxidative stress and inflammation. Human airway epithelial cells exposed to PM increase production of inflammatory cytokines (Quay *et al.*, 1998; Silbajoris *et al.*, 2011). Alveolar macrophages undergo oxidative burst in response to PM exposure, producing reactive oxygen species, reactive nitrogen species, TNF- $\alpha$ , and IL-1 (Driscoll *et al.*, 1990). ROS can also be directly formed from particle surfaces and have been shown to cause pulmonary damage in mice after a single exposure (Riva *et al.*, 2011). Oxidative damage is associated with primary development of asthma and COPD. DNA damage has been widely reported in response to PM, either through direct adduction by PM-associated chemicals or indirectly through oxidative stress (Claxton *et al.*, 2004).

Though inflammation and oxidative stress are associated with PM exposure and can lead to cardiopulmonary diseases, the molecular mechanisms underlying the initiation and progression from exposure to disease are not well characterized.

### **Quinones in PM**

Quinones are ubiquitous organic components of PM thought to mediate many of the adverse health effects associated with PM exposure (Valavanidis *et al.*, 2005). Quinones are produced through incomplete combustion of organic fuels, and as such are present in a variety of emissions, including diesel exhaust, cigarette smoke, wood fires (Jakober *et al.*, 2007; Eiguren-Fernandez *et al.*, 2008). Quinones are adsorbed onto the surface of particles during combustion. 1,2-Naphthoquinone (1,2-NQ) is a common quinone found in PM and has been detected in human serum in nanomolar concentrations (Lin *et al.*, 2009; Kumagai *et al.*, 2012). Additionally, the polycyclic aromatic hydrocarbon (PAH) naphthalene is the most abundant organic component of ambient air particulates and can be metabolized *in vivo* to 1,2-NQ through a cytochrome P450-mediated mechanism (Penning *et al.*, 1999; Preuss *et al.*, 2003; Miura and Kumagai, 2010), and this transformation has been demonstrated in lung cells (Zheng *et al.*, 1997). 1,2-NQ has been detected in human serum in nanomolar concentrations (Lin 2009). Other common quinones found in air pollution particulates include 9,10-phenanthrenequinone (9,10-PQ), 1,4-naphthoquinone (1,4-NQ), and 1,4-benzoquinone (BQ) (Cho *et al.*, 2004; Delgado-Saborit *et al.*, 2013).

Quinones, including 1,2-NQ, typically have two distinct mechanisms of toxicity: 1) Direct electrophilic attack through Michael addition and 2) generation of reactive oxygen species (ROS) through redox cycling. 1,2-NQ has an electrophilic carbon that can attack nucleophilic sites on numerous macromolecules, including DNA and proteins (Iwamoto *et al.*, 2007; Saeed *et al.*, 2007). In proteins, 1,2-NQ adducts the amino acids cysteine, histidine, and lysine (Labenski *et al.*, 2009). In addition, 1,2-NQ can undergo an enzymatically-mediated one-electron reduction to the semiquinone form and a subsequent one-electron reduction to a hydroquinone. Flavin-containing enzymes can mediate one electron reductions, including cytochrome P450 reductase within the endoplasmic reticulum and Complex I of the mitochondrial electron transport chain (Henry and Wallace, 1995). In the presence of strong reducing agents, such as ascorbate or dithiothreitol (DTT), this reduction can occur non-enzymatically (Charrier and Anastasio, 2012). The reduced forms, especially the semiquinone, can donate an electron to molecular O<sub>2</sub> to generate superoxide, leading to oxidative stress through a cascade of ROS (Cheng *et al.*, 2012; Shinkai *et al.*, 2012). Additionally, a 2-electron reduction can be enzymatically catalyzed by NAD(P)H Quinone Dehydrogenase 1 or aldo-keto reductases directly to the hydroquinone, bypassing the

labile semiquinone radical, and making the quinone more susceptible to conjugation reactions and favoring its excretion (Penning *et al.*, 1999).

Not all quinones participate in both redox cycling and Michael addition, as they vary in electrophilicity and redox potential (Song and Buettner, 2010). For example, 9,10-PQ is a potent redox cycler due to its high redox potential, but is not very electrophilic in biological systems (Figure 1-1). In contrast, BQ is a potent electrophile, but its low redox potential does not afford redox cycling in a cell. Interestingly, 1,2-NQ can continue to redox cycle even when adducted to proteins, while 1,4-NQ cannot (Brunmark and Cadenas, 1989). Although 1,2-NQ and other quinones have been studied for years, the relative contribution of electrophilic attacks and ROS production in mediating toxicologic effects is not well understood (Henry and Wallace, 1996).

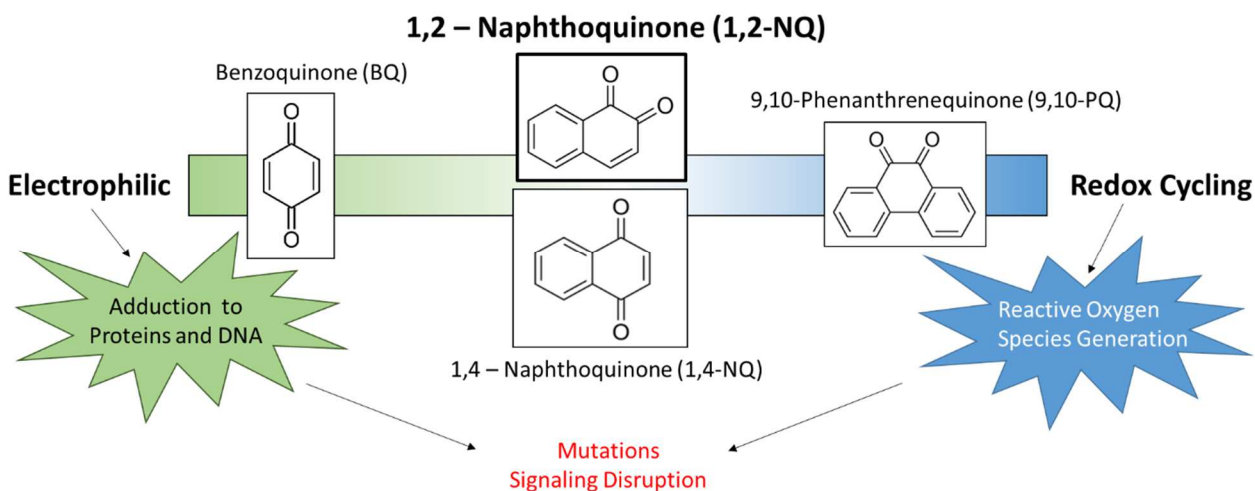


**Figure 1-1.** Ambient PM-associated quinones have different mechanisms of toxicity.

While some quinones are naturally occurring, such as vitamins K1 and K2, xenobiotic quinones are of toxicologic interest due to their ability to induce oxidative stress, acute cytotoxicity, immunotoxicity, and carcinogenesis (Rodriguez *et al.*, 2004; Kumagai *et al.*, 2012). Historically, quinones have been studied intensively due to their ability to adduct DNA and induce mutagenesis (Rodriguez *et al.*, 2004). 1,2-NQ has been shown to alter a number of cellular signaling pathways leading to adverse outcomes through inhibition of phosphatases. Phosphatases play a central role in signaling as they remove a phosphate group from proteins, such as kinases (e.g. epidermal growth factor receptor (EGFR)), and therefore govern signaling. Phosphatase inhibition by 1,2-NQ can lead to uncontrolled signaling and was

shown to lead to tracheal contraction in guinea pigs through inhibition of protein tyrosine phosphatases (Kikuno *et al.*, 2006). Additionally, 1,2-NQ inhibited nitric oxide synthase in endothelial cells, a key function in vasorelaxation which could lead to high blood pressure (Sun *et al.*, 2006). 1,2-NQ has also been shown to increase expression of pro-inflammatory proteins IL-8, COX-2, and the adaptive oxidative stress protein HO-1 (Cheng *et al.*, 2012).

Although 1,2-NQ is known to disrupt signaling pathways and cause adverse effects in cells, the initiating mechanisms of these effects are not well understood. Further characterization is needed especially in human airway cells to better predict the effect of 1,2-NQ and other PM-associated quinones on human health.

### **Toxicologic Investigation of Human Airways**

The respiratory tract is the first target for air pollution exposure. The human respiratory tract has a tree-like organization in which the trachea connects to branched conducting airways, ultimately terminating in alveoli (Kopf *et al.*, 2015). Alveoli have thin walls and are highly vascularized to facilitate the exchange of oxygen and carbon dioxide. The lungs have a high surface area (90 m<sup>2</sup>), especially compared to the gut (10 m<sup>2</sup>) or skin (2 m<sup>2</sup>) (Revoir and Bien, 1997). The distal airways filter roughly 8,000-9,000 liters of air every day (Kopf *et al.*, 2015). This means that alveoli and bronchioles are constantly exposed to a variety of inhaled pollutants, microbes, allergens. A functioning innate immune system in the lung is essential as a first defense to many of these insults.

#### ***Basic Lung Physiology***

Numerous cell types form the complex lung environment. Epithelial cells serve primarily as a barrier along the airways preventing the inhaled environment from reaching underlying tissue. Tight junctions link epithelial cells to form a nearly impermeable membrane, though ultrafine particles have been documented to cross tight junctions (Nemmar *et al.*, 2001; Proud and Leigh, 2011). In the upper and conducting airways, epithelial cells are pseudostratified columnar epithelial cells. Specialized epithelial cells, called goblet cells, secrete mucus to moisten the airways and trap inhaled pathogens or toxins (Lillehoj *et al.*, 2013). Mucus also has antioxidant (e.g., glutathione) and antimicrobial (B-defensins, lactoferrin) defenses that can protect against oxidant air pollutants (Parker and Prince, 2011). Epithelial cells have cilia that beat in coordination to form a mucociliary escalator to push the mucus and trapped

xenobiotics up to the throat, where they are typically swallowed and destroyed by stomach acid (Mall, 2008). Further down the airway, epithelial cells transition into cuboidal cells in the bronchioles. Alveolar epithelial cells are divided into type I squamous cells that provide structure and type II spherical cells that synthesize and release surfactant, important for water and ion transport regulation (Castranova *et al.*, 1988; Williams, 2003). Additionally, epithelial cells can secrete numerous inflammatory mediators to initiate the innate immune response when damaged or infected (Vareille *et al.*, 2011).

Resident macrophages (MAC) are the most common resident immune cells in a normal, healthy lung and thus are an essential part of the innate immune system. MAC phagocytose inhaled particles, microorganisms, and allergens. MAC also can release oxidants to destroy inhaled pathogens and infected cells in a process known as the respiratory burst (Laskin *et al.*, 2011). MAC can stimulate an inflammatory response and recruit other immune cells, such as neutrophils (PMN) and lymphocytes, through production of cytokines, to assist in repair and recovery. MAC have been shown to vary along the airway in phenotype and function (Franke-Ullmann *et al.*, 1996; Alexis *et al.*, 2000).

Recently, MAC have been phenotypically characterized into M1 pro-inflammatory and M2 anti-inflammatory MAC. From naïve monocytes, M1 MAC polarization is induced by LPS or IFN- $\gamma$ , and have increased production of pro-inflammatory cytokines, ROS, and RNS. In contrast, M2 MAC are polarized with IL-4 stimulation, leading to alternative activation and production of anti-inflammatory cytokines, tissue repair mediators, and express scavenger receptors (Laskin *et al.*, 2011). However, the M1/M2 phenotype classification is likely an oversimplification of how MAC exist *in vivo*, as much of its characterization occurred using *in vitro* systems with MAC derived from mice or peripheral blood/bone marrow monocytes. In reality, MAC are extremely plastic in their tissue microenvironments (Porcheray *et al.*, 2005; Mosser and Edwards, 2008). The M1/M2 MAC classification has not been well defined in the lung or using human MAC (Murray and Wynn, 2011).

Other important innate immune cells in the lung include dendritic cells, PMN (first cells recruited to the site of inflammation or injury), eosinophils, basophils, mast cells, and natural killer cells. The communication between all of these different cell types is essential for both homeostasis and proper initiation, coordination, and resolution of immune responses. Often, it is the epithelial cells and resident MAC that recognize damage and activate the immune response through production of cytokines and

chemokines, leading to the recruitment of blood circulating immune cells to the airway (Holgate, 2011). Interruption in these processes can lead to numerous respiratory diseases including asthma and COPD (Shaykhiev *et al.*, 2009; Kudo *et al.*, 2013).

### **Sampling Human Airways**

Several clinical techniques have been developed to sample different parts of the respiratory tract and gain valuable insight into pulmonary health and disease. Bronchoscopy has been the gold standard technique to evaluate lung health and inflammation clinically, but is also a useful technique in research. After anesthetizing of the upper airways and trachea, a small flexible bronchoscope is wedged in a segmental bronchus, typically of the lingual or right middle lobe when performed for research purposes (Hunninghake *et al.*, 1979). A brush can be lightly scraped across the surface of the bronchi to yield bronchial epithelial cells, which can be cultured and passaged (Romagnoli *et al.*, 1999). Several washes of sterile saline can be performed on small segments of lung to collect resident cells. The first wash typically samples the surfaces of the main bronchus; thus the sample is termed the bronchial fraction (BF). Subsequent washes are typically pooled and represent the distal airways, including the bronchioles and alveolar regions, and the sample is termed the bronchoalveolar lavage (BAL). BAL samples are usually over 90% MAC. BF samples are typically predominantly MAC, with a mix of PMN and lymphocytes (Hunninghake *et al.*, 1979; Alexis *et al.*, 2000; Moodley *et al.*, 2000). BAL analysis is useful in diagnosis of inflammatory pulmonary diseases including interstitial lung disease (Meyer *et al.*, 2012) and COPD (Rutgers *et al.*, 2000). Although the samples have a high utility in both clinical and experimental settings, bronchoscopy is a highly invasive technique and requires a board certified subspecialist to perform, limiting its application.

Induced sputum (IS) was developed as a less invasive technique to sample the large conducting airways (Alexis *et al.*, 2000; Moodley *et al.*, 2000). This procedure involves periods of inhalation of vaporized isotonic saline by the subject followed by production of an expectorant into a cup. Mucus plugs are counted and dissolved with 0.1% dithiothreitol to recover the cells. IS samples are often predominantly MAC, with PMN and lymphocytes making up the rest of the sample (Alexis *et al.*, 2000; Moodley *et al.*, 2000). This sample has been shown useful in indicating airway inflammation (Pizzichini *et al.*, 1996) and disease phenotypes, such as asthma (Fahy *et al.*, 1994) and COPD (Rutgers *et al.*, 2000).

While this sample typically yields fewer cells than BAL and production is less consistent across individuals, the lower invasiveness means it is well tolerated by human subjects and can be performed more often by trained technicians, making the technique more accessible for research purposes.

### ***Cell variability along airways***

Sampling from different anatomical locations along the airway has shown that respiratory tract cells are heterogeneous within a cell type. As mentioned earlier, epithelial cells change morphologically along the respiratory tract, transition from ciliated, pseudostratified columnar cells to thin type I or II alveolar epithelial cells. Since alveolar epithelial cells lack cilia and mucociliary clearance, it can be surmised that they are more susceptible to xenobiotics and microorganisms. MAC recovered from IS were phenotypically and functionally more active and pro-inflammatory than MAC recovered from BAL (Alexis *et al.*, 2000). However little is known whether MAC vary in susceptibility to air pollutants. Susceptibility could be altered both due to fewer protective mechanisms lower in the airways or to biochemical differences in the cells, such as lower antioxidant capacity or bioenergetics impairments.

### ***In vitro Models***

Although controlled human studies are the gold standard for evaluating air pollution toxicity, they are not ethical or practical for many mechanistic studies. Animal models provide an *in vivo* method of air pollution toxicity, but translation back to human airways is limited due to crucial differences. For example, rodent airways are known to be better at scrubbing air pollution, plus rodents have higher ventilation rate compared to humans (Winkler-Heil and Hofmann, 2016). Though outside of a complex body, *in vitro* models can provide essential mechanistic validation.

Numerous immortalized cell lines exist and are often utilized in toxicologic testing. However, it is known that clinical relevance to human exposures and processes is limited. Many cell lines have neoplastic phenotypes and thus typically do not represent normal, healthy cells. Some immortalized lines have a documented difference in oxidant process and baseline bioenergetics compared to their background, normal cells. Therefore, it is essential to validate redox and bioenergetic characteristics in a cell line for appropriateness to tissues found in intact, healthy humans. The bronchial epithelial cell line, BEAS-2B (Reddel *et al.*, 1988) was previously validated to maintain a similar oxidative capacity as primary human bronchial epithelial cells (Kinnula *et al.*, 1994).

Primary human airway epithelial cells grown at an air-liquid interface are presently the most representative *in vitro* model for air pollution toxicology studies. These cells can differentiate fully into pseudostratified epithelium with functioning cilia and goblet cells secreting mucus (Fulcher *et al.*, 2005). Likewise, primary lung MAC can be studied using BAL samples. Although primary airway cells grown in this manner are most appropriate as a model, they are notoriously difficult to use in mechanistic studies. They tend to be resistant to gene induction techniques (Pickles *et al.*, 1998) and the diversity of genotypes leads to noisy results that may mask a true effect.

*In vitro* toxicity tests are typically performed using monocultures, which do not resemble the complexity of human airways. MAC could be added to the epithelial air-liquid interface model described above to begin to investigate how multiple cell types play into toxicologic responses (Bauer *et al.*, 2015). Recent advancements have been made in multi-cell pulmonary models, including “lung-on-a-chip” (Benam *et al.*, 2016). While the field of toxicology needs to embrace these novel complex systems, they are currently not validated or sufficiently developed to study many toxicologic endpoints, especially for regulatory purposes.

### **Defining Oxidative Stress**

Despite the complexity of air pollution and the diversity of health effects, oxidative stress has been considered a unifying mechanism linking different types of air pollution exposure to inflammatory health effects (Kelly, 2003). Oxidative stress is a commonly cited mechanism of cellular injury caused by a wide variety of environmental compounds. However, oxidative stress is an extremely broad term that encompasses a wide variety of reactions. As the field of toxicology moves to a more mechanistic view of compound interactions, it is essential to investigate and understand which specific oxidant events are altered.

Many normal physiological processes rely on redox signaling to maintain homeostasis (Ray *et al.*, 2012). In the simplest terms, a reduction-oxidation (redox) reaction is the formal transfer of electrons from one molecule to another. In biology, redox reactions are frequent and are essential for many signaling processes. The cell maintains a tight balance on molecules that can both oxidize and reduce others to maintain homeostasis (Winterbourn and Hampton, 2008).

## **Reactive Oxygen Species**

Reactive oxygen species (ROS) are common oxidants with a strong oxidizing capacity. ROS have varying degrees of reactivity, which dictates half-life and specificity of reactions with other molecules. The strongest ROS oxidants are hydroxyl radicals ( $\text{HO}^\bullet$ ) and singlet oxygen ( $^1\text{O}_2$ ). These transients react with most compounds at a nearly diffusion-limited rate. They are thus promiscuous and so do not play a part in regulated signaling pathways, and react with most compounds at a nearly diffusion-limited rate. Superoxide ( $\text{O}_2^{\bullet-}$ ) is less reactive, with a half-life of seconds in a biological system. Superoxide rapidly reacts with another superoxide molecule, dismutating to form  $\text{H}_2\text{O}$  and  $\text{O}_2$ , or can form other reactive oxygen or nitrogen species. In contrast, hydrogen peroxide ( $\text{H}_2\text{O}_2$ ) is relatively stable with a half-life of months, making it an essential second messenger in numerous signaling pathways (Kalyanaraman, 2013).

### $\text{H}_2\text{O}_2$

$\text{H}_2\text{O}_2$  has many characteristics that make it an ideal second messenger within the cell. It is a small, diffusible and ubiquitous molecule that can be rapidly synthesized and destroyed in response to stimuli. It is also relatively less reactive and longer-lived than other ROS, according to its selectivity toward specific targets (Gough and Cotter, 2011).  $\text{H}_2\text{O}_2$  is an electrophile and can oxidize nucleophilic sites, most notably thiol sites of glutathione and amino acids, cysteine and methionine.

Production of  $\text{H}_2\text{O}_2$  was initially thought to be specific to immune phagocytes, wherein oxidative burst causes nicotinamide adenine dinucleotide phosphate (NADPH) oxidases to generate  $\text{O}_2^{\bullet-}$  which is converted enzymatically into  $\text{H}_2\text{O}_2$  by superoxide dismutases (SODs). However, it was shown that insulin produces  $\text{H}_2\text{O}_2$  in adipose cells, leading to the discovery that numerous ligands elicit a cellular  $\text{H}_2\text{O}_2$  response, including epidermal growth factor, cytokines (e.g. tumor necrosis factor- $\alpha$ , transforming growth factor- $\beta$ ), and granulocyte-macrophage colony-stimulating factor (May and De Haen, 1979; Lo and Cruz, 1995; Bae *et al.*, 1997; Sattler *et al.*, 1999). As discussed in detail later,  $\text{H}_2\text{O}_2$  is also produced as a byproduct of mitochondrial respiration in the cell. (Lambeth, 2004). The site of production of  $\text{H}_2\text{O}_2$  critically determines whether subsequent signaling changes are essential or harmful in the cell (Winterbourn and Hampton, 2008).

## **Redox Signaling**

### Sulfenylation and Redox Switches

Sulfenylation, or the oxidation of cysteine groups by  $\text{H}_2\text{O}_2$ , is essential to redox signaling in the cell. It is known to play an essential role in proliferation, growth, and other key signaling pathways (Gough and Cotter, 2011). Cysteine is scarce relative to other amino acids in the cell (~2% of all amino acid content in cells), but is highly conserved within functional sites of proteins (Huang *et al.*, 2009; Poole, 2015). Sulfenylation and subsequent reactions typically inactivate a protein, which can have a profound effect on signaling. However, not all cysteines can be readily oxidized by  $\text{H}_2\text{O}_2$ . Many cysteine groups are sterically inaccessible to oxidation. Additionally, oxidation by  $\text{H}_2\text{O}_2$  to sulfenic acid is energetically favorable only for the thiolate ( $-\text{S}^-$ ) form (Winterbourn and Hampton, 2008; Poole, 2015). The pKa of the cysteine sulfhydryl group (pH at which  $-\text{SH}$  deprotonates to  $-\text{S}^-$ ) is strongly influenced by the microenvironment within the protein, though there is debate as to the importance of pKa in thiolate formation (Poole, 2015; Adamson *et al.*, 2017).

Sulfenic acid is relatively reactive and short-lived. The sulfenic acid serves as the basis for many other post-translational modifications (PTMs). Oxidized cysteine may form a disulfide bond with a second cysteine group, either intra- or inter-molecularly. Formation of a disulfide bond with glutathione is termed S-glutathionylation. The disulfide can be reduced back to the original thiol form of the protein enzymatically by thioredoxin (Trx) or glutaredoxin (Grx) (Groitl and Jakob, 2014). Additionally, sulfenic acids can interact with protein amine groups to form a sulfenamide, though this modification is typically reversible. Often the sulfenic acid and resulting PTMs can inactivate the enzyme if the cysteine is critical for its function. PTMs stabilize the oxidation of the cysteine group and can lengthen the impact on signaling. Since the original form of the protein can be regenerated, proteins can act as “redox switches” as the activity of the protein is regulated by redox state. However,  $\text{H}_2\text{O}_2$  can further oxidize sulfenic acids to sulfinic and sulfonic acids. The more highly oxidized forms are considered irreversible and can lead to cytotoxicity (Janssen-Heininger *et al.*, 2008; Groitl and Jakob, 2014).

### Activation of Signaling Pathways

Protein tyrosine phosphatases (PTPs) were one of the first redox switches discovered. PTPs are essential signaling regulators through dephosphorylation of other proteins, primarily kinases. PTPs

contain a catalytic cysteine that is extremely sensitive to inactivation via sulfenylation by H<sub>2</sub>O<sub>2</sub>. When PTPs are inhibited, kinases that are regulated through dephosphorylation by PTPs are left “turned on,” which leads to altered signaling. For example, the well-studied PTP1B typically regulates EGFR, insulin-like growth factor receptor, c-Src, and Janus kinase 2 (Tonks, 2013). When EGF binds EGFR, H<sub>2</sub>O<sub>2</sub> is produced, which can inhibit PTP1B. With PTP1B temporarily inhibited, the EGFR signaling cascade proceeds unopposed. Inappropriate inactivation of redox switches, such as PTP1B, could have detrimental effects as cellular signaling continues unrestrained (Samet and Tal, 2010). Numerous pathologies, neurological disorders, and metabolic diseases are associated with overproduction of ROS and inappropriate redox signaling (Kalyanaraman, 2013).

### ***Antioxidant Capacity***

#### Enzymes

To maintain normal, homeostatic signaling, cells have numerous systems to counteract oxidant production. Sequential action by the superoxide dismutase (SOD) family and catalase generates O<sub>2</sub> and water from O<sub>2</sub><sup>•-</sup> in both the cytosol and mitochondria. Peroxiredoxin (Prxs) family of enzymes efficiently break down H<sub>2</sub>O<sub>2</sub> (K~ 10<sup>7</sup> M<sup>-1</sup> s<sup>-1</sup>) (Rhee *et al.*, 2012). Peroxiredoxins are localized in different subcellular compartments including the cytosol, mitochondria, endoplasmic reticulum, and peroxisomes. Native peroxiredoxin is restored through the specialized enzyme, sulfiredoxin, at the expense of ATP. Catalase, typically expressed in peroxisomes, is a potent H<sub>2</sub>O<sub>2</sub> scavenger (K~10<sup>7</sup> M<sup>-1</sup> s<sup>-1</sup>) (Ogura and Yamazaki, 1983). Glutathione peroxidases (GPx) utilize glutathione to break down H<sub>2</sub>O<sub>2</sub>.

The expression level and localization of antioxidant enzymes will dictate intracellular levels of H<sub>2</sub>O<sub>2</sub>, and thus redox-dependent signaling. The expression of antioxidant enzymes varies widely both within cells and between tissues. In the lung, differences have been identified even along the airways between epithelial cell and MAC. Expression of MnSOD was shown to be low in human alveolar macrophages and airway epithelial cells, though is induced by cytokines and inflammatory diseases (Wong and Goeddel, 1988; Coursin *et al.*, 1992). CuZnSOD was shown to be constitutively expressed in human bronchial and alveolar epithelial cells (Kinnula *et al.*, 1994). Extracellular SOD is excreted by human alveolar MAC (Oury *et al.*, 1994). Human bronchial epithelial cells, alveolar type II cells, and macrophages express catalase and glutathione peroxidase constitutively (Erzurum *et al.*, 1993a; Comhair

*et al.*, 2000). Prx 1, 3, 5, and 6 are expressed in the bronchial epithelium, though the alveolar epithelium expressed primarily Prx 5 and 6, and alveolar MAC expressed Prx 1 and 3 (Kinnula *et al.*, 2002).

### Glutathione

Other than enzymes, small molecules also serve as important antioxidants. Glutathione plays a central role in cellular antioxidant defense and as such, is typically found in millimolar concentrations in most cell types. Glutathione is a three amino acid peptide,  $\gamma$ -glutamylcysteinylglycine. Although  $H_2O_2$  is not likely to oxidize glutathione directly due to the pKa of the thiol (~8.8), it is an essential cofactor for GPx to scrub  $H_2O_2$  (Winterbourn and Hampton, 2008). GPx consumes two reduced glutathione molecules (GSH) to catalyze the reduction of  $H_2O_2$  to water, leaving glutathione disulfide (GSSG). GSH can be regenerated by the enzyme glutathione reductase (GR) at an energy cost in the form of NADPH (Flohé, 2013; Berndt *et al.*, 2014). Resting cells and tissues maintain a very high ratio of GSH to GSSG (100:1) (Van Laer *et al.*, 2013). In addition to intracellular sources, the epithelial lining fluid of the human lung has a glutathione level 100 times higher than circulating blood (Cantin *et al.*, 1987), which can directly protect against electrophilic attack and oxidation.

### NADPH

NADPH is the main reducing equivalent used to regenerate the antioxidant capacity of the cell. It is necessary for maintaining both the glutathione, thioredoxin, and glutaredoxin systems. The cellular NADPH/NAP<sup>+</sup> ratio ultimately determines the cellular redox status (Schafer and Buettner, 2001). NADPH is produced primarily through the pentose phosphate pathway, in which each molecule of oxidized glucose-6-phosphate generates 2 molecules of NADPH. NADPH levels can be modulated by glucose availability or diseases (Wamelink *et al.*, 2008). For example, deficiencies in glucose-6-phosphate dehydrogenase (G6PD), which catalyzes the first step of the pentose phosphate pathway, results in lower intracellular NADPH/NAP<sup>+</sup> ratios, and consequent increase in oxidative stress, and has been associated with a number of diseases (Ho *et al.*, 2007). Also notably, G6PD deficiency has been shown to lead to recurring infections in individuals associated with decreased NADPH, necessary for oxidative burst in neutrophils (Rosa-Borges *et al.*, 2001; Agudelo-Flórez *et al.*, 2004).

## ***Novel Redox Techniques***

Due to the central role of H<sub>2</sub>O<sub>2</sub> and redox signaling in cellular viability, it is imperative to develop sensitive and selective techniques to measure specific aspects of the redox state in a cell. Typically, these measurements attempt to quantify concentration of oxidant species (e.g., H<sub>2</sub>O<sub>2</sub>, superoxide), oxidized biomolecules (e.g., proteins, lipids), or intracellular antioxidants (e.g., GSH, ascorbate). However, measuring many of these molecules is notoriously difficult due to their labile nature. Many of the biochemical and analytical assays consume the sample, preventing serial collection from the same sample. Additionally, cell lysis or tissue disruption can cause oxidative damage, potentially introducing artifacts (Meyer and Dick, 2010).

### Live-Cell Imaging

Live-cell imaging approaches have been developed to study different redox events to overcome some of these issues (Wages *et al.*, 2016). Many redox events are rapid, but can be captured over time using live-cell approaches is desired to provide high temporal resolution. Live-cell imaging also preserves spatial information since cells are left intact under physiological conditions. Numerous genetically encoded probes have been developed to measure many different aspects of redox signaling (Wages *et al.*, 2016). roGFP measures GSH/GSSG redox potential in the cell, which provides a sense of overall redox status. HyPer specifically measures intracellular H<sub>2</sub>O<sub>2</sub>, and has been targeted to different subcellular compartments to show novel roles of H<sub>2</sub>O<sub>2</sub> in signaling (Malinouski *et al.*, 2011). The recent development of novel genetically-encoded NADPH sensors show great promise to study the role of this important reductant (Tao *et al.*, 2017). A genetically-encoded sensor utilizing the yeast transcription factor, Yap-1 has been developed to detect protein sulfenic acid formation (Takanishi *et al.*, 2007).

### Dimedone-based sulfenylation probes

As more is learned about the central role of cysteine oxidation in essential biological signaling, numerous methods have been developed to probe the proteome for redox switches and oxidative PTMs. Traditional methods rely on thiol modifying agents to deduce which thiols are lost after oxidation or those that are regained using reductants (Poole *et al.*, 2007). However, there are several limitations of these methods including the need for the reductant to be specific for that PTM and that it is a multistep procedure, and many PTMs are not stable. More direct approaches to specifically trap sulfenic acids and

allow identification of sites of cysteine oxidation have been developed to overcome these limitations. Many are based on the small molecule probe, 5,5-dimethyl-1,3-cyclohexanedione, more commonly known as dimedone. Dimedone is cell permeable and forms a thioether bond specifically and irreversibly with sulfenic acids. Dimedone does not reactive with all other cysteine PTMs and can be used to label sulfenic acid by mass spectrometric or immunoblotting methods (Bachi *et al.*, 2012).

Novel dimedone-based approaches have been developed to increase signal-to-noise ratio. The Carroll group has developed DYn-2 and DAz-2, which utilize dimedone warheads with alkynyl or azide tails, respectively (Paulsen and Carroll, 2013; Pan and Carroll, 2014). They are more reactive than dimedone and can be labelled with biotin through copper-catalyzed alkynyl-azo cycloaddition (better known as “Click Chemistry”) or the Staudinger Ligation, respectively, as biotin cannot cross the cell membrane (Presolski *et al.*, 2011). Once labeled, biotin-avidin separation approaches can dramatically improve sensitivity (Poole *et al.*, 2007; Yang *et al.*, 2014; Yang *et al.*, 2015). However, Click chemistry has been shown to damage the proteins it detects (Hong *et al.*, 2009). Advances in sulfenylation detection techniques have increased site-specific mapping of redox-sensitive cysteines in the proteome (Yang *et al.*, 2015).

### ***Oxidative Stress in Toxicology***

In toxicology, oxidative stress has traditionally been measured by markers of irreversible damage to the cell caused by a xenobiotic. This includes oxidative DNA adducts, irreversible oxidized proteins, and oxidized lipids. However, these are extreme forms of oxidative stress and many toxicants may cause more subtle changes in redox homeostasis that would not be apparent by only looking at these markers. Another generally accepted “functional” readout used by many toxicologists is the expression of heme oxygenase-1 (HO-1) (Ma, 2013). HO-1 is upregulated as result of the KEAP1/Nrf2 pathway activation. Typically, the transcription factor Nrf2 is bound to Keap1, preventing its function. Keap1 can be modified when a key disulfide bond is broken, either by electrophiles or oxidants. Nrf2 is released and translocates to the nucleus where it binds to antioxidant-responsive elements (ARE), found in the promoter regions of numerous phase II metabolism enzymes. These enzymes include HO-1, glutathione-S-transferases (GSTs), and NQO1 which are seen as an adaptive response to mitigate oxidative stress. However, this pathway is not specific for oxidative stress, since Nrf2 can be released from Keap1 through both

electrophilic attack of specific cysteine residues of Keap1 or phosphorylation of Nrf2 by a number of kinases (ERK, JNK, PKC) (Huang *et al.*, 2000; Kaspar *et al.*, 2009). HO-1 expression may be appropriately labelled as a good marker of overt oxidative stress (Choi and Alam, 1996; Wu *et al.*, 2012).

#### Oxidative Stress in PM Toxicity

Oxidative stress has been cited as a key mechanism in PM-induced human health effects. Diesel exhaust particles (DEP) have been shown to increase ROS in MAC, bronchial epithelial cells and lung microsomes (Hiura *et al.*, 1999; Li *et al.*, 2002). DEP has also been shown to induce HO-1, GST, and other phase II enzymes through activation of Nrf2 (Li *et al.*, 2004). Numerous investigations have been made into whether different components of PM could induce oxidative stress (Ghio *et al.*, 2012). A number of metals, such as zinc, lead, and cadmium can coordinate on reactive protein thiols, interrupting cellular function and promoting oxidation (Wu *et al.*, 2013). Ultrafine and nanoparticles have shown numerous hallmarks of oxidative stress, especially due to their increased surface area to mass ratio (Manke *et al.*, 2013).

While general makers of oxidative stress have previously been documented in response to PM exposure, the specific oxidative events have not been characterized, even as the technology to more accurately measure these events has improved. Previous studies in our lab showed that 1,2-NQ increased H<sub>2</sub>O<sub>2</sub> in both cytosolic and mitochondrial compartments, using the genetically encoded sensor HyPer, which is specific for H<sub>2</sub>O<sub>2</sub>. 1,2-NQ also caused an increase in the glutathione redox potential and induced transcription of HO-1, IL-6, and IL-8 (Cheng *et al.*, 2012). We also showed that 1,2-NQ induced both total sulfenylation and of key redox switches GAPDH and PTP1B in bronchial epithelial cells (Wages *et al.*, 2015). However, it is not known if 1,2-NQ induced sulfenylation causes a functional change in the cell.

#### **Bioenergetics: Needed for Life, Runs on Redox Signaling**

Bioenergetics is most simply defined as how cells produce, maintain, and use energy. Bioenergetics is a highly responsive process that can react within seconds to pO<sub>2</sub> and pH changes (Wilson, 2013). The two main processes of bioenergetics are oxidative phosphorylation, which occurs in the mitochondria, and glycolysis, which occurs in the cytosol.

## **Mitochondria**

Mitochondria are often known as “the powerhouse of the cell,” converting organic carbon into usable cellular energy in the form of ATP. Oxidative phosphorylation is fueled by the citric acid cycle to produce energy source NADH to drive ATP synthase. The citric acid cycle in turn is regulated by upstream substrate oxidation process including glycolysis, when glucose is the substrate, and glutaminolysis when amino acids are the substrate.

Nutrients (glucose, amino acids, or fatty acids) are converted into metabolic intermediates (pyruvate, acetyl-CoA, oxaloacetate, 2-oxoglutarate) which are metabolized in the tricarboxylic acid (TCA, or citric acid) cycle. Decarboxylation of the intermediates during this process produces NADH. NADH feeds into the electron transport chain as Complex I (NADH:ubiquinone oxidoreductase) oxidizes NADH and passes the electrons to the naturally occurring quinone, ubiquinone ( $Q \rightarrow QH_2$ ). Complex II (succinate dehydrogenase) and other electron sources also feed into the “Q pool”. Ubiquinone passes electrons to Complex III (coenzyme Q: cytochrome c-oxidoreductase), which reduces cytochrome c. Complex IV (cytochrome c oxidase) transfers 4 electrons from cytochrome c to reduce the terminal electron acceptor  $O_2$  to  $H_2O$ . This transfer of electrons from NADH to  $O_2$  is an energetically favorable process and is coupled to the pumping of protons through Complexes I, III, and IV into the intermembrane space. This stored energy, termed the proton motive force is used by Complex V (ATP Synthase) to produce ATP (Mailloux *et al.*, 2014).

As both a source and target of ROS, mitochondria play a central role in cellular redox signaling. Mitochondria can be a main site for ROS production within the cell, as ROS are an inevitable byproduct of respiration. There are at least seven sites of ROS production in the mammalian mitochondrion, including Complex I, Complex III, and TCA Cycle enzymes (Brand, 2010). Electrons can “spin-off” prematurely from Complexes I and III to reduce  $O_2$  and produce  $O_2^{\bullet-}$  which is quickly dismutated to  $H_2O_2$  through high levels of SOD activity present in the mitochondria.  $H_2O_2$  produced by the mitochondria has been shown to regulate insulin release, insulin signaling, the hypoxic response, adipocyte differentiation, regulation of cell cycle, and T cell receptor-initiated cell signaling (Guzy *et al.*, 2005; Hamanaka and Chandel, 2010; Tormos *et al.*, 2011). To control ROS production, there are several antioxidant systems present in the

mitochondria to scavenge superoxide and H<sub>2</sub>O<sub>2</sub> in the cell. They contain SOD2 and high levels of GSH (~5mM). Mitochondria also contain Prx3 which specifically targets H<sub>2</sub>O<sub>2</sub>.

Mitochondria use redox reactions to drive their function and also have a microenvironment that favors cysteine oxidation reactions, making them a center of redox regulation, and vulnerable target for oxidative stress. The pumping of protons into the intermembrane space lowers the redox potential of the mitochondrial matrix, favoring the thiolate form of protein sulfhydryls. Additionally, the mitochondrial proteome is rich in protein thiols, estimated to be 60-90 mM of exposed protein thiols (Kemp *et al.*, 2008; Requejo *et al.*, 2010). This is the most concentrated cellular location of thiols. There are numerous Fe-S clusters present in the respiratory complexes and TCA cycle enzymes. Enzymes sensitive to redox inactivation include aconitase, isocitrate dehydrogenase, 2-oxoglutarate dehydrogenase, pyruvate dehydrogenase, Complex II, and Complex I. Due to their short-lived nature, sulfenic acids themselves are unlikely to play an important regulatory role in mitochondria, and are most likely a precursor for other reactions such as S-glutathionylation (Mailloux *et al.*, 2014). The presence of high mitochondrial concentrations of GSH also enables rapid S-glutathionylation as a part redox signaling. S-glutathionylation could play a protective mechanism to prevent hyperoxidation and reduce further ROS production. S-glutathionylation has been found to be essential in protecting several mitochondrial enzymes from overoxidation by H<sub>2</sub>O<sub>2</sub>, including TCA enzyme 2-oxoglutarate dehydrogenase, Complex I, and the adenine nucleotide translocator (ANT) (McStay *et al.*, 2002; Applegate *et al.*, 2008; Hurd *et al.*, 2008).

Notably, ROS can also cause the opening of the mitochondrial permeability transition pore (MPTP). Opening of the MPTP is an apoptotic process that dissipates ion and metabolite gradients, collapsing the PMF, which induces swelling and rupture of the mitochondria (McStay *et al.*, 2002). A number of toxicants are known to induce MPTP, including semiquinones, through the generation of ROS (Kowaltowski *et al.*, 1995).

### **Glycolysis**

Glycolysis is an essential cellular process that converts glucose into pyruvate that feeds into oxidative phosphorylation. Glycolysis also produces a net of 2 ATP in the process and can be used for energy under anaerobic conditions. Though most cells only switch entirely to glycolysis when adequate

oxygen supply is low or mitochondria are inhibited, cancer cells constantly rely on glycolysis even under normoxia. This phenomenon is termed the Warburg phenomenon after it was discovered in the 1950s (Ganapathy *et al.*, 2009).

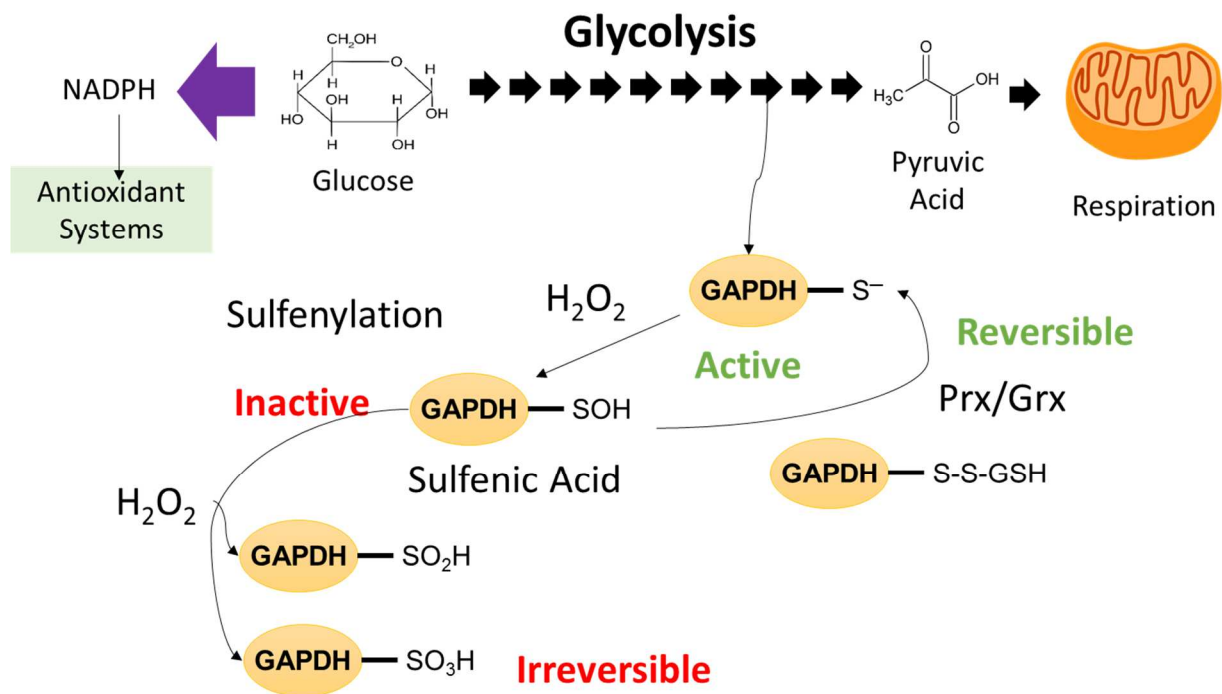


**Figure 1-2.** GAPDH acts a redox switch to shunt glucose through the pentose phosphate pathway to generate NADPH, an essential reductant for numerous antioxidant systems. GAPDH thiolate is also sensitive to hydroxylation to the irreversible sulfinic and sulfonic acid forms by H<sub>2</sub>O<sub>2</sub>.

## GAPDH

Glyceraldehyde-3-phosphate dehydrogenase (GAPDH) is an essential glycolytic enzyme and is needed for cellular viability. GAPDH catalyzes the conversion of glyceraldehyde-3-phosphate to 1,3-bisphosphoglycerate, yielding NADH in the process. GAPDH is expressed constitutively at high-levels in the cell, making it a popular housekeeping protein and experimental control. GAPDH has recently been shown to have several “moonlighting” functions including structural organization, signaling regulation of nuclear proteins, mRNA stabilization, and as a receptor (Hildebrandt *et al.*, 2015).

GAPDH is also an important redox switch with important antioxidant capacities within the cell (Figure 1-2). GAPDH has 2 cysteines in its active site, one of which is extremely reactive to H<sub>2</sub>O<sub>2</sub> oxidation, primarily based on its low pKa. Interestingly, the Dick group discovered that another Cys, 5

amino acids from the catalytic Cys, provides a proton-shuttle to enhance sulfenylation of the catalytic Cys (Peralta *et al.*, 2015). When GAPDH is sulfenylated by H<sub>2</sub>O<sub>2</sub>, it is inactivated and glycolysis slows. This allows glucose to shunt toward the pentose phosphate pathway and generates NADPH (Godon *et al.*, 1998; Ralser *et al.*, 2007). As mentioned previously, NADPH is an essential reductant for regeneration of many antioxidant cellular systems. Once NADPH levels reach sufficient levels for antioxidant systems to control the oxidant levels, GAPDH can be reduced through disulfide bonding and Trx or Grx to the thiol form (Peralta *et al.*, 2015).

### ***Novel Bioenergetic Techniques***

One of the key methods to study bioenergetics is through extracellular flux analysis. Extracellular flux analysis measures changes in levels of molecules used or excreted from cells over time. Bioenergetically, cells are constantly taking up oxygen for use in oxidative phosphorylation. The oxygen consumption rate (OCR) of the cell can be measured as a marker of mitochondrial respirational activity. In a normal cell, over 90% of the OCR is typically devoted to mitochondrial respiration. Other non-respirational processes can contribute to OCR, including NADPH oxidase activity (e.g. during oxidative burst response) and redox cycling of a xenobiotic. For decades, oxygen consumption by cells and isolated mitochondria has been measured using the Clark electrode. While accurate, this method is extremely low throughput and often requires mitochondrial isolation to obtain accurate readings.

During glycolysis, lactate is produced and excreted from the cell, which acidifies the media. The pH flux of the media can be measured over time and an extracellular acidification rate (ECAR) can be calculated. As with OCR, glycolysis is not the only process that contributes to ECAR. In fact, CO<sub>2</sub> produced during the TCA cycle in highly respirational cells can play a large role in ECAR. ECAR has traditionally been measured in a straightforward method with a pH meter. This method has similar limitations as the Clark Electrode.

The Seahorse XFe analyzer (originally developed by Seahorse Bioscience, now owned by Agilent Technologies) revolutionized the way extracellular flux is performed (Ferrick *et al.*, 2008). This system combines OCR and ECAR measurements into a plate-reader-like format using polymer-embedded fluorescent probes and optics. Additionally, each well has four ports that can be filled with various injections to be added at user-designated time. Complex calculations have gone into adjusting

measurements for background readings, yet the system overall is straight-forward and user friendly (Gerencser *et al.*, 2009). There is a high degree of customization that can be done by the investigator to adapt the system and conditions for specific experiments. Seahorse assays have been adapted for a variety of cell types, tissues, 3D spheroid cultures, and even zebrafish embryos. Of interest to lung research is adapting the technology to study fully differentiated murine lung epithelial cells grown at an air liquid interface (Xu *et al.*, 2014). A bioenergetic difference was noted between submerged and air-liquid interface cultures, highlighting the importance to move toward the most appropriate lung cell system for increased relevance.

Additionally, several assays have been developed with specific inhibitors to use in the injection ports to measure different bioenergetics parameters. The “Cell Mito Stress Test” has been the most widely used and recognized of the Seahorse assays as it provides eight different parameters of mitochondrial function. The first injection is Oligomycin, which inhibits ATP synthase (Complex V), providing a sense of how much OCR was devoted to ATP production. The next injection is the protonophore FCCP which uncouples the mitochondrial proton gradient, speeding up respiration to its maximum, providing the parameters Maximal respiration and spare capacity. Last is injection of rotenone and antimycin A, inhibitors of Complexes I and III respectively, which measures non-mitochondrial respiration. Through additional calculations the proton leak and basal respiration of the cells can be determined. Since this only utilizes three of the four injection ports, it is useful for toxicologists interested in acute effects to include a compound of interest as the first injection.

The assay most common for measuring glycolysis is termed the “Glycolytic Stress Test”. The media initially lacks glucose or pyruvate and the cell must rely on L-glutamine for energy. The first injection is glucose, producing a rise in ECAR equivalent to glycolysis occurring in the cell. The next injection is oligomycin A to force the cell to rely completely on glycolysis for ATP production, increasing ECAR and glycolysis to its maximum. The last injection is 2-deoxyglucose which inhibits glycolysis and shows the portion of ECAR derived from other processes. While this assay is useful, it has two flaws, especially in a toxicological application: 1) Cells are glucose starved for an hour prior to analysis, effectively depleting NADPH levels and making them more susceptible to oxidative stress, and 2) CO<sub>2</sub> production from mitochondrial respiration could confound results. As an improvement, the “Glycolytic Rate

Test” was recently developed to overcome both of these flaws and provide a more accurate readout of glycolytic function.

### ***Role in Immune Function***

Bioenergetics has taken a central role in function of many different immune cells, especially macrophages (Mills *et al.*, 2017). Metabolic reprogramming is shown to mediate macrophages’ polarization to different phenotypes. Pro-inflammatory “M1” macrophages are shown to upregulate glycolysis and downregulate mitochondrial respiration, with specific breaks in the TCA cycle and respiratory chain noted. In contrast, “M2” macrophages have an anti-inflammatory phenotype and are shown to be dependent on mitochondrial respiration (O’Neill *et al.*, 2016).

While there is clear evidence that metabolic shifts play a role in monocyte-derived macrophage polarization, the bulk of this work has been performed in differentiated rodent bone-marrow derived monocytes. A few studies have utilized *ex vivo* differentiated peripheral blood monocytes. While these are helpful to understanding the mechanisms of those cell types, it is widely established that macrophages are extremely plastic and resident macrophages, such as those of the liver, lung, and brain, are very different from circulating monocytes (Jha *et al.*, 2015). Recent work has begun to investigate the role of bioenergetics of rodent BAL alveolar MAC in airway diseases and dysfunction (Agarwal *et al.*, 2014; Bewley *et al.*, 2017). However, no studies have characterized the bioenergetics of human resident lung macrophages.

### ***Role in Air Pollution Toxicity***

Mitochondrial dysfunction has been identified as a key event in PM-induced cytotoxicity (Hiura *et al.*, 2000; Li *et al.*, 2003; Xia *et al.*, 2004). Organic PM components were previously shown to depolarize mitochondrial potential, inducing the Ca<sup>2+</sup>-dependent permeability transition pore to open in an alveolar macrophage cell line (Xia *et al.*, 2004). Previous evidence in our group indicated that 1,2-NQ increased H<sub>2</sub>O<sub>2</sub> concentration in the mitochondria, as treatment with the proton gradient uncoupler CCCP ablated cytosolic H<sub>2</sub>O<sub>2</sub> in human epithelial cells (Cheng *et al.*, 2012).

Though glycolysis has not been thoroughly studied in response to PM or diesel exhaust particle exposure, quinones have previously been found to inhibit GAPDH. Short-term cigarette smoke exposure was shown to decrease GAPDH activity and increase G63P activity of the pentose phosphate pathway in

mouse lungs (Agarwal *et al.*, 2012). This was coupled by an increase in activity of Complexes II, IV, and V of the electron transport chain.

### **Scope of the Dissertation**

Exposure to ambient air particulate matter (PM) is a global public health problem linked to cardiopulmonary morbidity and mortality. Oxidative stress has been cited as an initiating mechanism in PM-induced health effects, yet the specific events involved are not well characterized. There remains a critical need for a more detailed understanding of how specific redox events alter cellular signaling over time, leading to disease development. Characterizing how specific redox events are altered by air pollutant components will provide a molecular and mechanistic basis to understand the adverse outcomes of PM exposure. H<sub>2</sub>O<sub>2</sub> is an essential second messenger in numerous redox sensitive signaling pathways that control critical cellular functions, ranging from proliferation to energy production. This project will investigate the role of H<sub>2</sub>O<sub>2</sub> in the adverse effects of the ubiquitous PM-associated 1,2-naphthoquinone (1,2-NQ).

The aim of this research is to define how an oxidative air pollutant induces oxidative damage in the cell. The overarching hypothesis is that toxicologic responses to 1,2-NQ exposure result from peroxide-dependent oxidative modification of regulatory protein targets in human airway cells (Figure 1-3). To test this hypothesis, I examined the role of mitochondrial dysfunction in cellular production of H<sub>2</sub>O<sub>2</sub> in human epithelial cells exposed to 1,2-NQ (Chapter 2). Additionally, I assessed how 1,2-NQ affected glycolysis, a key cellular redox switch, and the role of H<sub>2</sub>O<sub>2</sub> production (Chapter 3). Finally, I expanded the model to primary human innate immune lung cells to characterize both baseline and altered bioenergetics in response to 1,2-NQ (Chapter 4).

The findings in this dissertation provide compelling evidence that H<sub>2</sub>O<sub>2</sub> and mitochondrial function play a profound role in mediating toxicologic responses to 1,2-NQ in human airway epithelial cells. I showed that 1,2-NQ exposure increases cellular H<sub>2</sub>O<sub>2</sub> through both redox cycling and mitochondrial dysfunction mechanisms. I showed that 1,2-NQ exposure causes glycolytic inhibition, partially due to a peroxide-dependent mechanism, and that GAPDH is likely both adducted and sulfenylated. Additionally, I found that bioenergetics impairments by 1,2-NQ hold true in primary human immune cells, emphasizing the utility of bioenergetics as a translational functional marker of air pollutant exposure.

Findings of this work will provide novel insights into the underlying mechanisms of PM-induced health effects.

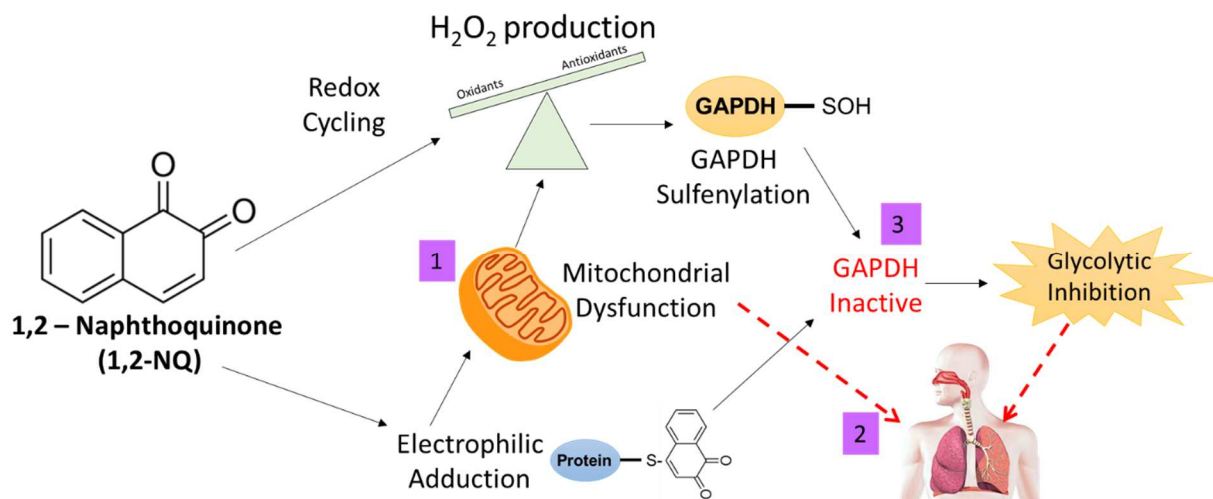


**Figure 1-3.** Overview of this dissertation which examines (1) The effect of 1,2-NQ on mitochondrial function as a source of H<sub>2</sub>O<sub>2</sub>. (2) The bioenergetics of primary human lung macrophages and whether mitochondrial dysfunction is similarly caused by 1,2-NQ. (3) The effect of 1,2-NQ on glycolysis, examining post-translational modifications of GAPDH to identify potential mechanisms.

## CHAPTER 2: INVESTIGATING MITOCHONDRIAL DYSFUNCTION IN HUMAN LUNG CELLS EXPOSED TO REDOX-ACTIVE PM COMPONENTS<sup>1</sup>

### Introduction

Ambient particulate matter (PM) is a global public health concern. Exposure to ambient PM is estimated to cause 3.3 million premature deaths worldwide annually and is linked to increased cardiovascular and respiratory morbidity and mortality (Pope and Dockery, 2006; Lelieveld *et al.*, 2015). Despite intensive investigation, the mechanism(s) that initiate the adverse health effects of PM exposure are not known. However, oxidative stress has been specifically implicated in the responses to PM inhalation (Kelly, 2003; Li *et al.*, 2008).

Mitochondrial dysfunction has been identified as a key event in PM-induced cytotoxicity (Hiura *et al.*, 2000; Li *et al.*, 2003; Xia *et al.*, 2004). In addition to their crucial role in cellular bioenergetics, mitochondria are important regulators of oxidative stress. In resting cells, mitochondria generate reactive oxygen species (ROS), the levels of which are highly controlled by multiple antioxidant systems (Murphy, 2009; Brand, 2010). A variety of xenobiotics disrupt mitochondrial function by inhibiting the electron transport chain or uncoupling mitochondrial membrane potential, processes which increase ROS generation (Kovacic *et al.*, 2005).

Typically found on particles surfaces, quinones are ubiquitous organic components of PM, typically absorbed on particles and implicated in PM-induced mitochondrial dysfunction (Flowers-Geary *et al.*, 1996). Quinones commonly found in ambient air include 1,2-naphthoquinone (1,2-NQ), 1,4-naphthoquinone (1,4-NQ), 9,10-phenanthrenequinone (9,10-PQ), and 1,4-benzoquinone (BQ) (Cho *et al.*, 2004; Delgado-Saborit *et al.*, 2013). Polyaromatic hydrocarbons (PAHs) can also be oxidized by cytochrome p450 to form quinones *in vivo* (Penning *et al.*, 1999). Quinones have been proposed to

---

<sup>1</sup> This chapter previously appeared as an article in *Toxicology and Applied Pharmacology*. The original citation is as follows: Lavrich, K.S., Corteselli, E., Wages, P., Bromberg, P., Simmons, S., Gibbs-Flournoy, E., Samet, J.M. (2018). Investigating Mitochondrial Dysfunction in Human Lung Cells Exposed to Redox-Active PM Components. *Toxicology and Applied Pharmacology*, 342, 99-107.

contribute to the health effects of PM inhalation (Valavanidis *et al.*, 2005). Previous work on environmentally relevant quinones has largely focused on their electrophilic properties, specifically their adduction of cellular macromolecules through Michael addition (Iwamoto *et al.*, 2007; Kumagai *et al.*, 2012). Less studied is the role played by ROS generated through redox cycling of specific quinone species (Watanabe and Forman, 2003). Redox-cycling quinones can undergo one-electron reduction to form unstable semiquinones (Figure 2-1). This reduction may be catalyzed by several flavin-containing enzymes, such as NADH:ubiquinone oxidoreductase (Complex I) of the mitochondrial electron transport chain and the cytochrome P450 system of the endoplasmic reticulum (Henry and Wallace, 1996). Semiquinones can donate an electron to oxygen ( $O_2$ ) to form superoxide ( $O_2^{\cdot-}$ ), which has an extremely short half-life due to its rapid dismutation to the more stable species, hydrogen peroxide ( $H_2O_2$ ), by abundant superoxide dismutases. Individual quinone species vary in their propensity to adduct and redox cycle, dependent on their electrophilicity and redox potential, respectively (Song and Buettner, 2010). Thus, 1,2-NQ and 1,4-NQ are capable of both mechanisms, while BQ is exclusively an electrophile and 9,10-PQ only redox cycles in the cell (Kumagai *et al.*, 2012). Prior studies have demonstrated that both redox-cycling and electrophilic quinones can depolarize mitochondrial membrane potential and deplete ATP production (reviewed in Henry and Wallace, 1996).

Previous work implicated mitochondria as a source of H<sub>2</sub>O<sub>2</sub> production in human airway epithelial

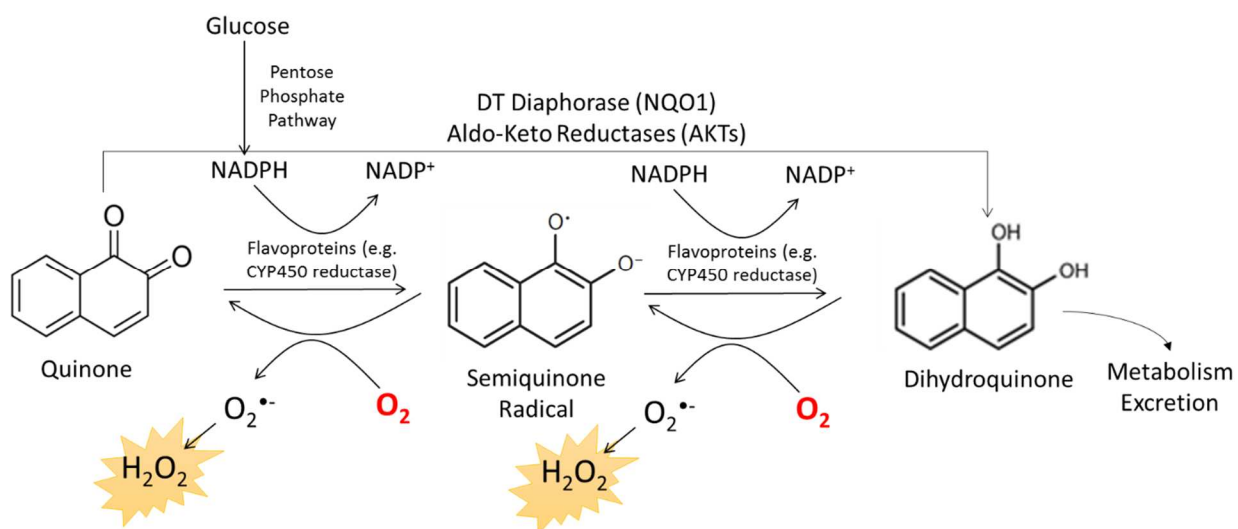


**Figure 2-1. 1,2-NQ redox cycles to produce ROS.** 1,2-NQ undergoes single-electron reduction to the semiquinone form catalyzed by flavoenzymes with NADPH as an electron source. NADPH is primarily produced by glucose metabolism through the pentose phosphate pathway. The semiquinone can auto-oxidize back to the quinone, reducing O<sub>2</sub> to form superoxide (O<sub>2</sub><sup>•-</sup>) and eventually hydrogen peroxide (H<sub>2</sub>O<sub>2</sub>). The semiquinone can also be further reduced to the dihydroquinone, which is more favorable for metabolism and excretion but can also reduce O<sub>2</sub> to O<sub>2</sub><sup>•-</sup>. Alternatively, the quinone can undergo two-electron reduction by DT Diaphorase (also known as NAD(P)H Quinone Dehydrogenase 1, NQO1) or Aldo-Keto Reductases (AKTs) to the dihydroquinone, bypassing the semiquinone form.

cells exposed to environmentally relevant concentrations of 1,2-NQ (Cheng *et al.*, 2012). We

hypothesized that 1,2-NQ impairs mitochondrial function, leading to increased mitochondrial H<sub>2</sub>O<sub>2</sub>. In the present study, we investigated whether 1,2-NQ disrupts mitochondrial function, as measured through extracellular flux analyses. We show here that 1,2-NQ exposure of the human bronchial epithelial cell line BEAS-2B impairs complex I-linked mitochondrial substrate oxidation, a novel mechanism of mitochondrial impairment by 1,2-NQ, and markedly increases oxygen consumption through a redox cycling mechanism, both potential sources of H<sub>2</sub>O<sub>2</sub>.

## Methods

### **Materials**

Tissue culture media and supplements were purchased from Lonza (Walkersville, MD, USA). The following chemicals were purchased from Sigma-Aldrich (St. Louis, MO): 1,2-naphthoquinone (1,2-NQ), 1,4-naphthoquinone (1,4-NQ), 9,10-phenanthrenequinone (9,10-PQ), 1,4-benzoquinone (BQ), DMSO, oligomycin, carbonyl cyanide-4-(trifluoromethoxy)phenylhydrazone (FCCP), rotenone, antimycin A,

glucose, sodium pyruvate, fatty acid-free bovine serum albumin (BSA), mannitol, sucrose, potassium phosphate monobasic (KH<sub>2</sub>PO<sub>4</sub>), magnesium chloride (MgCl<sub>2</sub>), EGTA, H<sub>2</sub>O<sub>2</sub>, and HEPES. XF Base Medium, XF Flux Paks, and XF PMP were purchased from Seahorse Bioscience (Billerica, MA, now Agilent Technologies). L-glutamine (Gibco) was purchased from ThermoFisher Scientific (Waltham, MA). Basic laboratory supplies were purchased from Fisher Scientific (Raleigh, NC, USA).

### **Cell Culture**

SV40 large T antigen-transformed human airway epithelial cells [BEAS-2B cells, subclone S6 (Reddel *et al.*, 1988)] were cultured in serum-free keratinocyte growth medium (KGM). BEAS-2B cells have been used extensively for *in vitro* testing of inhaled toxicants as a model of airway epithelium (Veljkovic *et al.*, 2011; Persoz *et al.*, 2012). BEAS-2B cell cultures were continually renewed from frozen stocks every 2–3 months for the duration of the study. Cells were deprived of growth factors overnight prior to experiment by changing the medium to keratinocyte basal medium (KBM), to induce cellular quiescence.

### **Quinone Preparation**

100 mM stocks of 1,2-NQ and 1,4-NQ and 15 mM stocks of 9,10-PQ were prepared in DMSO. Working solutions were diluted in cell media with final DMSO concentrations less than 0.1%. 50 mM stocks of BQ were prepared directly in cell media or mitochondrial assay solution. All stocks and working solutions were made fresh on the same day as exposure.

### **Protein Assay**

Where indicated, protein concentration was determined by a modified Bradford Assay (Bio-Rad Laboratories, Inc.).

### **Extracellular Flux Analysis**

Oxygen consumption rate (OCR) was measured at 37°C using the Seahorse XFe96 Analyzer (Agilent Technologies). BEAS-2B cells were seeded at 16,000 cells per well two days prior to assay in XFe96 cell plates with KGM. Four background wells without cells were included in all assays. XFe96 sensor cartridges were hydrated overnight with XF Calibrant at 37°C. Media was replaced the night before assay to KBM without growth factors. For intact cell experiments, XF Cell Mito Assay Media (XF Base Media with 10 mM glucose, 1 mM sodium pyruvate, 2 mM glutamine) was prepared fresh on the

day of assay and adjusted to pH 7.4 with 100 mM NaOH. Cell media was changed 1 hour prior to assay and cells were placed in a 37°C incubator without CO<sub>2</sub>. Stock concentrations of oligomycin, FCCP, rotenone, and antimycin A were prepared in DMSO and stored at -20°C. All compounds used for in-assay injections were prepared in XF Cell Mito Assay Media with final DMSO concentrations less than 0.1%. The concentration of FCCP that effects maximal OCR was optimized in preliminary experiments. For Cell Mito Stress Tests, the injections were ordered as follows unless otherwise noted: A) quinone; B) 1 μM oligomycin; C) 0.25 μM FCCP; D) 1 μM rotenone, 1 μM antimycin A. Mix-wait-measure times were 3 min-0 min-3 min.

Bioenergetic parameters were calculated through the standard Cell Mito Stress Test Assay (Agilent Technologies). Briefly, change in basal OCR after quinone addition was calculated as the measurement immediately after quinone addition minus the basal measurement directly before addition. ATP production was measured as the decrease in OCR after oligomycin addition. Non-mitochondrial respiration was measured as the minimum OCR after rotenone/antimycin A injection. Reserve capacity was measured as the increase in OCR after FCCP was added. Spare respiratory capacity was calculated as the maximal respiration after quinone treatment minus the basal respiration.

For glucose starvation experiments, cell media was changed to either XF Cell Mito Assay Media or XF Glycolysis media (XF Base Media supplemented with 2 mM glutamine) two hours prior to start of assay.

### ***Cell Viability***

Cell viability was measured by monitoring retention of pre-loaded calcein-AM (Molecular Probes, Eugene, OR, USA). BEAS-2B cells were plated in black-walled, clear-bottom 96-well plates (Costar, Corning Inc., Corning, NY) and grown until confluency. Cells were deprived of growth factors overnight before the experiment. Two hours before the assay, cell media were changed to XF Cell Mito Assay Media or XF Glycolysis media, and cells were placed in a non-CO<sub>2</sub> incubator at 37°C. Cells were washed twice with warm PBS and incubated with 2.5 μM calcein AM for 20 min at 37°C. After incubation, excess calcein AM was removed through two washes of warm PBS. Cells were treated in triplicate with the following: a media control; DMSO; 3-50 μM 1,2-NQ; 3-50 μM 1,4-NQ; 50 μM 9,10-PQ; or 0.1% saponin (positive control). Cells were immediately measured for calcein fluorescence at excitation 490

nm/emission 520 nm using a CLARIOstar microplate reader (BMG LABTECH, Ortenberg, Germany) at 37°C. Measurements were taken at 60 s intervals for 20 min. Cellular viability was expressed as percentage of media control.

### ***Permeabilized Cell Preparation***

Permeabilized cell experiments were conducted following a procedure similar to that described previously (Salabei *et al.*, 2014). BEAS-2B cells were plated and prepared as described above in *Extracellular Flux Analysis*. Mitochondrial Assay Solution (MAS, 220 mM mannitol, 210 mM sucrose, 10 mM KH<sub>2</sub>PO<sub>4</sub>, 5 mM MgCl<sub>2</sub>, 1 mM EGTA, pH 7.2) was prepared. All substrates were diluted in MAS and adjusted to pH 7.2. Immediately prior to extracellular flux assay, media was changed to MAS with freshly added 0.6% BSA and 1 nM XF PMP. No equilibration step was included on the XFe96 Analyzer, and mix-wait-measure times were 0.5min-0min-2min. For Complex I substrate oxidation tests, injections were sequenced as follows: A) quinone; B) 10 mM pyruvate/2 mM malate or 10 mM glutamate/ 10 mM malate, and 4 mM ADP; C) 3.16 μM oligomycin; D) 1 μM rotenone. Complex II substrate oxidation injections were sequenced as follows: A) quinone; B) 10 mM succinate, 4 mM ADP, 2 μM rotenone; C) 3.16 μM oligomycin; D) 4 μM antimycin A, 100 μM TMPD, 10 mM ascorbate.

To track mitochondria during permeabilization procedure, BEAS cells expressing the redox potential sensor roGFP targeted to the mitochondria were imaged using a Nikon Eclipse C1si spectral confocal imaging system (Nikon Instruments Corporation, Melville, NY) and the Andor Zyla 4.2 camera (Andor Technology Ltd, Belfast, UK). In a live cell imaging experiment at 37°C and 5% CO<sub>2</sub>, cells were imaged prior to permeabilization and at 150 s intervals immediately after permeabilization using excitation of 404 nm and 488 nm and emission at 515 nm. Injections of 10 μM 1,2-NQ and subsequent mitochondrial inhibitors were performed at the same intervals and concentrations as extracellular flux analysis experiments.

### ***Isolated Mitochondrial Preparation***

Mouse hearts were the generous gift of Dr. Kathleen Caron. C57/BL6 mice were treated humanely under practices approved by the Institutional Animal Care and Use Committee of the University of North Carolina at Chapel Hill. Mitochondria were isolated from hearts of middle-aged male C57/BL6 mice. Briefly, ventricles were minced in cold PBS and homogenized in 1 mL mitochondrial isolation buffer

(70 mM sucrose, 210 mM mannitol, 5 mM HEPES, 1 mM EGTA, 0.5% fatty-acid free BSA, pH 7.2) using a tissue processor (Tissue Tearer, Bio Spec Products Inc., Bartlesville, OK) on low speed for 2-3 strokes on ice, as described in (Palmer *et al.*, 1977). Homogenates were centrifuged at 800 x g for 10 min at 4°C. The fat/lipid layer was removed by aspiration and supernatant was centrifuged at 8000 x g for 10 min at 4°C. The resulting pellet was washed twice in ice-cold isolation buffer and resuspended in MAS and protein concentration was determined. Mitochondrial enrichment was verified by blotting cytochrome c as a marker of the mitochondrial fractions (Figure 2-14), as previously described (Wages *et al.*, 2014).

Extracellular flux analyses were conducted using a Seahorse XFe24 Analyzer (Seahorse Bioscience). Five µg of mitochondrial protein in 50 µL MAS were added per well of an XF24 cell plate, with 4 background wells containing no mitochondria. The mitochondria were immobilized on the plate by centrifugation at 2000 x g for 20 min at 4°C using centrifuge equipped with a swinging bucket (Eppendorf, Hauppauge, NY). Pre-warmed MAS + 0.6% BSA was added to each well and the assay began immediately. For Complex I substrate oxidation tests, injections were sequenced as follows: A) quinone; B) 10 mM pyruvate, 2 mM malate, 4 mM ADP; C) 3.16 µM oligomycin; D) 1 µM rotenone. Mix-wait-measure times of 0.5min-0min-2min were used and no equilibration step was included. After assay, cellular protein was extracted and subjected to Western Blotting analysis as previously (Wages *et al.*, 2015). A polyclonal antibody with affinity for 1,2-NQ protein adducts was developed by a custom antibody production service using a standard 70-day 2-rabbit immunization protocol (ThermoFisher Scientific, Waltham, MA). Unpurified rabbit serum was used at a concentration of 1:10,000 for immunoblotting.

To permit comparisons between isolated mitochondria and BEAS-2B experiments, we empirically determined the mitochondrial protein content in BEAS-2B cells. We first determined the ratio of mitochondrial protein to total cellular protein as follows. BEAS-2B cells were grown on 8 x 150 cm<sup>2</sup> flasks until confluent. Cells were disrupted using nitrogen cavitation (Gottlieb and Adachi, 1999). Mitochondrial fractions were obtained using differential centrifugation, at 800 x g and 8000 x g and the protein concentrations of cytosolic and mitochondrial fractions were determined. We determined the ratio to be  $0.0253 \pm 0.0064$  µg of mitochondrial protein per 1 µg total cellular protein (mean ± SD, n=3 independent experiments). In separate experiments, we determined that approximately 64,000 cells were present per well in BEAS-2B experiments at the time of assay, therefore corresponding to  $0.133 \pm 0.060$  µg of

mitochondrial protein/well. OCR values from all experiments were thusly expressed normalized per  $\mu\text{g}$  of mitochondrial protein.

### ***H<sub>2</sub>O<sub>2</sub> Production Assay***

Extracellular H<sub>2</sub>O<sub>2</sub> was measured using the Amplex Red Hydrogen Peroxide/Peroxidase Assay Kit (Thermo Fisher Scientific, Waltham, MA) following the manufacturer's instructions. Briefly, BEAS-2B cells were plated at 25,000 cells/well in a clear-bottom black-walled 96-well plate two days prior to assay. Eighteen hours prior to assay, the culture media was replaced with KBM. Cells were treated with DMSO, 3-25  $\mu\text{M}$  1,2-NQ, 3-25  $\mu\text{M}$  1,4-NQ, 3-25  $\mu\text{M}$  9,10-PQ, or 25  $\mu\text{M}$  BQ for 18 min. at 37°C in phenol red-free KBM. 100-250  $\mu\text{M}$  H<sub>2</sub>O<sub>2</sub> was used as a positive control. The media was incubated with Amplex Red and HRP for 30 min and the fluorescence of the resorufin produced by the reaction with H<sub>2</sub>O<sub>2</sub> was measured at excitation  $\lambda = 545$  nm, emission  $\lambda = 590$  nm on a CLARIOstar microplate reader (BMG LABTECH, Ortenberg, Germany).

### ***Complex I Activity Test***

The rate of NADH oxidation to NAD<sup>+</sup> was tested using the Complex I Enzyme Activity Microplate Assay Kit (Abcam, Cambridge, MA) per manufacturer's instructions. Briefly, BEAS-2B were treated with KBM, DMSO, 10  $\mu\text{M}$  or 50  $\mu\text{M}$  1,2-NQ for 15 min. Media was aspirated and cells were washed and scraped in ice-cold PBS. Following cell lysis and determination of protein content, 121.5  $\mu\text{g}$  of total protein was added to each assay well and incubated for 3 hrs at room temperature. Background wells containing no sample and background control wells without assay solution were included. The NADH-dependent reduction of the dye was measured at 450 nm at 1 min intervals for 30 min with shaking between readings. Complex I activity was calculated as the rate of absorbance increase over time (mOD/min). Data were normalized to background wells.

### ***Statistical Analyses***

Data are expressed as means  $\pm$  SEM from at least three separate experiments. Statistical significance ( $p < 0.05$ ) was determined with Prism version 7.00 (Graphpad Software, La Jolla, CA), using one-way ANOVA with Dunnett's post-test for comparisons to controls, Tukey's post-test for comparisons within groups, and Sidak's test for intergroup comparisons. Pairwise comparisons were conducted using Student's t-tests.

## **Results**

### ***1,2-NQ Induces Dose-Dependent Increase in Oxygen Consumption Rate (OCR) of BEAS Cells***

We previously reported that 1,2-NQ-induced H<sub>2</sub>O<sub>2</sub> production could be blocked with inhibitors of mitochondrial respiration (Cheng *et al.*, 2012). We therefore used extracellular flux analysis to characterize the effects of 1,2-NQ on indices of mitochondrial respiration. As shown in Figure 2-2, addition of 1,2-NQ (3-50  $\mu$ M) resulted in a striking, dose-dependent increase in the oxygen consumption rate (OCR) by BEAS cells relative to baseline within 6 min. of exposure, with 25  $\mu$ M 1,2-NQ inducing an approximately 80 pmol/min elevation in OCR (an increase of approximately 100%). Blank wells without cells showed no change in OCR, ruling out reactivity between 1,2-NQ and media components or the oxygen-sensing fluorophore as a possible signal artifact (data not shown). An increase in OCR is typically associated with mitochondrial membrane uncoupling, yet 1,2-NQ-induced OCR was higher than that by the model uncoupler FCCP (2.4-fold for 50  $\mu$ M 1,2-NQ vs 1.2-fold for 0.25  $\mu$ M FCCP). Addition of complex-specific inhibitors in the sequence prescribed by the standard Cell Mito Stress Test (Agilent Technologies) showed decreased maximal respiration, unaffected ATP production, as well as a marked increase in spare respiratory capacity and non-mitochondrial respiration, in cells treated with 1,2-NQ (Figure 2-3).

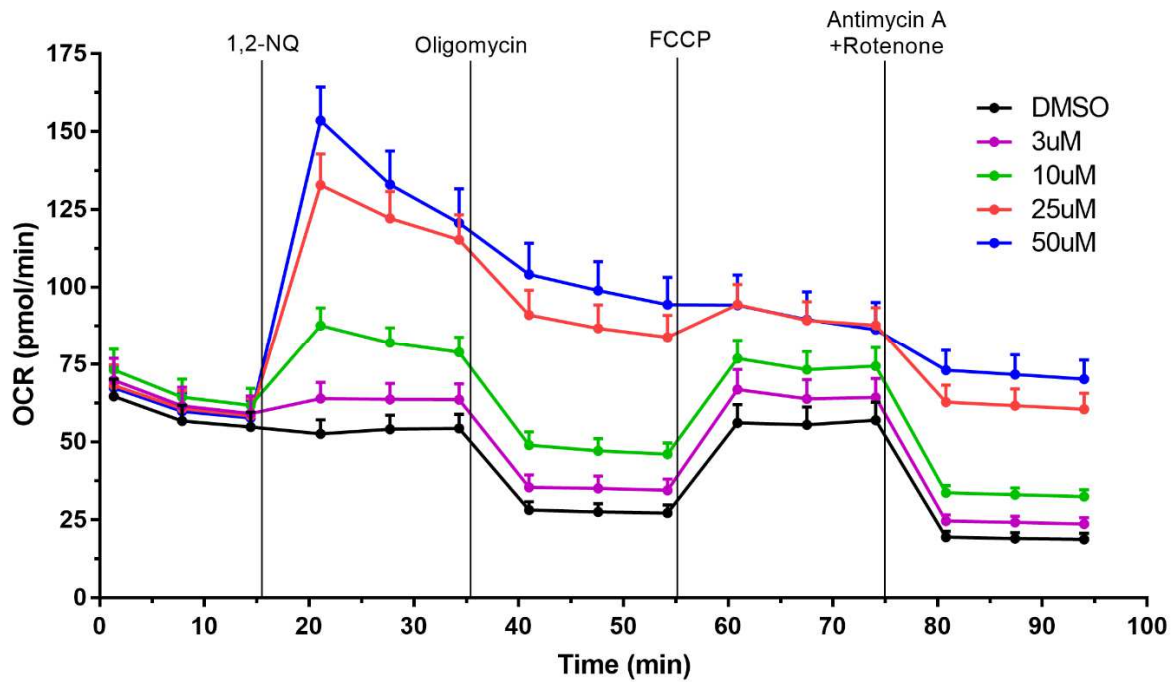


**Figure 2-2. 1,2-NQ increases basal Oxygen Consumption Rate (OCR, pmol/min).** (A) Bioenergetic effects of 1,2-NQ on BEAS cells were measured using the Cell Mito Stress Test on a XFe96 analyzer. An acute injection of 1,2-NQ was followed by additions of 1  $\mu$ M oligomycin, 0.25  $\mu$ M FCCP, and 1  $\mu$ M antimycin A and rotenone at the indicated times. Data displayed as mean  $\pm$  SEM,  $n \geq 10$ . One-sided error bars are used for clarity.

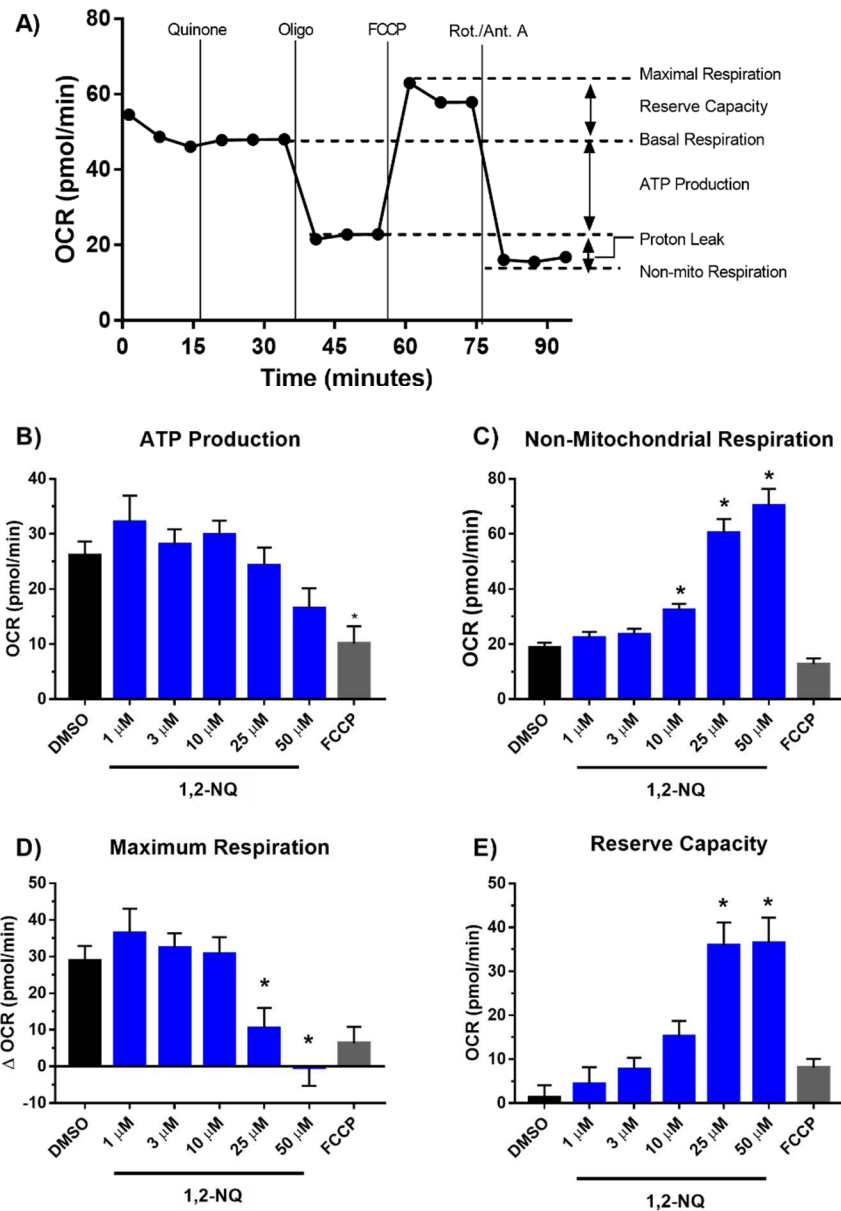


**Figure 2-3. 1,2-NQ alters bioenergetic parameters as measured by the Cell Mito Stress Test.** **A.** Seven different parameters can be tested by adding the following mitochondrial inhibitors in order as part of the Cell Mito Stress Test: (1) Oligomycin (Oligo), inhibits ATP Synthase, calculating the OCR attributed to ATP; (2) FCCP, a protonophore that dissipates the proton gradient across the inner mitochondrial membrane, forcing maximal mitochondrial respiration; (3) Rotenone (Rot.) and Antimycin A (Ant.A), inhibit Complex I and III, respectively, of the mitochondrial electron transport chain, leaving only non-mitochondrial OCR. BEAS cells were exposed to DMSO (vehicle), 1-50 μM 1,2-NQ, or 0.25 μM FCCP (positive control for uncoupling) as an acute injection prior to bioenergetic perturbation. **B.** ATP production was measured as the decrease in OCR after oligomycin addition. **C.** Non-mitochondrial respiration was measured as the minimum OCR after rotenone/antimycin A injection. **D.** Maximum respiration was measured as the increase in OCR after FCCP was added. **E.** Reserve capacity was calculated as the maximal respiration after quinone treatment minus the basal respiration. \* indicates significantly different from DMSO ( $p < 0.05$ ). Data shown as mean  $\pm$  SEM. For DMSO and 1,2-NQ,  $n \geq 7$ . For FCCP,  $n = 4$ .

### 1,2-NQ-Induced OCR is Not Dependent on Mitochondrial Respiration

Quinones (i.e., ubiquinone) play an essential physiological role in the mitochondrial electron transport chain by shuttling electrons in the inner membrane between Complexes I, II, and III. As a redox-active quinone, 1,2-NQ could possibly increase the basal OCR by enhancing the rate of electron transport in the inner membrane. To test this hypothesis, we pretreated BEAS cells with rotenone (Complex I inhibitor) and antimycin A (Complex III inhibitor) for 13 min. prior to the addition of 1,2-NQ. As shown in Figure 2-4, the 1,2-NQ (10-50  $\mu\text{M}$ )-induced dose-dependent rise in OCR was unaffected by pretreatment with these complex inhibitors. The efficacy of the rotenone and antimycin A pretreatment was demonstrated by the ablation of the OCR induced by the model uncoupler FCCP in cells not treated with 1,2-NQ. These findings suggested that a non-respirational process contributes significantly to the OCR

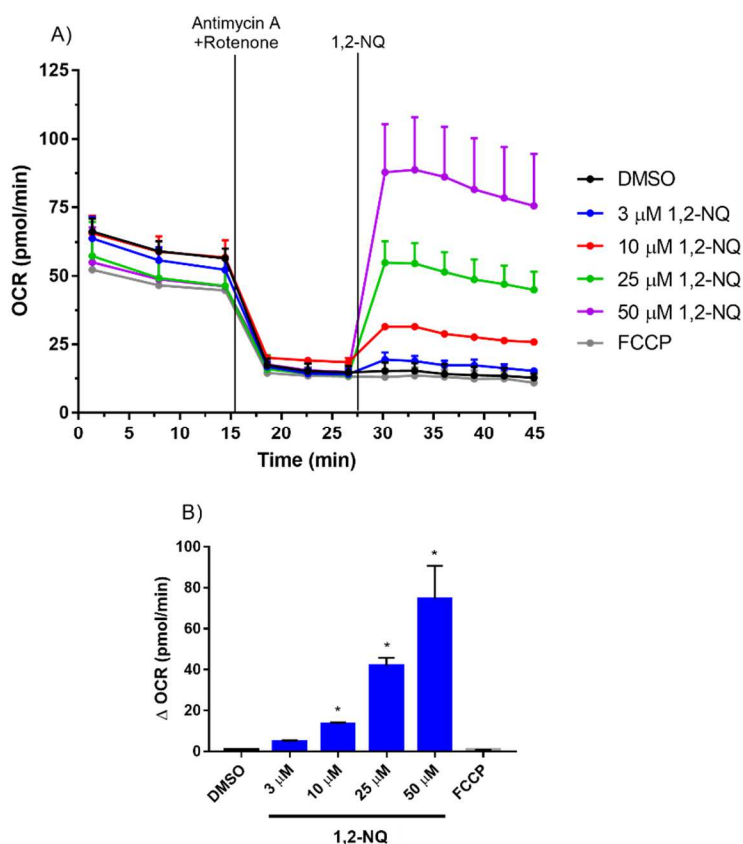


**Figure 2-4. 1,2-NQ-induced OCR increases are independent of mitochondrial electron transport.** **A.** BEAS cells were treated with 1  $\mu\text{M}$  antimycin A and 1  $\mu\text{M}$  rotenone for 13 min prior to addition of DMSO (vehicle), the indicated concentration of 1,2-NQ, or 0.25  $\mu\text{M}$  FCCP. **B.** The change in OCR after acute injection was calculated from rotenone/antimycin A-pretreated baseline, mean  $\pm$  SEM, n = 3, \* indicates significant difference from the pretreated baseline ( $p < 0.05$ ).

induced by exposure of BEAS cells to 1,2-NQ.

### ***Environmentally Relevant Redox Cycling Quinones Increase OCR in BEAS Cells***

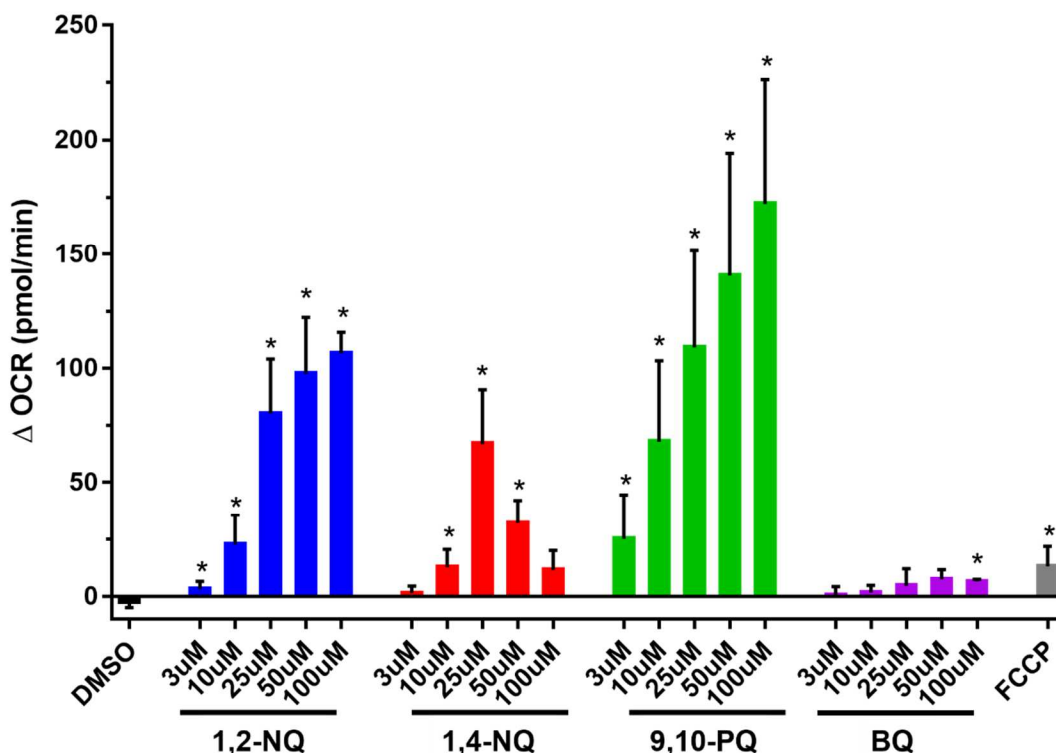
To examine the role of redox cycling in 1,2-NQ-induced increase in OCR, we next compared the effect of 1,2-NQ to that induced by three structurally distinct quinones that are also commonly found as contaminants of ambient air (Cho *et al.*, 2004). Like 1,2-NQ, 1,4-NQ is known to both redox cycle and adduct macromolecules within the cell. 9,10-PQ was examined as a quinone that is redox active but is not sufficiently electrophilic to participate in Michael addition. In contrast, BQ is potentially electrophilic but incapable of intracellular redox cycling (Kumagai *et al.*, 2012). As seen with 1,2-NQ, 9,10-PQ caused a dose-dependent increase in basal OCR, that exceeded that induced by FCCP by up to 15-fold (Figure 2-5). Similarly, 1,4-NQ also caused an increase in OCR that peaked at 25  $\mu$ M but decreased at higher doses. Following treatment with either 1,4-NQ or 9,10-PQ, cells were no longer responsive to mitochondrial inhibitors, suggesting inhibition of upstream metabolic processes (Figure 2-6). In marked contrast, treatment with BQ induced a comparatively small increase in OCR that was not dose-dependent and did not reach the level induced by FCCP (Figure 2-5). Unlike the cells treated with the redox active quinones, BEAS cells exposed to BQ remained responsive to the mitochondrial respiration inhibitors (Figure 2-6).

### ***1,2-NQ-induced Increase in OCR is NADPH-dependent***

The rate-limiting step in quinone redox cycling is the flavoenzyme-mediated one-electron reduction of the quinone to the semiquinone, a process that is dependent on NADPH as a source of electrons (Henry and Wallace, 1996; Figure 2-1). Thus, we determined whether 1,2-NQ-induced increases in OCR are influenced by intracellular NADPH levels. BEAS cells were deprived of glucose for two hours prior to assay, a treatment which we have previously shown depletes NADPH levels by approximately 65% (Gibbs-Flournoy *et al.*, 2013). Compared to control cells, the increase in OCR measured at 6 min following the addition of 25  $\mu$ M or 50  $\mu$ M 1,2-NQ was significantly blunted in glucose-deprived cells (Figure 2-7). For example, 25  $\mu$ M 1,2-NQ increased OCR by approximately 30 pmol/min (~50%) after a two-hour glucose starvation, compared to 80 pmol/min (100% increase) in presence of normal glucose. Similarly, glucose deprivation also diminished the increase in OCR in BEAS cells treated with 1,4-NQ or 9,10-PQ. In contrast, the OCR increase induced by FCCP was not affected by glucose

deprivation of the cells (Figure 2-7). To ensure that the blunted OCR after glucose starvation was not the result of cytotoxicity, cell viability was assessed. While exposure to the higher concentrations of 1,2-NQ and 1,4-NQ induced moderate loss of cell viability, we observed no significant differences between cell viability of glucose-deprived and glucose-sufficient BEAS cells (Figure 2-8).

To more definitively test if redox cycling of 1,2-NQ increased OCR, we attempted to inhibit flavoenzymes typically responsible for redox cycling using diphenyliodonium (DPI), a method suggested in previous reports (Dranka *et al.*, 2011). However, DPI inhibited mitochondrial function at low doses, as manifested by a low OCR that was no longer affected by rotenone treatment (Figure 2-15), rendering the experiment inconclusive. DPI had a minimal impact on the quinone-increased OCR at any dose of DPI



tested.

**Figure 2-5. Exposure to environmentally relevant redox-cycling quinones increases OCR.** BEAS cells were treated with DMSO (vehicle), the indicated concentrations of 1,2-NQ, 1,4-NQ, 9,10-PQ, BQ, or 0.25 μM FCCP following a baseline OCR collection period of 18 min on the extracellular flux analyzer. Shown is the change in OCR at 6 min of exposure relative to basal value. \* indicates the compound-induced OCR is significantly different from baseline OCR ( $p < 0.05$ ). For 1,2-NQ (3-50 μM),  $n \geq 11$ . For 1,4-NQ,  $n \geq 7$ . For 9,10-PQ (3-50 μM),  $n \geq 6$ . For 100 μM of all quinones,  $n = 3$ . For BQ,  $n = 3$ . For FCCP,  $n = 4$ . Data displayed as mean  $\pm$  SEM.

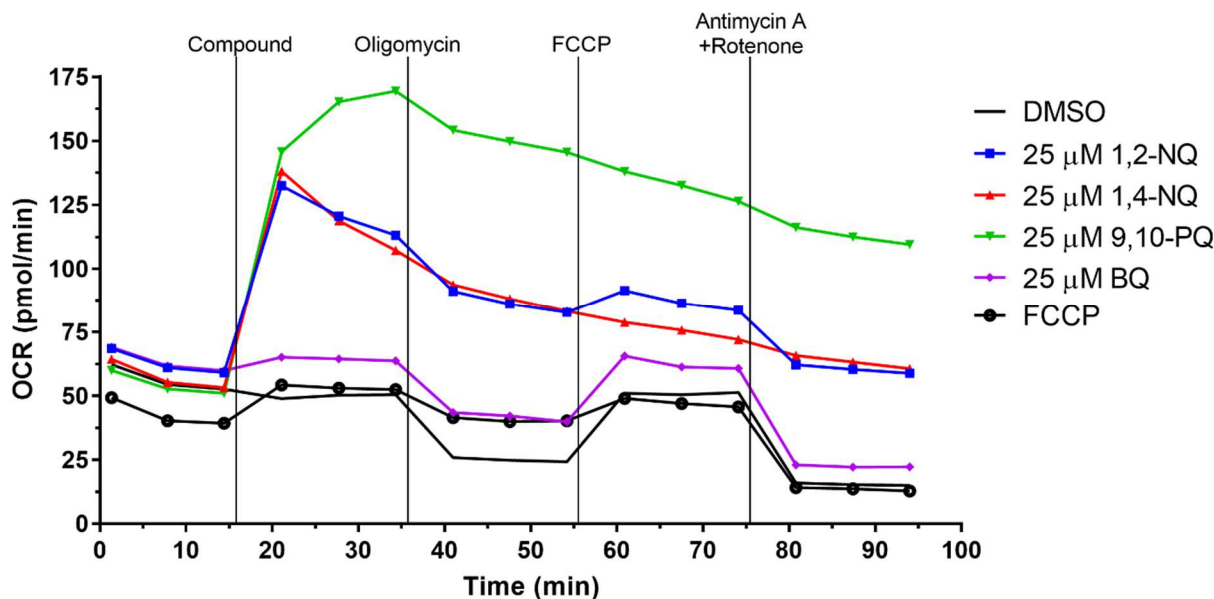
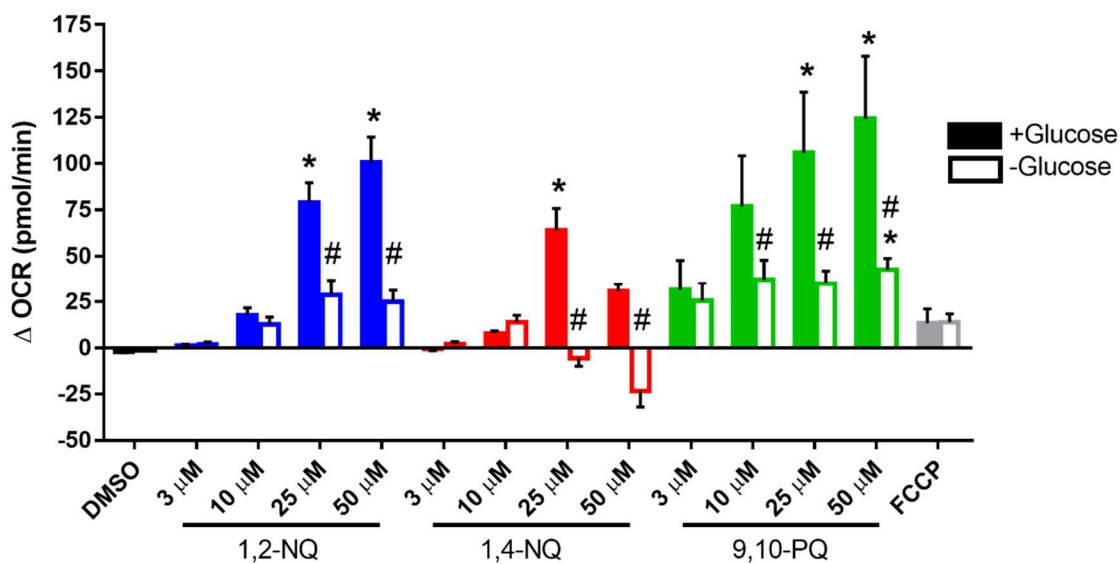


**Figure 2-6. Redox cycling quinones increase OCR and alter the bioenergetic profile in BEAS cells.** An acute injection of DMSO, 25 μM 1,2-NQ, 1,4-NQ, 9,10-PQ, or BQ was added and OCR was monitored using the Seahorse XFe96 analyzer. FCCP (0.25 μM) used as a positive control for uncoupling. The Cell Mito Stress Test was performed after the acute injection. Error bars were omitted for clarity. For DMSO,



1,2-NQ, n ≥ 7. For 1,4-NQ and 9,10-PQ, n = 6. For BQ, n = 3. For FCCP, n = 2.

**Figure 2-7 Exposure to environmentally relevant redox-cycling quinones increases OCR.** BEAS cells were treated with DMSO (vehicle), the indicated concentrations of 1,2-NQ, 1,4-NQ, 9,10-PQ, BQ, or 0.25 μM FCCP following a baseline OCR collection period of 18 min on the extracellular flux analyzer.

Shown is the change in OCR at 6 min of exposure relative to basal value. \* indicates the compound-induced OCR is significantly different from baseline OCR ( $p < 0.05$ ).  $n \geq 3$ , mean  $\pm$  SEM.

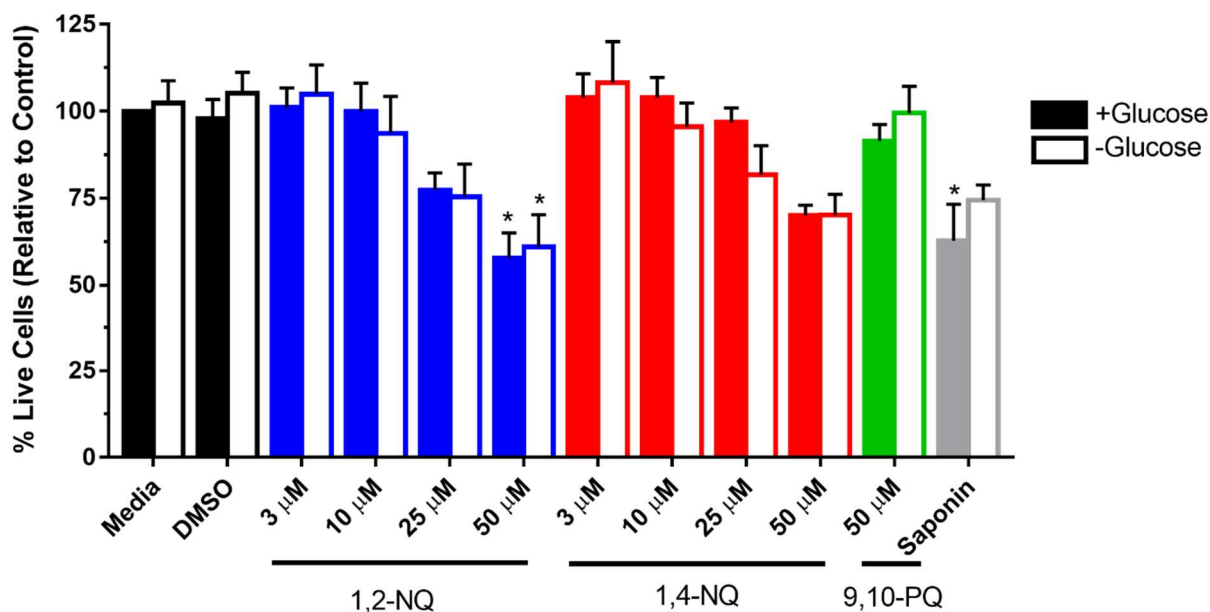


**Figure 2-8. Glucose starvation does not alter quinone-induced cytotoxicity.** BEAS cells were starved of glucose (open bars) or provided with 10 mM glucose (closed bars) 2 hours prior to start of assay. Cell viability was measured by retention of calcein AM with fluorescence measurement 6 min after exposure. The change in % viability is relative to media control. No significant difference was observed between glucose starved and supplemented cells. \* indicates the change in cell viability was significantly ( $p < 0.05$ ) different from media-treated controls. Data displayed as mean  $\pm$  SEM,  $n \geq 3$ .

### Redox-Cycling Quinones Increase $H_2O_2$ in BEAS cells

We hypothesized that the OCR increases induced in BEAS cells exposed to redox-cycling quinones is attributable to the conversion of dissolved oxygen in the media to reduced oxygen species that would not be detectable by the flux analyzer, leading to it being reported by the instrument as an increase in the rate of oxygen consumption. Superoxide produced during redox cycling is rapidly dismutated to  $H_2O_2$ , making its detection challenging during an acute exposure. We therefore measured  $H_2O_2$  levels in the medium of BEAS cells using Amplex Red after exposure to 3-25  $\mu$ M 1,2-NQ, 1,4-NQ, 9,10-PAQ or BQ. As we described previously for 1,2-NQ (Cheng *et al.*, 2012; Wages *et al.*, 2015), exposure to each of the three redox-active quinones resulted in dose-dependent increases in  $H_2O_2$  production. In contrast, 25  $\mu$ M BQ induced a comparatively modest increase in  $H_2O_2$  levels (Figure 2-9).

### 1,2-NQ-Induced OCR is Dependent on an Extra-Mitochondrial Process

To further identify the intracellular site of oxygen consumption, we tested the effect of 1,2-NQ on OCR in BEAS cells pretreated with the cholesterol-specific permeabilizing reagent perfringolysin (XF PMP) to permeabilize the cells and allow the intracellular compartment to equilibrate with the extracellular medium (Divakaruni *et al.*, 2013). Imaging analysis of BEAS cells expressing a mitochondrially-targeted fluorophore (roGFP) showed that the permeabilization procedure did not reduce the number of mitochondria present in the cells (Figure 2-10).

Relative to intact cells, permeabilized BEAS cells exposed to 10  $\mu$ M 50  $\mu$ M 1,2-NQ showed an increase in OCR that was significantly diminished in magnitude (Figure 2-11) yet a significant dose-dependent increase in OCR in permeabilized BEAS cells remained, suggesting that reductive activity is still present without the cytosol and could occur within another organelle, such as the mitochondria or the endoplasmic reticulum.

To specifically examine the contribution of mitochondria to the redox cycling of 1,2-NQ, we tested the effect of 1,2-NQ on OCR in mitochondria isolated by differential centrifugation of homogenates prepared from murine cardiac myocytes. Treatment of isolated mitochondria with 10 or 50  $\mu$ M 1,2-NQ did not significantly increase OCR, suggesting that mitochondria are not a major site of quinone metabolism contributing to redox cycling in BEAS cells (Figure 2-11).

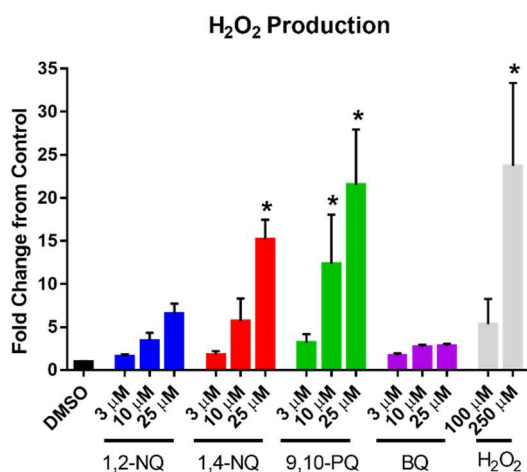


**Figure 2-9. Exposure to redox cycling quinones induces H<sub>2</sub>O<sub>2</sub> production.** BEAS cells were exposed to DMSO (vehicle) or the indicated concentrations of 1,2-NQ, 1,4-NQ, 9,10-PQ, BQ, or H<sub>2</sub>O<sub>2</sub> for 18 min. H<sub>2</sub>O<sub>2</sub> was measured in apical media as fluorescence at excitation  $\lambda$ = 545 nm, emission  $\lambda$ = 590 nm following a 30 min incubation in the presence of HRP and Amplex Red. n=3, mean +/- SEM.

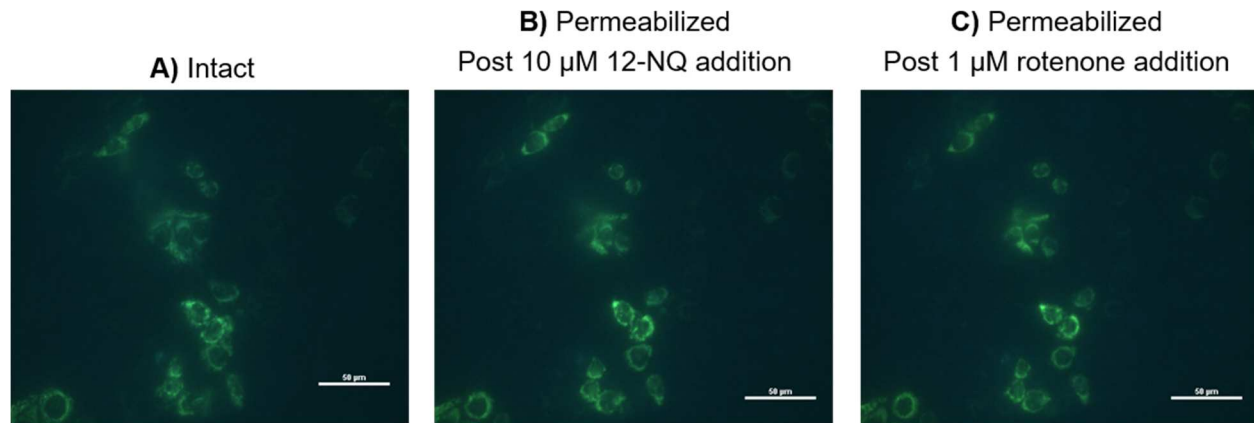
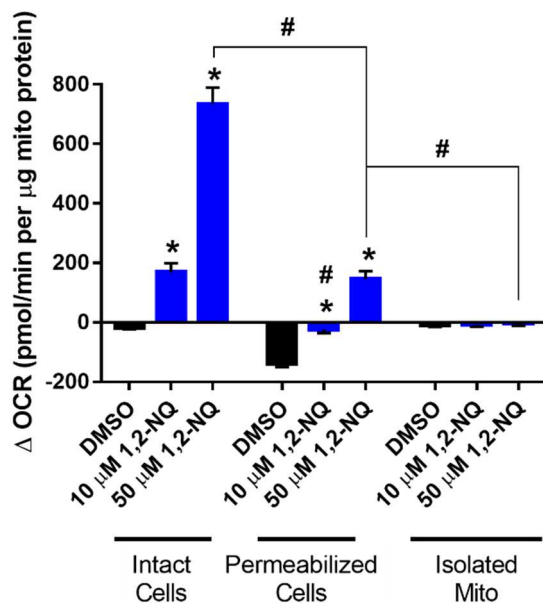


**Figure 2-10. Permeabilization by XF PMP leaves mitochondria intact.** BEAS cells expressing the redox potential sensor roGFP targeted to the mitochondria were imaged during a permeabilization procedure. A procedure similar to that done on the XFe96 was used. Media was changed to Mitochondrial Assay Solution and XF PMP at the beginning of the assay. Subsequent addition of substrates every 7.5 min to mimic XF assay was as follows: 1) 10  $\mu\text{M}$  1,2-NQ; 2) 10 mM pyruvate, 2 mM malate, 4 mM ADP; 3) 3.16  $\mu\text{M}$  oligomycin; 4) 1  $\mu\text{M}$  rotenone. Shown are co-localized displays of 515 nm emissions using 404 nm and 488 nm excitation wavelengths at time points: **A.** Immediately prior to permeabilization. **B.** 2.5 min after 10  $\mu\text{M}$  1,2-NQ addition, 10 min after permeabilization, **C.** 2.5 min after 1  $\mu\text{M}$  rotenone addition, 32.5 min after permeabilization. Images are representative of four independent



experiments.

**Figure 2-11. Mitochondrial preparations show a diminished 1,2-NQ-induced OCR increase.** All values shown as a change from basal OCR observed immediately after addition of DMSO or the indicated concentration of 1,2-NQ. All values were normalized to the mass of mitochondrial protein in each preparation. \* indicates the change in OCR was significantly ( $p < 0.05$ ) different from DMSO treatment within each preparation. # indicates the change in OCR was statistically different ( $p < 0.05$ )

between mitochondrial preparations. For intact cells,  $n \geq 11$ ; for permeabilized cells,  $n \geq 13$ ; for isolated mitochondria,  $n = 5$ . Data shown as mean  $\pm$  SEM.

### ***1,2-NQ Impairs Complex I-Linked Respiration***

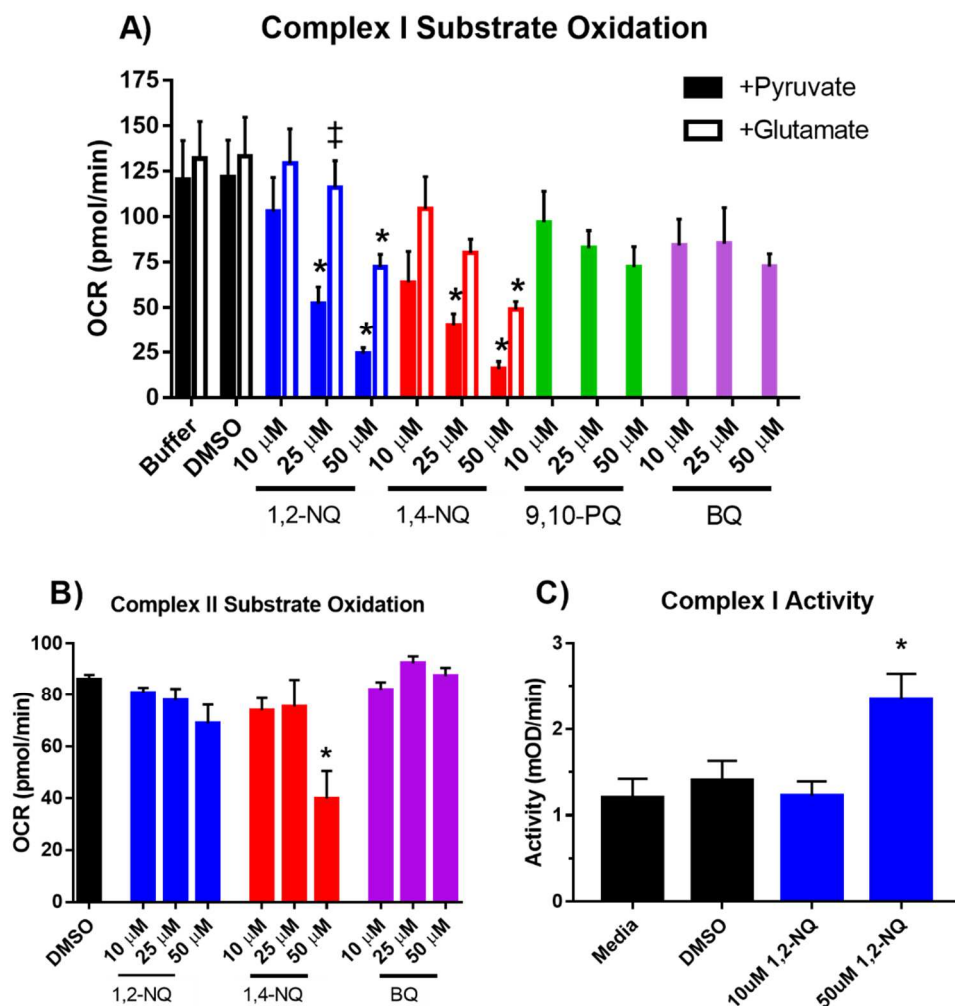
The preceding experiments strongly implicated extra-mitochondrial redox cycling as a major contributor to the large OCR induced in BEAS cells exposed to 1,2-NQ. However, the reduction in mitochondrial maximum respiration shown in Figure 2-3 suggested that 1,2-NQ may also impair mitochondrial respiratory function. We therefore next examined the effect of 1,2-NQ exposure on mitochondrial respiration in permeabilized BEAS cells unimpeded by redox cycling. Pyruvate, malate, and ADP were added as substrates to support respiration through Complex I. Exposure of permeabilized BEAS cells to 1,2-NQ for 10 min prior to substrate addition, resulted in a dose-dependent reduction in pyruvate-dependent respiration (Figure 2-12A) with exposure to 25  $\mu$ M 1,2-NQ resulting in an impairment of pyruvate-driven OCR by approximately 75 pmol/min (equivalent to a 60% decrease). While exposure to 1,4-NQ produced results similar to those induced by 1,2-NQ, pyruvate-driven respiration was not significantly impaired by exposure of permeabilized BEAS cells to either 9,10-PQ or BQ (Figure 2-12). Compared to the permeabilized cells, virtually the same result was obtained in isolated mitochondria exposed to 1,2-NQ (Figure 2-14B). Additionally, numerous protein adducts were detected by blotting with a 1,2-NQ-specific antibody, suggesting that 1,2-NQ binds to multiple mitochondrial proteins (Figure 2-14C). Substitution of glutamate for pyruvate in the medium as a Complex I-linked substrate partially rescued the 1,2-NQ-induced inhibition of OCR, suggesting that 1,2-NQ preferentially inhibits pyruvate-linked respiration (Figure 2-12A).

To further test whether 1,2-NQ inhibits downstream complexes in the electron transport chain, we used rotenone (Complex I inhibitor) and succinate (Complex II substrate) to bypass Complex I. As shown in Figure 7B, 1,2-NQ treatment did not affect Complex II-linked respiration using succinate as a substrate in permeabilized BEAS cells, suggesting no impairment of electron transport occurs downstream of Complex I and thus indicating that the functional loss occurs at or upstream of Complex I (Figure 2-12B).

### ***1,2-NQ Does Not Impair Complex I Activity***

Given the observed decrease in Complex I-linked substrate oxidation induced by 1,2-NQ, we next determined whether this was due to 1,2-NQ directly inhibiting Complex I activity. We assayed the effect of

1,2-NQ exposure on Complex I activity by measuring NADH oxidation by BEAS cell proteins immunocaptured with a mouse monoclonal antibody directed to bovine Complex I. As shown in Figure



2-12C, exposure of BEAS cells to 1,2-NQ did not inhibit Complex I activity, suggesting that 1,2-NQ-induced inhibition observed in permeabilized cells occurs upstream of Complex I.

**Figure 2-12. 1,2-NQ impairs Complex I-linked respiration in permeabilized cells.** **A.** BEAS cells were permeabilized with XF PMP and treated as indicated with buffer, DMSO, 1,2-NQ, 1,4-NQ, 9,10-PQ, BQ for 10 min, followed by an injection of 10 mM pyruvate/2 mM malate or 10 mM glutamate/10 mM malate, in a buffer containing 4 mM ADP, and mitochondrial respiration was measured as OCR. \* indicates activity was significantly ( $p < 0.05$ ) different from buffer control. # indicates a significant ( $p < 0.05$ ) difference between glutamate and pyruvate supplementation. For 1,2-NQ, 1,4-NQ, Buffer, and DMSO,  $n \geq 4$ . For 9,10-PQ and BQ,  $n \geq 3$ . **B.** Complex II-linked mitochondrial respiration measured by OCR after addition of 10 mM succinate/4 mM ADP/2 µM rotenone. BEAS cells were permeabilized with XF PMP and treated as indicated with DMSO, 1,2-NQ, 1,4-NQ, 9,10-PQ, BQ for 10 min, and substrate oxidation was measured as OCR. \* indicates activity was significantly ( $p < 0.05$ ) different from buffer control. For DMSO and 1,2-NQ,  $n$

= 4. For 1,4-NQ and BQ, n = 3. **C.** BEAS cells were treated with 10  $\mu\text{M}$  or 50  $\mu\text{M}$  1,2-NQ for 15 min and Complex I activity was assayed as the NADH-dependent reduction of a chromophore over 30 min. indicates activity was significantly ( $p < 0.05$ ) different from media control, n = 3. Data shown as mean  $\pm$  SEM.

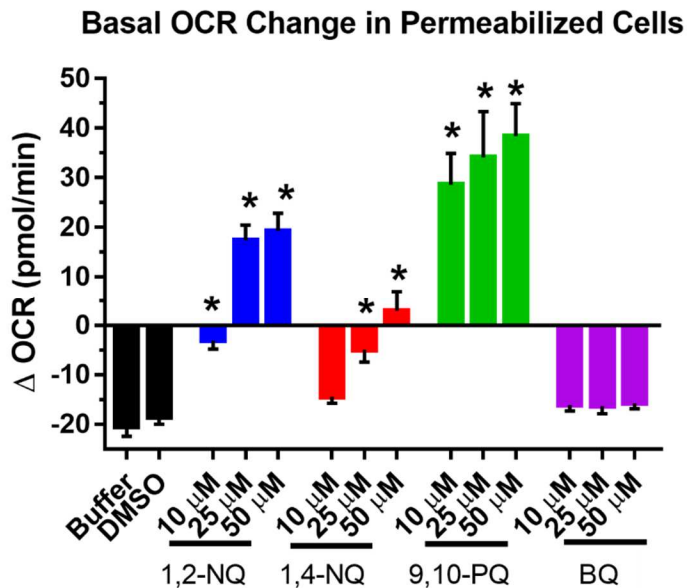


**Figure 2-13. Redox cycling quinones increase OCR in permeabilized cells.** BEAS cells were permeabilized with XF PMP and assayed in Mitochondrial Assay Solution (Buffer). An acute injection of buffer, DMSO, or indicated concentration of 1,2-NQ, 1,4-NQ, 9,10-PQ, or BQ was added after 7.5 min of basal OCR collection. The OCR change induced in 2.5 min of exposure to the acute injection without the presence of mitochondrial substrates is shown here. \* indicates the change in OCR was significantly ( $p < 0.05$ ) different from DMSO-treated controls. Data shown are mean  $\pm$  SEM. For DMSO and 1,2-NQ, n  $\geq$  13. For 1,4-NQ, n  $\geq$  11. For 9,10-PQ n  $\geq$  6. For BQ, n = 8.

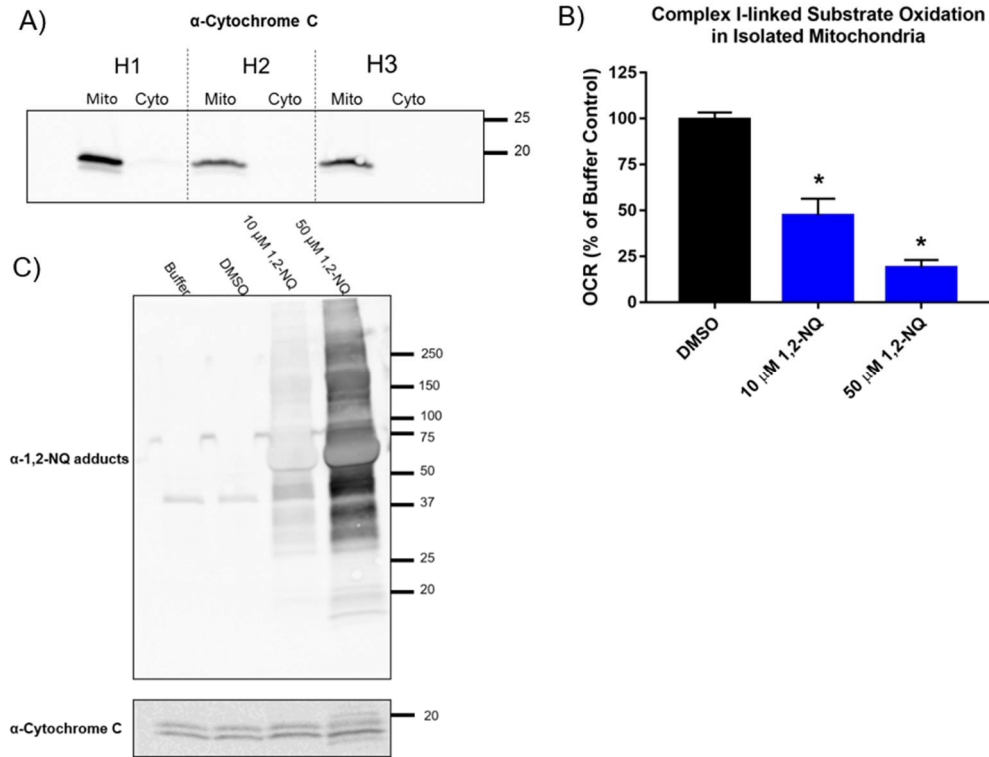


**Figure 2-14. 1,2-NQ decreases pyruvate-driven substrate oxidation in isolated mitochondria.**

Mitochondria were isolated from murine heart ventricles. **A.** Mitochondrial (Mito) and cytosolic (Cyto) fractions were analyzed for enrichment by Western Blotting. Approximately three  $\mu\text{g}$  of total protein was loaded per well. Three independent heart replicates (H1, H2, H3) are displayed. Samples were probed using the primary antibody rabbit anti-Cytochrome C (Cell Signaling Technologies, 1:1000) and anti-rabbit HRP secondary antibody (Cell Signaling Technologies, 1:1000). **B.** Isolated mitochondria were run on a Seahorse XFe24 analyzer and treated with buffer, DMSO, 10  $\mu\text{M}$  or 50  $\mu\text{M}$  1,2-NQ for 10 min. Subsequently, 10 mM pyruvate, 2 mM malate and 4 mM ADP were injected, and substrate oxidation was measured as OCR, relative to the buffer control. Data shown as mean  $\pm$  SEM, n=5. **C.** After assay, protein was lysed and analyzed via Western Blotting for 1,2-NQ adducts using a custom made polyclonal antibody. Samples were probed using the unpurified rabbit serum (ThermoFisher Scientific, 1: 10,000) and subsequent anti-rabbit HRP secondary antibody (Cell Signaling Technologies, 1:1000). Approximately three  $\mu\text{g}$  of total protein was loaded per well. Samples were probed for cytochrome C, as described above, for a loading control.

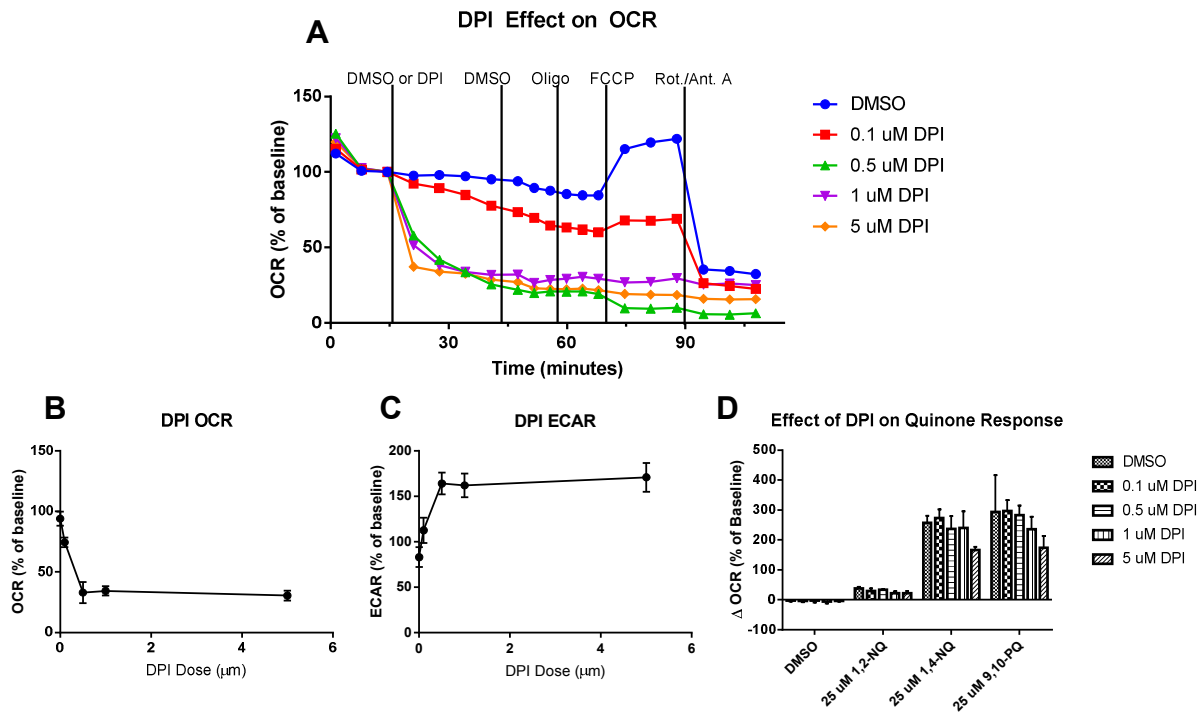


**Figure 2-15. DPI decreases basal OCR within 30 min. of exposure.** BEAS-2B were exposed to increasing doses of DPI (0 – 5  $\mu\text{M}$ ) for 30 min. prior to the Cell Mito Stress Test. OCR and ECAR was measured on the Seahorse XFe Analyzer. (A) OCR time course during DPI exposure. OCR (B) and ECAR (C) are shown after 30 min. of DPI exposure. After DPI exposure, an injection of DMSO, 25  $\mu\text{M}$  1,2-NQ, 25  $\mu\text{M}$  1,4-NQ, or 25  $\mu\text{M}$  9,10-PQ was made. (D) The change in OCR from the measurement immediately prior to quinone injection is shown. OCR and ECAR on all graphs was normalized as a percentage of the baseline OCR/ECAR. Shown as mean  $\pm$  SD, n=1.

## Discussion

In the present study, we utilized extracellular flux analysis to characterize the effect of environmentally relevant doses of 1,2-NQ exposure on mitochondrial function in human airway epithelial cells. We report that 1,2-NQ induces a large, dose-dependent increase in BEAS cell OCR that masks a frank impairment in mitochondrial respiration.

While initial observations suggested that 1,2-NQ could be a mitochondrial uncoupler, further study revealed that the increase in OCR induced by 1,2-NQ is primarily attributable to a non-mitochondrial NADPH-dependent redox-cycling process. This is supported by multiple lines of evidence. First, the magnitude of the 1,2-NQ-induced increase in OCR exceeded that produced by the model mitochondrial uncoupler FCCP. Second, inhibition of the electron transport chain with mitochondrial respiration inhibitors rotenone and antimycin A did not prevent 1,2-NQ-induced OCR increases. Third, only exposure to quinones with redox cycling potential produced elevations in OCR and H<sub>2</sub>O<sub>2</sub> production. Fourth, prior depletion of levels of NADPH, a cofactor required to support redox-cycling (Cohen and Doherty, 1987), significantly blunted 1,2-NQ-induced OCR increases. Given that the degradation of H<sub>2</sub>O<sub>2</sub> produced by the dismutation of O<sub>2</sub><sup>•-</sup> generates O<sub>2</sub>, the data in this study may underrepresent the true magnitude of the OCR increase induced by 1,2-NQ exposure.

Despite the masking effect of redox cycling, in this study we elucidate a novel mechanism of mitochondrial inhibition by 1,2-NQ. Our data show that that 1,2-NQ exposure impaired mitochondrial respiration through a mechanism that is dependent on oxidation of pyruvate and to a lesser extent, glutamate, two substrates that feed electrons to Complex I, in a dose-dependent manner. When succinate (Complex II substrate) was provided, mitochondrial respiration was not affected by 1,2-NQ exposure, suggesting that the electron transport chain was intact downstream of Complex I. That the enzymatic activity of Complex I itself was not inhibited by 1,2-NQ, leads us to conclude that 1,2-NQ inhibits upstream pyruvate transporters or Krebs's cycle enzymes (Brand and Nicholls, 2011). We have detected 1,2-NQ adducts in mitochondrial proteins (Figure 2-14C), indicating that 1,2-NQ adducts mitochondrial targets. However, since neither 9,10-PQ nor BQ caused inhibition in pyruvate-driven mitochondrial respiration, we are unable to infer the extent to which quinone-induced effects are mediated by ROS generation or by electrophilic adduction. An inherent limitation of comparing the effects of

different quinones is that they may vary in solubility and not compartmentalize similarly. Nonetheless, given the electrophilicity of 1,2-NQ, it is possible to speculate that key substrate transporters or dehydrogenases are attacked by 1,2-NQ. Additionally, we cannot exclude the possibility that H<sub>2</sub>O<sub>2</sub> produced extra-mitochondrially damages mitochondria, leading to the observed mitochondrial inhibition and further H<sub>2</sub>O<sub>2</sub> production. However, the lack of an inhibition of substrate oxidation by exposure to 9,10-PQ, a more potent redox cyler than 1,2-NQ, mediated, suggests that this is not a likely to be a major contribution. An unavoidable limitation of our study is that the assays to measure activity of specific electron transport Complexes require a disrupted cell preparation. Further investigation using novel methodological approaches is needed to identify potential sites of substrate oxidation inhibition by 1,2-NQ and determine the likelihood of it occurring in intact cells.

Inhibition of mitochondrial substrate oxidation could disrupt cellular ATP production and increase H<sub>2</sub>O<sub>2</sub> production. Though Complexes I and III are the most well-known, there are at least ten different sites of superoxide/H<sub>2</sub>O<sub>2</sub> generation in mitochondria, including upstream substrate oxidation processes (Quinlan *et al.*, 2013). Increased H<sub>2</sub>O<sub>2</sub> and resulting oxidative stress can induce downstream inflammatory responses, as we previously observed (Cheng *et al.*, 2012).

The intracellular localization of redox cycling by quinones in human airway epithelial cells has not been identified. A number of different flavin-containing enzymes are capable of 1-electron quinone reduction, including cytochrome P450 reductases located in the endoplasmic reticulum and NADH:ubiquinone oxidoreductase (Complex I) in the mitochondrion. It has previously been suggested that quinone redox cycling is preferentially compartmentalized within mitochondria, leading to permeabilization of the inner mitochondrial membrane and disrupting calcium homeostasis in hepatocytes (Henry and Wallace, 1996). Hydrophilic quinones have also been found to redox cycle at a rotenone-insensitive allosteric site in Complex I (King *et al.*, 2009). Furthermore, we have previously reported that 1,2-NQ-induced H<sub>2</sub>O<sub>2</sub> production was of mitochondrial origin (Cheng *et al.*, 2012). In contrast, the data presented herein support an extra-mitochondrial site for 1,2-NQ redox cycling leading to H<sub>2</sub>O<sub>2</sub> production. The ineffectiveness of electron transport chain inhibition in blunting the 1,2-NQ-induced OCR increase, combined with the diminished magnitude of the OCR in isolated mitochondria, further suggest that the mitochondrion plays a relatively minor role in the 1,2-NQ-induced OCR in BEAS cells.

. Reductases bound to the endoplasmic reticulum and possibly other cytosolic enzymes are likely key players in quinone redox cycling. Sepiapterin reductase is a cytosolic NADPH-dependent enzyme found to readily reduce 1,2-NQ in murine lung epithelial cells and could also be responsible for mediating 1,2-NQ redox cycling in human airway epithelial cells (Yang *et al.*, 2013).

To our knowledge, this is the first application of extracellular flux technology to elucidate the bioenergetic effects of ambient air pollution in human airway epithelial cells. Technological innovations in cellular metabolism have increased accessibility and standardized approaches to measure mitochondrial function (Ferrick *et al.*, 2008; Pelletier *et al.*, 2014). Extracellular flux technology can advance our understanding of the role of bioenergetic processes as both targets of environmental agents and mediators of response, and has the potential to revolutionize screening for mitochondrial toxicity. While the technology is rapidly gaining in popularity, this report shows the need for caution when interpreting extracellular flux findings in toxicologic research. A decrease in OCR is not the only indicator of mitochondrial toxicity. On the other hand, as demonstrated in this study, an increase in OCR may not always indicate an uncoupling effect. It is important to consider alternative pathways that consume oxygen, including redox cycling and the activities of xanthine oxidase, NADPH oxidase and cytochrome p450 oxidase.

By consuming oxygen, redox-active compounds can induce OCR, confounding changes in respiration and bioenergetics when using extracellular flux analysis. Organic and inorganic redox cycling compounds of toxicological concern include paraquat, menadione, doxorubicin and transition metals. Use of the NADPH oxidoreductase inhibitor diphenyleneiodonium (DPI) has been recommended as an adequate control for redox cycling to measure bioenergetic function using extracellular flux analysis (Dranka *et al.*, 2010; Dranka *et al.*, 2011). However, we found that DPI and other pharmacologic redox cycling interventions (e.g., dicoumarol) inhibit mitochondrial respiration at doses lower than those required to suppress 1,2-NQ-induced redox cycling (Figure 2-15, data not shown). As demonstrated in this study, the use of a permeabilized cell system allows examination of the contribution of mitochondrial and extra-mitochondrial processes to OCR changes induced by redox-active compounds. In spite of these limitations, extracellular flux technology can be used as a powerful tool to measure O<sub>2</sub> consumption and bioenergetic effects in cells exposed to redox-active compounds. The burden is therefore on the

investigator to be aware of the limitations and devise appropriate experimental strategies to address them in order to better interpret findings for toxicological research applications.

The environmental relevance of the concentrations of 1,2-NQ used in this study are based on our previously published calculations modelling a plausible *in vivo* exposure (Cheng *et al.*, 2012). Briefly, a realistic 3 hr inhalational exposure to diesel exhaust (e.g., at a bus depot) could result in human airway epithelial cells experiencing concentrations of 1,2-NQ between 0.6 and 6  $\mu\text{M}$ , comparable to the levels that showed clear effects in this study. Moreover, ambient air pollution contains a varied mixture of redox-active components that includes multiple quinone species and precursors to which *in vivo* airway epithelial cells are exposed simultaneously (Mastral and Callen, 2000; Alves *et al.*, 2015). For example, naphthalene, the most prevalent and abundant polycyclic aromatic hydrocarbon in the air is rapidly converted in airway cells to 1,2-NQ through cytochrome p450 oxidation (Zheng *et al.*, 1997; Lanza *et al.*, 1999), and thus represents an additional source of exposure to 1,2-NQ and the accompanying oxidative burden on the cells. Additional dose modeling is needed to gain a more accurate concentration of the total quinone burden experienced by airway epithelial cells during PM exposure.

### **Summary**

The data presented here suggest that 1,2-NQ induces  $\text{H}_2\text{O}_2$  production in human airway epithelial cells through extra-mitochondrial redox cycling, though mitochondrial impairment also contributes to the oxidative stress induced by quinone exposure. This indicates that an organic PM component can have significant oxidative effects in human airway epithelial cells and is a potential initiating mechanism leading to downstream adverse effects. This study also highlights the strengths and limitations of extracellular flux technology for investigating the bioenergetics effects of environmental agents.

## CHAPTER 3: CHARACTERIZING THE BIOENERGETIC PROFILE OF HUMAN LUNG MACROPHAGES FROM HEALTHY VOLUNTEERS<sup>2</sup>

### Introduction

Resident lung macrophages (MAC) are found throughout the respiratory tract and are a key part of the innate immune defense to inhaled biological and xenobiotic agents. Altered MAC function is associated with numerous respiratory diseases, including chronic obstructive pulmonary disease (COPD), asthma, and cystic fibrosis (Hiemstra, 2013; Belchamber and Donnelly, 2017). Functionally, MAC clear pathogens and debris through phagocytic processing and produce a repertoire of cytokines, chemokines, reactive oxygen species, and proteases that are vital to their function in host defense (Laskin *et al.*, 2011).

The bioenergetic activity of immune cells, including monocyte-derived MAC, has been reported to be a key determinant of their response to pathogenic challenges. Metabolic dysfunction of respiratory immune cells is thought to be involved in the initiation or progression of a number of inflammatory airway diseases, including COPD and asthma, where mitochondrial respiration is either reduced or dysfunctional (Mabalirajan *et al.*, 2008; Wiegman *et al.*, 2015; Yoon *et al.*, 2016).

Recently, metabolic reprogramming has been identified as a critical factor in committing innate immune cells toward a pro- or anti-inflammatory phenotype following exposure to an appropriate stimulus (O'Neill *et al.*, 2016). For example, MAC derived from rodent bone marrow monocytes (BMDM) or human peripheral blood monocytes (PBMC) stimulated with lipopolysaccharide (LPS) and/or interferon  $\gamma$  induce a M1 pro-inflammatory phenotype that is more reliant on glycolysis than mitochondrial respiration for ATP production. This shift is caused by a reduction in Krebs cycle production of NADH, as the metabolic intermediates succinate and citrate are utilized for non-energy functions, such as membrane biogenesis and HIF1 $\alpha$  activation, respectively. In contrast, alternatively activated M2 MAC have an anti-inflammatory

---

<sup>2</sup> This chapter has been submitted for publication in April 2018. Lavrich, K.S., Speen, A.M., Ghio, A.J., Bromberg, P.A., Samet, J.M., Alexis, N.E. (2018). *Characterizing the Bioenergetic Profiles of Human Lung Macrophages from Healthy Volunteers*.

phenotype and primarily use oxidative phosphorylation for ATP generation (Tannahill *et al.*, 2013; Galván-Peña and O'Neill, 2014; Jha *et al.*, 2015; Van den Bossche *et al.*, 2015). Although the M1/M2 classification involves both phenotype and functional criteria, energy metabolism plays an important role in mediating the plasticity that MAC display following activation (Xue *et al.*, 2014). Much of the pioneering immunometabolism work on MAC has utilized rodent BMDM or human PBMC. Relatively little is known about the *in vivo* bioenergetic profiles of lung MAC acquired from human volunteers.

Previous work by our group demonstrated that innate immune cells recovered from induced sputum (IS), a technique that samples the surfaces of large central airways, were phenotypically (CD11b, HLA-DR, CD64) and functionally (phagocytosis, intracellular oxidative burst) more active and pro-inflammatory than innate immune cells recovered from distal alveolar airways using bronchoalveolar lavage (BAL) (Alexis *et al.*, 2000). These findings suggest that the bioenergetic profiles of these two cell populations may also differ from each other, leading us to hypothesize that cells derived from IS are more glycolytic and less reliant on mitochondrial respiration as their primary bioenergetic process for ATP production relative to BAL MAC.

In the present study, we utilized BAL, the first aliquot of BAL (bronchial fraction, BF), or IS to recover MAC from the distal alveolar, bronchial and central airways surfaces of the respiratory tract, respectively, of healthy volunteers. The recovered MAC were subjected *ex vivo* to extracellular flux analyses to characterize their bioenergetic profile at baseline and following xenobiotic challenge. We report that MAC obtained by IS are highly dependent on glycolysis for their energy needs, while BAL MAC primarily rely on mitochondrial respiration for energy production. Notably, despite mounting a robust inflammatory response, BAL or IS MAC stimulated with LPS did not produce the expected shift in metabolic profile as previously reported for BMDM (Tannahill *et al.*, 2013; Palsson-McDermott *et al.*, 2015), revealing a potentially novel *in vivo* phenotype wherein the disposition of the MAC toward an inflammatory response appears uncoupled from the bioenergetic profile.

## **Methods**

### ***Materials***

All chemicals were purchased from Sigma-Aldrich (St. Louis, MO, USA), unless otherwise noted. XF Base Medium and XF FluxPaks, were purchased from Agilent Technologies (Santa Clara, CA, USA).

L-glutamine (Gibco), the BCA Protein Assay Kit, RPMI Medium 1640 (Gibco, with L-glutamine, phenol red), fetal bovine serum (FBS, Gibco), Penicillin-Streptomycin (Pen-Strep, Gibco), and Gentamicin (Gent, Gibco) was purchased from ThermoFisher Scientific (Waltham, MA, USA). Basic laboratory supplies were purchased from Fisher Scientific (Raleigh, NC, USA).

### ***Subject Participants***

The study protocol was approved by the Institutional Review Board at the University of North Carolina Medical School in Chapel Hill and the US Environmental Protection Agency (EPA). Informed consent was obtained from all subjects before their participation in the study. All subjects underwent a physical examination prior to participation. For induced sputum, 12 healthy, non-smoking volunteers participated in this study ranging from age 23 to 60. Three subjects provided multiple IS samples, procedures separated by over 6 weeks, giving a total of 16 independent cell collections. Separately, 25 nonsmoking healthy volunteers between 20 and 37 years of age were recruited for bronchoscopy. Of those that underwent bronchoscopy, the BF was utilized from 17 subjects, based on cell yield. Subject characteristics are shown in Table 3-1.

### ***Induced Sputum Collection***

Sputum was collected as described previously (Alexis *et al.*, 2009). Briefly, subjects underwent three 7-min. inhalation periods of nebulized hypertonic saline (3, 4, and 5%; UltraNeb 99 ultrasonic nebulizer; DeVilbiss, Jackson, TN), followed by expectoration of sputum into a sterile specimen cup. Cell-rich mucus plugs were selected and incubated in dilute 0.1% dithiothreitol (Sputolysin; Calbiochem, San Diego, CA) in Dulbecco's PBS. The sample was then washed in Dulbecco's PBS and gravity filtered through a 48- $\mu$ m pore mesh filter.

### ***Bronchoalveolar Lavage***

Bronchoalveolar lavage was performed by a board certified pulmonologist, as described previously (Ghio and Devlin, 2001). A fiberoptic bronchoscope was wedged into a segmental bronchus of the lingual. One 20 mL aliquot and five 50 mL aliquots of sterile saline were sequentially instilled and immediately aspirated. Samples were put on ice immediately following aspiration and pelleted by centrifugation at 300 g for 10 min., 4°C. BF was classified as the first 20 mL aliquot. Cells from the

remaining 5 washes were pooled and classified as BAL. Cells were washed once in RPMI (+0.25% gentamicin).

For matched BAL and peripheral blood mononuclear cell comparisons, whole blood was drawn from an antecubital site prior to bronchoscopy. Purified blood mononuclear cells (PBMCs) were purified using BD Vacutainer® CPT™ Cell Preparation Tube with Sodium Heparin according to manufacturer's instructions.

Subject Characteristics			
	BAL	BF	IS
Age (years)	27 (20-37)	26 (20-37)	29 (23-60)
BMI (kg/m <sup>2</sup> )	28.3 (19.7-36.9)	28.1 (19.7-36.9)	29.8 (18.8-44.8)
Sex			
Female	10	9	5
Male	15	8	6
Race			
Black	12	7	3
White	11	9	8
Hispanic	1	0	0
Bi-Racial	1	1	0

**Table 3-1. Characteristics of healthy subjects who underwent bronchoscopy (BAL, BF) or induced sputum (IS).** Shown as mean (range). Of note, BF donors represent a subset of bronchoscopy subjects. Some IS donors provided multiple samples over the course of the study.

Sample Type	% PMN	% Mac	% Eos	% Lym	%Bec
IS	31.3 (8.3-68)	68.3 (30.9-92)	0.2 (0-2.6)	0 (0-0)	0.06 (0-0.7)
BAL	2.9 (0-8)	96.8 (91.2-100)	0.17 (0-1)	0.08 (0-1)	0.05 (0-0.85)
BF*	12.33 (6-17)	84.0 (80-88)	0 (0-0)	0 (0-0)	3.67 (2-6)

**Table 3-2. Differential Cell Count Percentages.** Shown as Mean (Range). For Sputum, n=15; BAL, n=20. Eos (Eosinophils), Lym (lymphocytes), Bec (bronchial epithelial cells). \*For BF samples, differentials were conducted on separate samples (n=3) from those run in experimental procedures due limited sample size.

### **Cell Differentials**

Cell samples were counted and their viability was determined by Trypan blue exclusion, as previously described (Alexis *et al.*, 2006). Samples were cytocentrifuged onto slides and stained (Hema-Stain-3; Fisher Scientific, Hampton, NH). At least 500 cells per slide were counted. Results of cell differentials are shown in Table 2. BF cell differentials were not performed on the samples used for this study. Additional BF samples were collected in healthy individuals to provide representative differentials as shown in Table 3-2.

### **Bioenergetic Analyses**

Cellular oxygen consumption rate (OCR) and extracellular acidification rate (ECAR) were measured using the Seahorse XFe24 Analyzer (Agilent Technologies, Santa Clara, CA, USA) (Gerencser *et al.*, 2009). With the exception of 24-hr challenges, all samples were assayed the day of collection. Bioenergetic parameters were calculated using a modified Cell Mitochondrial (Mito) Stress Test (Van den Bossche *et al.*, 2015). Briefly, measurements were made after addition of glucose to stimulate glycolysis, followed by sequential addition of oligomycin to block ATP synthase (Complex V), carbonyl cyanide-pentriylfluoromethoxyphenylhydrazone (FCCP) to stimulate maximal mitochondrial oxygen consumption, and rotenone/antimycin A to inhibit electron transport through Complexes I and III.

XFe24 sensor cartridges were hydrated for at least 4 hr with XF Calibrant at 37°C. Cells were seeded at 60,000 cells per well in XF24 cell culture plates. For BF and BAL cells, media was changed from RPMI to assay media prior to cell seeding. Sputum cells were plated in isotonic saline and replaced with assay media immediately prior to assay. Cells were allowed to settle for approximately 40 min prior to assay in a non-CO<sub>2</sub> incubator at 37°C. After attachment, Assay media was either XF Glycolysis media (XF Base Media supplemented with only 2 mM glutamine) or XF Cell Mito Assay Media (XF Base Media with 10 mM glucose, 1 mM sodium pyruvate, and 2 mM glutamine). Both media were prepared fresh on the day of assay and adjusted to pH 7.4. For 24-hr challenges, media was changed from RPMI to XF Cell Mito Assay Media one hr prior to assay to allow proper degassing. Basal OCR and ECAR were recorded in the presence of 10 mM glucose, 2 mM glutamine, and sometimes 1 mM sodium pyruvate, though the presence of sodium pyruvate did not affect basal OCR or ECAR in our samples (data not shown). Sequential mix-wait-measurement times were set at 3 min-2 min-3 min.

### **Modified Cell Mito Stress Test**

Bioenergetic parameters were calculated using a modified Cell Mito Stress Test (Van den Bossche *et al.*, 2015). This assay tests nine different parameters of glycolytic and mitochondrial function using injection of specific bioenergetic modulators. The first injection of glucose allows measurement of glycolysis using the ECAR, as the glucose-deficient cells process the glucose and produce lactate, acidifying the media. Oligomycin, an ATP Synthase inhibitor, is the second injection allowing calculation of glycolytic capacity using ECAR, glycolysis must now be used exclusively for ATP production. Additionally, the OCR linked to ATP production and proton leak of the inner mitochondrial membrane can be determined. Next, the protonophore FCCP is injected, which collapses the proton gradient and allows measurement of the maximal rate of respiration and spare respiratory capacity using the OCR. The last injection is rotenone and antimycin A, Complex I and III inhibitors respectively, which shut off mitochondrial electron transport, and provide the OCR linked to non-mitochondrial respiration processes.

Stock concentrations of oligomycin, FCCP, rotenone, and antimycin A were prepared in DMSO and stored at -20°C. Working solutions were diluted in cell media with final DMSO concentrations less than 0.1%. Stock concentrations of glucose were prepared in XF Glycolysis media and stored at -20°C. Injections were ordered as follows: A) 10 mM glucose B) 1 uM oligomycin C) 1 uM FCCP D) 0.5 uM rotenone, 0.5 uM antimycin A. For bioenergetics parameter calculations, all measurements were normalized as a percentage of the basal OCR and ECAR. Mitochondrial and glycolytic parameters were calculated as recommended by the instrument manufacturer (Agilent Technologies).

### **LPS Challenge**

A stock of lipopolysaccharide (LPS; 1 mg/mL) was made in PBS and stored at -80°C. Airway macrophages were exposed to a final concentration of 50 or 100 ng/mL LPS for either 6 or 24 hours, after which media was collected for cytokine analysis. For experiments with a 6-hr exposure, the stimulus was the first injection after 3 baseline measurements were collected. Measurements were performed every 8 min. thereafter for 4 hrs, prior to the introduction of oligomycin, FCCP, and rotenone/antimycin A per Cell Mito Stress Test. For 24-hr exposures, cells were allowed to settle for 1hr, then media was switched to RPMI (100 U/mL Pen-strep, 10% FBS). Cells were incubated with stimuli overnight in at 37°C, 5% CO<sub>2</sub>. After 24 hrs, the media was changed to Cell Mito Stress Test media an hour prior to assay.

### ***Acute Challenges***

Ten  $\mu\text{M}$  1,2-naphthoquinone (100mM stock made fresh in DMSO) was used as an environmentally relevant model redox cycling ambient air contaminant (Lavrich et al. 2018, *in resubmission*). The protein kinase C activator phorbol myristate acetate (PMA; stock made in DMSO, stored at  $-20^{\circ}\text{C}$ ) was included as a model inducer of the oxidative burst (final concentration of 100 ng/mL). Both stimuli were diluted to 10X port solutions in Cell Mito Assay Media. Both stimuli were diluted to 10X working solutions in Cell Mito Assay Media and loaded as the first port injection.

### ***Protein Normalization***

Immediately after extracellular flux analysis, the media was carefully aspirated from each well and the plate was stored at  $-80^{\circ}\text{C}$  overnight. BCA protein assay reagent was prepared according to manufacturer's instructions (ThermoFisher Scientific, Waltham, MA). BSA protein standards (0, 250, 500, 750  $\mu\text{g}/\text{mL}$ ) were pipetted directly into Seahorse "blank" wells. In-plate BCA assays were performed by lysing cells in RIPA buffer (25 mM Tris-HCl, pH 7.6, 150 mM NaCl, 1% NP-40, 1% sodium deoxycholate, 0.1% SDS) and adding BCA working reagent directly to each well. After 30 min. incubation at  $37^{\circ}\text{C}$ , absorbance was read at 562 nm using a CLARIOstar microplate reader (BMG LABTECH, Ortenberg, Germany). For each group, protein values were averaged and basal OCR and ECAR values were normalized for protein mass.

### ***Cytokine Production Measurements***

IL-6 and IL-1 $\beta$  in media were measured using commercially available ELISA kits (BD OptEIA, Franklin Lakes, NJ. Absorbance was measured using a CLARIOstar microplate reader (BMG Labtech, Ortenberg, Germany).

### ***Statistical Analyses***

OCR and ECAR values represent the averages of at least 3 replicate wells per group. For comparison between sample types, nonparametric Kruskal-Wallis test and a subsequent Dunn's multiple comparison test were used. Between BAL and BF samples, a paired nonparametric t-test (Wilcoxon) was used. A  $p < 0.05$  was considered statistically significant. PRISM (Graphpad Software, La Jolla, CA) was used for statistical analyses.

## **Results**

### ***Induced sputum macrophages are highly energetic***

We examined the bioenergetic profiles of cells recovered by the BAL or IS sampling techniques. Table 3-2 shows that both samples contained a majority of MAC, as previously reported (Alexis *et al.*, 2006; Heron *et al.*, 2012). However, IS samples also contained on average 30 % PMN (Table 3-2).

In the presence of glucose, the basal oxygen consumption rate (OCR) and the extracellular acidification rate (ECAR), indicators of mitochondrial respiration and glycolytic activity respectively, were measured using extracellular flux analyses. Figure 3-1A shows the cell energy phenotype (OCR vs. ECAR) plotted for BAL, IS, and BF MAC. Quadrants depict the relative tendency towards different bioenergetic phenotypes. Relative to BAL and BF MAC, IS MAC were found to be the most energetic cells, showing the highest OCR and ECAR, although IS MAC also showed the greatest variability among sample types. The ECAR and OCR values were significantly correlated in each of the samples (Figure 3-1B-D). There was no correlation between PMN content and the baseline OCR or ECAR of IS samples (Figure 3-4A, B), consistent with previous reports that PMN exhibit a relatively quiescent bioenergetic phenotype (Borregaard and Herlin, 1982; Chacko *et al.*, 2013).

### ***Bronchoalveolar macrophages are more reliant on mitochondrial respiration***

We next examined individual bioenergetics parameters in samples using a modified mitochondrial stress test, wherein glucose and site-specific inhibitors of the electron transport chain are added sequentially to the cells and the effect on OCR is measured. Six parameters of mitochondrial respiration were quantified using this assay (Figure 3-2). IS MAC showed an increase in OCR following glucose addition, indicating that these cells are more reliant on glucose over glutamine as a substrate for mitochondrial respiration (Figure 3-2A). In contrast, BAL MAC showed little change in OCR in response to glucose, suggesting their preference for L-glutamine as a substrate (Figure 3-2B). As shown in Figure 3-2C, BAL MAC showed a higher dependence on mitochondrial respiration for ATP production than did IS MAC. Similarly, BAL MAC exhibited higher maximal respiration than IS MAC (Figure 3-2D). Reserve capacity and proton leak did not differ between BAL and IS MAC (Figure 3-2E, F). In contrast, the rate of non-mitochondrial oxygen utilization was higher in IS MAC than BAL MAC (Figure 3-2G).

BF MAC had a bioenergetic profile that was similar to that of BAL MAC (Figure 3-5). However, like the IS MAC, BF MAC showed a lower mitochondrial oxygen-dependent ATP production and higher non-mitochondrial respiration than BAL MAC when samples from the same subject were compared.

We also examined the association between percentage of PMN in IS and maximal respiration. Initially, we noted a positive correlation that was statistically significant. However, the exclusion of a single outlier (noted in red, Figure 3-4C) resulted in a loss of statistical significance in the correlation. Similarly, Figure 3-4D shows that a trend toward a significant correlation between IS %PMN and non-mitochondrial oxygen consumption was observed, but the trend disappeared by removing the same outlier from the data (noted in red, Figure 3-4D).

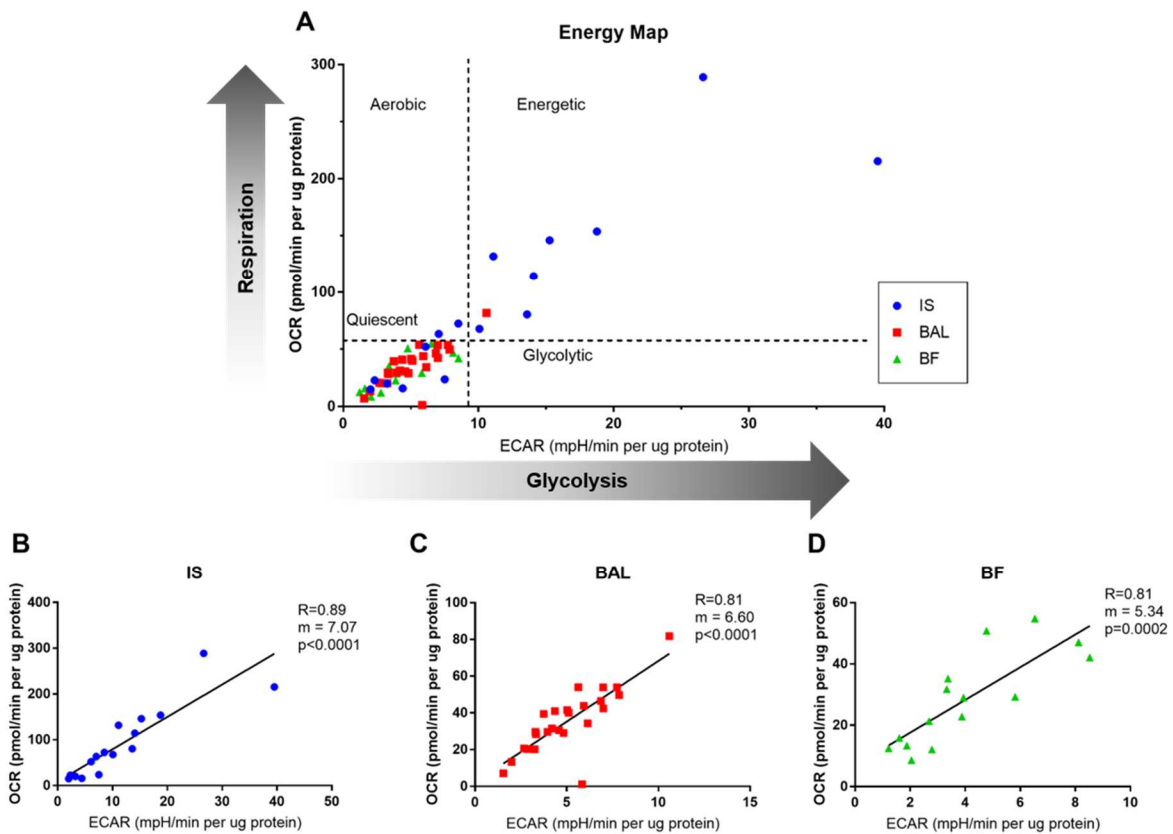


**Figure 3-1. Bioenergetic Profiles of Macrophages Sampled from Different Regions of the Human Lung.** MAC obtained by induced sputum (IS), bronchial fraction (BF), or bronchoalveolar lavage (BAL) from normal volunteers undergoing extracellular flux analysis. Basal oxygen consumption rate (OCR) and extracellular acidification rate (ECAR), as measures of mitochondrial respiration and glycolysis activities, respectively, were assessed. Basal OCR and ECAR was measured in the presence of 10 mM glucose and 2 mM L-glutamine. **A.** A comparative representation of the range of bioenergetics profiles of MAC obtained by IS or BAL. **B-D.** Plots of the OCR versus ECAR for cell samples recovered by IS or bronchoalveolar lavage. Shown is goodness of fit, slope and  $p$  for individual samples representing, IS ( $n=16$ ), BF ( $n=15$ ), BAL ( $n=25$ ).

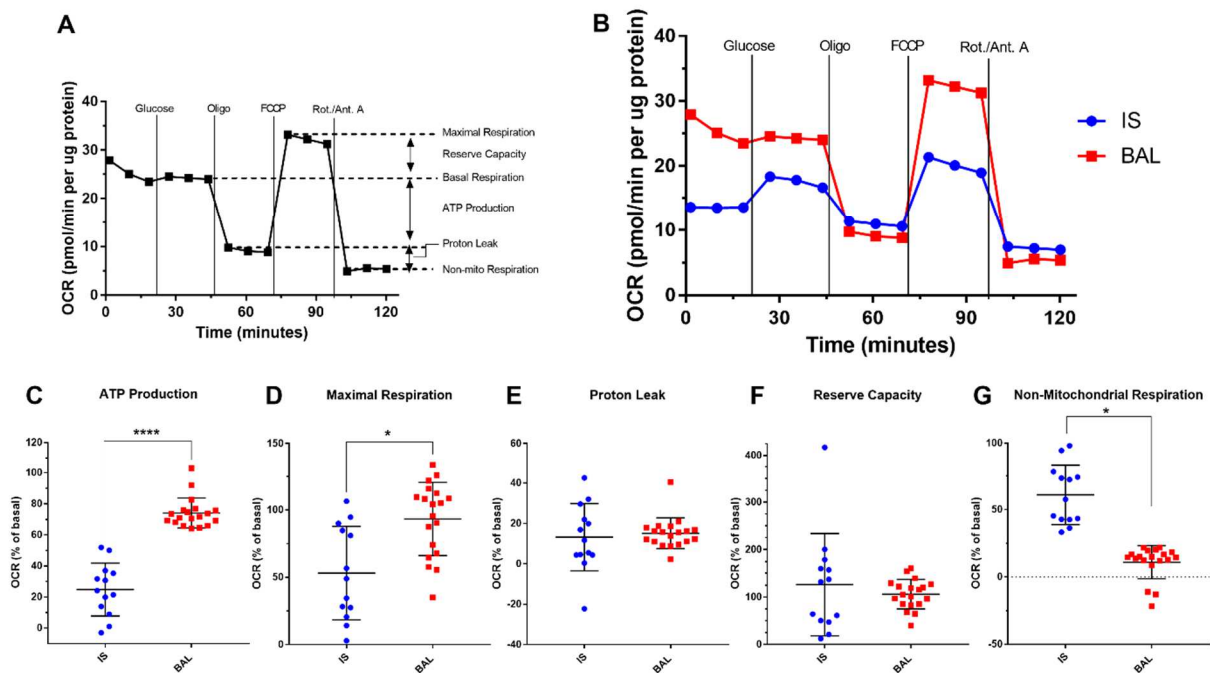


**Figure 3-2 Bronchoalveolar Macrophages Are Highly Dependent on Mitochondrial Respiration for Energy Production.** **A.** Oxygen consumption rate (OCR) can be modulated by addition of glucose and followed by a mitochondrial stress test to yield different bioenergetic parameters. The mitochondrial stress test involves sequential addition of site-specific inhibitors of the electron transport chain: oligomycin (Oligo), FCCP, and rotenone/antimycin A (Rot./Ant. A). **B.** The mitochondrial stress test was performed on MAC sampled from the central airways (IS) or distal airways (BAL) of normal volunteers. Representative OCR graphs for each sample type is shown. **C-G.** Individual parameters measured from the mitochondrial stress test data for IS and BAL MAC. \* denotes  $p < 0.05$  and \*\*\*\* denotes  $p < 0.001$  for comparison of group means. Shown are mean  $\pm$  SD, IS (n=13) and BAL (n=19).

### ***Central airway macrophages have a higher glycolytic activity***

The modified mitochondrial stress test also allowed us to quantify three parameters of glycolytic function, as assessed by the ECAR of the MAC (Figure 3-3). In this assay, IS MAC showed a marked increase in ECAR in response to the introduction of glucose, reaching nearly full glycolytic capacity (Figure 3-3B). In contrast, the ECAR in the BAL MAC was not changed by the addition of glucose (Figure 3-3B). Furthermore, glycolysis and glycolytic capacity were significantly elevated and no difference in glycolytic reserve was observed in IS vs BAL MAC (Figure 3-3C-E). BF MAC displayed a similar glycolytic profile to that of BAL MAC, but also showed a slight, yet significant, increase in glycolytic capacity (Figure 3-5). As observed for other bioenergetic parameters, the PMN content of IS samples was not positively correlated with the glycolytic capacity of the IS samples (Figure 3-4E).

### ***Environmental challenges differentially affect bronchoalveolar lavage and sputum macrophage bioenergetics***

We characterized and compared the influence of various environmental challenges on cellular bioenergetics in MAC obtained by IS, BAL, and BF MAC. LPS is a potent activating stimulus of MAC and, to a lesser extent, PMN. Exposure of IS, BAL, and BF MAC to 50-100 ng/mL LPS for 6 hr or 24 hr (BAL MAC only) did not alter baseline OCR nor mitochondrial parameters measured in these cells (Figure 3-6A, Figure 3-7A, C, E, G). ECAR parameters were similarly unchanged in IS, BAL, and BF MAC following LPS exposure (Figure 3-6B, Figure 3-7B, D, F, H).

Given the surprising lack of an effect of LPS on MAC bioenergetics, we investigated whether the BAL MAC examined in our study were capable of mounting an inflammatory response to LPS stimulation by measuring their production of IL-1 $\beta$  and IL-6. As shown in Figure 3-6C, D, BAL MAC responded to 6 hr LPS treatment with an approximately 10-fold increase in the production of these inflammatory cytokines.

We then determined whether the lack of a bioenergetic response to LPS challenge in lung MAC also extended to other monocytic cells in the same study volunteers. We compared the bioenergetic profiles of BAL MAC with PBMC obtained from the same individual volunteers. Matched BAL MAC and PBMC were exposed to LPS for 4 hr or 24 hr and subjected to the mitochondrial stress test. As shown in Figure 3-6F, there was a significant LPS-induced increase in basal ECAR in the PBMC but not in the BAL MAC sample after 4 hr. No significant changes in basal OCR were seen in response to LPS in either PBMC or BAL (Figure 3-6E). After 24 hr of LPS exposure, BAL OCR was non-significantly decreased,

though no further changes were noted in BAL and PBMC bioenergetics compared to media controls (Figure 3-7E, F, G, H).

We also tested the effect of activation of PMA, a potent protein kinase C activator, on IS, BAL, and BF MAC. Treatment of BF MAC with PMA significantly increased the baseline OCR (Figure 3-8A, G), while BAL and IS MAC showed a modest increase and no change, respectively (Figure 3-8A, E). There were no changes in subsequent mitochondrial parameters associated with OCR in IS, BAL, or BF MAC (Figure 3-8C, E, G). In contrast, glycolytic parameters were affected by PMA exposure, as demonstrated by increased ECAR in BAL and BF MAC (Figure 3-8B, F, H). The ECAR of IS MAC was not significantly affected by PMA treatment (Figure 3-8B, D).

Redox-cycling quinones such as 1,2-NQ are contaminants of ambient air that are thought to contribute to the health effects of air pollution exposure (Valavanidis *et al.*, 2005; Kumagai *et al.*, 2012). Relative to baseline, the addition of 10  $\mu$ M 1,2-NQ had no significant effect on IS or BAL MAC OCR (Figure 3-9A), but did increase OCR in BF MAC. Further perturbation with bioenergetic inhibitors produced no response in BAL and BF MAC, indicating that the exposure to 1,2-NQ effectively suppressed mitochondrial respiration, including ATP production and maximum respiration (Figure 3-9E, G). In the glycolytic pathway, exposure to 1,2-NQ significantly decreased the ECAR in BAL MAC, but had no effect on glycolysis in BF or IS MAC (Figure 3-9B).

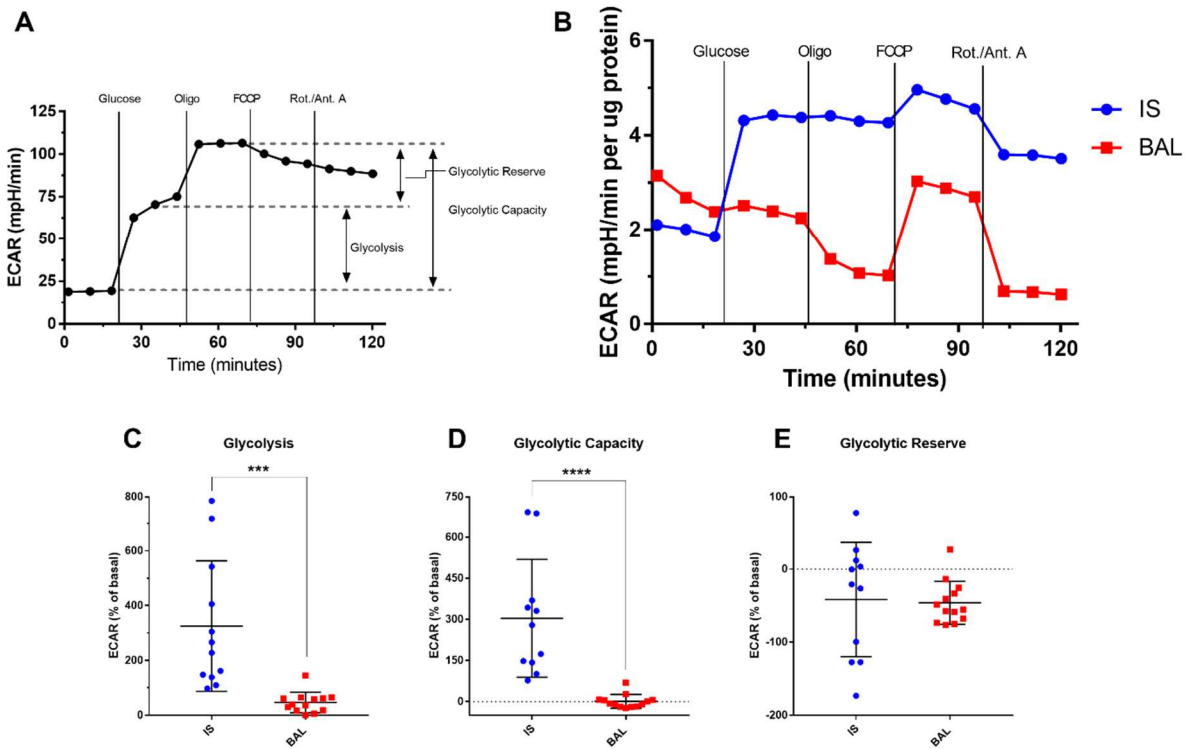


**Figure 3-3. Induced Sputum Macrophages Rely on Glycolysis.** **A.** A glycolytic stress test with the sequential addition of glucose and oligomycin (Oligo) provides measurements of three glycolytic parameters using the extracellular acidification rate (ECAR). **B.** The ECAR was measured in MAC sampled from the upper airways (IS) or bronchoalveolar region (BAL) of normal volunteers in response to the glycolytic stress test. Representative ECAR plots are shown for each sample type. **C-G.** Individual parameters derived from the data produced by the glycolytic stress test described in A. for IS and BAL MAC. \*\*\*denotes  $p < 0.001$  and \*\*\*\* denotes  $p < 0.0001$  for comparison of group means. Shown are mean  $\pm$  SD, IS ( $n = 11$ ) and BAL ( $n = 13$ ).

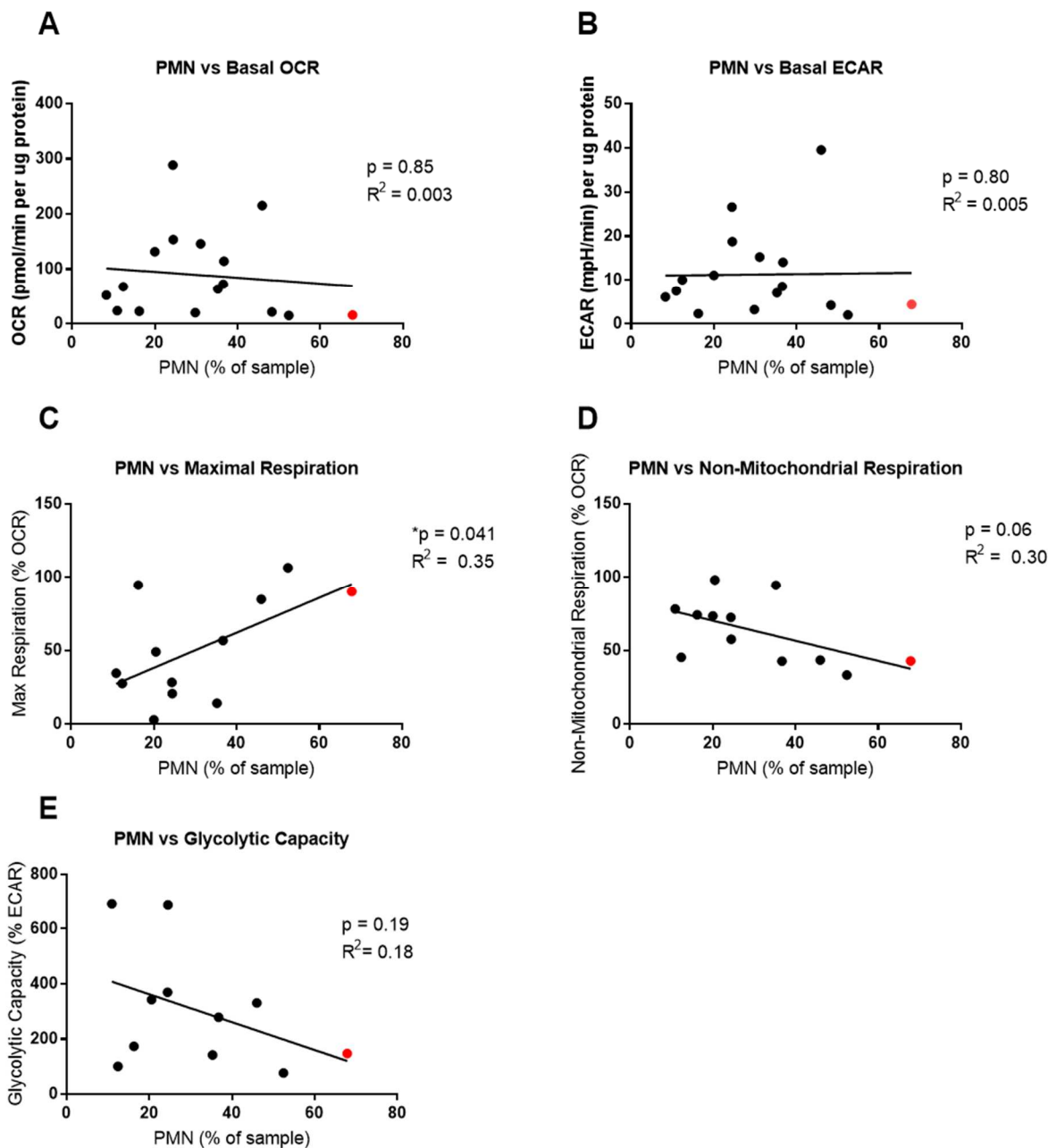


**Figure 3-4. Neutrophil content does not significantly correlate with bioenergetic parameters.**

Percentage of neutrophils (PMN) in each sample was plotted against **A.** Basal OCR, **B.** Basal ECAR **C.** Maximal Respiration, **D.** Non-mitochondrial respiration, and **E.** Glycolytic Capacity. Linear regression was performed and the resulting significance of a non-zero slope and correlation coefficient ( $R^2$ ) is shown. An outlier was identified as higher than two standard deviations from the mean (red marker). When the outlier was excluded from analysis, the parameters changed for each graph as follows: A. Basal OCR,  $p=0.88$ ;  $R^2=0.016$ , B. Basal ECAR,  $p=0.58$ ,  $R^2=0.02$ , C. Maximal Respiration,  $p=0.10$ ;  $R^2=0.26$ , D. Non-Mitochondrial Respiration,  $p=0.11$ ,  $R^2=0.25$ , E. Glycolytic Capacity,  $p=0.30$ ,  $R^2=0.13$ .

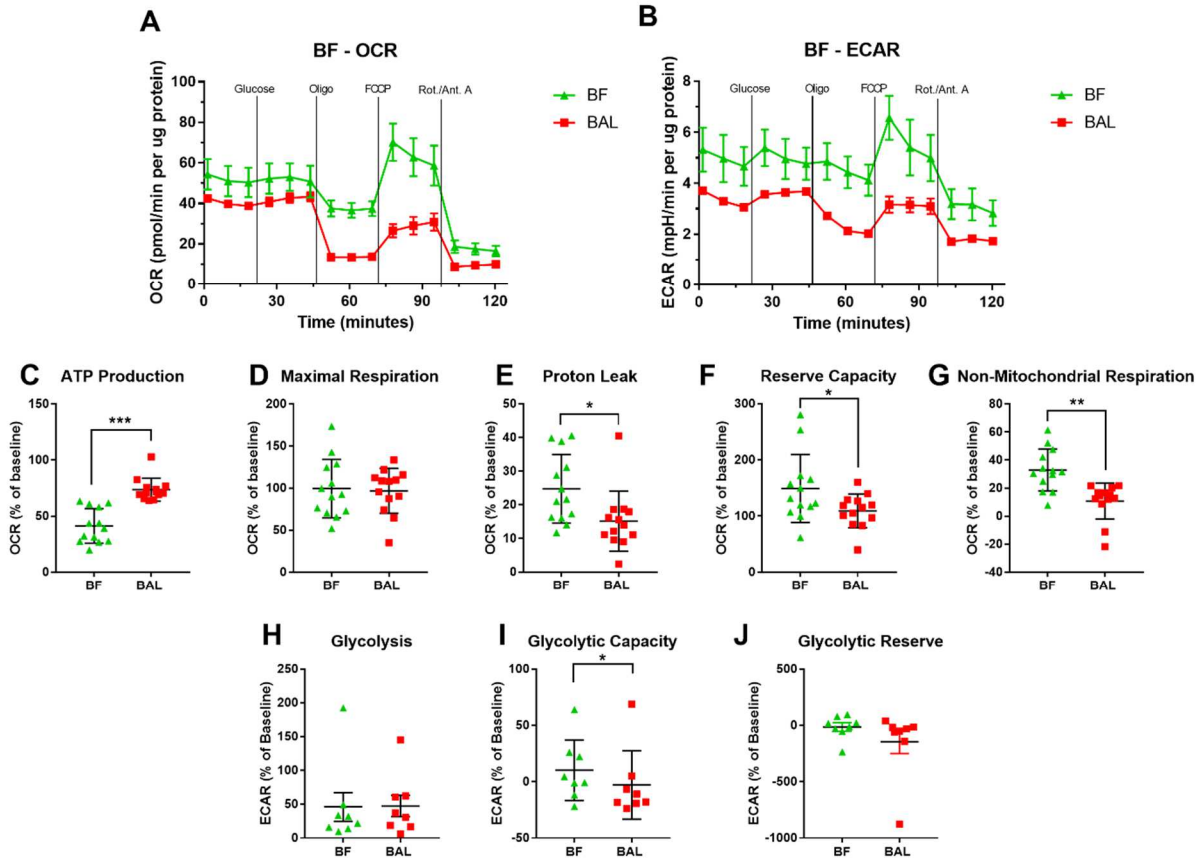


**Figure 3-5. Bioenergetic profile of BF MAC resemble that of BAL MAC.** Bioenergetic parameters in MAC from BF and paired BAL were measured using extracellular flux analysis and a mitochondrial stress test. Representative **A**. OCR and **B**. ECAR are plotted for the BAL and BF MAC from the same subject. The following mitochondrial parameters were calculated using OCR: **C**. ATP Production, **D**. Maximal Respiration, **E**. Proton Leak, **F**. Reserve Capacity **G**. Non-Mitochondrial Respiration. Data shown as mean  $\pm$  SD, N=13. The following glycolytic parameters were calculated using ECAR: **H**. Glycolysis, **I**. Glycolytic Capacity, (**J**) Glycolytic Reserve. Data shown as mean  $\pm$  SD, N = 8. For all graphs, \* indicates  $p < 0.05$ , \*\* indicates  $p < 0.01$ , and \*\*\* indicates  $p < 0.001$ .

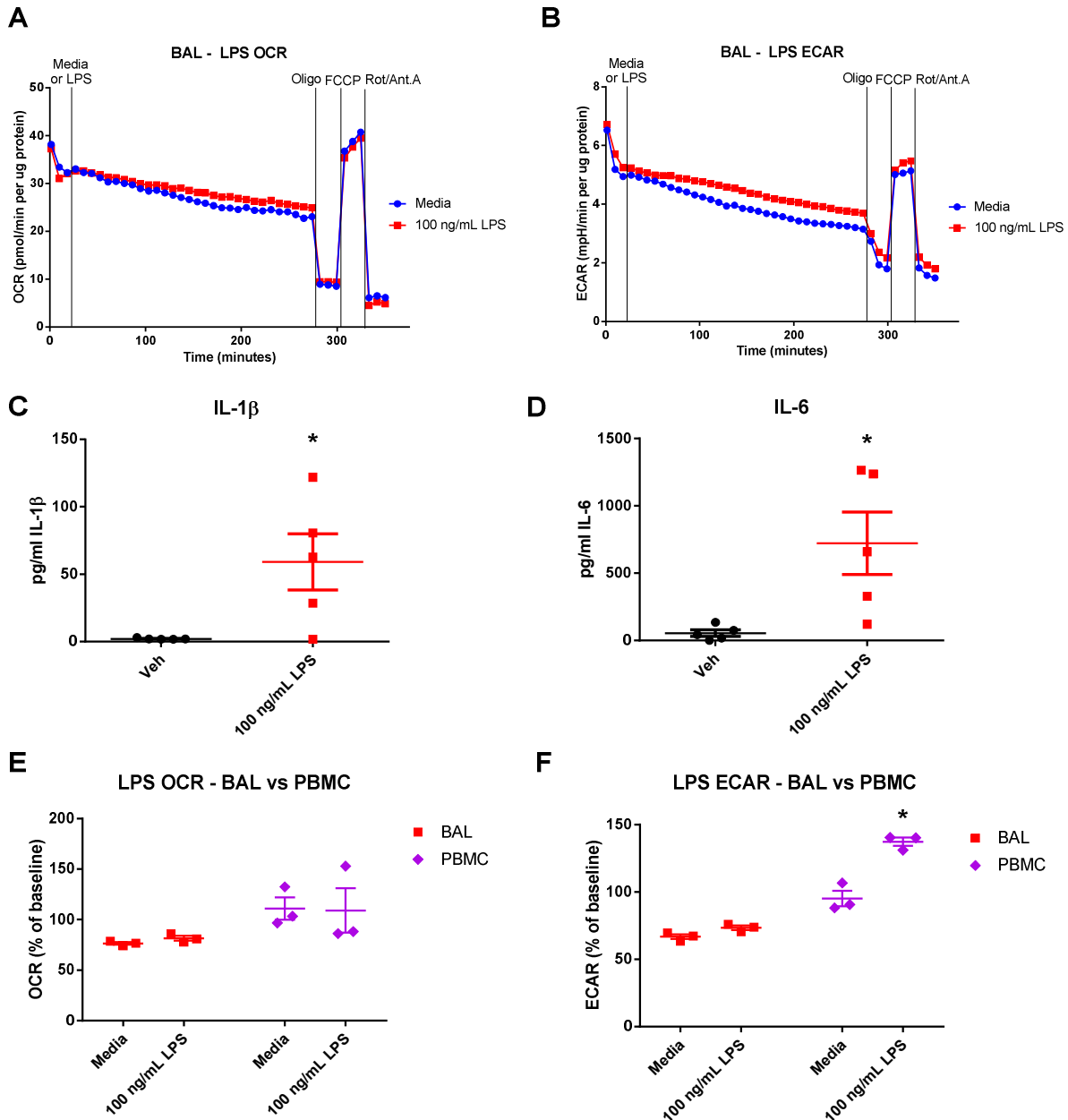


**Figure 3-6. Acute LPS Challenge Does Not Alter BAL Macrophage Bioenergetics.** BAL MAC were subjected to extracellular flux analyses in which **A.** the oxygen consumption rate (OCR) and **B.** extracellular acidification rate (ECAR) were measured in response to exposure of 100 ng/mL LPS for 4 hr were then of the cells. After 4 hrs of exposure, a mitochondrial stress test was performed using sequential addition of site-specific inhibitors of the electron transport chain (oligomycin, FCCP, and rotenone/antimycin A). OCR and ECAR values are expressed normalized for protein content, n=6. Levels of **C.** IL-1B and **D.** IL-6, produced by BAL MAC after 4 hr challenge with media or 100 ng/mL LPS. **E., F.** BAL MAC and peripheral blood monocytes (PBMC) from the same subject were stimulated with media or 100 ng/mL LPS for 4 hr prior to measurement of their OCR and ECAR. Data are expressed as a percent of the baseline value. \*denotes p<0.05 from vehicle or media controls, mean  $\pm$  SD, n  $\geq$  3.

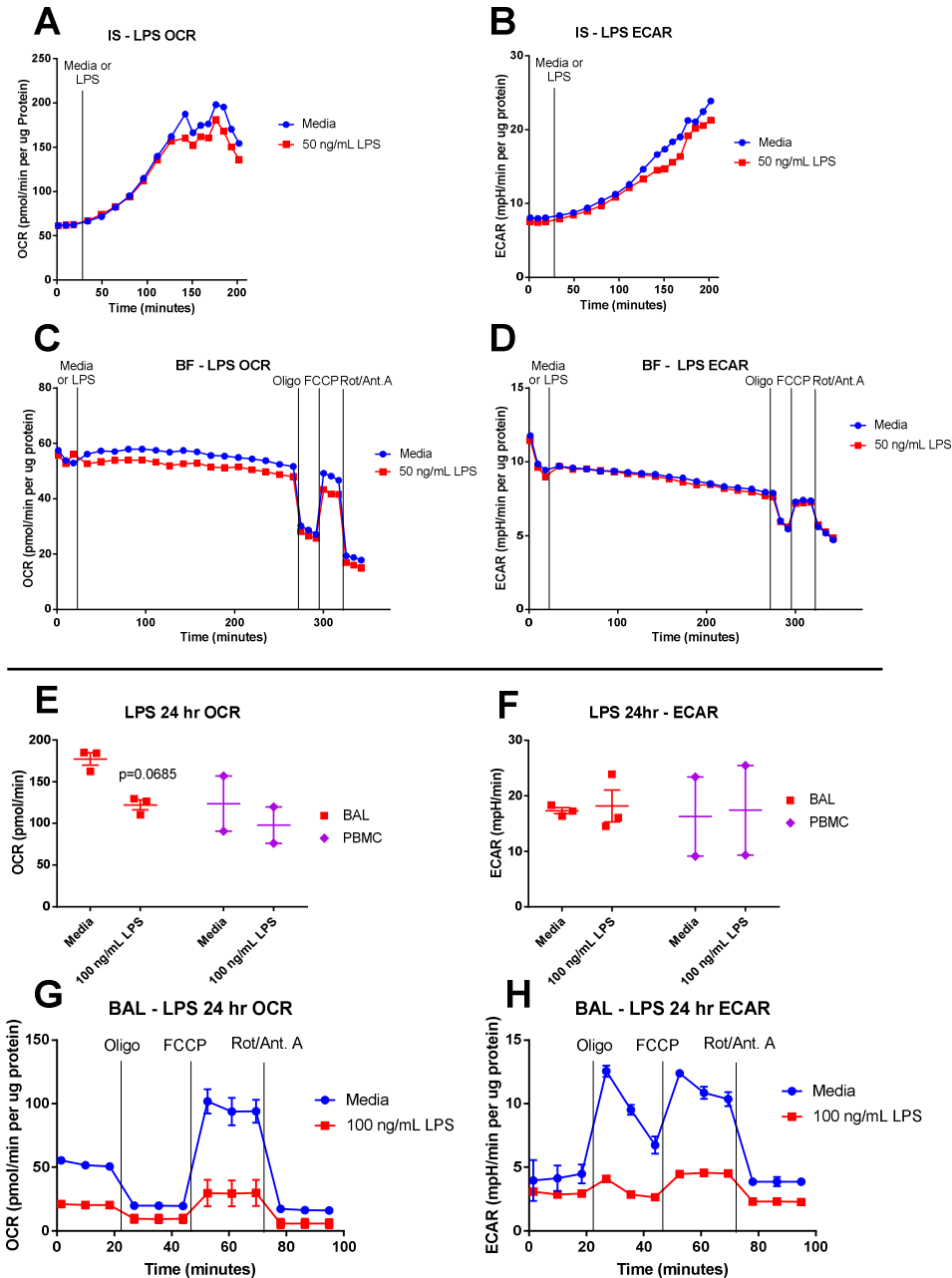


**Figure 3-7 Acute LPS Challenge Does Not Alter the Bioenergetics of Human Lung Macrophages.** The OCR and ECAR of IS (**A, B**) and BF (**C, D**) cells were monitored using extracellular flux analysis during exposure to 50 ng/mL LPS for 3-4 hr. For BF cells, this exposure was followed by a mitochondrial stress test (oligomycin, FCCP, and rotenone/antimycin A). Activity data are expressed normalized for protein content. **E, F.** BAL MAC and peripheral blood monocytes (PBMC) from the same subject were stimulated with media or 100 ng/mL LPS for 24 hr before their basal OCR and ECAR were measured. Shown are mean  $\pm$  SEM,  $n \geq 2$ . Representative **G.** OCR and **H.** ECAR graphs from BAL MAC that were exposed to media or 100 ng/mL LPS for 24 hr and subjected to a mitochondrial stress test. Representative of  $n = 3$  subjects.

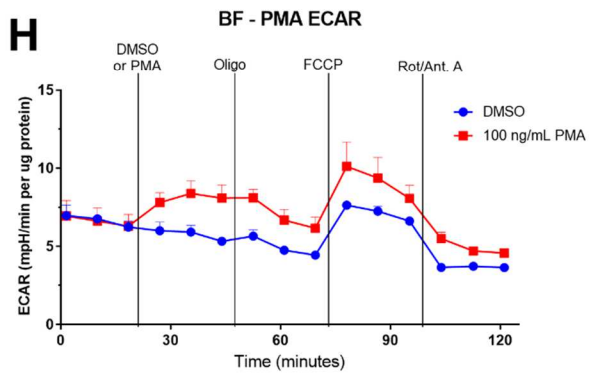
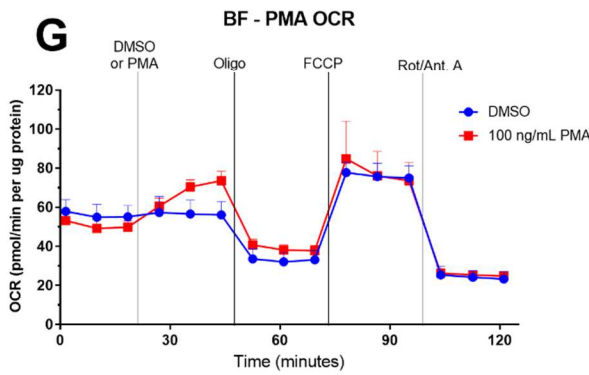
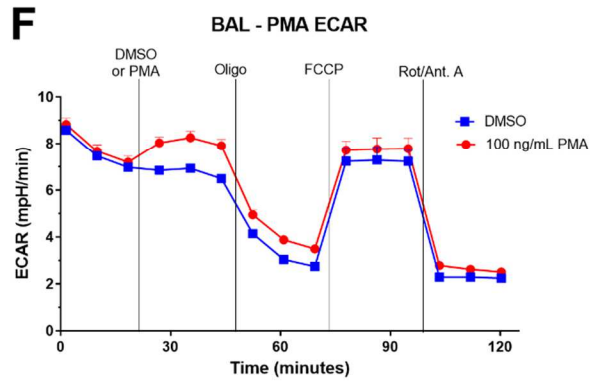
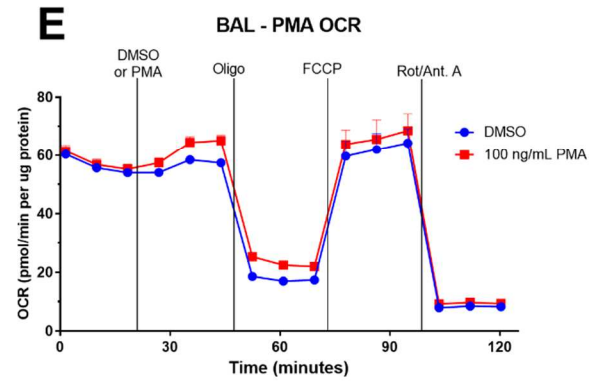
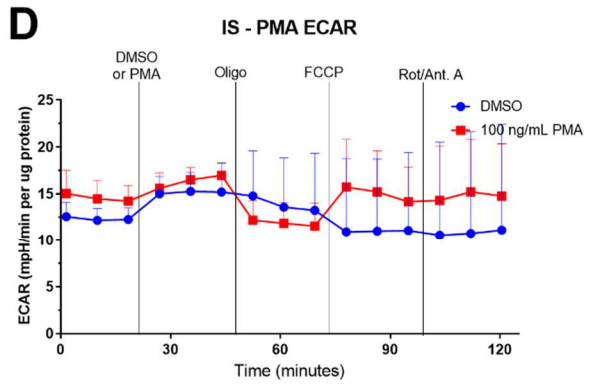
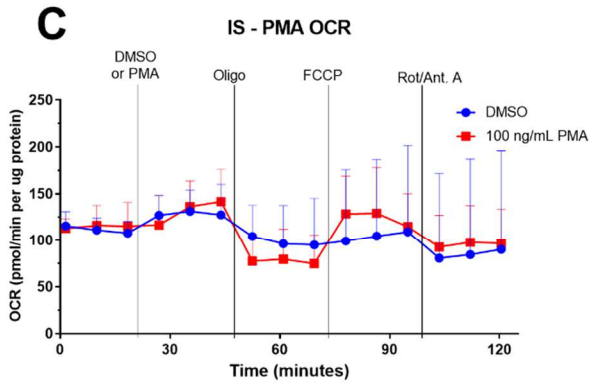
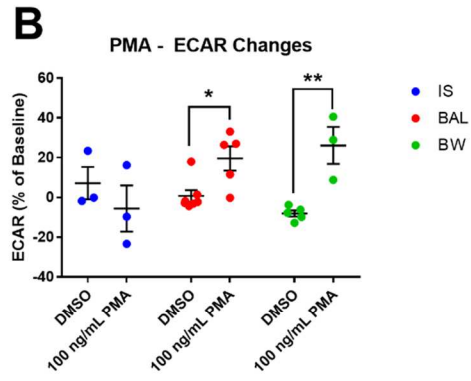
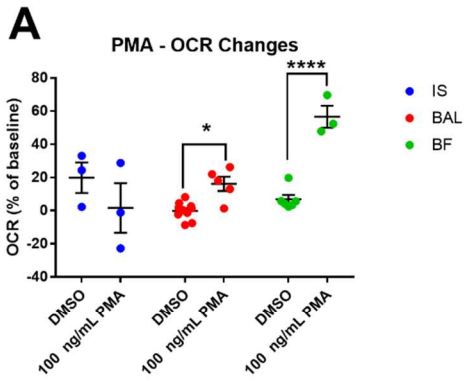


**Figure 3-8. Activation of Protein Kinase C Induces Bronchoalveolar and Bronchial Fraction Macrophage OCR and ECAR.** Cells collected by IS, BAL, and BF were stimulated with the protein kinase C activator, PMA, and bioenergetic changes were monitored by extracellular flux analysis. OCR and ECAR were measured at basal conditions, following the addition of 100 ng/mL PMA and in response to a mitochondrial stress test (oligomycin, FCCP, rotenone/antimycin A). The data are expressed as the mean **A**. OCR and **B**. ECAR changes in response to PMA addition over a 24 min exposure are shown as a percentage of the basal OCR or ECAR. Representative OCR and ECAR graphs are shown for IS (**C**, **D**), BAL (**E**, **F**), and BF (**G**, **H**),  $n \geq 3$ , mean + SD. OCR and ECAR data were normalized to total protein content in the sample. \* denotes  $p < 0.05$  and \*\*\*\* denotes  $p < 0.001$  between means of DMSO control and PMA groups.

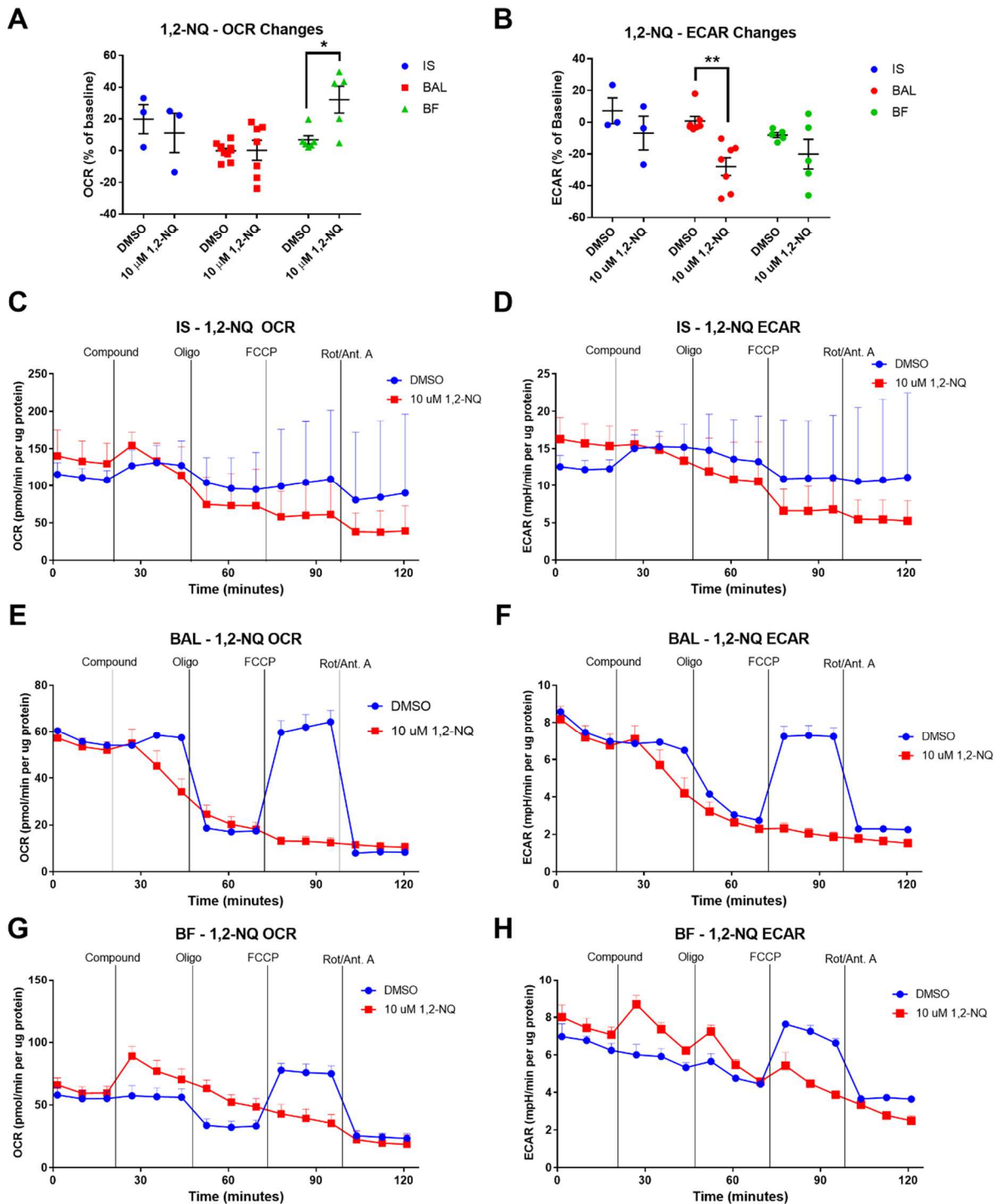


**Figure 3-9. Exposure to 1,2-Naphthoquinone Impairs Mitochondrial Respiration in Human Bronchoalveolar Macrophages.** The effect of 1,2-naphthoquinone (1,2-NQ) on IS, BAL, and BF MAC was measured using extracellular flux analysis. The OCR and ECAR were measured at basal conditions, following the addition of 10  $\mu$ M 1,2-NQ and in response to a mitochondrial stress test (oligomycin, FCCP, and rotenone/antimycin A). The data are expressed as the mean **A.** OCR and **B.** ECAR changes in response to 1,2-NQ addition over a 24 min exposure are shown as a percentage of baseline.

Representative OCR and ECAR plots are shown for IS (**C, D**), BAL (**E, F**), and BF (**G, H**),  $n \geq 3$ , mean + SD. OCR and ECAR data were normalized to total protein content in the sample. \* denotes  $p < 0.05$  and \*\* denotes  $p < 0.01$  between means of DMSO control and 1,2-NQ groups within sample type.

## Discussion

To our knowledge, this is the first report describing the bioenergetic profile of MAC recovered from different regions in the respiratory tract of human volunteers. This study provides evidence that depending on their location within the respiratory tract, MAC populations demonstrate metabolically distinct profiles. We observed that IS MAC recovered from the surfaces of the central airways had constitutively higher OCR and ECAR levels compared to BAL and BF MAC, suggesting a heightened basal metabolic state occurs in MAC from the central versus distal airway regions. Interestingly, the majority of the basal OCR in IS MAC was non-mitochondrial, suggesting oxygen consumption occurs through non-mitochondrial processes, such as oxidative burst. Furthermore, IS MAC had higher glycolytic activity, reflecting the M1 phenotype. In contrast, BAL MAC were highly reliant on mitochondrial respiration, a reflection of the M2 phenotype. These observations are consistent with our previous work that showed greater functional activity (phagocytosis, oxidative burst) and upregulated cell surface phenotype expression (CD11b) in IS versus BAL and BF MAC sampled from the same individuals (Alexis *et al.*, 2000).

Based on these findings, we speculate that increased glycolytic state of IS MAC may reflect their functional need as first responder immune cells to generate ATP quickly via glycolysis rather than slowly via oxidative phosphorylation, in order to optimally respond to the continued exposure and interaction with inhaled microorganisms and pathogen-associated molecular patterns. During immune response, nitric oxide can inhibit Complex I, II, and IV, leading to a collapse in mitochondrial membrane potential (Beltrán *et al.*, 2000). To mount an appropriate immune response, MAC may repurpose mitochondria to generate required reactive oxygen species signals, as shown in Complex I, to stimulate inflammation and phagocytosis (Chandel *et al.*, 2001; Pearce and Pearce, 2013). BAL MAC on the other hand, are located more distally from inhaled pathogens and therefore less likely to undergo inflammatory metabolic reprogramming, consistent with their bioenergetic similarity to the anti-inflammatory M2 profile. Overall, the metabolic differences that we report here, together with previously reported functional and phenotypic

differences between IS, BAL, and BF MAC, support the notion that functionally heterogeneous MAC populations exist in the lung and that bioenergetic profiles play distinct roles in supporting the respective activities of MAC from the upper and lower respiratory tract.

An unexpected finding from this study was the lack of metabolic reprogramming toward glycolysis in BAL MAC after acute LPS stimulation. This metabolic reprogramming has been previously reported in MAC differentiated from both mice BMDMs (Vats *et al.*, 2006; Palsson-McDermott *et al.*, 2015) and human PBMC (Huang *et al.*, 2014) and has been hypothesized to be necessary for the production of inflammatory cytokines (Tannahill *et al.*, 2013). In the present study, BAL MAC were metabolically unresponsive to an acute LPS exposure despite the fact that LPS recognition and associated signal transduction processes were functional, as evidenced by a robust IL-6 and IL-1 $\beta$  cytokine response. In addition, subject-matched PBMC did show an increase in ECAR in response to LPS, as previously seen using MAC differentiated *in vitro* from PBMC (Huang *et al.*, 2014). These data suggest that in terms of their ability to undergo metabolic reprogramming toward the glycolytic phenotype, human BAL MAC *in vivo* are unlike both murine or human MAC differentiated in culture from BMDM or PBMC, respectively. While we did note a decrease in OCR in BAL MAC after 24hr exposure to LPS which could be a sign of metabolic reprogramming, we did not observe a concomitant increase in ECAR, suggesting a decrease in cellular viability rather than metabolic reprogramming. Additional investigation is needed to determine whether glycolytic IS MAC can be reprogrammed toward oxidative phosphorylation (M2 phenotype) in the presence of IL-4, a process that has been shown not to occur in murine MAC (Van den Bossche *et al.*, 2016).

We further characterized the metabolic profile of our samples by challenging them with PMA, a protein kinase C activator known to induce the intracellular oxidative burst activity, and 1,2-NQ, a redox-active air pollutant that induces oxidative stress. BAL and BF MAC responded with the expected increase in OCR and ECAR following PMA, likely indicating increases in oxidative burst and a shift toward glycolysis respectively. IS MAC bioenergetics did not change in response to PMA exposure, likely due to the high basal activation (high OCR and ECAR) of the IS samples. Interestingly, BF MAC were the only cells to show an increase in OCR following 1,2-NQ exposure, an effect attributable to the redox-cycling activity of the quinone. Indeed, BF and BAL MAC demonstrated decreases in mitochondrial function when

treated with 1,2-NQ, as previously reported in human bronchial epithelial cells (Lavrich *et al.*, 2018). Such mitochondrial dysfunction could also induce oxidative stress, leading to adaptive changes or even apoptosis in MAC (Ott *et al.*, 2007).

It is important to note that although our sample types contained predominately MAC, some IS and BF samples contained significant numbers of PMN (on average, 30%), which is also in keeping with previously published findings (Alexis *et al.*, 2000; Rutgers *et al.*, 2000). Due to limited cell yield of these samples, it was not possible to remove PMN from the bioenergetic profile and enrich for MAC. However, we contend that PMN were unlikely contributors to the MAC OCR and ECAR measurements for multiple reasons. First, it is well established that resting PMN have relatively few mitochondria per cell, rendering these cells bioenergetically quiescent (Borregaard and Herlin, 1982; Chacko *et al.*, 2013). Second, although there was a positive correlation between the fractional PMN content and the maximal respiration of the IS sample, this correlation was found to be driven by a single outlier in whom the percent PMN was more than two standard deviations from the group mean in this study. Third, given their phagocytic capacity, if anything, PMN would be expected to contribute to non-mitochondrial oxygen consumption and/or the glycolytic capacity of the IS samples. However, no positive correlations were observed between PMN content and either parameter in the IS samples. Therefore, while we cannot completely rule out the possibility that PMN contribute to the bioenergetic profile of the IS samples, we take our results of the analysis of IS and BF samples in this study to represent the bioenergetic profile of MAC from the surfaces of the large central airways. In addition, the presence of neutrophils in sputum samples may contribute to the altered bioenergetics of IS MAC, though more investigation is needed into potential mechanisms.

### **Summary**

Recent advances in extracellular flux technology have greatly facilitated the characterization of the bioenergetic profile of immune cells, affording unprecedented insights into how energy metabolism can influence immune cell function during homeostasis and in response to challenge (Mills *et al.*, 2017). Here, we show for the first time that lung MAC derived from the surfaces of the central airways (IS) are more basally energetic overall than BAL and BF MAC. Furthermore, IS MAC have a higher dependence on glycolysis, reflective of a M1 phenotype, than BAL and BF MAC, which appear to rely heavily on

mitochondrial respiration. Notably, human lung MAC examined *ex vivo* do not undergo metabolic reprogramming during their inflammatory responses to LPS, showing a clear difference from MAC differentiated in culture from monocytic lineage. Although in its infancy, translational bioenergetics can inform clinical research by revealing critical mechanisms underlying innate immune cell function both in healthy and diseases in the airways.

## CHAPTER 4: GLYCOLYSIS IS INHIBITED THROUGH PEROXIDE-MEDIATED INACTIVATION OF GLYCERALDEHYDE-3-PHOSPHATE DEHYDROGENASE<sup>3</sup>

### Introduction

Ambient particulate matter (PM) exposure is a leading cause of morbidity and mortality worldwide. The World Health Organization estimated that ambient PM caused roughly 3 million premature deaths worldwide in 2012, primarily through cardiopulmonary diseases with inflammatory phenotypes (World Health Organization, 2014). Oxidative stress has been cited as the primary mechanism linking PM exposure and inflammatory human health effects (Valavanidis *et al.*, 2005). However, oxidative stress is a broad term that encompasses diverse redox events that mechanistically cause different physiologic outcomes. The specific oxidative changes induced by PM that initiate inflammatory signaling are not well characterized.

Quinones are ubiquitous organic components of PM suggested to play a key role in oxidative stress induction. Quinones have two primary mechanisms of toxicity: (1) electrophilic adduction to macromolecules, and (2) redox cycling to generate reactive oxygen species (ROS). 1,2-naphthoquinone (1,2-NQ) is a quinone commonly found in ambient air and is capable of both mechanisms of toxicity (Kumagai *et al.*, 2012). We have previously shown that 1,2-NQ increases ROS production, namely H<sub>2</sub>O<sub>2</sub>, in human airway epithelial cells leading to downstream activation of inflammatory and adaptive pathways (Cheng *et al.*, 2012).

H<sub>2</sub>O<sub>2</sub> is a key signaling mediator for numerous physiological functions, including proliferation and bioenergetics (Rhee *et al.*, 2005a). Importantly, H<sub>2</sub>O<sub>2</sub> can oxidize key cysteine residues of proteins in a process known as sulfenylation, often leading to inactivation of the protein. Since this modification is

---

<sup>3</sup> Portions of this chapter appeared previously in Wages, P. A., Lavrich, K. S., Zhang, Z., Cheng, W. Y., Corteselli, E., Gold, A., Bromberg, P.A., Simmons, S.O., & Samet, J. M. (2015). Protein Sulfenylation: A Novel Readout of Environmental Oxidant Stress. *Chemical Research in Toxicology*, 28(12), 2411-2418. Copyright 2015. American Chemical Society. Used with permission.

usually reversible, the proteins sensitive to sulfenylation can act as “redox switches” in the cell and maintain redox homeostasis (Barford, 2004).

Glyceraldehyde-3-phosphate dehydrogenase (GAPDH) is an important cellular redox switch in the cell and is particularly sensitive to inactivation by  $H_2O_2$ , with a rapid rate constant ( $10^2$ - $10^3$   $M^{-1}s^{-1}$ ) (Winterbourn and Hampton, 2008). GAPDH is an essential glycolytic enzyme pathway for ATP production and cell viability. Due to its high constitutive expression, it is a popular housekeeping protein, but several “moonlighting” functions have recently been characterized including its role in nuclear signaling, mRNA stabilization, and structural organization (Hildebrandt *et al.*, 2015; Millet *et al.*, 2016).

As a redox switch, GAPDH also plays an essential role in regulating cellular NADPH levels, an essential reductant for the regeneration of many antioxidant systems in the cell. When  $H_2O_2$  is sufficiently high, either due to physiological or pathologic mechanisms, GAPDH is sulfenylated and inactivated (Grant *et al.*, 1999). This reduces glycolytic activity in the cell and allows glucose to be shunted through the pentose phosphate pathway, the primary source of cellular NADPH (Ralser *et al.*, 2007). With sufficient NADPH, antioxidant systems, including glutaredoxin and thioredoxin, can mediate the rescue of the reduced active form of GAPDH and glycolysis can be restored. While the mechanism of GAPDH as a redox switch is well-characterized, several other glycolytic enzymes have shown to be sensitive to  $H_2O_2$ , including pyruvate kinase 2 (Yang *et al.*, 2014).

Through redox switches, numerous essential signaling pathways are sensitive to  $H_2O_2$  production. Inappropriate production of  $H_2O_2$  by a toxicant could lead to pathologic signaling changes. If excess  $H_2O_2$  is present, sulfenylated proteins can be further oxidized to the sulfinic and sulfonic acid forms, often considered irreversible (Poole, 2015). In the case of glycolysis, pathological inhibition of GAPDH could lead to a loss of cellular viability and growth. We specifically identified GAPDH as a target of  $H_2O_2$  oxidation induced by 1,2-NQ exposure in human bronchial epithelial cells, but had not characterized the functional impacts (Wages *et al.*, 2015).

In addition to increasing  $H_2O_2$  production, 1,2-NQ is a strong electrophile and could directly inhibit GAPDH or other proteins through Michael addition. A previous study showed that 1,2-NQ can adduct recombinant GAPDH and inhibit GAPDH activity. However, this inhibition was not detected in an

adenocarcinomic alveolar epithelial cell line, despite finding 1,2-NQ adducts on GAPDH (Miura *et al.*, 2011). The role of H<sub>2</sub>O<sub>2</sub> in the inactivation of GAPDH was not thoroughly investigated.

Here, we examined the functional effect of 1,2-NQ on glycolysis in the human bronchial epithelial cell line, BEAS-2B. We hypothesized that 1,2-NQ reduces glycolytic activity in the cell through a H<sub>2</sub>O<sub>2</sub>-mediated inactivation of GAPDH and other essential enzymes. We utilized other quinones with varying propensities for redox cycling and adduction to compare potential mechanisms. We found that environmentally-relevant doses of 1,2-NQ rapidly inhibited glycolytic function as measured using extracellular flux analyses. Overexpression of catalase, an enzyme that scavenges H<sub>2</sub>O<sub>2</sub>, reversed the glycolytic inhibition caused by low doses of 1,2-NQ, suggesting an underlying H<sub>2</sub>O<sub>2</sub>-dependent mechanism to inactivate glycolytic proteins rather than adduction.

## **Methods**

### **Reagents**

Tissue culture media and supplements were purchased from Lonza (Walkersville, MD). Adenoviral vectors were obtained from the Gene Therapy Center Virus Vector Core Facility (University of North Carolina at Chapel Hill, Chapel Hill, NC). The following chemicals were obtained from Sigma-Aldrich (St. Louis, MO): hydrogen peroxide (H<sub>2</sub>O<sub>2</sub>), 1,2-naphthoquinone (1,2-NQ), 1,4-naphthoquinone (1,4-NQ), 9,10-phenanthrenequinone (9,10-PQ), 1,4-benzoquinone (BQ), dimethyl sulfoxide (DMSO), dimedone (DMD), dithiothreitol (DTT), oligomycin (Oligo), rotenone (Rot.), antimycin A (Ant. A), D-glucose, L-glutamine, sodium pyruvate, and polybrene. Dimethoxy-1,4-naphthoquinone (DMNQ) and 2-deoxy-d-glucose (2-DG) was purchased from Cayman Chemical (Ann Arbor, MI). Seahorse Analyzer consumables were purchased from Agilent Technologies, including XF FluxPaks (XFe96 and XFe24), XF Base Medium (minimal DMEM without phenol red), and HEPES. Basic laboratory supplies were obtained from Fisher Scientific (Raleigh, NC).

### **Cell Culture**

SV40 large T antigen-transformed human airway epithelial cells (BEAS-2B, subclone S6) were obtained from the Environmental and Public Health Division, NHEERL, U.S. EPA and cultured as previously described in keratinocyte growth medium (KGM) (Reddel *et al.*, 1988; Tal *et al.*, 2008). Prior to

assay, cells were deprived of growth factors overnight by changing cell media to un-supplemented keratinocyte basal media (KBM).

### ***Viral Transduction***

For cytosolic catalase overexpression, BEAS-2B cells were transduced with an adenoviral vector encoding human catalase driven by a cytomegalovirus promoter at a MOI of 200 with 10 µg/mL polybrene in KBM for 4 hr the day prior to assay (Erzurum *et al.*, 1993b). KGM was added and cells were incubated with the virus for an additional 4 hr. After the incubation with virus (8 hr total), cells were washed with PBS and KBM was added overnight. Assays were performed the following morning.

### ***Quinone Preparation***

100 mM stocks of 1,2-NQ, 1,4-NQ, and DMNQ were prepared in DMSO. 15 mM stocks of 9,10-PQ were prepared in DMSO. Working solutions were diluted in cell media with final DMSO concentrations less than 0.1%. 50 mM stocks of BQ were prepared directly in cell media or mitochondrial assay solution. All stocks, with the exception of DMNQ, and working solutions were made fresh on the same day as exposure. DMNQ stocks were stored at -20°C for less than 6 months.

### ***Extracellular Flux Analysis***

Oxygen consumption rate (OCR) and Extracellular Acidification Rate (ECAR) was measured at 37°C using the Seahorse XFe24 and XFe96 Analyzers (Agilent Technologies). BEAS-2B were seeded at 30,000 cells (XF24) or 16,000 cells (XF96) per well two days prior to assay in KGM. Four background wells without cells were included in all assays. XFe24 and XFe96 sensor cartridges were hydrated overnight with XF Calibrant at 37°C. Media was replaced the night before assay to KBM without growth factors.

Stock concentrations of oligomycin, rotenone, and antimycin A were prepared in DMSO and stored at -20°C. Glucose and 2-deoxy-D-glucose (2-DG) stocks were prepared in XF Base Media and stored at -20°C. All compounds used for in-assay injections were diluted in the appropriate assay media with final DMSO concentrations less than 0.1%.

For the glycolytic stress test experiments, XF Base Media with 2 mM L-glutamine was prepared fresh on the day of assay and adjusted to pH 7.4 with 0.1 N NaOH. Cell media was changed 1 hr prior to assay and cells were placed in a 37°C incubator without CO<sub>2</sub>. The injections were ordered as follows

unless otherwise noted: A) quinone; B) 10 mM glucose; C) 1  $\mu$ M oligomycin; D) 50 mM 2-DG. As a brief summary of parameters measured during the glycolytic stress test, the second injection of glucose (post-1 hr glucose starvation) stimulates glycolysis in the cell to yield a measurement of glycolysis. The third injection of oligomycin shuts off ATP synthase, forcing the cells to upregulate glycolysis for their ATP needs and is a measurement of glycolytic capacity. The last injection of 2-DG inhibits the second step of glycolysis and confirms that the ECAR displayed is linked to glycolytic function. Mix-wait-measure times were 3 min – 2 min – 3 min for the XFe24 and 3 min – 0 min – 3 min for the XFe96.

For the glycolytic rate assay, XF Base Media (without phenol red) was prepared with 2mM L-glutamine, 10 mM glucose, 1 mM pyruvate, and 5 mM HEPES, and adjusted to pH 7.4 with 1 N NaOH. Cell media was changed 1 hr prior to assay and again immediately before cells were transferred to the machine for assay. The injections were ordered as follows: A) quinone; B) 0.5  $\mu$ M rotenone, 0.5  $\mu$ M antimycin A; C) 50 mM 2-DG. Mix-wait-measure times were 3 min – 2 min – 3 min.

Bioenergetic parameters were calculated using the manufacturer's recommendations (Agilent Technologies).

### ***GAPDH Activity Assay***

Activity of GAPDH in BEAS-2B lysates was measured using the KD Knockout Alert Assay Kit (ThermoFisher) kit following manufacturer's recommendations. BEAS-2B cells were prepared in same manner as for the glycolytic stress test on the extracellular analyzer. Cells were exposed to indicated doses of 1,2-NQ, 1,4-NQ, and DMNQ in XF Base Media (+2 mM L-glutamine, pH 7.4) for 24 min to mimic conditions in extracellular flux assays. After exposure, cells were washed in 100  $\mu$ L ice-cold PBS and lysed in 200  $\mu$ L lysis buffer (provided) for 20 min. at 4°C. 10  $\mu$ L of the cell lysate was transferred to a 96-well, clear bottom, black walled plate. 90  $\mu$ L of provided master mix was added to each sample and fluorescence was measured at room temperature for a 4 min interval, with an excitation wavelength of 560 nm and an emission wavelength of 590 nm, using a CLARIOstar plate reader (BMG LABTECH, Ortenberg, Germany). A standard curve using recombinant GAPDH was ran as a positive control.

### ***Detection of Recombinant Protein Sulfenylation***

Recombinant GAPDH from rabbit muscle (Sigma-Aldrich) in Tris-HCl (1 M, pH 7.6) was first reduced with 1 mM DTT on ice for 30 min. Samples were passed through Bio-Spin P-6 columns (Bio-

Rad) and protein concentration determined using a Bradford Assay. 25  $\mu$ M reduced GAPDH was incubated with varying molar equivalencies of 1,2-NQ or H<sub>2</sub>O<sub>2</sub> for indicated time at 37°C.

Protein was labelled with 200  $\mu$ M - 1 mM dimedone (DMD, dissolved in DMSO) for the indicated period and subsequently prepared for Western Blotting. In some experiments, catalase (33.3 U/mL) was added to the reduced GAPDH immediately prior to exposure. Catalase boiled at 90°C for 10 min. was included as an inactive control.

### ***Intracellular Sulfenylation Labelling***

Cells were exposed to KBM containing H<sub>2</sub>O<sub>2</sub>, 1,2-NQ, 1,4-NQ, or 9,10-PQ at the indicated concentrations for 15 min. or as otherwise noted. Cells were then quickly rinsed with PBS and then labeled in KBM with 5 mM dimedone with DMSO at 1:200 dilution for one hr.

Cells labeled with dimedone were washed with ice-cold PBS and lysed in a mild-detergent buffer (1% NP40, 150 mM Tris-HCl, pH 7.4, 150 mM NaCl, 5 mM DTT) supplemented with Calbiochem protease inhibitor cocktail set III (EMD Millipore, Temecula, CA) for 20 min on ice. Lysates were centrifuged at 4°C, 12000g for 10 min. Supernatant was collected and normalized for protein concentration via Bradford assay.

### ***Immunoblotting***

Samples were prepared for Western Blotting with 4X Laemmli Sample Buffer and boiled for 10 min. Samples were then loaded into Mini-PROTEAN TGX Precast Gels (Bio-Rad, Hercules, CA) alongside Precision Plus Protein Kaleidoscope Standards (Bio-Rad) and electrophoresed for size separation. Gels were transferred using the Trans-Blot Turbo Transfer System onto nitrocellulose membranes (Bio-Rad). Membranes were then blocked with 5% Milk in TBST for one hr at room temperature. Primary antibodies were incubated overnight at 4°C and secondary antibodies were incubated for one hr at room temperature. The following antibodies were used: anti-sulfenic acid modified cysteine (2-Thiodimedone-Specific Ig) antibody (EMD Millipore, Temecula, CA), anti-GAPDH (6C5), anti-Catalase (A-7), goat anti-mouse IgG-HRP, goat anti-rabbit IgG-HRP (all from Santa Cruz, Dallas, TX). After antibody incubation, membranes were developed in Clarity Western ECL Blotting Substrate (Bio-Rad) for 5 min and imaged with the LAS-3000 FujiFilm.

A polyclonal antibody detecting 1,2-NQ protein adducts was made by a custom antibody production service using a standard 70-day 2-rabbit immunization protocol (ThermoFisher Scientific, Waltham, MA). Briefly, 1 mg of 1,2-NQ was conjugated to 10 mg of reduced KLH to form a conjugated peptide antigen. Rabbits were injected with 0.5 mg antigen in Complete Freund's Adjuvant on Day 1. Three subsequent boosters of 0.25 mg antigen in Incomplete Freund's Adjuvant were injected at Days 14, 28, and 42. Serum was collected on Days 35 and 58 and tittered using ELISA. Unpurified rabbit serum was used at a concentration of 1:10,000 for immunoblotting.

### ***Imaging Intracellular Sulfenylation***

Intracellular sulfenylation was detected using manufacturer's recommendations of the Sulfenylated Protein Cell-Based Detection Kit (Cayman Chemical, Ann Arbor, MI). Briefly, Cells were plated in a clear bottom black-walled 96-well plate (Costar) at a density of 10,000 per well and grown to 80% confluency. Cells were starved of growth factors overnight. Cells were treated with indicated concentrations of H<sub>2</sub>O<sub>2</sub> or 1,2-NQ for 15 min. and labelled with DAZ-2 for 1 hr. Cells were fixed and underwent Staudinger Ligation. Cells were read on a CLARIOstar plate reader (BMG LABTECH, Ortenberg, Germany) at 485 nm and emission was collected at 535 nm. Subsequent pictures were taken on a Nikon Eclipse C1si (Nikon Instruments Inc., Melville, NY) with laser excitation at 488 nm and 525/30 nm emission with identical laser settings. Images were then imported to ImageJ (NIH, Bethesda, MD) for Lookup Table editing to enhance visual determination of fluorescence by converting images to 16-bit monochromatic images, implementing Green Lookup Table edited to an interpolated 4 color table (0 Green, 150 Green, 175 Green, 255 Green) followed by a median filter of 2.0-pixel radius.

### ***Statistical Analysis***

All statistical analyses were performed using PRISM (Graphpad Software, La Jolla, CA) and significance was determined as  $p < 0.05$ . One-way ANOVA was used with Dunnett's post-test for comparisons to DMSO controls, and Sidak's test for intergroup comparisons. Where noted, measurements from same day were considered paired.

## Results

### ***1,2-NQ and 1,4-NQ Impair Glycolytic Function***

Glycolytic function was first measured in BEAS-2B in response to 1,2-NQ, 1,4-NQ, 9,10-PQ, BQ, and DMNQ using the extracellular flux analyzer and the glycolytic stress test. A dose-dependent decrease in glycolysis and glycolytic function was observed in response to 1,2-NQ (Figure 4-1). This decrease was statistically significant starting at 25  $\mu$ M, though 3-10  $\mu$ M showed decreases as well. 1,4-NQ induced a similar, but steeper dose response curve for glycolysis and glycolytic function. Doses of 10  $\mu$ M 1,4-NQ and higher showed a statistically significant impairment. While 9,10-PQ exposure showed decreases in glycolytic function and capacity, it was not statistically significant. Treatment with BQ slightly increased glycolytic function and capacity, but not significantly.

To mimic a more physiological system and possibly prevent increased sensitivity to oxidants from a 1 hr glucose starvation, we also performed the glycolytic rate test using the XFe24 (Figure 4-2). Results were similar to the glycolytic stress test for 1,2-NQ, 1,4-NQ, and DMNQ. 25  $\mu$ M 1,2-NQ and 25  $\mu$ M DMNQ produced similar decreases in basal and compensatory glycolysis. Though 10  $\mu$ M 1,4-NQ treatment did not affect basal or compensatory glycolysis, 25  $\mu$ M 1,4-NQ significantly depleted both parameters in BEAS-2B cells.

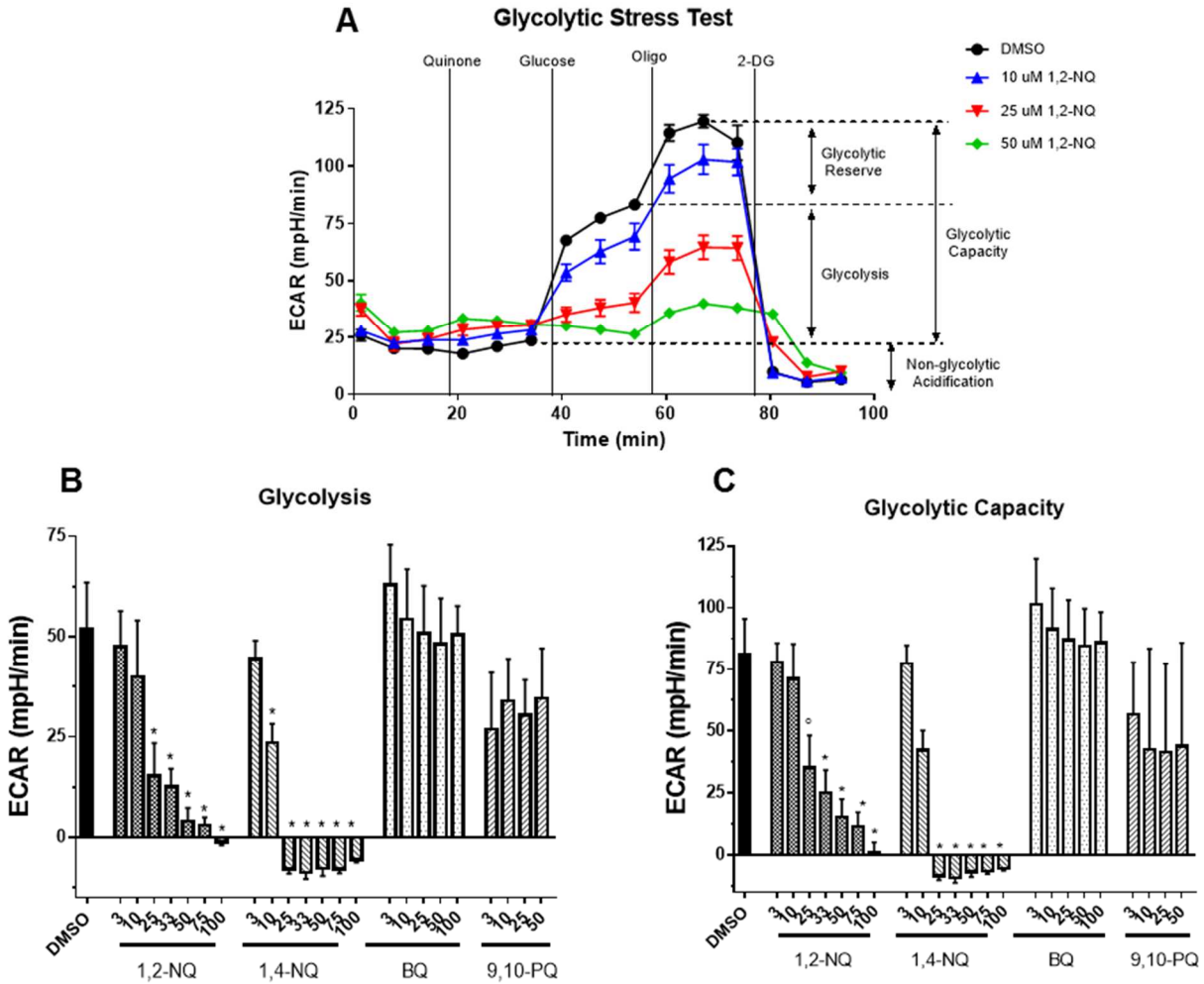


**Figure 4-1. 1,2-NQ decreases glycolytic function and glycolytic capacity in a dose-dependent manner.** **A.** Extracellular acidification rate (ECAR) was measured in BEAS-2B cells in response to DMSO or 1,2-NQ treatment and subsequent glycolytic stress test inhibitors using the Seahorse XFe96 Analyzer. For clarity, representative ECAR plot is shown, representative of  $n \geq 3$ . **B.** Glycolysis and **C.** Glycolytic Capacity were calculated for BEAS-2B cells exposed to 1,2-NQ, 1,4-NQ, BQ, or 9,10-PQ on the XFe96. Data shown as mean  $\pm$  SE,  $n \geq 3$ . In all plots, \* indicates  $p < 0.05$ .

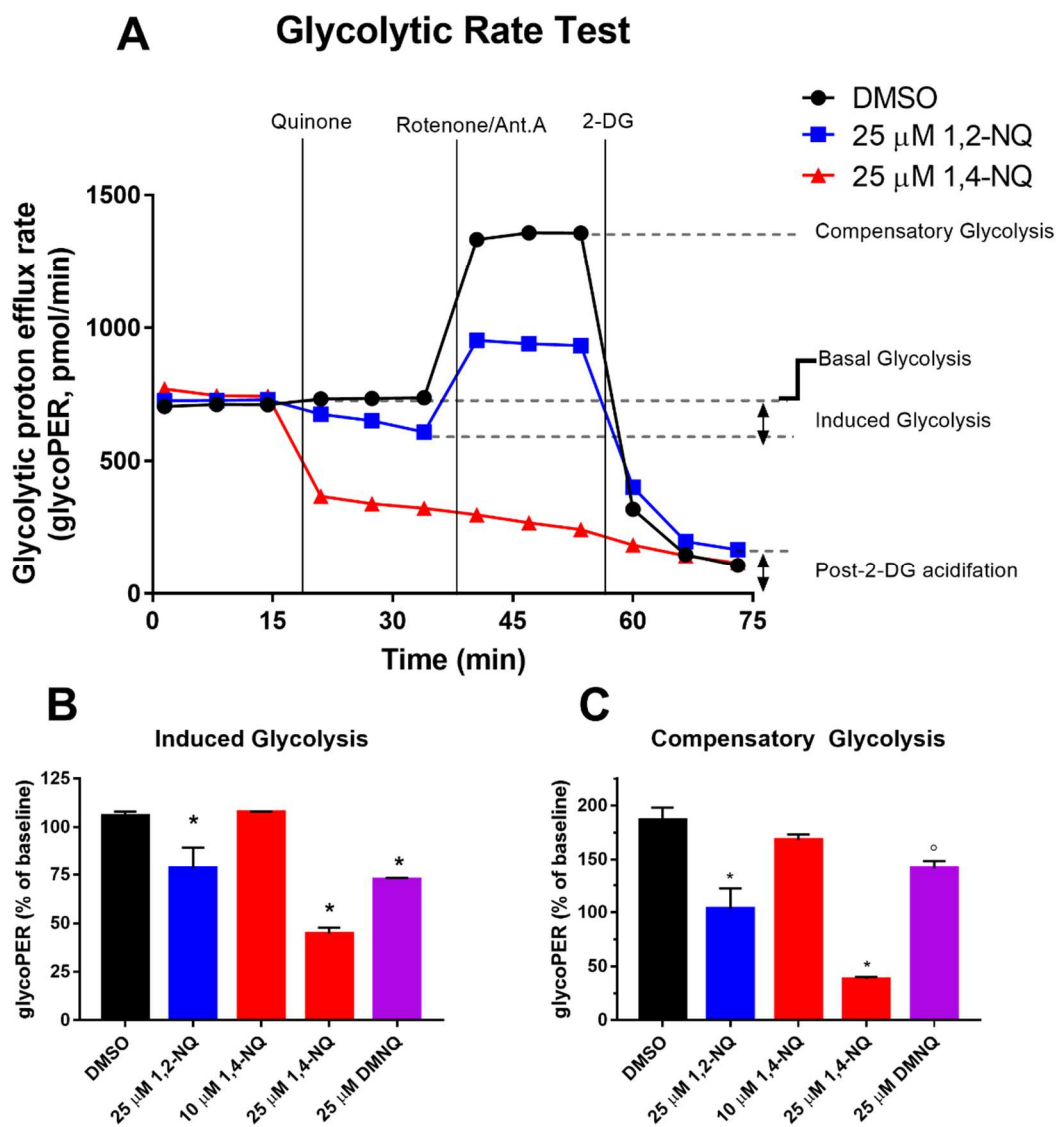


**Figure 4-2. Even in the presence of glucose, 1,2-NQ decreases glycolytic function and glycolytic capacity in a dose-dependent manner.** BEAS-2B were analyzed exposed to DMSO, 25  $\mu$ M 1,2-NQ, 10-25  $\mu$ M 1,4-NQ, or 25  $\mu$ M DMNQ, followed by the glycolytic rate test on the Seahorse XFe24 analyzer. The Glycolytic proton efflux rate (glycoPER) was calculated using the ECAR, OCR, and buffering capacity of the media. (A) Representative plot of glycoPER over time and resulting glycolytic parameters. (B) Induced Glycolysis and (C) Compensatory Glycolysis were calculated as shown in (A). GlycoPER values were normalized to the baseline. Shown are mean  $\pm$  SE,  $n \geq 3$ . Significance is shown as \*  $p < 0.05$ ,  $^{\circ} p < 0.1$ .

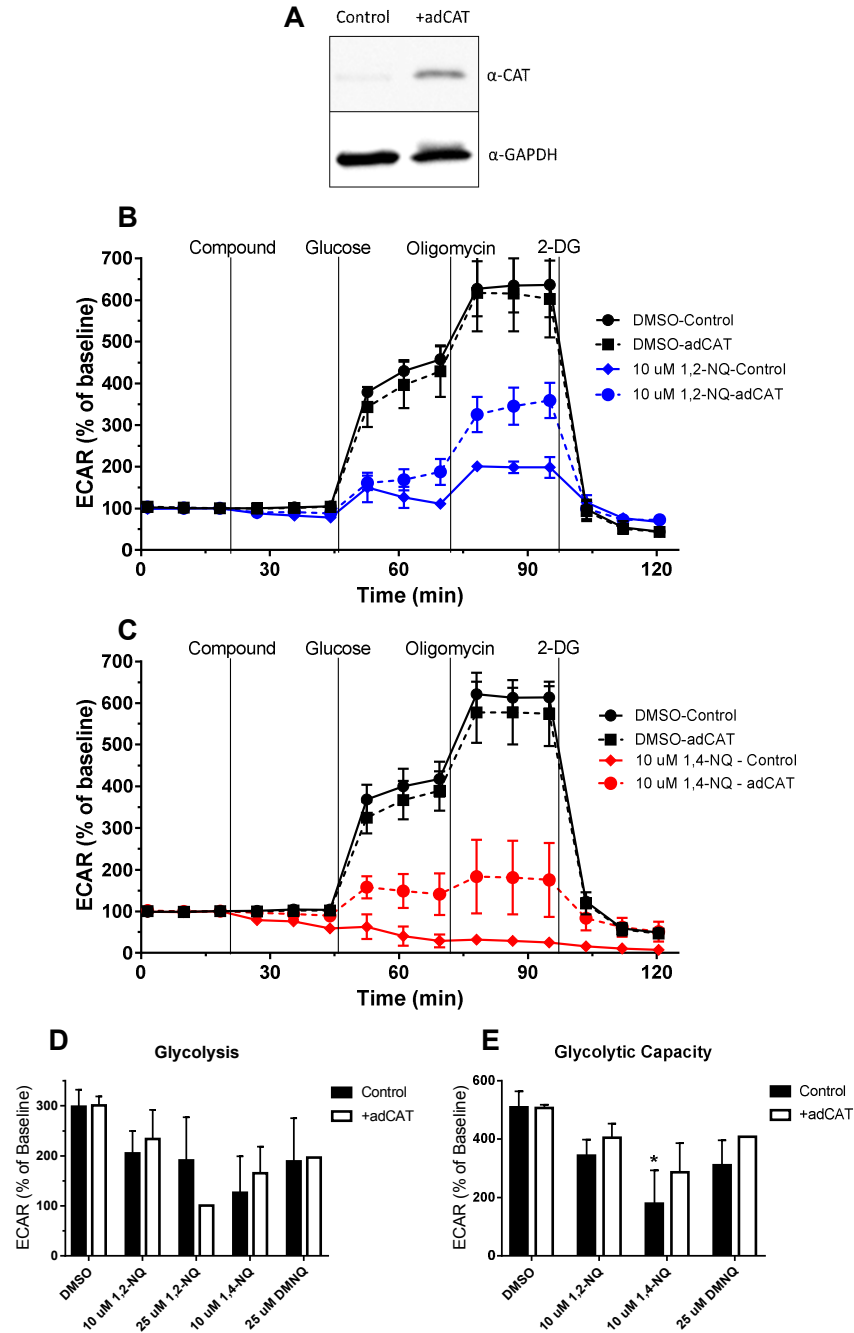


**Figure 4-3. Catalase overexpression partially rescues 1,2-NQ and 1,4-NQ-induced glycolytic inhibition.** BEAS-2B were transduced with an adenoviral vector to overexpress cytosolic catalase (adCAT). (A) Lysates from control and adCAT cells were immunoblotted and probed for catalase. GAPDH was used as a loading control. Control and adCAT cells were exposed to (B) 1,2-NQ or (C) 1,4-NQ, then underwent the glycolytic stress test. ECAR is plotted as a percentage of the baseline and data are shown as mean  $\pm$  SD for one representative experiment,  $n=3-6$ . (D) Glycolysis and (E) Glycolytic Capacity were calculated after control or adCAT cells were exposed to 10-25  $\mu$ M 1,2-NQ, 10  $\mu$ M 1,4-NQ, or 25  $\mu$ M DMNQ. \* indicates significantly different from DMSO control,  $p<0.05$ . Data shown as mean  $\pm$  SE,  $n=1-6$ .

### **Catalase overexpression partially blunts effect of 1,2-NQ on glycolysis**

To explore the contribution of H<sub>2</sub>O<sub>2</sub> in the quinone-mediated inhibition of glycolysis, we overexpressed catalase, a scavenger specific for H<sub>2</sub>O<sub>2</sub>, using an adenoviral vector (Figure 4-3A) in BEAS-2B (adCAT). BEAS-2B, control or adCAT, were exposed to DMSO, 10-25 μM 1,2-NQ, 10 μM 1,4-NQ, or 25 μM DMNQ and underwent the glycolytic stress test (Figure 4-3B, C). Though not statistically significant, catalase overexpression blunted the glycolytic capacity decreases induced by 10 μM 1,2-NQ, 10 μM 1,4-NQ, and 25 μM DMNQ (Figure 4-3D, E).

### **1,2-NQ may impair GAPDH activity**

Since GAPDH is known to be sensitive to H<sub>2</sub>O<sub>2</sub> inactivation and adduction by 1,2-NQ, we next tested whether GAPDH activity was affected by 1,2-NQ treatment. Intact BEAS-2B were exposed to increasing doses of 1,2-NQ, 1,4-NQ, and DMNQ and the resulting cell lysate was assayed for GAPDH activity (Figure 4-4). GAPDH was significantly decreased in response to exposure to 25 μM 1,4-NQ, though 25 μM 1,2-NQ also trended downward. DMNQ treatment did not alter GAPDH activity in BEAS-2B. BEAS-2B overexpressing catalase did not significantly alter quinone-induced effects on GAPDH activity.

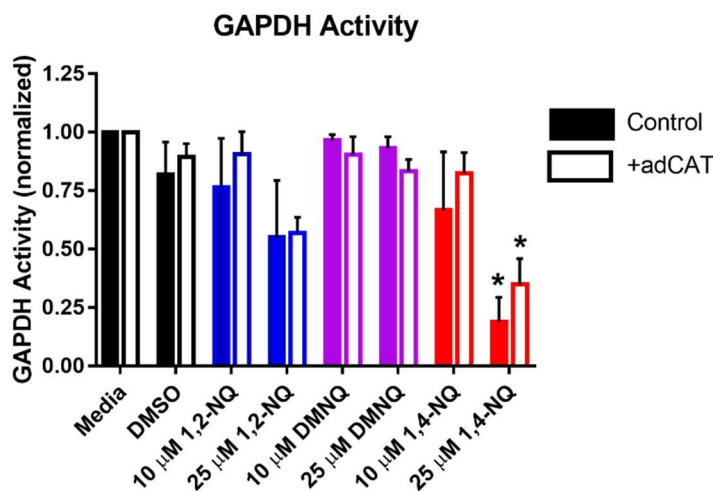


**Figure 4-4. 1,2-NQ and 1,4-NQ impair GAPDH activity in BEAS-2B cells.** GAPDH activity was assessed in BEAS-2B lysates using the KD Knockout Alert Assay Kit (ThermoFisher). Lysates were measure for fluorescence at excitation 560 nm and emission 590 nm every minute for 4 min. Slopes were determined between t=0 and t=4 min. Activity was normalized to media control. Data shown as mean ± SEM, n = 3. \* indicates p<0.05 when compared to DMSO control using a two-way ANOVA and subsequent Dunnett's post-test.

### 1,2-NQ sulfenylates and adducts recombinant GAPDH in a time-dependent manner

Recombinant GAPDH was incubated with increasing molar equivalents of 1,2-NQ for 15 min. and sulfenic acids were labelled through incubation with 1 mM dimedone for one hour 37°C. Sulfenylation of GAPDH was increased with 0.5-2 equivalents of 1,2-NQ over the DMSO control (Figure 4-5). Samples underwent immunoblotting for sulfenylation using an anti-thio-dimedone antibody. Addition of recombinant catalase blunted 1,2-NQ-induced sulfenylation. To control for off-target effects, the catalase was inactivated by boiling, restoring 1,2-NQ-induced sulfenylation. We also assessed 1,2-NQ adduction of GAPDH using a custom-made antibody and immunoblotting. 1,2-NQ adducts were detected on recombinant GAPDH in a dose-dependent manner. Catalase addition did not impact 1,2-NQ adduction of

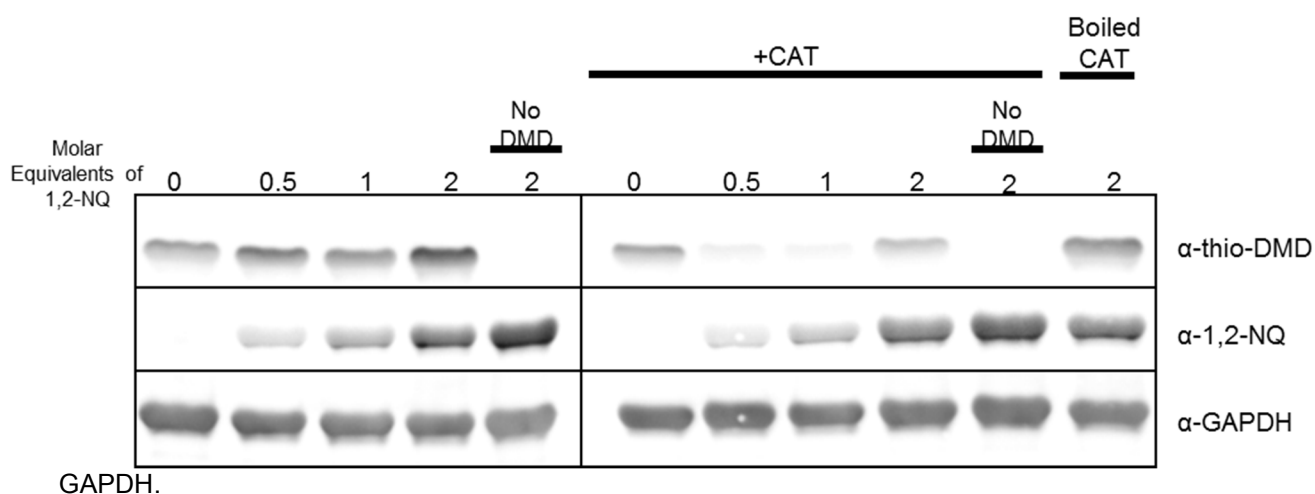
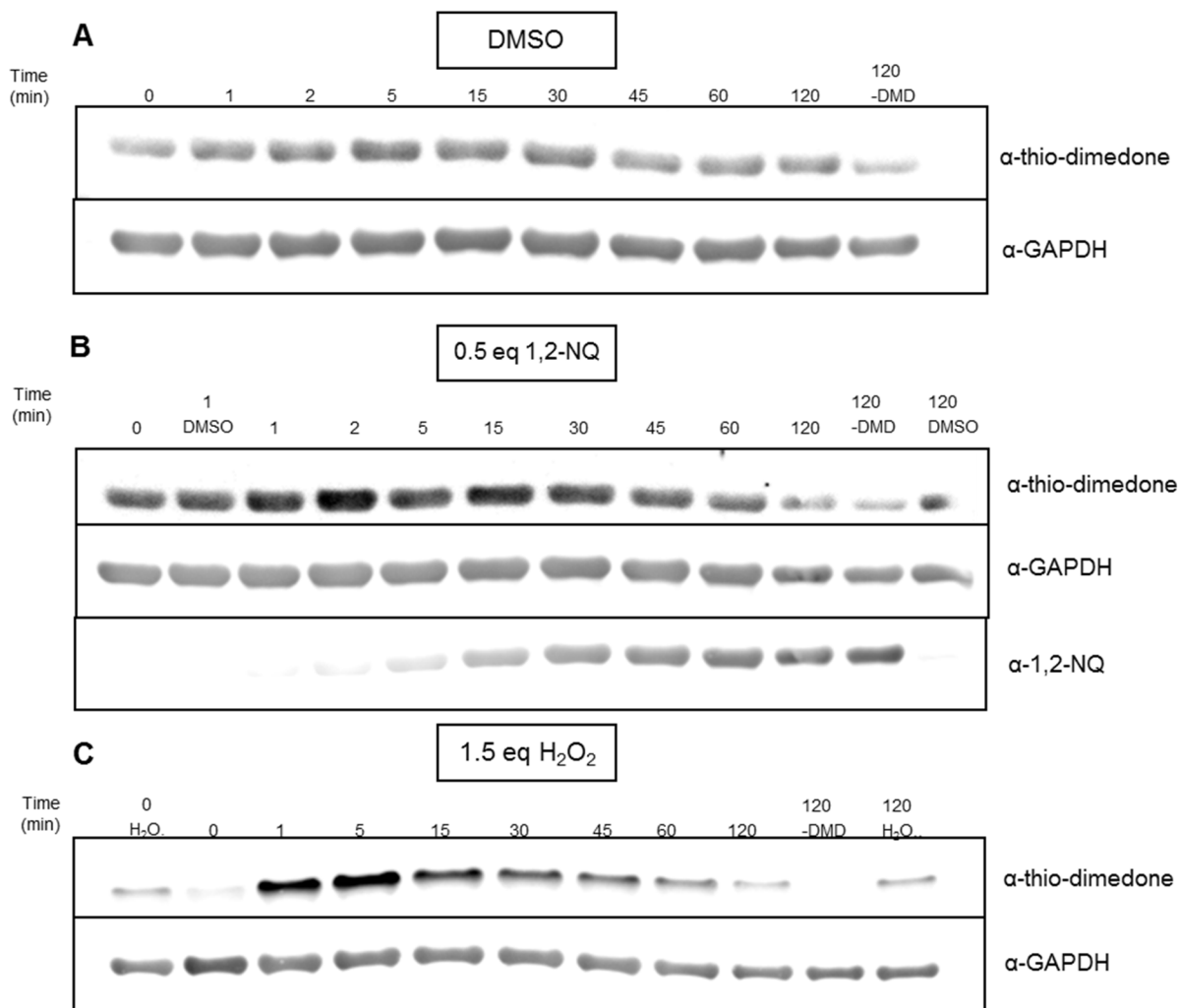


**Figure 4-5. 1,2-NQ produces H<sub>2</sub>O<sub>2</sub> *in vitro* to sulfenylate recombinant GAPDH.** Recombinant GAPDH was incubated with either 1,2-NQ or DMSO control with active recombinant catalase (CAT) or inactive catalase (Boiled CAT) for 15 min. The protein then underwent dimedone (DMD) labeling and was analyzed using immunoblotting. Blots were probed using antibodies against thio-DMD and 1,2-NQ adducts. Total GAPDH was probed as a loading control. Blot is shown representative of three independent experiments.

Next, we sought to determine if sulfenylation or adduction by 1,2-NQ changed over time. Recombinant GAPDH was incubated with DMSO, 0.5 molar equivalents of 1,2-NQ, or 1.5 molar equivalents of H<sub>2</sub>O<sub>2</sub> for a total of 2 hr at 37°C. Aliquots were removed from the primary reaction tube at the indicated time and incubated with 1 mM dimedone for 1 min. The reaction was stopped with addition of loading buffer containing 50 mM DTT and samples were analyzed by immunoblotting. No changes in

sulfenylation were observed with DMSO treatment (Figure 4-6A). When exposed to 0.5 eq 1,2-NQ, sulfenylation of GAPDH steadily increased until 15 min., then decreased over the remaining time. 1,2-NQ adduction increased steadily throughout the 120 min. time period (Figure 4-6B). GAPDH sulfenylation



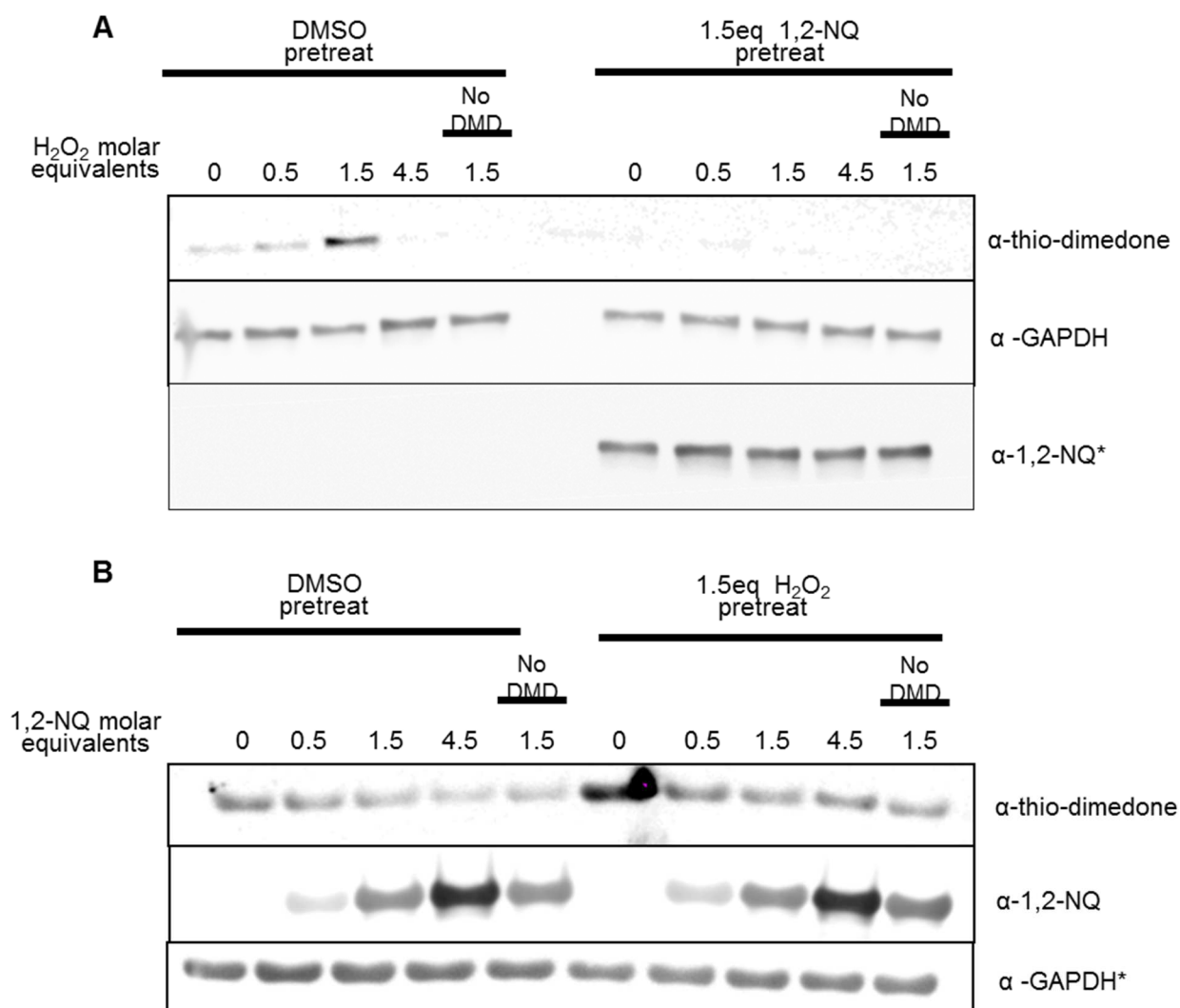
increased when treated with 1.5 eq H<sub>2</sub>O<sub>2</sub> until 5 min., then decreased for the remainder of the time period (Figure 4-6C).

**Figure 4-6. Sulfenylation of recombinant GAPDH peaks at 5 min. with 1,2-NQ, but increases adduction over time *in vitro*.** Recombinant GAPDH (25 μM) was incubated with (A) DMSO, (B) 0.5 molar equivalents (12.5 μM) 1,2-NQ, or (C) 1.5 molar equivalents H<sub>2</sub>O<sub>2</sub> for two hours, with aliquots taken from the same reaction tube at indicated times. Protein was labelled with dimedone for 1 min. at 37°C, then Laemmli loading buffer was added to stop the reaction. Protein was immunoblotted and probed for thio-dimedone and 1,2-NQ adducts. Total GAPDH was probed as loading control. Representative blots shown, n≥3. 0 min. = before treatment.

### 1,2-NQ pretreatment decreases sulfenylation by H<sub>2</sub>O<sub>2</sub>, but not the reverse

Since it was apparent that 1,2-NQ could both sulfenylate and adduct GAPDH in an *in vitro* system, we investigated whether each of these mechanisms prevented the other. Recombinant GAPDH was pre-incubated with 1.5 molar equivalents of 1,2-NQ or a DMSO control for 5 min. After the pretreatment, increasing doses of H<sub>2</sub>O<sub>2</sub> and 200  $\mu$ M dimedone was added and the reaction was incubated for 1 hr at 37°C and analyzed using immunoblotting. Sulfenylation induced by H<sub>2</sub>O<sub>2</sub> was blunted when GAPDH was pretreated with 1,2-NQ (Figure 4-7A).

The reverse experiment was performed in the same manner, pretreating with 1.5 eq H<sub>2</sub>O<sub>2</sub> for 5 min., then adding increasing doses of 1,2-NQ. No differences in adduction of GAPDH by 1,2-NQ were detected due to the pretreatment (Figure 4-7B). No differences were observed in GAPDH sulfenylation



with the addition of 1,2-NQ, and that was not altered by H<sub>2</sub>O<sub>2</sub> pretreatment.

**Figure 4-7. Pretreatment of recombinant GAPDH with 1,2-NQ reduces sulfenylation by H<sub>2</sub>O<sub>2</sub>, but prior sulfenylation does not reduce 1,2-NQ adduction *in vitro*.** Recombinant GAPDH (25 uM) was incubated in two parallel scenarios: (A) 1.5 molar equivalents 1,2-NQ for 5 min. prior to addition of indicated H<sub>2</sub>O<sub>2</sub>, exposure to both for 1 hr. (B) H<sub>2</sub>O<sub>2</sub> for 5 min. prior to addition of 1,2-NQ, exposure to both for 1 hr. Simultaneous to exposure, samples were labeled with 200 uM dimedone at 37°C and the reaction was stopped with the addition of 200 uM DTT. Representative blots are shown of three independent experiments. \* indicates that same samples were run on a parallel blot due to potential antibody interference.

### ***1,2-NQ, 1,4-NQ, and 9,10-PQ increase global sulfenylation in BEAS-2B***

While we determined that 1,2-NQ could sulfenylate GAPDH *in vitro*, we sought to confirm whether this was possible in cells. First, we visualized total sulfenylation changes in BEAS-2B after 15 min. 1,2-NQ exposure by labeling sulfenic acids in intact cells with dimedone analogue, DAz-2. Cells were then fixed, and imaged utilizing Staudinger Ligation and a FITC tag. We showed that 1,2-NQ increased sulfenylation at 3 and 10 μM 1,2-NQ, but 100 μM 1,2-NQ was lower than 10 μM (Figure 4-8A). A positive control of 1 mM H<sub>2</sub>O<sub>2</sub> also increased sulfenylation over control.

To give more insight into the potential proteins sulfenylated by 1,2-NQ, we compared cell lysates by immunoblotting. BEAS-2B were exposed to increasing doses of 1,2-NQ for 15 min. and sulfenic acids were labelled with 5 mM dimedone for 1 hr. Global sulfenylation was increased at 10 μM 1,2-NQ and higher (Figure 4-8B). In a separate experiment, cells were exposed to varying doses of 1,2-NQ, 1,4-NQ and 9,10-PQ for comparison (Figure 4-9A). 25 μM 9,10-PQ increased global sulfenylation, but few changes were observed at lower doses. 10 μM 1,4-NQ and higher doses elevated global sulfenylation. When comparing 10 μM across quinones, 1,4-NQ showed the highest response. When comparing 25 μM across the quinones, 1,2-NQ induced the highest global sulfenylation.

### ***1,2-NQ adducts proteins in BEAS-2B***

Total cell lysates were also examined for 1,2-NQ adducts using immunoblotting. While some adducts were detected after 10 μM 1,2-NQ exposure for 15 min., numerous bands were shown with 25 μM 1,2-NQ (Figure 4-9B). No bands were detected in cells exposed to 1,4-NQ or 9,10-PQ, demonstrating the antibody's specificity.

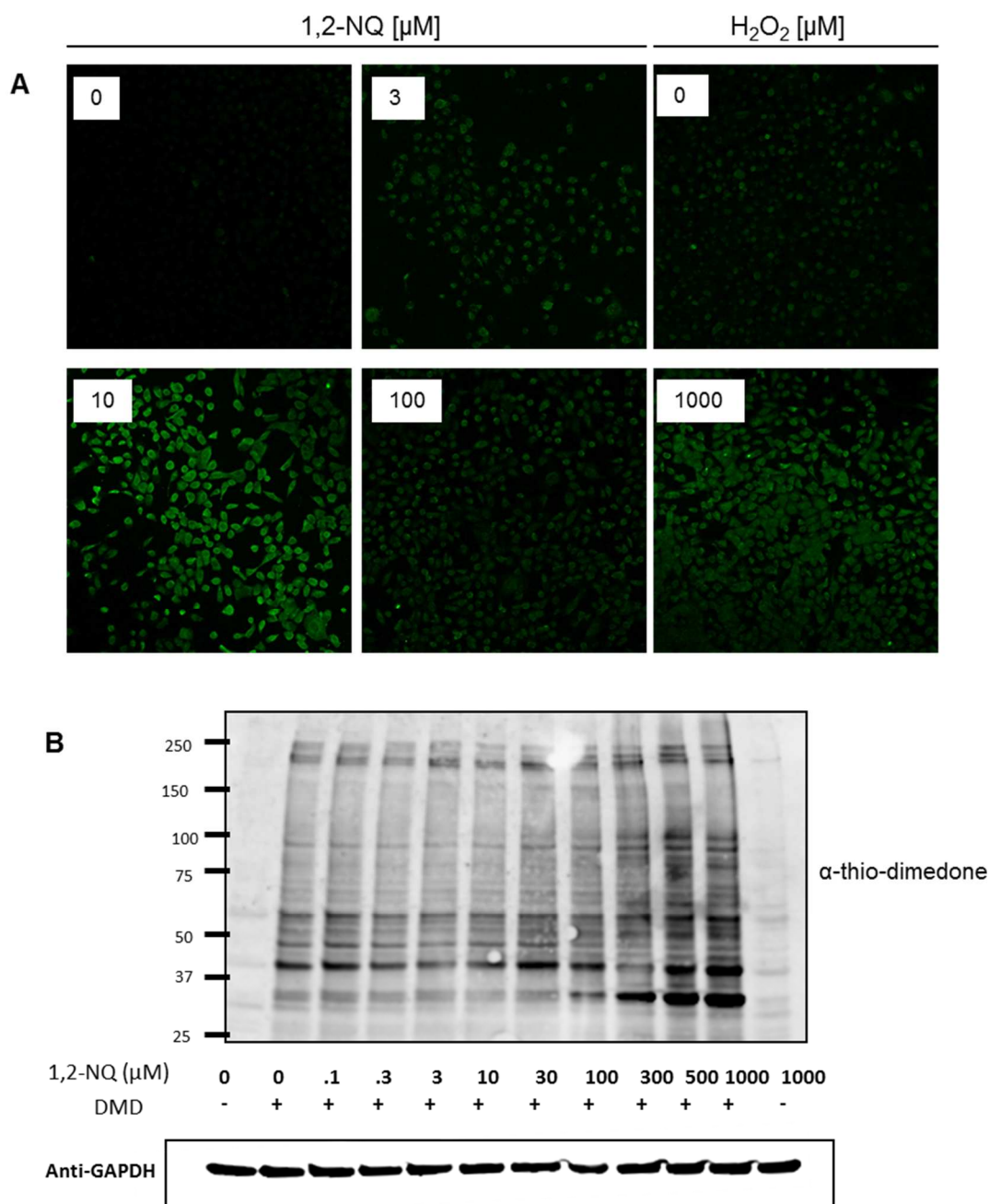


**Figure 4-8. 1,2-naphthoquinone induces intracellular protein sulfenylation.** (A) BEAS-2B cells were exposed to H<sub>2</sub>O<sub>2</sub> (0-1000  $\mu\text{M}$ ) or 1,2-NQ (0-100  $\mu\text{M}$ ) for 15 minutes, labeled with DAZ-2 followed by conjugation to FITC by Staudinger Ligation. Cells were imaged on a Nikon Eclipse C1si with laser excitation at wavelength 488 nm and emission wavelength 525/30 nm. (B) BEAS-2B were treated with indicated concentration of 1,2-NQ for 15 min. and labelled with dimedone. Cell lysates were immunoblotted for sulfenylation using anti-thio-dimedone and anti-GAPDH as a loading control. Reproduced in part with permission from the American Chemical Society. Wages, P. A., Lavrich, K. S., Zhang, Z., Cheng, W. Y., Corteselli, E., Gold, A., Bromberg, P.A., Simmons, S.O., & Samet, J. M. (2015). Protein Sulfenylation: A Novel Readout of Environmental Oxidant Stress. *Chemical Research in Toxicology*, 28(12), 2411-2418. Copyright 2015. American Chemical Society.

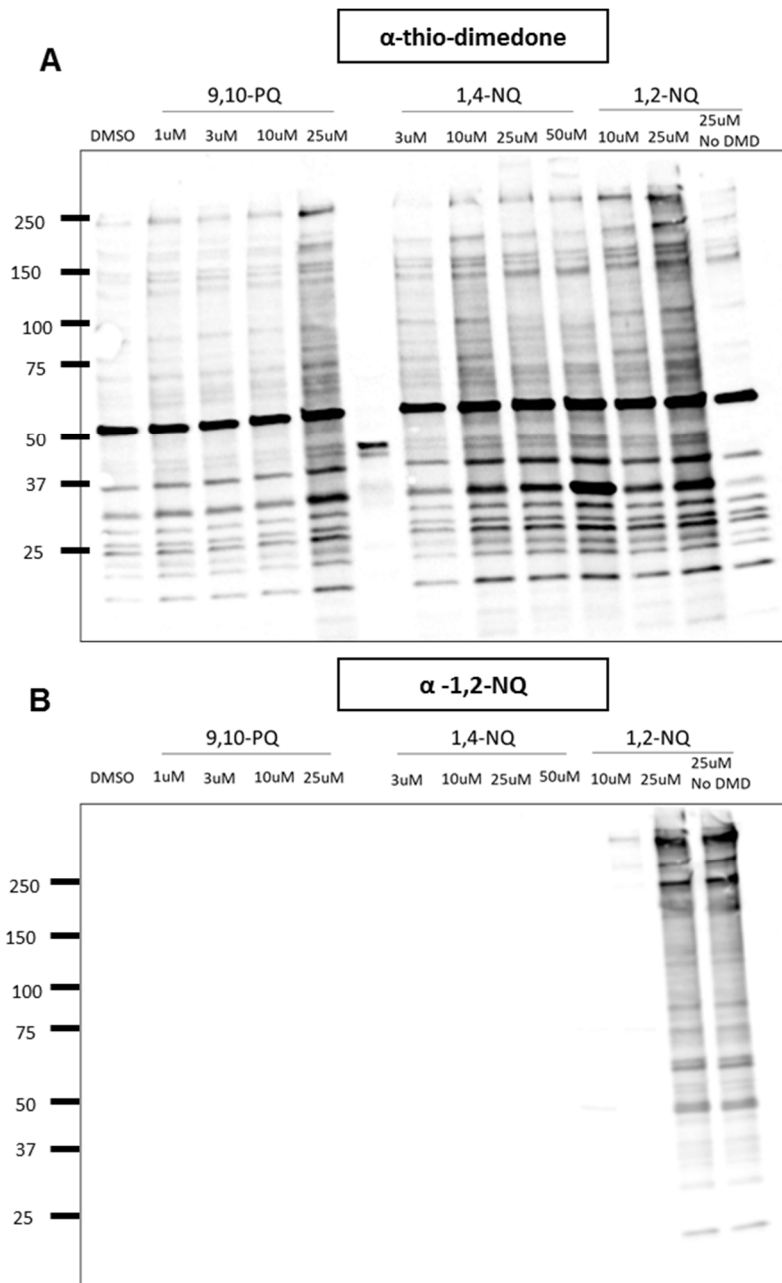


**Figure 4-9. 1,2-NQ, 1,4-NQ, and 9,10-PQ increase global sulfenylation in BEAS-2B.** BEAS-2B were treated for 15 min. with DMSO or indicated concentrations of 9,10-PQ, 1,4-NQ, or 1,2-NQ. Cells were then labelled with dimedone and immunoblotted for sulfenylation with anti-thio-dimedone and for 1,2-NQ adducts. Representative blot shown of two independent experiments.

## Discussion

We show that 1,2-NQ and other redox cycling quinones inhibit glycolytic function in cells in a peroxide-mediated manner. To our knowledge, this is the first report that exposure to environmentally relevant doses of a toxicant results in a functional inhibition of glycolysis through peroxide-mediated mechanisms. Our results here show that GAPDH is a likely target for inactivation by 1,2-NQ, either indirectly by sulfenylation or directly by adduction.

Since the extracellular flux analyzer was released about a decade ago, the glycolytic stress test has become a standard measure of glycolytic function. However, this assay has several limitations. First, an hour of glucose starvation is required to prior to assay. Glucose starvation has previously been shown to deplete NADPH levels and make potentially cells more sensitive to toxicants, particularly those known to cause oxidative stress (Gibbs-Flournoy *et al.*, 2013). In the case of quinones, the effect of glucose starvation is more complex as the redox cycling process often relies on NADPH-dependent reduction. In theory, glucose starvation could limit quinone redox cycling and H<sub>2</sub>O<sub>2</sub> production. We have previously reported that 2 hr glucose starvation blunts the increase in oxygen consumption rate (OCR), consistent with decreased quinone redox cycling (Lavrich *et al.*, 2018). In the case of quinones, glucose starvation could skew the toxicologic effects to electrophilic adduction. Additionally, the glycolytic stress test did not take into account the production of CO<sub>2</sub> in the citric acid cycle contributes to acidification in the media (Mookerjee *et al.*, 2016).

The glycolytic rate test was developed as a more relevant and accurate method to measure glycolytic activity, which was shown to directly correlate with lactate production (Romero *et al.*, 2017). This assay uses the OCR and the buffering capacity of the assay medium to calculate the proton efflux rate attributed to mitochondrial function. In this manner, the proton efflux rate due to glycolysis can be more accurately calculated. This assay also avoids the oxidative issues associated with glucose starvation, as it is performed in a medium with normal supplementation of glucose, pyruvate, and L-glutamine.

For sulfenylation detected in both recombinant GAPDH and total cells, a bell-shaped curve was observed with both dose of 1,2-NQ and exposure time. This may be explained by considering that at high

doses of 1,2-NQ or long exposure times, hyperoxidation of the sulfenic acids can occur to the sulfinic or sulfonic forms, which would not be detected by dimedone.

Our results suggest that hydrogen peroxide mediates the glycolytic inhibition caused by 1,2-NQ. Catalase, unlike peroxiredoxins, specifically breaks down  $H_2O_2$  into  $H_2O$  and  $O_2$  (Rhee *et al.*, 2005b; Perkins *et al.*, 2015). Catalase overexpression experiments in conjunction with the glycolytic stress test suggest that approximately half of the inhibition caused by 25  $\mu M$  1,2-NQ is mediated by  $H_2O_2$ . Additionally, DMNQ which only redox cycles in the cell and is not capable of adduction produced similar results to 1,2-NQ. In contrast, the potent electrophile BQ did not cause glycolytic inhibition. The potent redox cycling quinone, 9,10-PQ showed moderate glycolytic inhibition in our system, though this quinone has shown inhibition of GAPDH in other studies through both aerobic and anaerobic mechanisms (Rodriguez *et al.*, 2004; Rodriguez *et al.*, 2005).

However, additional experiments are required to more definitively show the role of sulfenylation and adduction by 1,2-NQ. To more distinctly identify the modifications of GAPDH, it could be immunoprecipitated and examined by immunoblotting for sulfenylation, GSH conjugates, or 1,2-NQ adducts. Mass spectrometry has previously shown that treatment with 0.4  $\mu M$  1,2-NQ adducts the catalytic cysteine in recombinant GAPDH (Miura *et al.*, 2011), though mass spectrometry of cellular GAPDH has not been performed. Additionally, GAPDH was immunoprecipitated from A549 cells, a adenocarcinomic human alveolar basal epithelial cell line, and examined for 1,2-NQ adducts using a similar antibody to the one we developed. However, no 1,2-NQ adducts of GAPDH were detected in the cell. Miura *et al.* (2011) detected a GSH adduct on the catalytic cysteine *in vivo* instead and attributed it to a “transarylation” reaction with GSH. Interestingly, a GSH adduct is a very likely outcome of sulfenic acid formation. Sulfenic acids are extremely unstable and very likely to form a disulfide with GSH, which is present in millimolar concentrations in the cytosol. Miura *et al.* (2011) did not control nor investigate the involvement of a  $H_2O_2$ -dependent mechanism.

Our preliminary experiment indicated that GAPDH activity is inhibited in BEAS-2B following treatment with 1,2-NQ. However, more replicates and experiments performed in the presence of catalase need to be conducted to verify that GAPDH activity is inhibited through peroxide-dependent inactivation

by 1,2-NQ. Recombinant GAPDH activity has previously been shown to be inhibited by 1,2-NQ in a dose dependent manner (Miura *et al.*, 2011).

Additionally, a GAPDH mutant developed by the Dick research group could provide more insight into the relative importance of adduction and sulfenylation in GAPDH (Peralta *et al.*, 2015). They used site-specific mutagenesis to generate a C156S mutant, where a cysteine nearby the catalytic cysteine (C152) is mutated to a serine. They have shown that this mutant is detectably less sensitive to sulfenylation at C152 by H<sub>2</sub>O<sub>2</sub>, likely do to the disruption of a proton-stabilized leaving group, which normally encourages sulfenylation. Though less sensitive to sulfenylation, the C156S mutant retains full glycolytic activity. Further experiments using both the recombinant C156S GAPDH mutant and expression of the mutant in BEAS-2B would provide valuable mechanistic insight by examining the contribution from H<sub>2</sub>O<sub>2</sub>-mediated sulfenylation of GAPDH has in 1,2-NQ-induced decrease in glycolytic activity.

From the perspective of air pollution health effects, sulfenylation may be a bigger player in an even more relevant setting. Quinones are absorbed onto the surfaces of particles. When inhaled and deposited in the lung, they likely dissolve into aqueous surfactant, which has numerous nucleophilic proteins that could be adducted. Quinones can also redox cycle in the surfactant in the presence of strong reducing agents, such as ascorbate. It is likely that only a small dose of 1,2-NQ actually reaches the epithelial airway cells. Even if only a relatively small amount of 1,2-NQ enters the cell and is capable of redox cycling, the process will continue to generate H<sub>2</sub>O<sub>2</sub> as long as reductases and/or reducing sources (e.g., NADPH) are present. H<sub>2</sub>O<sub>2</sub> is relatively long lived and can diffuse through membranes to induce an intracellular effect, even when produced extracellularly.

While GAPDH was examined as a potential target of 1,2-NQ in this study, there are a total of 9 enzymes involved in glycolysis. Of these, at least a few of them are likely targets for electrophilic adduction and/or sulfenylation by H<sub>2</sub>O<sub>2</sub> due to their thiol content. Protein kinase 2 and hexokinase have also been shown to be capable of sulfenylation (Mailloux *et al.*, 2014). Further investigation is needed to identify the glycolytic enzyme(s) affected by 1,2-NQ quinone exposure. Using our novel 1,2-NQ antibody, immunoprecipitation could be performed in conjunction with either immunoblotting or mass spectrometry to identify all potential targets of 1,2-NQ adduction. Likewise, sulfenylation detection using a dimedone analogue, like DYn-2, and subsequent biotin labelling and avidin pull-down to label the sulfenic acids in

the cell. Then, with immunoblotting and/or mass spectrometric methods, the “sulfenylome” of 1,2-NQ exposure could be determined.

Glycolytic inhibition is a functional biomarker of oxidative stress that also plays a crucial role in cellular bioenergetics and vitality. Glycolytic inhibition could be used as a novel biomarker of oxidative stress in cells. These results also could be used to suggest novel approaches to cancer therapies, as cancer cells are highly reliant on glycolysis for energy production. This study, therefore, informs our mechanistic understanding of PM-induced human health effects.

### **Summary**

Glycolysis is an essential intracellular energy process. Here, we show that the PM-associated quinones 1,2-NQ and 1,4-NQ inhibit glycolysis in the bronchial epithelial cell line, BEAS-2B. Overexpression of catalase blunted this inhibition, suggesting a hydrogen peroxide-dependent mechanism. Although sulfenylation of GAPDH is a likely mechanism underlying this effect, future studies are required to elucidate the mechanism of 1,2-NQ-induced inhibition of glycolysis.

## CHAPTER 5: ADDITIONAL EXPERIMENTS

### Normalization of Seahorse Results

#### *Introduction*

Energy metabolism and bioenergetics are key indicators of cellular function. Metabolic shifts are linked to tumorigenesis, differentiation, stress, aging, disease, and xenobiotic effects. Extracellular flux analysis is a useful tool for the study of bioenergetics. The recently developed Seahorse XFe Analyzer increased access and ease of use for non-specialists to measure bioenergetics. There is a great need for Seahorse XFe Analyzer users and other high throughput assays to normalize results to make accurate comparisons across plates, cell types, and individuals. While baselining results to the basal OCR or ECAR is very useful in some situations, especially when using cell lines, it does not accurately represent some changes in metabolism, particularly when the starting conditions vary between groups. Normalization is essential when using cells from different individuals, long-term exposure experiments, and different cell type comparisons.

The four key factors that determine mitochondrial energetic measurements include cell number, cell mass, mitochondrial mass or number, and mitochondrial complex activity. Normalization approaches for cellular populations include expression based on cell number, nuclear DNA content, and total protein. To compare differences between mitochondrial populations, mitochondrial DNA copy number, mitochondrial protein, and mitochondrial enzyme activity have been suggested (Seahorse Bioscience, 2016).

To date, there is no standardized method recommended for normalization of data generated by extracellular flux analysis with the Seahorse XFe Analyzer. Our objective was to compare different DNA and protein normalization methods to determine and pick the optimal method for use after experiments on the Seahorse XFe Analyzer. We used the bronchial epithelial cell line, BEAS-2B, and primary lung

immune cells collected by induced sputum (IS) or bronchoalveolar lavage (BAL) from healthy human volunteers for optimization.

## **Methods**

### Cell Seeding

BEAS-2B were seeded at increasing densities in a XF24 plate, leaving 4 blank wells in 100  $\mu$ L KGM. Plates were allowed to settle at room temperature for 30 min before being moved to the incubator (37°C, 5% CO<sub>2</sub>) overnight. Cells were allowed to grow overnight in the incubator.

In some experiments, innate immune cells were collected by induced sputum (IS) or bronchoalveolar lavage (BAL) from healthy human volunteers, as described in Chapter 3, following protocols approved by the Institutional Review Board at the University of North Carolina Medical School in Chapel Hill and the US Environmental Protection Agency (EPA). Informed consent was obtained from all subjects before their participation in the study. IS or BAL cells were seeded at the indicated concentration and allowed to settle for 4 hrs at 37°C in a non-CO<sub>2</sub> incubator.

Media was aspirated and plates were frozen at -80°C at least overnight. Plates were thawed at room temperature immediately prior to assay.

### BCA Assay

The Pierce BCA Protein Assay Kit was performed according to manufacturer's instructions (ThermoFisher Scientific). In-plate BCA assay was performed by adding 25  $\mu$ L of RIPA (25 mM Tris-HCl, pH 7.6, 150 mM NaCl, 1% NP-40, 1% SDS) to each well containing cells. BSA protein standards (0, 250, 500, 750, 1000  $\mu$ g/mL) were added to blank wells. Plate was incubated at 37°C for 15 min. and complete cell lysis was ensured by checking under a microscope. If a significant portion of cells were intact, a wide mouth pipette tip was used to scrape. BCA Working Reagent was prepared by mixing BCA Reagent A with Reagent B in a 50:1 dilution. After lysis, 200  $\mu$ L of BCA Working Reagent was added to each well and mixed briefly on a plate shaker. The plate was covered and incubated at 37°C for 30 min. At room temperature, absorbance at 562 nm was measured using a CLARIOstar microplate reader (BMG LABTECH, Ortenberg, Germany).

For comparison, BCA assay was also performed out of the original XF24 plate by adding 75  $\mu$ L RIPA and transferring to a 96-well plate to create three 25  $\mu$ L technical replicates. BSA protein standards (0, 50, 100, 250, 500, 750, 1000, 2000  $\mu$ g/mL) were run in triplicate.

#### DC Bradford Assay

The Thermo Scientific Pierce Detergent Compatible (DC) Bradford Assay Kit was ran in the XF24 plate, following manufacturer's instructions. 10  $\mu$ L of RIPA was added to each well containing cells. 10  $\mu$ L of BSA protein standards (0, 500, 750, 1000  $\mu$ g/mL) were added to blank wells. 300  $\mu$ L of DC Bradford Reagent was added to each well and mixed. The plate was incubated for 10 min. at room temperature and the absorbance at 595 nm was measured using a CLARIOstar microplate reader (BMG LABTECH, Ortenberg, Germany).

#### CyQuant

The CyQuant Cell Proliferation Assay was performed according to manufacturer's instructions (ThermoFisher Scientific). Briefly, CyQuant GR was diluted to 200-fold in provided cell lysis buffer. 200  $\mu$ L of the dye/cell lysis buffer mixture was added to each well. Standard DNA curve (0, 250, 500, 1000 ng/mL) was added to blank wells. Samples were incubated for 5 min. at room temperature and fluorescence was measured using a CLARIOstar microplate reader (BMG LABTECH, Ortenberg, Germany) with excitation of 480 nm and emission of 520 nm.

#### Hoechst 33324 Staining

Hoechst 33324 dye was purchased from ThermoFisher Scientific (#62249) and dye was diluted to 2  $\mu$ g/mL in PBS. Cell culture medium was aspirated and 50  $\mu$ L of dye solution was added to each well of the XF24 plate. Sample was incubated for 5-10 min. protected by light. Fluorescence was measure in plate at excitation wavelength of 361 nm and emission of 497 nm using a top or bottom read.

#### Clariostar Plate Settings

To read assays in-plate, a custom plate design was created on a CLARIOstar microplate reader (BMG LABTECH, Ortenberg, Germany) using the XF24 dimensions of Top Left X-Axis - 18.88 mm, Top Left Y-axis - 15.74 mm.

## Data display

Unless otherwise indicated, graphs are representative of one experiment and are shown as mean +/- standard deviation. Depending on assay type, 1-4 technical replicates were used for each measurement.

## **Results**

### In-plate BCA Assay provides most consistent protein values in BEAS-2B

We first seeded BEAS-2B at six increasing densities and compared the consistency of three different protein assay designs: an in-plate BCA assay, an out-of-plate BCA assay, and an in-plate DC Bradford Assay. All assays produced strongly linear standard curves using BSA ( $R^2 \geq 0.98$ ; Figure 5-1 A, C, E). When comparing total protein, the in-plate BCA assay produced the most linear results over increasing cell density. The assays held relatively consistent average protein content for each cell density, however the BCA out-of-plate and DC Bradford assays had higher standard deviation overall for each measurement (Figure 5-1B, D, E).

### CyQuant Assay provides consistent DNA content in BEAS-2B

Next, we compared two different DNA quantification methods, the CyQuant assay and Hoechst 33324 staining. BEAS-2B were seeded at increasing densities. Although a standard curve was not used for Hoechst 33324 staining, the DNA standard curve for the CyQuant Assay was highly linear ( $R^2 = 0.988$ ; Figure 5-2A). The CyQuant produced a linear increase in DNA content over increasing BEAS-2B cell density and overall variation was low (Figure 5-2B). While the variation in the Hoechst 33324 was extremely low, it did not produce a linear increase in fluorescence over cell density ( $R^2 = 0.79$ ; Figure 5-2C).

### CyQuant Assay has highest signal-to-noise ratio

To compare all assays regardless of their measurement type, the signal-to-noise ratio was calculated for each assay over increasing BEAS-2B cell density. Overall, the CyQuant assay showed the highest signal-to-noise ratio for all cell densities tested (Figure 5-3). The BCA in-plate assay had the next highest ratio.

### BAL cells can be measured by BCA-In Plate Protein or CyQuant DNA Assays

We then sought to compare protein and DNA normalization methods using primary lung cells where normalization is essential. BAL cells from the same subject were plated into XF24 plates and analyzed using the BCA in-plate protein assay or the CyQuant assay. Both assays produced strongly linear standard curves (Figure 5-4 A, C). The BCA in-plate assay produced a linear correlation ( $R^2 = 0.916$ ) between protein content and BAL cell density, though variation was high at some concentrations (Figure 5-4B). The CyQuant assay showed a linear correlation between cell density and DNA content ( $R^2 = 0.96$ ) with low variation (Figure 5-4D).

### IS cells show consistent protein content using BCA in-plate assay

To ensure that protein content could be reliably measured for IS cells using the BCA in-plate assay, IS cells from the same subject were plated into 3 wells of an XF24 plate at 60,000 cells per well. BSA standards were added to the plate and the protein content was assessed using the in-plate BCA assay. The average absorbance of the IS cells fell in the linear range of the standard curve (Figure 5-5A). The three wells produced consistent protein values (Avg. = 23.7  $\mu$ g, SD = 0.82  $\mu$ g, Figure 5-5 B).

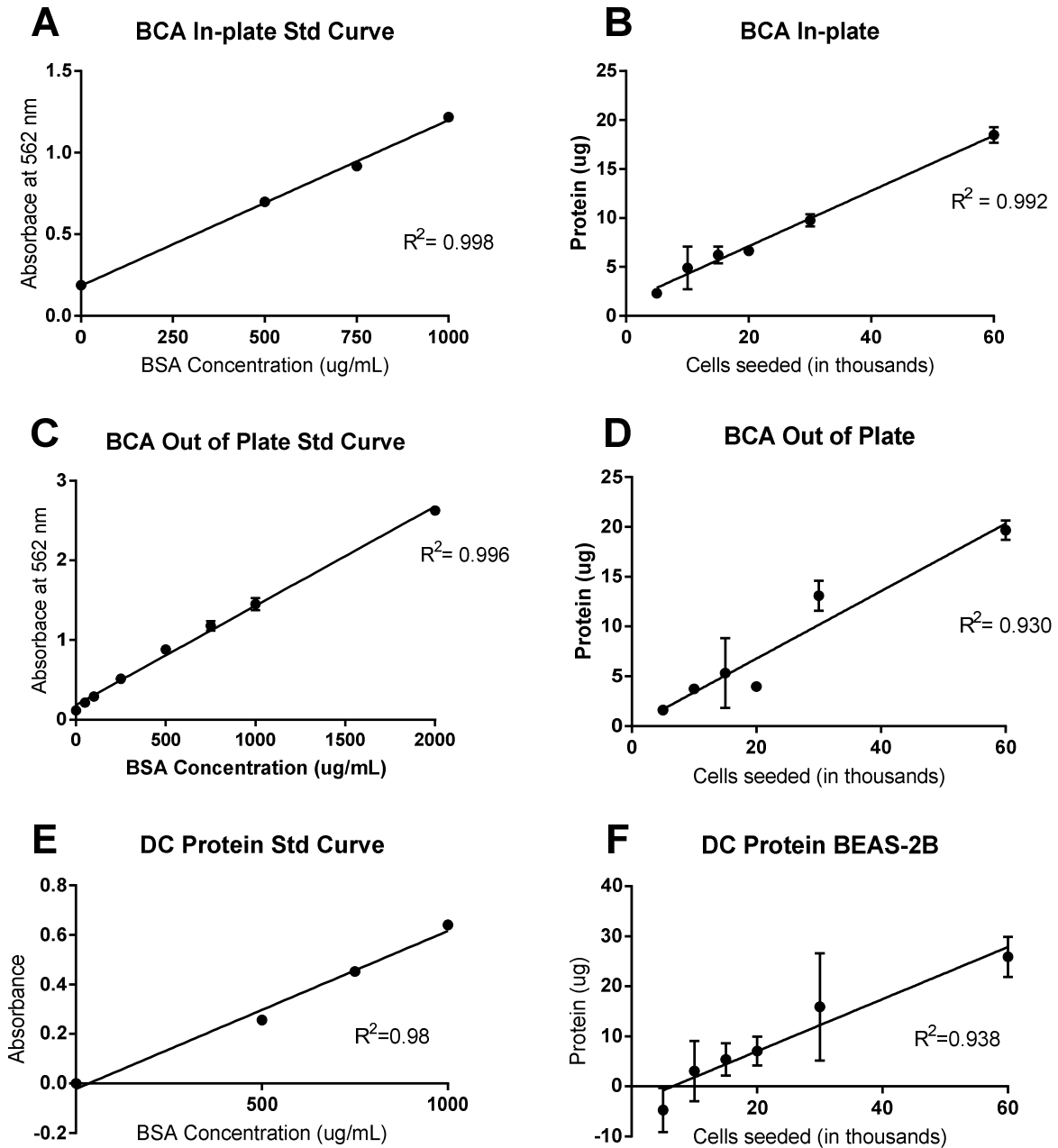


**Figure 5-1. In-plate BCA-based protein assay measures protein linearly over cell density.** BEAS-2B were seeded at indicated density in XF24 plates and allowed to settle overnight and subsequently frozen at  $-80^{\circ}\text{C}$  the next morning. Protein analysis was conducted using an in-plate BCA, out-of-plate BCA, or Detergent Compatible Bradford protein assay (B, D, F). Standard curves were performed using BSA protein standards and used to calculate total protein in samples (A, C, E).

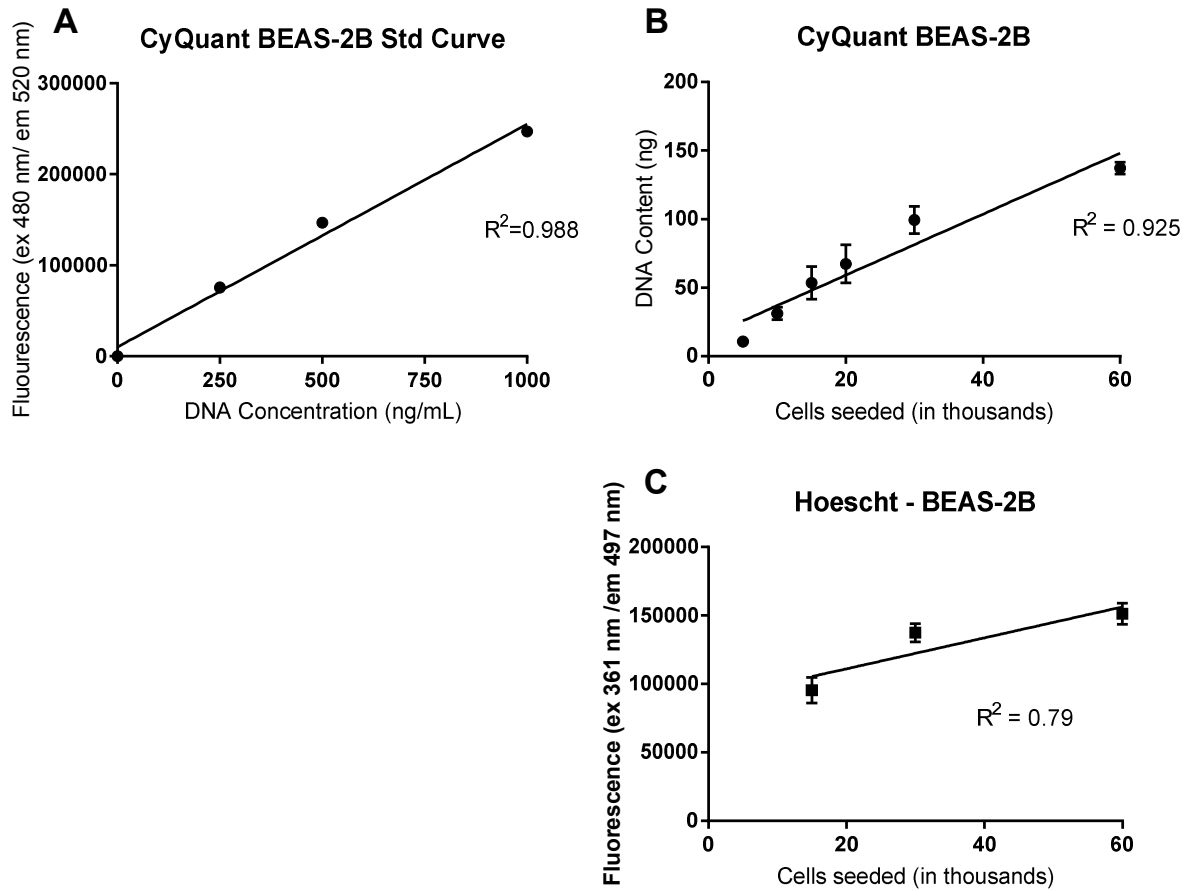


**Figure 5-2. CyQuant provides consistent linear DNA content over cell density.** BEAS-2B were seeded at indicated concentrations and allowed to settle overnight before being frozen at  $-80^{\circ}\text{C}$ . DNA content was analyzed using the (B) CyQuant assay or (C) Hoechst 33324 staining. (A) A standard curve using stock DNA was prepared for the Cyquant assay.

### Assay Comparison - Signal to Noise

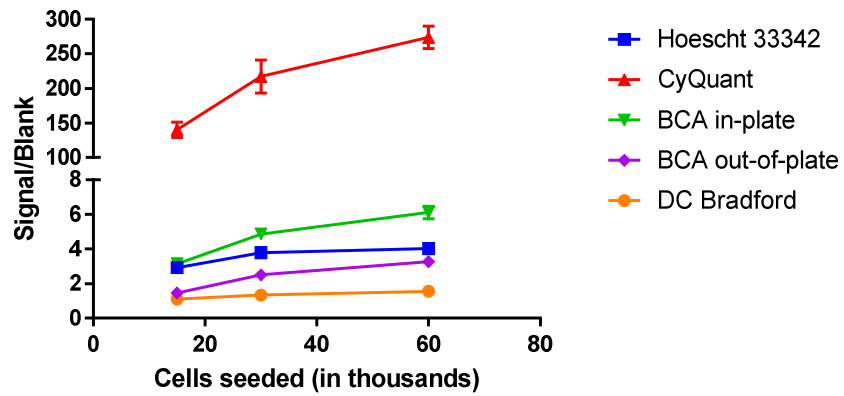


**Figure 5-3. CyQuant consistently has the highest signal-to-noise ratio.** BEAS-2B were seeded at indicated concentrations and allowed to settle overnight before being frozen at -80°C. DNA or protein content was analyzed using indicated assay. Signal-to-noise ratio was determined by dividing the sample measurements by the blank measurement.

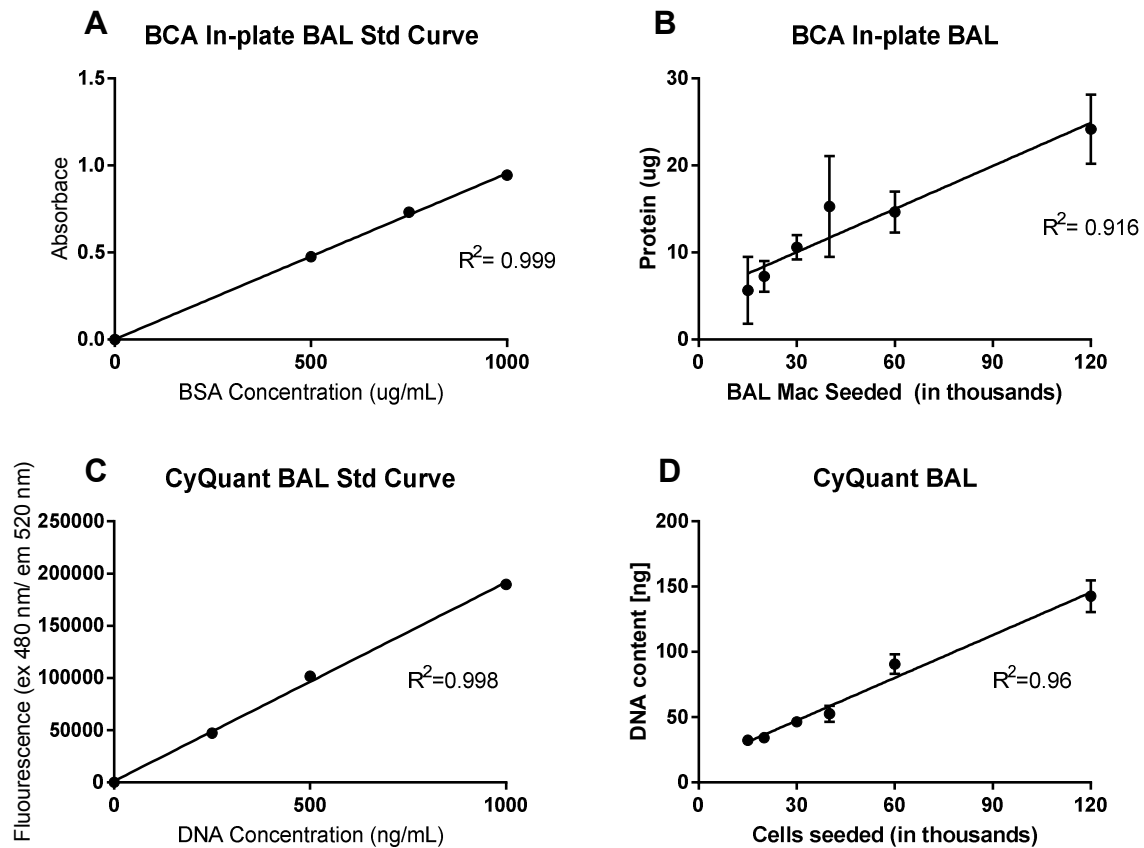


**Figure 5-4. Comparison between BCA protein and CyQuant DNA assays using BAL cells.** BAL cells from healthy human volunteers was seeded at increasing doses and allowed to settle for 4 hr before being frozen at  $-80^{\circ}\text{C}$ . Protein content was analyzed using an in-plate BCA assay and BSA standard curve (A, B). DNA content was analyzed using a CyQuant assay and a DNA standard curve (C, D).

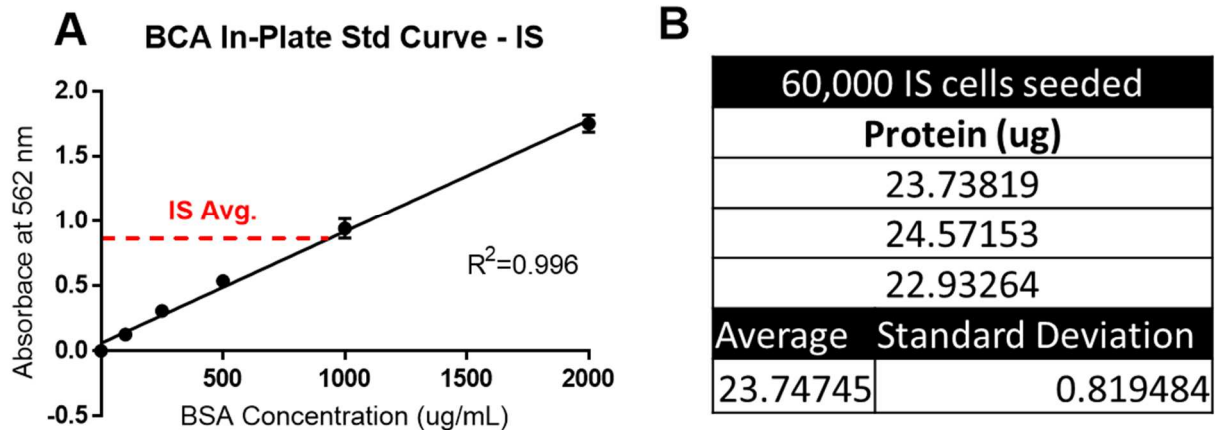


**Figure 5-5. Protein content of IS cells is consistent.** IS cells from healthy human subjects were seeded in 3 wells at 60,000 cells per well and allowed to settle for 4 hr. Protein content was determined using an in-plate BCA Assay (B) and a BSA standard curve (A). The red dotted line signifies the average absorbance of the IS cells. An average protein content and standard deviation was determined for the three wells.

### Discussion

Normalization of cell samples is essential for comparing bioenergetics results across individuals, cell types, and experimental groups. Despite the rapidly growing use of the Seahorse XFe analyzer, there is not a standard technique to perform normalization, nor are there detailed methods frequently described in the “Methods” section of publications. Here, we sought to optimize a normalization method for use after assays on the XFe24 Analyzer. Although there are several parameters that could be used for normalization, the current methodology only allows two to be practical for a project with numerous plates: protein and DNA. We tested three different protein assay designs and two DNA assay designs.

All of our assays were optimized using plates where the media had been carefully aspirated from each well and the plate was frozen at -80°C at least overnight. This was done to simulate real conditions where experiments are completed over many months to allow for batch analysis.

Protein measurement tends to be utilized more universally in publications using the Seahorse XFe Analyzer. Therefore, we sought to test out several different protein assays and designs to see which

yielded the most consistent results over a range of cell densities. The intricacies of performing the assay in-plate or out-of-plate, lysis conditions, plate storage are not typically stated. Of the protein assays tested, the in-plate BCA assay gave the highest signal-to-noise ratio and lowest variation across BEAS-2B cell densities. In addition, two of our primary cell types, BAL and IS cells, worked well with the in-plate BCA assay.

Unlike the protein assays which rely on absorbance, both DNA assays are fluorescence-based. Fluorescence is less sensitive to interference by numerous substances and tends to have a higher signal-to-noise ratio. The CyQuant assay consistently had strongly linear standard curves and minimal well-to-well variation compared to the other assays. The CyQuant assay also showed linearity between DNA content and cell density. Although a DNA standard curve was not performed for Hoechst 33342 assay, it showed less between signal and cell density.

Our choice came down to whether protein or DNA normalization was optimal for our experiments. The fact that protein is widely used would help to compare our data to existing publications and draw new conclusions. Additionally, DNA could vary greatly depending on whether a cell line or primary cell is being used, as many cell lines have acquired numerous mutations and have extra chromosomes. For example, almost 20% of the BEAS-2B cell line was characterized to have over 80 chromosomes compared to the normal 46 found in primary healthy human bronchial epithelial cells (Reddel *et al.*, 1988). Additionally, the CyQuant dye is proprietary and more expensive than the BCA reagents. In larger experiments, this cost of the CyQuant assay could be a limiting factor. However, the CyQuant assay may provide a more robust normalization method when there are no concerns regarding DNA changes between cell types and comparison to established protein-normalized data.

After preliminary experiments comparing individual well OCR or ECAR to protein levels, we did not find a strong correlation between the subtle differences when all the wells were seeded with the same cell type at the same density (data not shown). This is expected due to the natural variation in the protein assay, and lack of technical repeats. For this reason, we chose not to normalize results on a well-to-well basis but rather on an experimental group. Additional experiments are needed utilizing cell density experiments to see how well protein or DNA correlates with OCR or ECAR baseline readings.

**Summary**

The in-plate BCA assay was optimal for protein normalization of a variety of lung cell types, including a cell line and primary samples. The CyQuant assay provided consistent normalization for DNA content. Due to the broader applicability of protein normalization, we chose to use the BCA in-plate assay for future normalization of Seahorse XF Analyzer results.

## **Influence of Lung MAC Donor Characteristics on Bioenergetics**

### ***Introduction***

Recent investigation has shown the central role of bioenergetics in numerous diseases, such as cancer, neurodegenerative diseases, and arthritis (Alam *et al.*, 2016; Swerdlow, 2016; Rosas-Ballina, 2017). As bioenergetic measurements are utilized more frequently on clinical samples, it is important to understand whether demographic characteristics influence basal bioenergetics. Previous clinical studies have shown that individual characteristics, such as age, BMI, and sex, may influence mitochondrial and glycolytic parameters, but these relationships have not been extensively characterized (Karakelides *et al.*, 2010).

Few studies have utilized extracellular flux measurements to analyze these parameters. Whether these parameters influence bioenergetic parameters in lung macrophages (MAC) has also not been tested. To determine if any such relationships existed in our current study utilizing clinical lung samples (Chapter 3), basal oxygen consumption rate (OCR), basal extracellular acidification rate (ECAR), and maximal respiration was stratified according to characteristics of the donor.

### ***Methods***

The lung MAC were assayed for bioenergetic activity as they were available and were not pre-selected based on donor characteristics. Upon conclusion of experiments, subject characteristics were requested from the EPA Clinical Research Branch and the UNC-CH Environmental Medicine, Asthma and Lung Biology. For comparison between categorical groups, non-parametric analyses were used to compare bioenergetic outcomes as several distributions were not normally distributed. For numerical groups, linear regression was performed and the p-value was determined to test the hypothesis whether the slope was significantly nonzero. All statistical analyses were performed using GraphPad Prism (La Jolla, CA).

### ***Results***

#### **Basal Bioenergetics were consistent over repeated IS sampling of the same individuals**

We had three subjects who donated induced sputum (IS) samples two or three different times, separated by at least 6 weeks between procedures. We examined whether the baseline OCR and ECAR

changed at these separate sample times (Figure 5-6). Compared to the overall variance of IS MAC, the intra-individual variability remained relatively constant in the basal OCR and ECAR.

#### Race may affect IS MAC Bioenergetic Outcomes

Next, we stratified IS bioenergetic data by sex, age, BMI, and race (Figure 5-7). Data were distributed relatively evenly across the demographic parameters, except for race, where donors were predominately white. IS MAC from white subjects tended to have a significantly higher basal OCR and ECAR ( $p=0.0059$  and  $p=0.018$  respectively). This effect was reversed for maximal respiration, as IS MAC from African American donors had significantly increased maximal respiration ( $p=0.024$ ). No other significant differences were observed with the other demographic parameters. BMI tended to have a negative correlation with basal OCR and ECAR ( $p=0.064$  and  $p=0.057$  respectively).

#### Donor characteristics do not influence BAL MAC

We then examined bioenergetic data on BAL MAC for potential correlations with the demographics of the donor (Figure 5-8). Donors were relatively evenly distributed between male and female and across ages (within our subject criteria of 18-40). BMI tended to cluster around 29. While donors were evenly distributed between black and white, other races were not adequately represented. Overall, no significant differences were observed between donor demographic parameters and BAL MAC basal OCR, ECAR, nor maximal respiration.

#### No differences seen in donor characteristics of BF MAC

BF donor distributions mirrored that of BAL MAC, though race was limited to only black and white. Similar to BAL MAC, no significant correlations were seen between BF MAC bioenergetic parameters and subject characteristics (Figure 5-9). However, BF MAC maximal respiration appeared to increase with age ( $p=0.09$ ).

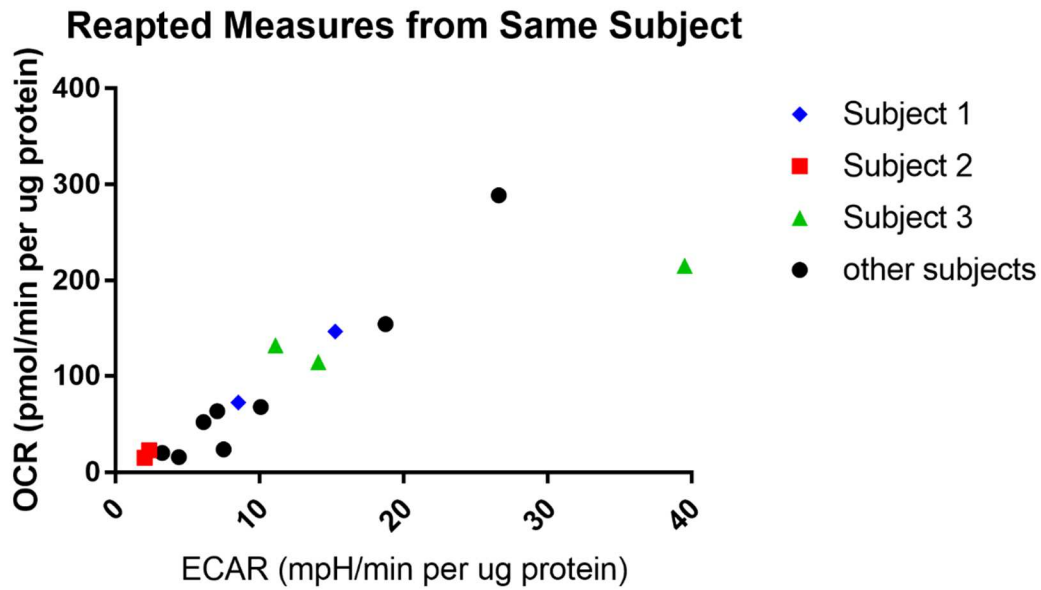


**Figure 5-6. IS cells from same subject have similar bioenergetic profile.** The basal extracellular acidification rate (ECAR) and oxygen consumption rate (OCR) was plotted for cell obtained by induced sputum (IS) from each subject. Two of the subjects donated IS samples at two separate occasions (Subject 1 and 2). One subject donated IS samples on three separate occasions (Subject 3). Repeated IS sampling was separated by at least 6 weeks between procedures. Other subjects who donated once are shown for comparison. All OCR and ECAR values were normalized to total protein for that day.

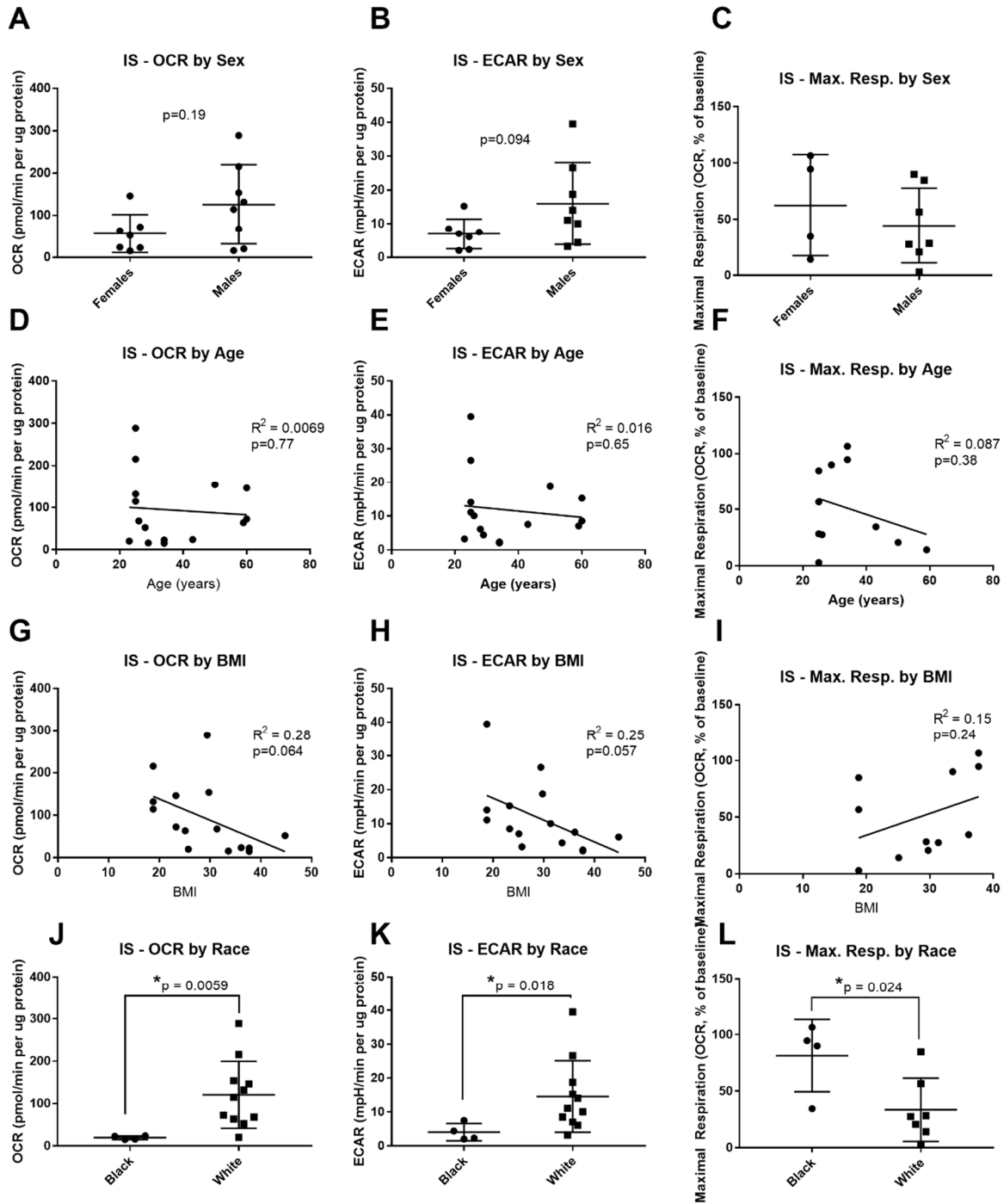


**Figure 5-7. Race may affect the bioenergetics of MAC from central airways.** Basal OCR, ECAR, and maximal respiration of IS cells was analyzed by subject Sex (A-C), Age (D-F), BMI (G-I), and Race (J-L). Repeat donors were included as separate measurements. A Mann-Whitney test was used to compare Sex and Race categories. Significant differences ( $p < 0.05$ ) were found between races for basal OCR, ECAR, and maximal respiration. Age and BMI were analyzed using linear correlation. No significant differences were found in any other parameter.

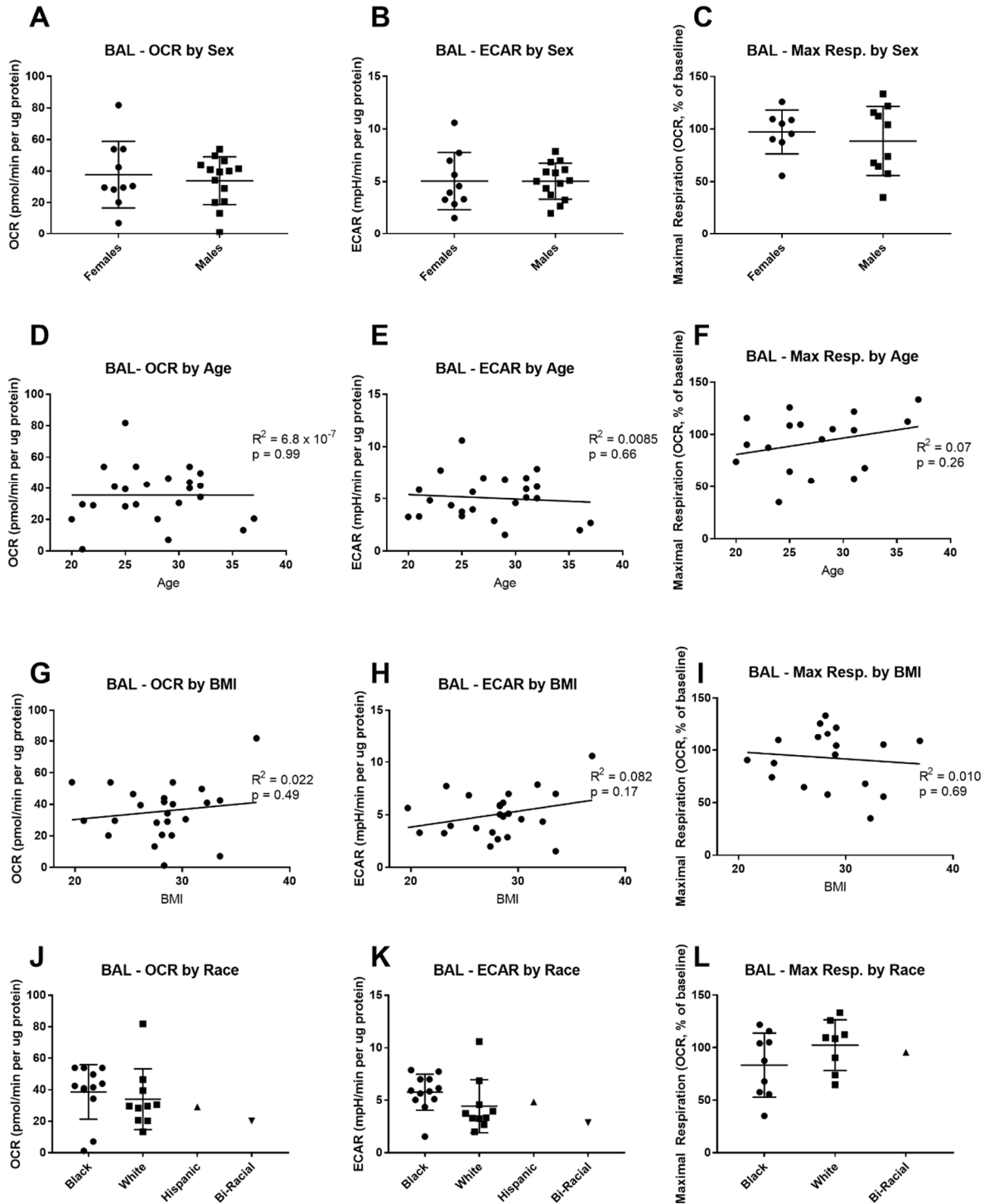


**Figure 5-8. BAL MAC Bioenergetic Outcomes and donor characteristics.** Basal OCR, ECAR, and maximal respiration of BAL cells was analyzed by subject Sex (A-C), Age (D-F), BMI (G-I), and Race (J-L). A Mann-Whitney test was used to compare Sex group differences. Age and BMI were analyzed using linear correlation. Race was analyzed by a one-way ANOVA for differences between groups. No significant differences were found in any parameter.

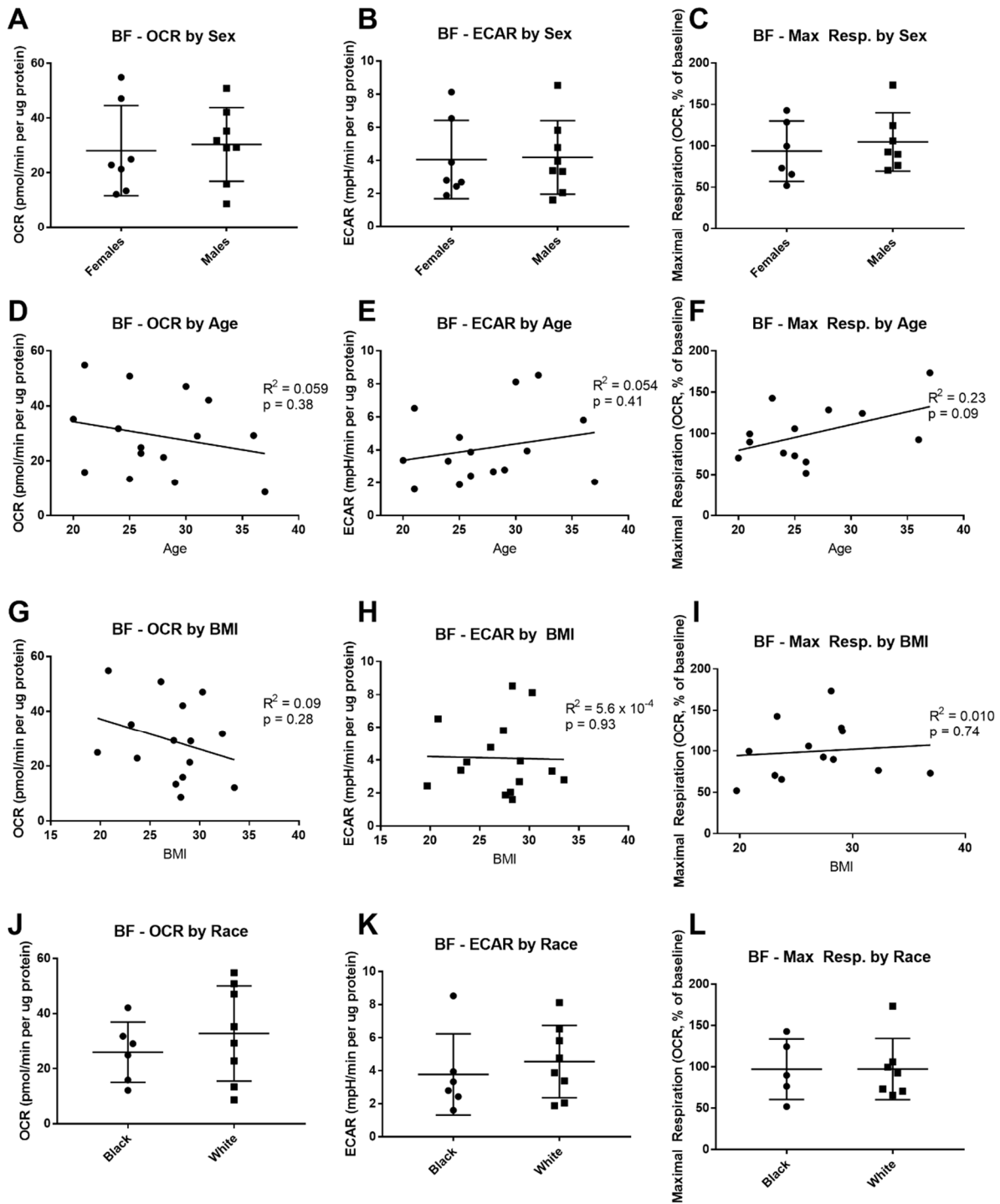


**Figure 5-9. BF MAC Bioenergetic Outcomes and Donor Characteristics.** Basal OCR, ECAR, and maximal respiration of BF cells was analyzed by subject Sex (A-C), Age (D-F), BMI (G-I), and Race (J-L). A Mann-Whitney test was used to compare Sex and Race group differences. Age and BMI were analyzed using linear correlation. No significant differences were found in any parameter.

### ***Discussion/Summary***

The effect of donor characteristics on lung immune cells has yet to be fully characterized. We analyzed the effect age, race, sex, and BMI may affect baseline bioenergetic parameters in a relatively small sample size (n = 15-25). Unsurprisingly given the limited sample size, most of the demographic parameters were not associated with any bioenergetic differences in IS, BAL, or BF MAC.

However, there was a significant correlation between race (Black vs White) and IS MAC bioenergetics. If the correlation is indeed true, it may mean the IS MAC from white donors overall have more energetic (ECAR and OCR) than black donors. However, IS MAC from black donors have increased maximal respiration over those from white donors, indicating that IS MAC are still highly functional. Due to the skewing of donors (more white than black), a larger, more balanced study needs to be performed to elucidate these effects.

The trends observed here need to be verified in larger studies. The preliminary data presented here could be useful in power calculations to design future studies to examine the role different demographics may have on basal bioenergetic parameters.

## CHAPTER 6: CONCLUSIONS, PERSPECTIVES, AND FUTURE DIRECTIONS

The research presented in this dissertation suggests that an inherent link between bioenergetics and redox signaling plays a central role in maintaining cellular homeostasis and is thus a vulnerable target for toxicants, such as PM-associated quinones.

### **The Oxygen Paradox: Linking Redox and Bioenergetics**

Bioenergetic processes and redox signaling have been intrinsically linked since the introduction of O<sub>2</sub> into Earth's atmosphere approximately 2.5 billion years ago, which led to the great paradox that is aerobic oxidation. As O<sub>2</sub> slowly increased to the current 21% of atmosphere, selective pressure favored organisms that relied on the reduction of O<sub>2</sub> instead of H<sub>2</sub> to create energy. Mitochondria were developed as an evolutionary beneficial symbiotic relationship between O<sub>2</sub>-consuming bacteria and a eukaryotic cell. With the immense energy produced by mitochondria and aerobic respiration, cells and organisms evolved to be more complex and advanced than their ancestors. Over the evolutionary timeline, roughly 300 million years ago, lungs were developed for efficient gas exchange in air, taking in O<sub>2</sub> and releasing CO<sub>2</sub> (Benzie, 2000; Rogers and Cismowski, 2017). While O<sub>2</sub> played a pivotal role in the evolution of numerous higher species, including humans, aerobic respiration also leads to destruction.

### ***Metabolism as key producer of ROS***

Aerobic respiration is not a perfect process and electrons tend to prematurely leave the defined metabolic reactions (Figure 6-1). The mitochondrial electron transport chain is notably inefficient and is directly linked to ROS production. ROS are produced in the mitochondria as electrons either have off-target effects on nearby molecules or directly by mitochondrial enzymes. Though Complex I and III have been typically named as the key generators of mitochondrial H<sub>2</sub>O<sub>2</sub>, at least 7 sites of H<sub>2</sub>O<sub>2</sub> formation have been identified so far in the mitochondria (Brand, 2010). Many of these enzymes are essential in carbon metabolism, further linking metabolism and redox signaling. The primary source of electrons in the mitochondria is NADH, which is produced by the Krebs's cycle, and ubiquinone QH<sub>2</sub> and utilized by

Complex I and II. The normal metabolism of carbohydrates, lipids, and proteins leads to primarily NADH generation through the Krebs's cycle. Though NADH is usually oxidized as part of the electron transport chain to drive oxidative phosphorylation, premature reduction of O<sub>2</sub> leads to O<sub>2</sub><sup>•-</sup> production, and subsequently H<sub>2</sub>O<sub>2</sub>. Through the generation of ROS, namely H<sub>2</sub>O<sub>2</sub>, cellular redox signaling can be initiated by nutrient metabolism.

H<sub>2</sub>O<sub>2</sub> levels, therefore, will be highest at sites of production within the mitochondria. This could create a gradient of oxidized antioxidants around the site of H<sub>2</sub>O<sub>2</sub> production. As such, where H<sub>2</sub>O<sub>2</sub> is produced could greatly influence the signaling effects. Although H<sub>2</sub>O<sub>2</sub> is typically released into the mitochondrial matrix, different tissues have varying preferences for metabolic substrates, which influences where H<sub>2</sub>O<sub>2</sub> is produced. As hypothesized by Dean Jones, nutrients and metabolism create a spatiotemporal flux of H<sub>2</sub>O<sub>2</sub> production and subsequent signaling as part of the "Redox Code" of cells (Jones and Sies, 2015).

At very high levels, ROS lead to destruction of vital cellular structures, including DNA, protein, and lipids, and can cause cell death. This harmful role of O<sub>2</sub> is especially relevant in the lung, as the key site of O<sub>2</sub> exchange. An estimated 2% of all inhaled oxygen is converted into ROS (Domej *et al.*, 2006) (Domej 2014). Insufficient O<sub>2</sub> leads to reductive stress, including impaired function of the mitochondrial electron transport chain. This introduces an oxygen paradox in which life depends on the unique chemical reactivity of O<sub>2</sub> for aerobic life, but that same reactivity damages the cell. Over time, this damage, characterized as aging, leads to senescence and death of the organism (Sthijns *et al.*, 2016).

### ***Co-evolution of antioxidant processes***

Since molecular O<sub>2</sub> and resulting ROS produced by metabolism can be potent toxins in the cell, antioxidant defenses developed evolutionarily alongside aerobic metabolism. Organisms that could defend themselves or limit harmful ROS were evolutionarily selected for. Metabolism also has the inherent link to the antioxidant systems through the production of NADPH. As previously mentioned, NADPH is primarily generated through the processing of glucose in the pentose phosphate pathway. NADPH is crucial for the regeneration of numerous antioxidant systems. As mentioned previously, inactivation of GAPDH serves as an essential redox switch to shunt glucose through the pentose phosphate pathway and replenish NADPH pools.

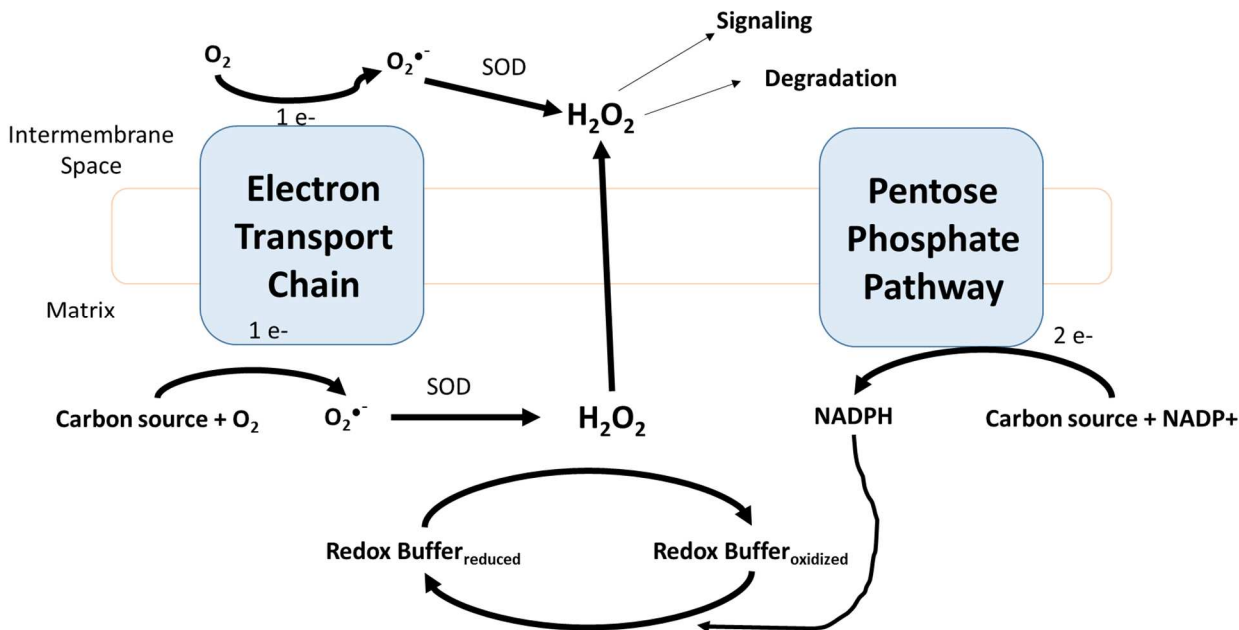


**Figure 6-1.** Inherent link between metabolism and redox signaling occurs in the mitochondria. Adapted from (Mailloux et al., 2013).

### Defining Redox Toxicology Mechanisms Using Bioenergetics

#### ***Mitochondria as an initiator of xenobiotic-induced oxidative stress***

Under physiologic conditions, mitochondria are a key source of intracellular ROS. Previous studies have focused on antioxidants targeted to the mitochondria showing altered cellular growth and gene expression, highlighting the vital role of mitochondrial ROS in redox biology (Mailloux *et al.*, 2014). Xenobiotics can disrupt mitochondrial redox homeostasis, often leading to increased ROS production in the mitochondria. Since mitochondria have the highest concentration of thiol groups among organelles, they are extremely susceptible to electrophilic attack by a toxicant. The glutathione redox potential is lower in the mitochondrial matrix, making it more likely that these protein cysteines are reduced and susceptible to attack by an electrophile or  $H_2O_2$ , despite potential steric hindrance (Smith *et al.*, 2016). Mitochondrial proteins adducted by potent electrophiles, such as aldehydes, have been shown to decrease their activity and in return, lead to an increase in ROS production, as electrons are more likely to leave the defined transfer pathway when it is slowed (Aitken *et al.*, 2012).

### ***Mitochondria as a target of xenobiotic-induced oxidative stress***

Mitochondria are also sensitive to external oxidative stress. As mentioned previously, numerous key mitochondrial enzymes are regulated by redox switches, inherently linking oxidative phosphorylation function to oxidative stress in the cell. If H<sub>2</sub>O<sub>2</sub> is generated in large quantities extra-mitochondrially, such as through redox cycling of a xenobiotic, key mitochondrial enzymes could be inactivated and generate increased ROS. This cycle of H<sub>2</sub>O<sub>2</sub> and mitochondrial dysfunction could lead to overt oxidative stress and adverse cellular outcomes.

Mitochondria are also a major target for nitric oxide (NO) signaling and S-nitrosylation. NO is an important gaseous second messenger with a central role in vasodilation. In the mitochondria, NO binds the heme or copper group of Complex IV, decreasing oxidative phosphorylation. Additionally, several mitochondrial proteins have been modified by S-nitrosylation when NO binds free thiol groups, including Complex I, ATP synthase, TCA cycle enzymes, and  $\beta$ -oxidation enzymes (Mailloux *et al.*, 2014; Mailloux and Treberg, 2016). However, the mechanisms underlying S-nitrosylation and mitochondrial sources of NO are still debated. Toxicants that induce NO production could affect mitochondria in this way.

One of the hallmarks of mitochondrial toxicity is the opening of the mitochondrial transition pore (MPTP). Opening of this pore dissipates the highly regulated membrane potential and initiates apoptotic signaling. Although there is some evidence that MPTP opening is induced by S-glutathionylation of ANT, there is still much debate and many questions about the role of redox signaling in this process (Mailloux and Treberg, 2016). If the MPTP is opened either through toxicant-induced oxidative stress or electrophilic mechanisms, apoptosis could be induced in the cell.

### ***Quinones and mitochondria***

As demonstrated, mitochondria are a part of the complex redox system in the cell, which is highly controlled at normal physiological conditions to keep the system functioning. Toxicants can easily disrupt mitochondrial function through uncontrolled and nonspecific reactions. Quinones could have a significant impact on mitochondria, both directly through adduction and indirectly through H<sub>2</sub>O<sub>2</sub> production by redox cycling.

Our lab had previously detected 1,2-NQ increased mitochondrial H<sub>2</sub>O<sub>2</sub>, but it was not certain whether this was a direct effect of 1,2-NQ on mitochondria or a byproduct of H<sub>2</sub>O<sub>2</sub> production elsewhere.

Here, we sought to better define the effect of 1,2-NQ on the mitochondria (Chapter 2). In isolated mitochondria and in permeabilized cells, where the redox cycling of 1,2-NQ was minimized, we observed substantial decrements in Complex I-linked substrate oxidation, but downstream mitochondrial function was not affected. 1,2-NQ adducts were detected in mitochondria isolated from cells that were exposed to 1,2-NQ when they were intact. This suggests that 1,2-NQ directly targets mitochondrial enzymes to inhibit mitochondrial function, thereby increasing ROS production. We then confirmed that 1,2-NQ induced mitochondrial dysfunction in primary lung macrophages (Chapter 3).

These results suggest that 1,2-NQ has the potential to cause direct effects on the mitochondria, likely through electrophilic adduction of key thiols, which could increase H<sub>2</sub>O<sub>2</sub> production. However, it is still unclear whether this mechanism occurs in an intact cellular system. Further experiments are needed to better clarify whether 1,2-NQ-induced mitochondrial dysfunction is an initiating event or a byproduct of oxidative signaling mechanisms elsewhere. First, the mechanism of substrate oxidation inhibition by 1,2-NQ in the mitochondria should be detailed in a permeabilized cell system. Mitochondria can be analyzed for 1,2-NQ adducts using mass spectrometry to determine exactly which proteins are being targeted and whether these adducts would have a functional inhibition of the enzymes. Addition of catalase into the substrate oxidation assays could more definitively determine the role of H<sub>2</sub>O<sub>2</sub> in these processes. Follow-up experiments should analyze proteins for sulfenylation modifications if a significant role of H<sub>2</sub>O<sub>2</sub> is detected, potentially through modified dimedone probes that localize to the mitochondria (McLain *et al.*, 2013). Although substrate oxidation experiments are not easily performed in intact cells due to the impermeability of ATP, the protein alterations detected in permeabilized cell experiments could be verified in intact cells, eventually primary airway epithelial cells.

### ***Identifying Role of H<sub>2</sub>O<sub>2</sub> in Mitochondrial Redox Signaling and Beyond***

Although H<sub>2</sub>O<sub>2</sub> is known to play a central role in mitochondrial signaling, it is still unclear how H<sub>2</sub>O<sub>2</sub> serves as second messenger in redox biology. This uncertainty limits the predictive ability of measuring H<sub>2</sub>O<sub>2</sub> in response to environmental exposures. There are three main concerns that challenge the direct role of H<sub>2</sub>O<sub>2</sub> in redox signaling. H<sub>2</sub>O<sub>2</sub> has weak interactions with most nucleophilic protein thiols, and the thiol needs to be in a unique microenvironment to encourage thiolate formation (Poole, 2015). Secondly, there are abundant peroxidases, including peroxiredoxin, glutathione peroxidase, and catalase

found in the cell with relatively high reaction rates ( $\sim 10^7 \text{ M}^{-1}\text{s}^{-1}$ ) that would rapidly scrub  $\text{H}_2\text{O}_2$  (Rhee *et al.*, 2003). Peroxidases are found to be particularly concentrated in mitochondria, therefore a direct role of  $\text{H}_2\text{O}_2$  causing mitochondrial redox changes is less likely. Lastly, sulfenic acids are known to be highly unstable and are documented to react with other electrophilic groups at rates  $>10^5 \text{ M}^{-1}\text{s}^{-1}$  (Mailloux and Treberg, 2016). There is concern that sulfenylation lacks the specificity needed to be the key regulatory intermediate in redox signaling.

Two main theories have been proposed for how  $\text{H}_2\text{O}_2$  mediates signaling – the flood-gate hypothesis and the chaperone theory. Briefly, the flood-gate hypothesis proposes that close to the source of  $\text{H}_2\text{O}_2$ , most of the peroxidases would be oxidized and not readily regenerated due to the high concentration of  $\text{H}_2\text{O}_2$ . The farther from the  $\text{H}_2\text{O}_2$  source, the more antioxidant resources are available and the effects of  $\text{H}_2\text{O}_2$  are less likely to be observed. However, this would mean that all peroxide-dependent changes in signaling would need to occur very close to the source of  $\text{H}_2\text{O}_2$  generation, which may be the case in some instances, but perhaps not all (Karplus, 2015). The competing theory is that some other protein chaperone is first generated through oxidation by  $\text{H}_2\text{O}_2$  and that in turn alters the redox sensitive pathways. However, it is not understood which proteins or modifications relay that signal. Peroxiredoxins (Prxs) have been proposed to play a crucial role in mediating redox signaling from  $\text{H}_2\text{O}_2$  production to having a direct effect on redox switches (Karplus and Poole, 2012). There is evidence that S-glutathionylation (S-GSH) may be the direct modifier of redox signaling.  $\text{H}_2\text{O}_2$  flux directly influences changes in GSH/GSSG (Mailloux and Treberg, 2016). Additionally, glutaredoxins (Grx) can enzymatically mediate S-GSH transfers. There are two known Grxs, Grx1 found in the cytosol and intermembrane space of the mitochondria and Grx2, found in micromolar concentrations in the mitochondrial matrix. Grx2 has been shown to be directly regulated by ROS. In the mitochondria, proteins known to undergo S-GSH modifications include Krebs cycle enzymes, OXPHOS enzymes, solute anion carriers, antioxidant enzymes, and proteins that control mitochondrial shape. Clarification of the basic mechanisms underlying redox signaling will improve biological detection and allow toxicologists to identify oxidative initiating events, leader to improved adverse outcome pathway modeling.

### **Role of Quinones in PM-Induced Health Effects**

The studies presented in this dissertation, we used the ubiquitous 1,2-NQ as model of quinones found in PM to investigate mechanisms of oxidative stress. We showed that 1,2-NQ disrupts multiple redox-sensitive processes, including mitochondrial function and glycolysis. However, we used *in vitro* and *ex vivo* techniques for these observations and must consider how likely these effects are to occur in human lungs.

#### ***Dose of Quinones***

A previous estimation calculated that a 3 hr exposure to diesel exhaust (e.g., at a bus depot) could result in human airway epithelial cells experiencing concentrations of 1,2-NQ between 0.6 and 6  $\mu\text{M}$  (Cheng *et al.*, 2012). This calculation does not take into account naphthalene metabolism. Naphthalene is the most abundant organic component of ambient air and can be rapidly converted in airway cells to 1,2-NQ through cytochrome P450 oxidation (Zheng *et al.*, 1997; Lanza *et al.*, 1999). However, better measurements of the P450 activity in human airways is required to more accurately estimate the capacity of bronchial epithelial cells to generate 1,2-NQ from naphthalene. Moreover, PM contains a varied mixture of multiple quinone species and precursors to which *in vivo* airway epithelial cells are exposed simultaneously (Mastral and Callen, 2000; Alves *et al.*, 2015). The quinones found most abundantly and frequently across sampling sites are 1,2-NQ, 1,4-NQ, 9,10-PQ, and BQ.

In addition to quinones, other PM components are redox active, electrophilic, or have known oxidative effects. For example, zinc is a redox inert metal that is extremely electrophilic. Previous studies have shown that  $\text{Zn}^{2+}$  increases cytosolic and mitochondrial  $\text{H}_2\text{O}_2$  inhibits Complex IV of mitochondria, and activates Nrf2 signaling by binding Keap1 and subsequent HO-1 induction (Wages *et al.*, 2014). Iron is another prevalent transition metal frequently found in PM and has strong redox cycling capability (Samet and Wages, 2017).

These components all contribute to the overall redox potential of PM. Additional dose modeling is needed to gain a more accurate concentration of the total redox and electrophile burden experienced by airway epithelial cells during PM exposure. Though the experiments in this dissertation utilize 1,2-NQ as a model, it would be more relevant would to use concentrated ambient particulate (CAPs) or diesel exhaust particles (DEP), as their composition is more similar to ambient PM. Studying the impact of mixtures is

complicated by the varying composition of test CAPs or DEP. To begin to understand the synergistic role of mixtures in PM, intermediate experiments could utilize varying mixtures of quinones and/or PAHs in environmentally relevant proportions tested in metabolically competent cells.

### ***Adduction vs Redox-Cycling Peroxide-Mediated Toxicity***

One quinone equivalent can generate multiple equivalents of superoxide, eventually  $H_2O_2$  and overwhelm the protective antioxidant systems. Additionally, 1,2-NQ can continue to redox cycle when adducted if it has access to reducing electrons. A “fixed” redox cycling quinone on a protein or other macromolecule may be longer lived and be more directly toxic locally to that protein (Monks *et al.*, 1992) (Monks and Lau, 1992). It is likely that at low, environmentally relevant doses in terms of ambient PM,  $H_2O_2$  production plays a bigger role than adduction in adverse cellular effects.

While we studied this question in the terms of purified 1,2-NQ, ambient PM contains a mix of quinones with varying propensities for redox cycling and adduction. Flavoproteins are the most likely one-electron reductants in the cell, with the optimal reducing potential range between -0.27 and -0.16V based on thermodynamic consideration of electron transfer from cytochrome p450 reductase and reduction of  $O_2$  by a reduced quinone (O'brien, 1991; Rodriguez *et al.*, 2004). 1,4-benzoquinone has a large redox potential that exceeds the range significant for redox cycling (0.1 V compared to normal hydrogen electrode) and therefore its toxicity is largely to be considered due to its electrophilic properties. On the other hand, 9,10-phenanthrenequinone (9,10-PQ) has a redox potential of -0.12V and is a potent redox cyclers (Brunmark and Cadenas, 1989). This means that both electrophilic and redox cycling likely both contribute to the associated toxicities of PM.

### ***Acute vs Chronic Exposure***

It is important to understand how oxidative stress can go from an initiating mechanism to health effects when evaluating the toxicity of a compound. In this dissertation, I examined the acute effects of a potent  $H_2O_2$  producer. However, less is known about the chronic effects of low doses of pro-oxidants, such as PM-associated quinones. Since the KEAP1/Nrf2 has been shown to be activated in response to 1,2-NQ in bronchial epithelial cells, genes with the antioxidant response element will be activated. Chronic oxidative stress could continue to induce transcriptional, epigenetic, and potentially genomic

changes (Stijns *et al.*, 2016). Insights from long term adaption of cells to oxidative stress could be useful in predicting those toxicities.

### **Translating bioenergetics as a marker of redox disruption**

Since bioenergetics is intimately linked to oxidative stress as both a direct target and a secondary propagator, measurements could be especially useful as a biomarker of oxidative stress induced by environmental toxicants. Additionally, bioenergetics is involved in pathology of numerous diseases and could be a potential diagnostic measure of disease. The central and adaptive role of bioenergetics in environmental health makes it an attractive translational research area to further understand xenobiotic-induced health effects on both an individual and public health scale.

### ***Limitations in translating redox markers***

Although new technologies are being developed to investigate the role of redox signaling using *in vitro* methods, these methods have limited translation to more relevant primary human cells or clinical samples. For example, the most specific and accessible sensor to detect H<sub>2</sub>O<sub>2</sub> is the genetically-encoded sensor HyPer. However, the recombinant protein has been shown to be unstable and primary cells are notoriously resistant to gene transfer techniques (Belousov *et al.*, 2006).

This dissertation and previous work in our lab has shown the utility of protein sulfenic acids as powerful biomarker after xenobiotic exposure of H<sub>2</sub>O<sub>2</sub> production and indicative of potential outcomes (Wages *et al.*, 2015). While we used dimedone and its analogues to detect sulfenic acids, due to long incubation of dimedone or similar analogues and need of large amounts of starting material, it may not be amenable to detection in clinical samples.

### ***Translational Bioenergetics***

Advances in extracellular flux technology, especially the development of the Seahorse XFe Analyzer, has been critical in advancing the study of bioenergetics both in normal physiology and in response to toxicants. The technology is easily adaptable to numerous physiological systems and experiments are customizable to examine specific bioenergetic questions.

Because of these benefits, extracellular flux analysis has lent itself to translational research. The XF Analyzer has great promise into becoming a translational marker of bioenergetics function. The Darley-Usmar group is investigating how to use the bioenergetics profiles of cells isolated from 10-20 mL

of human blood to provide crucial insights into innate immunity and numerous diseases (Chacko *et al.*, 2014). To this end, they have developed a new parameter termed the “Bioenergetic Health Index,” (BHI) which provides a single number to encompass four different mitochondrial parameters that can be easily measured in a medium-to-high throughput manner. They showed that low doses of the redox cycling quinone, DMNQ, caused a measurable increase in BHI in human monocytes (Chacko *et al.*, 2016). Extensive validation of what is “normal” bioenergetic function is needed, especially since it is not known how individual characteristics influence bioenergetics. The ideal outcome is that BHI becomes a new health index that could allow physicians to quickly assess mitochondrial function and diagnose either disease development or exposure to toxicants. One limitation to more widespread use of this technology is the need for a standard normalization technique to compare across laboratories or cell types. In this dissertation, I optimized protein normalization techniques (Chapter 5), which could be readily adaptable to numerous projects and cell types.

The development of a quick and meaningful marker of bioenergetic function could greatly impact disease treatment and prevention at both the individual and public scale. Inter-individual susceptibility to xenobiotic-induced health effects is still largely not well understood. Bioenergetics could play a key role as to why certain people are more or less susceptible to certain chemicals at certain times of their lives. Additionally, the development of modulation of bioenergetic function, either through pharmaceuticals or nutritional supplements, could serve as public health strategies to prevent diseases. While the possibilities seem endless in the utilization of individualized bioenergetic translation, much more research is needed to directly link different health outcomes or environmental exposures to changes in bioenergetic function.

### ***Measuring Airway Bioenergetics in Primary Human Lung Cells***

Here, we demonstrate the usefulness of XFe Technology in measuring the basal and perturbed bioenergetics of lung Mac (Chapter 3). This translational ability has allowed unprecedented insight into the bioenergetics of these key immune airway immune cells. We showed that human lung Macs produce an inflammatory response without undergoing metabolic reprogramming, a critical difference from the extensive reliance of peripheral blood monocytes on metabolic shifts for function (Mills *et al.*, 2017). Further investigation is needed into the role of metabolism of lung macrophages and how induced

inflammatory responses may differ from those characterized in other macrophages, since little is known. Using the techniques optimized in this dissertation, novel insights could be made into the pathology of numerous airway diseases and environmental toxicants.

However, XFe technology is currently limited in investigating one of the most relevant *in vitro* models of epithelial cells, which are primary airway epithelial cells, typically collected by brush bronchoscopy, and grown at air liquid interface. Although one group, adapted a culture system for the XF24 plates, it is not commercially available limiting its use (Xu *et al.*, 2014). Additionally, the XF Analyzer involves the submersion of cells, which could cause additional stress. A technique to measure the O<sub>2</sub> and pH flux in the basal media could be developed as an alternative.

In the short term, bioenergetics is being used as a new physiologic outcome in clinical experiments, including controlled human exposure studies to ambient air pollutants to see if bioenergetics function is altered. Both mitochondrial function and glycolytic function changes could be useful global readouts of potential redox changes due to air pollutant or other toxicant exposures.

### **Conclusions & Public Health Policy Implications of Elucidating Cellular Mechanisms**

The data presented in this dissertation supports the growing body of evidence that oxidative stress is a key mechanism involved in exposure to PM. This work identifies novel mechanistic links between oxidative stress, bioenergetics, and disrupted cellular function, leading to PM-associated adverse health outcomes. Using these mechanisms described here, susceptible groups could be better defined and individual-scale actions taken. Though ultimately air pollution exposure is largely out of the control of the individual and requires policies to be set at local, national, and international levels. Increased biomonitoring of oxidative effects and regulations set on the PM-components that cause these effects could improve public health.

## REFERENCES

- Adamson, H., Robinson, M., Bond, P.S., Soboh, B., Gillow, K., Simonov, A.N., Elton, D.M., Bond, A.M., Sawers, R.G., Gavaghan, D.J., 2017. Analysis of HypD Disulfide Redox Chemistry via Optimization of Fourier Transformed ac Voltammetric Data. *Analytical chemistry* **89**, 1565-1573.
- Agarwal, A.R., Yin, F., Cadenas, E., 2014. Short-term cigarette smoke exposure leads to metabolic alterations in lung alveolar cells. *American journal of respiratory cell and molecular biology* **51**, 284-293.
- Agarwal, A.R., Zhao, L., Sancheti, H., Sundar, I.K., Rahman, I., Cadenas, E., 2012. Short-term cigarette smoke exposure induces reversible changes in energy metabolism and cellular redox status independent of inflammatory responses in mouse lungs. *American Journal of Physiology-Lung Cellular and Molecular Physiology* **303**, L889-L898.
- Agudelo-Flórez, P., Costa-Carvalho, B.T., Alvaro López, J., Redher, J., Newburger, P.E., Olalla-Saad, S.T., Condino-Neto, A., 2004. Association of glucose-6-phosphate dehydrogenase deficiency and X-linked chronic granulomatous disease in a child with anemia and recurrent infections. *American journal of hematology* **75**, 151-156.
- Aitken, R.J., Whiting, S., De Iuliis, G.N., McClymont, S., Mitchell, L.A., Baker, M.A., 2012. Electrophilic aldehydes generated by sperm metabolism activate mitochondrial reactive oxygen species generation and apoptosis by targeting succinate dehydrogenase. *Journal of Biological Chemistry* **287**, 33048-33060.
- Alam, M.M., Lal, S., FitzGerald, K.E., Zhang, L., 2016. A holistic view of cancer bioenergetics: mitochondrial function and respiration play fundamental roles in the development and progression of diverse tumors. *Clinical and translational medicine* **5**, 3.
- Alexis, N., Soukup, J., Ghio, A., Becker, S., 2000. Sputum phagocytes from healthy individuals are functional and activated: a flow cytometric comparison with cells in bronchoalveolar lavage and peripheral blood. *Clinical Immunology* **97**, 21-32.
- Alexis, N.E., Lay, J.C., Zeman, K.L., Geiser, M., Kapp, N., Bennett, W.D., 2006. In vivo particle uptake by airway macrophages in healthy volunteers. *American journal of respiratory cell and molecular biology* **34**, 305-313.
- Alexis, N.E., Zhou, H., Lay, J.C., Harris, B., Hernandez, M.L., Lu, T.-S., Bromberg, P.A., Diaz-Sanchez, D., Devlin, R.B., Kleeberger, S.R., 2009. The glutathione-S-transferase Mu 1 null genotype modulates ozone-induced airway inflammation in human subjects. *Journal of Allergy and Clinical Immunology* **124**, 1222-1228. e1225.

- Alves, C.A., Barbosa, C., Rocha, S., Calvo, A., Nunes, T., Cerqueira, M., Pio, C., Karanasiou, A., Querol, X., 2015. Elements and polycyclic aromatic hydrocarbons in exhaust particles emitted by light-duty vehicles. *Environmental Science and Pollution Research* **22**, 11526-11542.
- Anderson, J.O., Thundiyil, J.G., Stolbach, A., 2012. Clearing the air: a review of the effects of particulate matter air pollution on human health. *Journal of Medical Toxicology* **8**, 166-175.
- Applegate, M.A., Humphries, K.M., Szveda, L.I., 2008. Reversible inhibition of  $\alpha$ -ketoglutarate dehydrogenase by hydrogen peroxide: glutathionylation and protection of lipoic acid. *Biochemistry* **47**, 473-478.
- Bachi, A., Dalle-Donne, I., Scaloni, A., 2012. Redox proteomics: chemical principles, methodological approaches and biological/biomedical promises. *Chemical reviews* **113**, 596-698.
- Bae, Y.S., Kang, S.W., Seo, M.S., Baines, I.C., Tekle, E., Chock, P.B., Rhee, S.G., 1997. Epidermal growth factor (EGF)-induced generation of hydrogen peroxide Role in EGF receptor-mediated tyrosine phosphorylation. *Journal of Biological Chemistry* **272**, 217-221.
- Barford, D., 2004. The role of cysteine residues as redox-sensitive regulatory switches. *Current opinion in structural biology* **14**, 679-686.
- Bauer, R.N., Müller, L., Brighton, L.E., Duncan, K.E., Jaspers, I., 2015. Interaction with epithelial cells modifies airway macrophage response to ozone. *American journal of respiratory cell and molecular biology* **52**, 285-294.
- Belchamber, K.B., Donnelly, L.E., 2017. *Macrophage Dysfunction in Respiratory Disease, Macrophages*. Springer, pp. 299-313.
- Belousov, V.V., Fradkov, A.F., Lukyanov, K.A., Staroverov, D.B., Shakhbazov, K.S., Terskikh, A.V., Lukyanov, S., 2006. Genetically encoded fluorescent indicator for intracellular hydrogen peroxide. *Nature methods* **3**, 281-286.
- Beltrán, B., Mathur, A., Duchon, M.R., Erusalimsky, J.D., Moncada, S., 2000. The effect of nitric oxide on cell respiration: a key to understanding its role in cell survival or death. *Proceedings of the National Academy of Sciences* **97**, 14602-14607.
- Benam, K.H., Villenave, R., Lucchesi, C., Varone, A., Hubeau, C., Lee, H.-H., Alves, S.E., Salmon, M., Ferrante, T.C., Weaver, J.C., 2016. Small airway-on-a-chip enables analysis of human lung inflammation and drug responses in vitro. *Nature methods* **13**, 151-157.
- Benzie, I.F., 2000. Evolution of antioxidant defence mechanisms. *European journal of nutrition* **39**, 53-61.

- Berndt, C., Lillig, C.H., Flohé, L., 2014. Redox regulation by glutathione needs enzymes. *Frontiers in pharmacology* **5**.
- Bewley, M.A., Preston, J.A., Mohasin, M., Marriott, H.M., Budd, R.C., Swales, J., Collini, P., Greaves, D.R., Craig, R.W., Brightling, C.E., 2017. Impaired Mitochondrial Microbicidal Responses in Chronic Obstructive Pulmonary Disease Macrophages. *American Journal of Respiratory And Critical Care Medicine*.
- Borregaard, N., Herlin, T., 1982. Energy metabolism of human neutrophils during phagocytosis. *Journal of Clinical Investigation* **70**, 550.
- Brand, M.D., 2010. The sites and topology of mitochondrial superoxide production. *Experimental gerontology* **45**, 466-472.
- Brand, M.D., Nicholls, D.G., 2011. Assessing mitochondrial dysfunction in cells. *Biochemical Journal* **435**, 297-312.
- Brook, R.D., Rajagopalan, S., Pope, C.A., Brook, J.R., Bhatnagar, A., Diez-Roux, A.V., Holguin, F., Hong, Y., Luepker, R.V., Mittleman, M.A., 2010. Particulate matter air pollution and cardiovascular disease. *Circulation* **121**, 2331-2378.
- Brown, J., Cook, K., Ney, F.G., Hatch, T., 1950. Influence of particle size upon the retention of particulate matter in the human lung. *American Journal of Public Health and the Nations Health* **40**, 450-480.
- Brunmark, A., Cadenas, E., 1989. Redox and addition chemistry of quinoid compounds and its biological implications. *Free Radical Biology and Medicine* **7**, 435-477.
- Cantin, A., North, S., Hubbard, R., Crystal, R., 1987. Normal alveolar epithelial lining fluid contains high levels of glutathione. *Journal of applied physiology* **63**, 152-157.
- Castranova, V., Rabovsky, J., Tucker, J., Miles, P., 1988. The alveolar type II epithelial cell: a multifunctional pneumocyte. *Toxicology and applied pharmacology* **93**, 472-483.
- Chacko, B.K., Kramer, P.A., Ravi, S., Benavides, G.A., Mitchell, T., Dranka, B.P., Ferrick, D., Singal, A.K., Ballinger, S.W., Bailey, S.M., 2014. The Bioenergetic Health Index: a new concept in mitochondrial translational research. *Clinical science* **127**, 367-373.
- Chacko, B.K., Kramer, P.A., Ravi, S., Johnson, M.S., Hardy, R.W., Ballinger, S.W., Darley-Usmar, V.M., 2013. Methods for defining distinct bioenergetic profiles in platelets, lymphocytes, monocytes, and neutrophils, and the oxidative burst from human blood. *Laboratory investigation* **93**, 690-700.
- Chacko, B.K., Zhi, D., Darley-Usmar, V.M., Mitchell, T., 2016. The Bioenergetic Health Index is a sensitive measure of oxidative stress in human monocytes. *Redox biology* **8**, 43-50.

- Chahine, T., Baccarelli, A., Litonjua, A., Wright, R.O., Suh, H., Gold, D.R., Sparrow, D., Vokonas, P., Schwartz, J., 2007. Particulate air pollution, oxidative stress genes, and heart rate variability in an elderly cohort. *Environmental health perspectives* **115**, 1617.
- Chandel, N.S., Schumacker, P.T., Arch, R.H., 2001. Reactive oxygen species are downstream products of TRAF-mediated signal transduction. *Journal of Biological Chemistry* **276**, 42728-42736.
- Charrier, J., Anastasio, C., 2012. On dithiothreitol (DTT) as a measure of oxidative potential for ambient particles: evidence for the importance of soluble transition metals. *Atmospheric chemistry and physics (Print)* **12**, 11317.
- Cheng, W.-Y., Currier, J., Bromberg, P.A., Silbajoris, R., Simmons, S.O., Samet, J.M., 2012. Linking oxidative events to inflammatory and adaptive gene expression induced by exposure to an organic particulate matter component. *Environmental Health Perspectives* **120**, 267.
- Cho, A.K., Di Stefano, E., You, Y., Rodriguez, C.E., Schmitz, D.A., Kumagai, Y., Miguel, A.H., Eiguren-Fernandez, A., Kobayashi, T., Avol, E., 2004. Determination of four quinones in diesel exhaust particles, SRM 1649a, and atmospheric PM<sub>2.5</sub> special issue of aerosol science and technology on findings from the fine particulate matter supersites program. *Aerosol Science and Technology* **38**, 68-81.
- Choi, A., Alam, J., 1996. Heme oxygenase-1: function, regulation, and implication of a novel stress-inducible protein in oxidant-induced lung injury. *American journal of respiratory cell and molecular biology* **15**, 9-19.
- Chuang, K.-J., Chan, C.-C., Su, T.-C., Lee, C.-T., Tang, C.-S., 2007. The effect of urban air pollution on inflammation, oxidative stress, coagulation, and autonomic dysfunction in young adults. *American journal of respiratory and critical care medicine* **176**, 370-376.
- Churg, A., Brauer, M., 1997. Human lung parenchyma retains PM<sub>2.5</sub>. *American journal of respiratory and critical care medicine* **155**, 2109-2111.
- Claxton, L.D., Matthews, P.P., Warren, S.H., 2004. The genotoxicity of ambient outdoor air, a review: Salmonella mutagenicity. *Mutation Research/Reviews in Mutation Research* **567**, 347-399.
- Cohen, A.J., Brauer, M., Burnett, R., Anderson, H.R., Frostad, J., Estep, K., Balakrishnan, K., Brunekreef, B., Dandona, L., Dandona, R., 2017. Estimates and 25-year trends of the global burden of disease attributable to ambient air pollution: an analysis of data from the Global Burden of Diseases Study 2015. *The Lancet* **389**, 1907-1918.
- Comhair, S.A., Thomassen, M.J., Erzurum, S.C., 2000. Differential induction of extracellular glutathione peroxidase and nitric oxide synthase 2 in airways of healthy individuals exposed to 100% O<sub>2</sub> or cigarette smoke. *American Journal of Respiratory Cell and Molecular Biology* **23**, 350-354.

- Coursin, D.B., Cihla, H.P., Oberley, T.D., Oberley, L.W., 1992. Immunolocalization of antioxidant enzymes and isozymes of glutathione S-transferase in normal rat lung. *American Journal of Physiology-Lung Cellular and Molecular Physiology* **263**, L679-L691.
- Curjuric, I., Imboden, M., Schindler, C., Downs, S., Hersberger, M., Liu, S., Matyas, G., Russi, E., Schwartz, J., Thun, G., 2010. HMOX1 and GST variants modify attenuation of FEF25–75% decline due to PM10 reduction. *European Respiratory Journal* **35**, 505-514.
- Delgado-Saborit, J.M., Alam, M.S., Pollitt, K.J.G., Stark, C., Harrison, R.M., 2013. Analysis of atmospheric concentrations of quinones and polycyclic aromatic hydrocarbons in vapour and particulate phases. *Atmospheric Environment* **77**, 974-982.
- Devlin, R.B., Smith, C.B., Schmitt, M.T., Rappold, A.G., Hinderliter, A., Graff, D., Carraway, M.S., 2014. Controlled exposure of humans with metabolic syndrome to concentrated ultrafine ambient particulate matter causes cardiovascular effects. *Toxicological Sciences* **140**, 61-72.
- Divakaruni, A.S., Wiley, S.E., Rogers, G.W., Andreyev, A.Y., Petrosyan, S., Loviscach, M., Wall, E.A., Yadava, N., Heuck, A.P., Ferrick, D.A., 2013. Thiazolidinediones are acute, specific inhibitors of the mitochondrial pyruvate carrier. *Proceedings of the National Academy of Sciences* **110**, 5422-5427.
- Domej, W., Foldes-Papp, Z., Flogel, E., Haditsch, B., 2006. Chronic obstructive pulmonary disease and oxidative stress. *Current pharmaceutical biotechnology* **7**, 117-123.
- Dominici, F., Peng, R.D., Bell, M.L., Pham, L., McDermott, A., Zeger, S.L., Samet, J.M., 2006. Fine particulate air pollution and hospital admission for cardiovascular and respiratory diseases. *Jama* **295**, 1127-1134.
- Dranka, B.P., Benavides, G.A., Diers, A.R., Giordano, S., Zelickson, B.R., Reily, C., Zou, L., Chatham, J.C., Hill, B.G., Zhang, J., 2011. Assessing bioenergetic function in response to oxidative stress by metabolic profiling. *Free Radical Biology and Medicine* **51**, 1621-1635.
- Dranka, B.P., Hill, B.G., Darley-Usmar, V.M., 2010. Mitochondrial reserve capacity in endothelial cells: The impact of nitric oxide and reactive oxygen species. *Free Radical Biology and Medicine* **48**, 905-914.
- Driscoll, K.E., Lindenschmidt, R.C., Maurer, J.K., Higgins, J.M., Ridder, G., 1990. Pulmonary response to silica or titanium dioxide: inflammatory cells, alveolar macrophage-derived cytokines, and histopathology. *Am J Respir Cell Mol Biol* **2**, 381-390.
- Eiguren-Fernandez, A., Miguel, A.H., Di Stefano, E., Schmitz, D.A., Cho, A.K., Thurairatnam, S., Avol, E.L., Froines, J.R., 2008. Atmospheric distribution of gas-and particle-phase quinones in Southern California. *Aerosol Science and Technology* **42**, 854-861.

Environmental Protection Agency, 2013. America's Children and the Environment, Third Edition, Updated August 2017, pp.

Erzurum, S.C., Danel, C., Gillissen, A., Chu, C.-S., Trapnell, B.C., Crystal, R.G., 1993a. In vivo antioxidant gene expression in human airway epithelium of normal individuals exposed to 100% O<sub>2</sub>. *Journal of Applied Physiology* **75**, 1256-1262.

Erzurum, S.C., Lemarchand, P., Rosenfeld, M.A., Yoo, J.-H., Crystal, R.G., 1993b. Protection of human endothelial cells from oxidant injury by adenovirus-mediated transfer of the human catalase cDNA. *Nucleic Acids Research* **21**, 1607-1612.

Fahy, J.V., Liu, J., Wong, H., Boushey, H.A., 1994. Analysis of cellular and biochemical constituents of induced sputum after allergen challenge: a method for studying allergic airway inflammation. *Journal of allergy and clinical immunology* **93**, 1031-1039.

Ferrick, D.A., Neilson, A., Beeson, C., 2008. Advances in measuring cellular bioenergetics using extracellular flux. *Drug Discovery Today* **13**, 268-274.

Flohé, L., 2013. The fairytale of the GSSG/GSH redox potential. *Biochimica et Biophysica Acta (BBA)-General Subjects* **1830**, 3139-3142.

Flowers-Geary, L., Blecinski, W., Harvey, R.G., Penning, T.M., 1996. Cytotoxicity and mutagenicity of polycyclic aromatic hydrocarbon o-quinones produced by dihydrodiol dehydrogenase. *Chemico-Biological Interactions* **99**, 55-72.

Franke-Ullmann, G., Pfortner, C., Walter, P., Steinmüller, C., Lohmann-Matthes, M.-L., Kobzik, L., 1996. Characterization of murine lung interstitial macrophages in comparison with alveolar macrophages in vitro. *The Journal of Immunology* **157**, 3097-3104.

Fulcher, M.L., Gabriel, S., Burns, K.A., Yankaskas, J.R., Randell, S.H., 2005. Well-differentiated human airway epithelial cell cultures. *Human Cell Culture Protocols*, 183-206.

Galván-Peña, S., O'Neill, L.A., 2014. Metabolic reprogramming in macrophage polarization. *Frontiers in immunology* **5**.

Ganapathy, V., Thangaraju, M., Prasad, P.D., 2009. Nutrient transporters in cancer: relevance to Warburg hypothesis and beyond. *Pharmacology & therapeutics* **121**, 29-40.

Gerencser, A.A., Neilson, A., Choi, S.W., Edman, U., Yadava, N., Oh, R.J., Ferrick, D.A., Nicholls, D.G., Brand, M.D., 2009. Quantitative microplate-based respirometry with correction for oxygen diffusion. *Analytical chemistry* **81**, 6868-6878.

- Ghio, A.J., Carraway, M.S., Madden, M.C., 2012. Composition of air pollution particles and oxidative stress in cells, tissues, and living systems. *Journal of Toxicology and Environmental Health, Part B* **15**, 1-21.
- Ghio, A.J., Devlin, R.B., 2001. Inflammatory lung injury after bronchial instillation of air pollution particles. *American journal of respiratory and critical care medicine* **164**, 704-708.
- Ghio, A.J., Kim, C., Devlin, R.B., 2000. Concentrated ambient air particles induce mild pulmonary inflammation in healthy human volunteers. *American journal of respiratory and critical care medicine* **162**, 981-988.
- Gibbs-Flournoy, E.A., Simmons, S.O., Bromberg, P.A., Dick, T.P., Samet, J.M., 2013. Monitoring intracellular redox changes in ozone-exposed airway epithelial cells. *Environmental Health Perspectives* **121**, 312.
- Godon, C., Lagniel, G., Lee, J., Buhler, J.-M., Kieffer, S., Perrot, M., Boucherie, H., Toledano, M.B., Labarre, J., 1998. The H<sub>2</sub>O<sub>2</sub> stimulon in *Saccharomyces cerevisiae*. *Journal of Biological Chemistry* **273**, 22480-22489.
- Gottlieb, R.A., Adachi, S., 1999. Nitrogen cavitation for cell disruption to obtain mitochondria from cultured cells. *Methods in Enzymology* **322**, 213-221.
- Gough, D., Cotter, T., 2011. Hydrogen peroxide: a Jekyll and Hyde signalling molecule. *Cell death & disease* **2**, e213.
- Grant, C.M., Quinn, K.A., Dawes, I.W., 1999. Differential protein S-thiolation of glyceraldehyde-3-phosphate dehydrogenase isoenzymes influences sensitivity to oxidative stress. *Molecular and cellular biology* **19**, 2650-2656.
- Groitel, B., Jakob, U., 2014. Thiol-based redox switches. *Biochimica et Biophysica Acta (BBA)-Proteins and Proteomics* **1844**, 1335-1343.
- Guzy, R.D., Hoyos, B., Robin, E., Chen, H., Liu, L., Mansfield, K.D., Simon, M.C., Hammerling, U., Schumacker, P.T., 2005. Mitochondrial complex III is required for hypoxia-induced ROS production and cellular oxygen sensing. *Cell metabolism* **1**, 401-408.
- Hamanaka, R.B., Chandel, N.S., 2010. Mitochondrial reactive oxygen species regulate cellular signaling and dictate biological outcomes. *Trends in biochemical sciences* **35**, 505-513.
- Health Effects Institute, 2017. State of Global Air 2017. Special Report., Boston, MA, pp.

- Henry, T., Wallace, K., 1995. The role of redox cycling versus arylation in quinone-induced mitochondrial dysfunction: a mechanistic approach in classifying reactive toxicants. *SAR and QSAR in Environmental Research* **4**, 97-108.
- Henry, T.R., Wallace, K.B., 1996. Differential mechanisms of cell killing by redox cycling and aryating quinones. *Archives of Toxicology* **70**, 482-489.
- Heron, M., Grutters, J., ten Dam-Molenkamp, K., Hijdra, D., van Heugten-Roeling, A., Claessen, A., Ruven, H., Van den Bosch, J., van Velzen-Blad, H., 2012. Bronchoalveolar lavage cell pattern from healthy human lung. *Clinical & Experimental Immunology* **167**, 523-531.
- Hiemstra, P.S., 2013. Altered macrophage function in chronic obstructive pulmonary disease. *Annals of the American Thoracic Society* **10**, S180-S185.
- Hildebrandt, T., Knesting, J., Berndt, C., Morgan, B., Scheibe, R., 2015. Cytosolic thiol switches regulating basic cellular functions: GAPDH as an information hub? *Biological chemistry* **396**, 523-537.
- Hiura, T.S., Kaszubowski, M.P., Li, N., Nel, A.E., 1999. Chemicals in diesel exhaust particles generate reactive oxygen radicals and induce apoptosis in macrophages. *The Journal of Immunology* **163**, 5582-5591.
- Hiura, T.S., Li, N., Kaplan, R., Horwitz, M., Segrave, J.-C., Nel, A.E., 2000. The role of a mitochondrial pathway in the induction of apoptosis by chemicals extracted from diesel exhaust particles. *The Journal of Immunology* **165**, 2703-2711.
- Ho, H.-y., Cheng, M.-I., Chiu, D.T.-y., 2007. Glucose-6-phosphate dehydrogenase—from oxidative stress to cellular functions and degenerative diseases. *Redox Report* **12**, 109-118.
- Holgate, S.T., 2011. The sentinel role of the airway epithelium in asthma pathogenesis. *Immunological reviews* **242**, 205-219.
- Hong, V., Presolski, S.I., Ma, C., Finn, M., 2009. Analysis and Optimization of Copper-Catalyzed Azide–Alkyne Cycloaddition for Bioconjugation. *Angewandte Chemie International Edition* **48**, 9879-9883.
- Huang, B., Chen, S.C., Wang, D.L., 2009. Shear flow increases S-nitrosylation of proteins in endothelial cells. *Cardiovascular research* **83**, 536-546.
- Huang, H.-C., Nguyen, T., Pickett, C.B., 2000. Regulation of the antioxidant response element by protein kinase C-mediated phosphorylation of NF-E2-related factor 2. *Proceedings of the National Academy of Sciences* **97**, 12475-12480.

- Huang, S.C.-C., Everts, B., Ivanova, Y., O'sullivan, D., Nascimento, M., Smith, A.M., Beatty, W., Love-Gregory, L., Lam, W.Y., O'Neill, C.M., 2014. Cell-intrinsic lysosomal lipolysis is essential for alternative activation of macrophages. *Nature immunology*.
- Hunninghake, G.W., Gadek, J., Kawanami, O., Ferrans, V., Crystal, R., 1979. Inflammatory and immune processes in the human lung in health and disease: evaluation by bronchoalveolar lavage. *The American journal of pathology* **97**, 149.
- Hurd, T.R., Requejo, R., Filipovska, A., Brown, S., Prime, T.A., Robinson, A.J., Fearnley, I.M., Murphy, M.P., 2008. Complex I within Oxidatively Stressed Bovine Heart Mitochondria Is Glutathionylated on Cys-531 and Cys-704 of the 75-kDa Subunit POTENTIAL ROLE OF CYS RESIDUES IN DECREASING OXIDATIVE DAMAGE. *Journal of Biological Chemistry* **283**, 24801-24815.
- Iwamoto, N., Sumi, D., Ishii, T., Uchida, K., Cho, A.K., Froines, J.R., Kumagai, Y., 2007. Chemical knockdown of protein-tyrosine phosphatase 1B by 1, 2-naphthoquinone through covalent modification causes persistent transactivation of epidermal growth factor receptor. *Journal of Biological Chemistry* **282**, 33396-33404.
- Jakober, C.A., Riddle, S.G., Robert, M.A., Destailats, H., Charles, M.J., Green, P.G., Kleeman, M.J., 2007. Quinone emissions from gasoline and diesel motor vehicles. *Environmental science & technology* **41**, 4548-4554.
- Janssen-Heininger, Y.M., Mossman, B.T., Heintz, N.H., Forman, H.J., Kalyanaraman, B., Finkel, T., Stamler, J.S., Rhee, S.G., van der Vliet, A., 2008. Redox-based regulation of signal transduction: principles, pitfalls, and promises. *Free Radical Biology and Medicine* **45**, 1-17.
- Jha, A.K., Huang, S.C.-C., Sergushichev, A., Lampropoulou, V., Ivanova, Y., Loginicheva, E., Chmielewski, K., Stewart, K.M., Ashall, J., Everts, B., 2015. Network integration of parallel metabolic and transcriptional data reveals metabolic modules that regulate macrophage polarization. *Immunity* **42**, 419-430.
- Jones, D.P., Sies, H., 2015. The redox code. *Antioxidants & redox signaling* **23**, 734-746.
- Kalyanaraman, B., 2013. Teaching the basics of redox biology to medical and graduate students: oxidants, antioxidants and disease mechanisms. *Redox biology* **1**, 244-257.
- Karakelides, H., Irving, B.A., Short, K.R., O'brien, P., Nair, K.S., 2010. Age, obesity, and sex effects on insulin sensitivity and skeletal muscle mitochondrial function. *Diabetes* **59**, 89-97.
- Karplus, P.A., 2015. A primer on peroxiredoxin biochemistry. *Free Radical Biology and Medicine* **80**, 183-190.
- Karplus, P.A., Poole, L.B., 2012. Peroxiredoxins as molecular triage agents, sacrificing themselves to enhance cell survival during a peroxide attack. *Molecular cell* **45**, 275-278.

- Kaspar, J.W., Niture, S.K., Jaiswal, A.K., 2009. Nrf2: INrf2 (Keap1) signaling in oxidative stress. *Free Radical Biology and Medicine* **47**, 1304-1309.
- Kelly, F.J., 2003. Oxidative stress: its role in air pollution and adverse health effects. *Occupational and Environmental Medicine* **60**, 612-616.
- Kemp, M., Go, Y.-M., Jones, D.P., 2008. Nonequilibrium thermodynamics of thiol/disulfide redox systems: a perspective on redox systems biology. *Free Radical Biology and Medicine* **44**, 921-937.
- Kikuno, S., Taguchi, K., Iwamoto, N., Yamano, S., Cho, A.K., Froines, J.R., Kumagai, Y., 2006. 1, 2-Naphthoquinone activates vanilloid receptor 1 through increased protein tyrosine phosphorylation, leading to contraction of guinea pig trachea. *Toxicology and applied pharmacology* **210**, 47-54.
- King, M.S., Sharpley, M.S., Hirst, J., 2009. Reduction of Hydrophilic Ubiquinones by the Flavin in Mitochondrial NADH: Ubiquinone Oxidoreductase (Complex I) and Production of Reactive Oxygen Species†. *Biochemistry* **48**, 2053-2062.
- Kinnula, V., Lehtonen, S., Kaarteenaho-Wiik, R., Lakari, E., Pääkkö, P., Kang, S., Rhee, S., Soini, Y., 2002. Cell specific expression of peroxiredoxins in human lung and pulmonary sarcoidosis. *Thorax* **57**, 157-164.
- Kinnula, V., Yankaskas, J., Chang, L., Virtanen, I., Linnala, A., Kang, B., Crapo, J., 1994. Primary and immortalized (BEAS 2B) human bronchial epithelial cells have significant antioxidative capacity in vitro. *American journal of respiratory cell and molecular biology* **11**, 568-576.
- Kodavanti, U.P., Thomas, R., Ledbetter, A.D., Schladweiler, M.C., Shannahan, J.H., Wallenborn, J.G., Lund, A.K., Campen, M.J., Butler, E.O., Gottipolu, R.R., 2011. Vascular and cardiac impairments in rats inhaling ozone and diesel exhaust particles. *Environmental health perspectives* **119**, 312.
- Kopf, M., Schneider, C., Nobs, S.P., 2015. The development and function of lung-resident macrophages and dendritic cells. *Nature immunology* **16**, 36-44.
- Kovacic, P., Pozos, R.S., Somanathan, R., Shangari, N., O'Brien, P.J., 2005. Mechanism of mitochondrial uncouplers, inhibitors, and toxins: focus on electron transfer, free radicals, and structure-activity relationships. *Current Medicinal Chemistry* **12**, 2601-2623.
- Kowaltowski, A.J., Castilho, R.F., Vercesi, A.E., 1995. Ca (2+)-induced mitochondrial membrane permeabilization: role of coenzyme Q redox state. *American Journal of Physiology-Cell Physiology* **269**, C141-C147.
- Kudo, M., Ishigatsubo, Y., Aoki, I., 2013. Pathology of asthma. *Frontiers in microbiology* **4**.

- Kumagai, Y., Shinkai, Y., Miura, T., Cho, A.K., 2012. The chemical biology of naphthoquinones and its environmental implications. *Annual Review of Pharmacology and Toxicology* **52**, 221-247.
- Labenski, M.T., Fisher, A.A., Lo, H.-H., Monks, T.J., Lau, S.S., 2009. Protein electrophile-binding motifs: lysine-rich proteins are preferential targets of quinones. *Drug Metabolism and Disposition* **37**, 1211-1218.
- Lambeth, J.D., 2004. NOX enzymes and the biology of reactive oxygen. *Nature Reviews Immunology* **4**, 181-189.
- Lanza, D.L., Code, E., Crespi, C.L., Gonzalez, F.J., Yost, G.S., 1999. Specific dehydrogenation of 3-methylindole and epoxidation of naphthalene by recombinant human CYP2F1 expressed in lymphoblastoid cells. *Drug Metabolism and Disposition* **27**, 798-803.
- Laskin, D.L., Sunil, V.R., Gardner, C.R., Laskin, J.D., 2011. Macrophages and tissue injury: agents of defense or destruction? *Annual review of pharmacology and toxicology* **51**, 267-288.
- Laumbach, R.J., Kipen, H.M., 2010. Acute effects of motor vehicle traffic-related air pollution exposures on measures of oxidative stress in human airways. *Annals of the New York Academy of Sciences* **1203**, 107-112.
- Lavrich, K.S., Corteselli, E.M., Wages, P.A., Bromberg, P.A., Simmons, S.O., Gibbs-Flournoy, E., Samet, J.M., 2018. Investigating Mitochondrial Dysfunction in Human Lung Cells Exposed to Redox-Active PM Components. *Toxicology and Applied Pharmacology* **342**, 99-107.
- Lelieveld, J., Evans, J., Fnais, M., Giannadaki, D., Pozzer, A., 2015. The contribution of outdoor air pollution sources to premature mortality on a global scale. *Nature* **525**, 367-371.
- Li, N., Alam, J., Venkatesan, M.I., Eiguren-Fernandez, A., Schmitz, D., Di Stefano, E., Slaughter, N., Killeen, E., Wang, X., Huang, A., 2004. Nrf2 is a key transcription factor that regulates antioxidant defense in macrophages and epithelial cells: protecting against the proinflammatory and oxidizing effects of diesel exhaust chemicals. *The Journal of Immunology* **173**, 3467-3481.
- Li, N., Sioutas, C., Cho, A., Schmitz, D., Misra, C., Sempf, J., Wang, M., Oberley, T., Froines, J., Nel, A., 2003. Ultrafine particulate pollutants induce oxidative stress and mitochondrial damage. *Environmental Health Perspectives* **111**, 455.
- Li, N., Wang, M., Oberley, T.D., Sempf, J.M., Nel, A.E., 2002. Comparison of the pro-oxidative and proinflammatory effects of organic diesel exhaust particle chemicals in bronchial epithelial cells and macrophages. *The Journal of Immunology* **169**, 4531-4541.
- Li, N., Xia, T., Nel, A.E., 2008. The role of oxidative stress in ambient particulate matter-induced lung diseases and its implications in the toxicity of engineered nanoparticles. *Free Radical Biology and Medicine* **44**, 1689-1699.

- Lillehoj, E.P., Kato, K., Lu, W., Kim, K.C., 2013. Cellular and molecular biology of airway mucins. *International review of cell and molecular biology* **303**, 139.
- Lin, M., Chen, Y., Burnett, R.T., Villeneuve, P.J., Krewski, D., 2002. The influence of ambient coarse particulate matter on asthma hospitalization in children: case-crossover and time-series analyses. *Environmental health perspectives* **110**, 575.
- Lin, P.-H., Chen, D.-R., Wang, T.-W., Lin, C.-H., Chuang, M.-C., 2009. Investigation of the cumulative tissue doses of naphthoquinones in human serum using protein adducts as biomarker of exposure. *Chemico-biological interactions* **181**, 107-114.
- Lo, Y.Y., Cruz, T.F., 1995. Involvement of reactive oxygen species in cytokine and growth factor induction of c-fos expression in chondrocytes. *Journal of Biological Chemistry* **270**, 11727-11730.
- Logan, W., 1953. Mortality in the London fog incident, 1952. *The lancet* **261**, 336-338.
- Ma, Q., 2013. Role of nrf2 in oxidative stress and toxicity. *Annual review of pharmacology and toxicology* **53**, 401-426.
- Mabalirajan, U., Dinda, A.K., Kumar, S., Roshan, R., Gupta, P., Sharma, S.K., Ghosh, B., 2008. Mitochondrial structural changes and dysfunction are associated with experimental allergic asthma. *The Journal of Immunology* **181**, 3540-3548.
- Mailloux, R.J., Jin, X., Willmore, W.G., 2014. Redox regulation of mitochondrial function with emphasis on cysteine oxidation reactions. *Redox biology* **2**, 123-139.
- Mailloux, R.J., McBride, S.L., Harper, M.-E., 2013. Unearthing the secrets of mitochondrial ROS and glutathione in bioenergetics. *Trends in biochemical sciences* **38**, 592-602.
- Mailloux, R.J., Treberg, J.R., 2016. Protein S-glutathionylation links energy metabolism to redox signaling in mitochondria. *Redox biology* **8**, 110-118.
- Malinouski, M., Zhou, Y., Belousov, V.V., Hatfield, D.L., Gladyshev, V.N., 2011. Hydrogen peroxide probes directed to different cellular compartments. *PloS one* **6**, e14564.
- Mall, M.A., 2008. Role of cilia, mucus, and airway surface liquid in mucociliary dysfunction: lessons from mouse models. *Journal of aerosol medicine and pulmonary drug delivery* **21**, 13-24.
- Manke, A., Wang, L., Rojanasakul, Y., 2013. Mechanisms of nanoparticle-induced oxidative stress and toxicity. *BioMed research international* **2013**.

- Mastral, A.M., Callen, M.S., 2000. A review on polycyclic aromatic hydrocarbon (PAH) emissions from energy generation. *Environmental Science & Technology* **34**, 3051-3057.
- May, J.M., De Haen, C., 1979. Insulin-stimulated intracellular hydrogen peroxide production in rat epididymal fat cells. *Journal of Biological Chemistry* **254**, 2214-2220.
- McLain, A.L., Cormier, P.J., Kinter, M., Szveda, L.I., 2013. Glutathionylation of  $\alpha$ -ketoglutarate dehydrogenase: the chemical nature and relative susceptibility of the cofactor lipoic acid to modification. *Free Radical Biology and Medicine* **61**, 161-169.
- McStay, G.P., Clarke, S.J., Halestrap, A.P., 2002. Role of critical thiol groups on the matrix surface of the adenine nucleotide translocase in the mechanism of the mitochondrial permeability transition pore. *Biochemical Journal* **367**, 541-548.
- Meyer, A.J., Dick, T.P., 2010. Fluorescent protein-based redox probes. *Antioxidants & redox signaling* **13**, 621-650.
- Meyer, K.C., Raghu, G., Baughman, R.P., Brown, K.K., Costabel, U., Du Bois, R.M., Drent, M., Haslam, P.L., Kim, D.S., Nagai, S., 2012. An official American Thoracic Society clinical practice guideline: the clinical utility of bronchoalveolar lavage cellular analysis in interstitial lung disease. *American journal of respiratory and critical care medicine* **185**, 1004-1014.
- Millet, P., Vachharajani, V., McPhail, L., Yoza, B., McCall, C.E., 2016. GAPDH binding to TNF- $\alpha$  mRNA contributes to posttranscriptional repression in monocytes: a novel mechanism of communication between inflammation and metabolism. *The Journal of Immunology* **196**, 2541-2551.
- Mills, E.L., Kelly, B., O'Neill, L.A., 2017. Mitochondria are the powerhouses of immunity. *Nature Immunology* **18**, 488-498.
- Miura, T., Kumagai, Y., 2010. Immunochemical method to detect proteins that undergo selective modification by 1, 2-naphthoquinone derived from naphthalene through metabolic activation. *The Journal of toxicological sciences* **35**, 843-852.
- Miura, T., Shinkai, Y., Hirose, R., Iwamoto, N., Cho, A.K., Kumagai, Y., 2011. Glyceraldehyde-3-phosphate dehydrogenase as a quinone reductase in the suppression of 1, 2-naphthoquinone protein adduct formation. *Free Radical Biology and Medicine* **51**, 2082-2089.
- Monks, T.J., Hanzlik, R.P., Cohen, G.M., Ross, D., Graham, D.G., 1992. Quinone chemistry and toxicity. *Toxicology and applied pharmacology* **112**, 2-16.
- Montero, R., Araujo, A., Carranza, P., Mejía-Loza, V., Serrano, L., Albores, A., Salinas, J.E., Camacho-Carranza, R., 2007. Genotype frequencies of polymorphic GSTM1, GSTT1, and cytochrome P450 CYP1A1 in Mexicans. *Human biology* **79**, 299-312.

- Moodley, Y., Krishnan, V., Lalloo, U., 2000. Neutrophils in induced sputum arise from central airways. *European Respiratory Journal* **15**, 36-40.
- Mookerjee, S.A., Nicholls, D.G., Brand, M.D., 2016. Determining maximum glycolytic capacity using extracellular flux measurements. *PloS one* **11**, e0152016.
- Mosser, D.M., Edwards, J.P., 2008. Exploring the full spectrum of macrophage activation. *Nature reviews immunology* **8**, 958-969.
- Murphy, M., 2009. How mitochondria produce reactive oxygen species. *Biochemistry* **417**, 1-13.
- Murray, P.J., Wynn, T.A., 2011. Obstacles and opportunities for understanding macrophage polarization. *Journal of leukocyte biology* **89**, 557-563.
- Nemmar, A., Hoylaerts, M.F., Hoet, P.H., Dinsdale, D., Smith, T., Xu, H., Vermylen, J., Nemery, B., 2002. Ultrafine particles affect experimental thrombosis in an in vivo hamster model. *American journal of respiratory and critical care medicine* **166**, 998-1004.
- Nemmar, A., Vanbilloen, H., Hoylaerts, M., Hoet, P., Verbruggen, A., Nemery, B., 2001. Passage of intratracheally instilled ultrafine particles from the lung into the systemic circulation in hamster. *American journal of respiratory and critical care medicine* **164**, 1665-1668.
- Nordenhäll, C., Pourazar, J., Ledin, M., Levin, J.-O., Sandström, T., Ädelroth, E., 2001. Diesel exhaust enhances airway responsiveness in asthmatic subjects. *European respiratory journal* **17**, 909-915.
- O'brien, P., 1991. Molecular mechanisms of quinone cytotoxicity. *Chemico-biological interactions* **80**, 1-41.
- O'Neill, L.A., Kishton, R.J., Rathmell, J., 2016. A guide to immunometabolism for immunologists. *Nature Reviews Immunology*.
- Ogura, Y., Yamazaki, I., 1983. Steady-state kinetics of the catalase reaction in the presence of cyanide. *The Journal of Biochemistry* **94**, 403-408.
- Ott, M., Gogvadze, V., Orrenius, S., Zhivotovsky, B., 2007. Mitochondria, oxidative stress and cell death. *Apoptosis* **12**, 913-922.
- Oury, T.D., Chang, L.-Y., Marklund, S.L., Day, B.J., Crapo, J.D., 1994. Immunocytochemical localization of extracellular superoxide dismutase in human lung. *Laboratory investigation* **70**, 889-898.

- Palmer, J.W., Tandler, B., Hoppel, C.L., 1977. Biochemical properties of subsarcolemmal and interfibrillar mitochondria isolated from rat cardiac muscle. *Journal of Biological Chemistry* **252**, 8731-8739.
- Palsson-McDermott, E.M., Curtis, A.M., Goel, G., Lauterbach, M.A., Sheedy, F.J., Gleeson, L.E., van den Bosch, M.W., Quinn, S.R., Domingo-Fernandez, R., Johnston, D.G., 2015. Pyruvate kinase M2 regulates Hif-1 $\alpha$  activity and IL-1 $\beta$  induction and is a critical determinant of the warburg effect in LPS-activated macrophages. *Cell metabolism* **21**, 65-80.
- Pan, J., Carroll, K.S., 2014. Chemical biology approaches to study protein cysteine sulfenylation. *Biopolymers* **101**, 165-172.
- Parker, D., Prince, A., 2011. Innate immunity in the respiratory epithelium. *American journal of respiratory cell and molecular biology* **45**, 189-201.
- Paulsen, C.E., Carroll, K.S., 2013. Cysteine-mediated redox signaling: chemistry, biology, and tools for discovery. *Chemical reviews* **113**, 4633-4679.
- Pearce, E.L., Pearce, E.J., 2013. Metabolic pathways in immune cell activation and quiescence. *Immunity* **38**, 633-643.
- Pearson, J.F., Bachireddy, C., Shyamprasad, S., Goldfine, A.B., Brownstein, J.S., 2010. Association between fine particulate matter and diabetes prevalence in the US. *Diabetes care* **33**, 2196-2201.
- Pelletier, M., Billingham, L.K., Ramaswamy, M., Siegel, R.M., 2014. Extracellular flux analysis to monitor glycolytic rates and mitochondrial oxygen consumption. *Methods in Enzymology* **542**, 125-149.
- Penning, T.M., Burczynski, M.E., Hung, C.-F., McCoull, K.D., Palackal, N.T., Tsuruda, L.S., 1999. Dihydrodiol dehydrogenases and polycyclic aromatic hydrocarbon activation: generation of reactive and redox active o-quinones. *Chemical Research in Toxicology* **12**, 1-18.
- Peralta, D., Bronowska, A.K., Morgan, B., Dóka, É., Van Laer, K., Nagy, P., Gräter, F., Dick, T.P., 2015. A proton relay enhances H<sub>2</sub>O<sub>2</sub> sensitivity of GAPDH to facilitate metabolic adaptation. *Nature chemical biology* **11**, 156-163.
- Perkins, A., Nelson, K.J., Parsonage, D., Poole, L.B., Karplus, P.A., 2015. Peroxiredoxins: guardians against oxidative stress and modulators of peroxide signaling. *Trends in biochemical sciences* **40**, 435-445.
- Persoz, C., Achard, S., Momas, I., Seta, N., 2012. Inflammatory response modulation of airway epithelial cells exposed to formaldehyde. *Toxicology letters* **211**, 159-163.

- Pickles, R.J., McCarty, D., Matsui, H., Hart, P.J., Randell, S.H., Boucher, R.C., 1998. Limited entry of adenovirus vectors into well-differentiated airway epithelium is responsible for inefficient gene transfer. *Journal of virology* **72**, 6014-6023.
- Pietropaoli, A.P., Frampton, M.W., Hyde, R.W., Morrow, P.E., Oberdörster, G., Cox, C., Speers, D.M., Frasier, L.M., Chalupa, D.C., Huang, L.-S., 2004. Pulmonary function, diffusing capacity, and inflammation in healthy and asthmatic subjects exposed to ultrafine particles. *Inhalation toxicology* **16**, 59-72.
- Pizzichini, E., Pizzichini, M., Efthimiadis, A., Evans, S., Morris, M.M., Squillace, D., Gleich, G.J., Dolovich, J., Hargreave, F.E., 1996. Indices of airway inflammation in induced sputum: reproducibility and validity of cell and fluid-phase measurements. *American journal of respiratory and critical care medicine* **154**, 308-317.
- Poole, L.B., 2015. The basics of thiols and cysteines in redox biology and chemistry. *Free Radical Biology and Medicine* **80**, 148-157.
- Poole, L.B., Klomsiri, C., Knaggs, S.A., Furdui, C.M., Nelson, K.J., Thomas, M.J., Fetrow, J.S., Daniel, L.W., King, S.B., 2007. Fluorescent and affinity-based tools to detect cysteine sulfenic acid formation in proteins. *Bioconjugate chemistry* **18**, 2004-2017.
- Pope 3rd, C., 2000. Epidemiology of fine particulate air pollution and human health: biologic mechanisms and who's at risk? *Environmental health perspectives* **108**, 713.
- Pope, C.A., Burnett, R.T., Thurston, G.D., Thun, M.J., Calle, E.E., Krewski, D., Godleski, J.J., 2004. Cardiovascular mortality and long-term exposure to particulate air pollution. *Circulation* **109**, 71-77.
- Pope, C.A., Dockery, D.W., 2006. Health effects of fine particulate air pollution: lines that connect. *Journal of the Air & Waste Management Association* **56**, 709-742.
- Pope, C.A., Thun, M.J., Namboodiri, M.M., Dockery, D.W., Evans, J.S., Speizer, F.E., Heath, C.W., 1995. Particulate air pollution as a predictor of mortality in a prospective study of US adults. *American journal of respiratory and critical care medicine* **151**, 669-674.
- Porcheray, F., Viaud, S., Rimaniol, A.C., Leone, C., Samah, B., Dereuddre-Bosquet, N., Dormont, D., Gras, G., 2005. Macrophage activation switching: an asset for the resolution of inflammation. *Clinical & Experimental Immunology* **142**, 481-489.
- Presolski, S.I., Hong, V.P., Finn, M., 2011. Copper-Catalyzed Azide-Alkyne Click Chemistry for Bioconjugation. *Current protocols in chemical biology*, 153-162.
- Preuss, R., Angerer, J., Drexler, H., 2003. Naphthalene—an environmental and occupational toxicant. *International archives of occupational and environmental health* **76**, 556-576.

- Proud, D., Leigh, R., 2011. Epithelial cells and airway diseases. *Immunological reviews* **242**, 186-204.
- Quay, J.L., Reed, W., Samet, J., Devlin, R.B., 1998. Air pollution particles induce IL-6 gene expression in human airway epithelial cells via NF- $\kappa$  B activation. *American Journal of Respiratory Cell and Molecular Biology* **19**, 98-106.
- Quinlan, C.L., Perevoshchikova, I.V., Hey-Mogensen, M., Orr, A.L., Brand, M.D., 2013. Sites of reactive oxygen species generation by mitochondria oxidizing different substrates. *Redox Biology* **1**, 304-312.
- Rabinovitch, N., Strand, M., Gelfand, E.W., 2006. Particulate levels are associated with early asthma worsening in children with persistent disease. *American journal of respiratory and critical care medicine* **173**, 1098-1105.
- Ralser, M., Wamelink, M.M., Kowald, A., Gerisch, B., Heeren, G., Struys, E.A., Klipp, E., Jakobs, C., Breitenbach, M., Lehrach, H., 2007. Dynamic rerouting of the carbohydrate flux is key to counteracting oxidative stress. *Journal of biology* **6**, 10.
- Ray, P.D., Huang, B.-W., Tsuji, Y., 2012. Reactive oxygen species (ROS) homeostasis and redox regulation in cellular signaling. *Cellular signalling* **24**, 981-990.
- Reddel, R.R., Ke, Y., Gerwin, B.I., McMenamin, M.G., Lechner, J.F., Su, R.T., Brash, D.E., Park, J.-B., Rhim, J.S., Harris, C.C., 1988. Transformation of human bronchial epithelial cells by infection with SV40 or adenovirus-12 SV40 hybrid virus, or transfection via strontium phosphate coprecipitation with a plasmid containing SV40 early region genes. *Cancer Research* **48**, 1904-1909.
- Requejo, R., Hurd, T.R., Costa, N.J., Murphy, M.P., 2010. Cysteine residues exposed on protein surfaces are the dominant intramitochondrial thiol and may protect against oxidative damage. *The FEBS journal* **277**, 1465-1480.
- Revoir, W., Bien, C., 1997. *Respiratory protection handbook*. Boca Raton: CRC press LLC, pp.
- Rhee, S.G., Chang, T.-S., Bae, Y.S., Lee, S.-R., Kang, S.W., 2003. Cellular regulation by hydrogen peroxide. *Journal of the American Society of Nephrology* **14**, S211-S215.
- Rhee, S.G., Kang, S.W., Jeong, W., Chang, T.-S., Yang, K.-S., Woo, H.A., 2005a. Intracellular messenger function of hydrogen peroxide and its regulation by peroxiredoxins. *Current opinion in cell biology* **17**, 183-189.
- Rhee, S.G., Woo, H.A., Kil, I.S., Bae, S.H., 2012. Peroxiredoxin functions as a peroxidase and a regulator and sensor of local peroxides. *Journal of Biological Chemistry* **287**, 4403-4410.

- Rhee, S.G., Yang, K.-S., Kang, S.W., Woo, H.A., Chang, T.-S., 2005b. Controlled elimination of intracellular H<sub>2</sub>O<sub>2</sub>: regulation of peroxiredoxin, catalase, and glutathione peroxidase via post-translational modification. *Antioxidants & redox signaling* **7**, 619-626.
- Riediker, M., Devlin, R.B., Griggs, T.R., Herbst, M.C., Bromberg, P.A., Williams, R.W., Cascio, W.E., 2004. Cardiovascular effects in patrol officers are associated with fine particulate matter from brake wear and engine emissions. *Particle and fibre toxicology* **1**, 2.
- Ritz, B., Wilhelm, M., 2008. Ambient air pollution and adverse birth outcomes: methodologic issues in an emerging field. *Basic & clinical pharmacology & toxicology* **102**, 182-190.
- Riva, D., Magalhaes, C., Lopes, A.A., Lancas, T., Mauad, T., Malm, O., Valenca, S., Saldiva, P., Faffe, D., Zin, W., 2011. Low dose of fine particulate matter (PM<sub>2.5</sub>) can induce acute oxidative stress, inflammation and pulmonary impairment in healthy mice. *Inhalation toxicology* **23**, 257-267.
- Rodriguez, C.E., Fukuto, J.M., Taguchi, K., Froines, J., Cho, A.K., 2005. The interactions of 9, 10-phenanthrenequinone with glyceraldehyde-3-phosphate dehydrogenase (GAPDH), a potential site for toxic actions. *Chemico-biological interactions* **155**, 97-110.
- Rodriguez, C.E., Shinyashiki, M., Froines, J., Yu, R.C., Fukuto, J.M., Cho, A.K., 2004. An examination of quinone toxicity using the yeast *Saccharomyces cerevisiae* model system. *Toxicology* **201**, 185-196.
- Rogers, L.K., Cismowski, M.J., 2017. Oxidative Stress in the Lung—The Essential Paradox. *Current Opinion in Toxicology*.
- Romagnoli, M., Vachier, I., Vignola, A., Godard, P., Bousquet, J., Chanez, P., 1999. Safety and cellular assessment of bronchial brushing in airway diseases. *Respiratory medicine* **93**, 461-466.
- Romero, N., Swain, P., Neilson, A., Dranka, B.P., 2017. Improving Quantification of Cellular Glycolytic Rate Using Agilent Seahorse XF Technology Agilent Technologies Inc.
- Rosa-Borges, A., Sampaio, M.G., Condino-Neto, A., Barreto, O.C., Nudelman, V., Carneiro-Sampaio, M., Nogueira, S.A., Abreu, T.F.d., Rehder, J., Costa-Carvalho, B.T., 2001. Glucose-6-phosphate dehydrogenase deficiency with recurrent infections: case report. *Jornal de pediatria* **77**, 331-336.
- Rosas-Ballina, M., 2017. Energy Homeostasis of Immune Cells: Translating Cell Bioenergetics into Clinical Application in Rheumatoid Arthritis, Next-Generation Therapies and Technologies for Immune-Mediated Inflammatory Diseases. Springer, pp. 123-144.
- Ruckerl, R., Ibaldo-Mulli, A., Koenig, W., Schneider, A., Woelke, G., Cyrys, J., Heinrich, J., Marder, V., Frampton, M., Wichmann, H.E., 2006. Air pollution and markers of inflammation and coagulation in patients with coronary heart disease. *American journal of respiratory and critical care medicine* **173**, 432-441.

- Rutgers, S., Timens, W., Kaufmann, H., van der Mark, T.W., Koeter, G., Postma, D., 2000. Comparison of induced sputum with bronchial wash, bronchoalveolar lavage and bronchial biopsies in COPD. *European Respiratory Journal* **15**, 109-115.
- Sacks, J.D., Stanek, L.W., Luben, T.J., Johns, D.O., Buckley, B.J., Brown, J.S., Ross, M., 2011. Particulate matter–induced health effects: Who is susceptible? *Environmental health perspectives* **119**, 446.
- Saeed, M., Higginbotham, S., Rogan, E., Cavalieri, E., 2007. Formation of depurinating N3adenine and N7guanine adducts after reaction of 1, 2-naphthoquinone or enzyme-activated 1, 2-dihydroxynaphthalene with DNA: Implications for the mechanism of tumor initiation by naphthalene. *Chemico-biological interactions* **165**, 175-188.
- Salabei, J.K., Gibb, A.A., Hill, B.G., 2014. Comprehensive measurement of respiratory activity in permeabilized cells using extracellular flux analysis. *Nature Protocols* **9**, 421-438.
- Samet, J.M., Dominici, F., Curriero, F.C., Coursac, I., Zeger, S.L., 2000. Fine particulate air pollution and mortality in 20 US cities, 1987–1994. *New England journal of medicine* **343**, 1742-1749.
- Samet, J.M., Rappold, A., Graff, D., Cascio, W.E., Berntsen, J.H., Huang, Y.-C.T., Herbst, M., Bassett, M., Montilla, T., Hazucha, M.J., 2009. Concentrated ambient ultrafine particle exposure induces cardiac changes in young healthy volunteers. *American journal of respiratory and critical care medicine* **179**, 1034-1042.
- Samet, J.M., Tal, T.L., 2010. Toxicological disruption of signaling homeostasis: tyrosine phosphatases as targets. *Annual review of pharmacology and toxicology* **50**, 215-235.
- Samet, J.M., Wages, P.A., 2017. Oxidative Stress from Environmental Exposures. *Current Opinion in Toxicology*.
- Sattler, M., Winkler, T., Verma, S., Byrne, C.H., Shrikhande, G., Salgia, R., Griffin, J.D., 1999. Hematopoietic growth factors signal through the formation of reactive oxygen species. *Blood* **93**, 2928-2935.
- Schafer, F.Q., Buettner, G.R., 2001. Redox environment of the cell as viewed through the redox state of the glutathione disulfide/glutathione couple. *Free Radical Biology and Medicine* **30**, 1191-1212.
- Schicker, B., Kuhn, M., Fehr, R., Asmis, L., Karagiannidis, C., Reinhart, W., 2009. Particulate matter inhalation during hay storing activity induces systemic inflammation and platelet aggregation. *European journal of applied physiology* **105**, 771-778.
- Schrenk, H.H., Heimann, H., Clayton, G.D., Gafafer, W., Wexler, H., 1949. Air Pollution in Donora, Pa. Epidemiology of the Unusual Smog Episode of October 1948. Preliminary Report. Air Pollution in Donora, Pa. Epidemiology of the Unusual Smog Episode of October 1948. Preliminary Report.

- Schwarze, P., Øvrevik, J., Låg, M., Refsnes, M., Nafstad, P., Hetland, R., Dybing, E., 2006. Particulate matter properties and health effects: consistency of epidemiological and toxicological studies. *Human & experimental toxicology* **25**, 559-579.
- Seahorse Bioscience, 2016. Normalizing XF metabolic data to cellular or mitochondrial parameters, pp.
- Shah, P.S., Balkhair, T., Births, K.S.G.o.D.o.P.L., 2011. Air pollution and birth outcomes: a systematic review. *Environment international* **37**, 498-516.
- Shaykhiev, R., Krause, A., Salit, J., Strulovici-Barel, Y., Harvey, B.-G., O'Connor, T.P., Crystal, R.G., 2009. Smoking-dependent reprogramming of alveolar macrophage polarization: implication for pathogenesis of chronic obstructive pulmonary disease. *The Journal of immunology* **183**, 2867-2883.
- Shinkai, Y., Iwamoto, N., Miura, T., Ishii, T., Cho, A.K., Kumagai, Y., 2012. Redox cycling of 1, 2-naphthoquinone by thioredoxin1 through Cys32 and Cys35 causes inhibition of its catalytic activity and activation of ASK1/p38 signaling. *Chemical research in toxicology* **25**, 1222-1230.
- Silbajoris, R., Osornio-Vargas, A., Simmons, S., Reed, W., Bromberg, P., Dailey, L.A., Samet, J.M., 2011. Ambient particulate matter induces IL-8 expression through an alternative NF-κB mechanism in human airway epithelial cells. *Environ Health Perspect* **119**, 1379-1383.
- Smith, M.R., Vayalil, P.K., Zhou, F., Benavides, G.A., Beggs, R.R., Golzarian, H., Nijampatnam, B., Oliver, P.G., Smith, R.A., Murphy, M.P., 2016. Mitochondrial thiol modification by a targeted electrophile inhibits metabolism in breast adenocarcinoma cells by inhibiting enzyme activity and protein levels. *Redox biology* **8**, 136-148.
- Snow, S., Cheng, W., Wolberg, A., Carraway, M., 2014. Air pollution upregulates endothelial cell procoagulant activity via ultrafine particle-induced oxidant signaling and tissue factor expression. *Toxicological Sciences* **140**, 83-93.
- Song, Y., Buettner, G.R., 2010. Thermodynamic and kinetic considerations for the reaction of semiquinone radicals to form superoxide and hydrogen peroxide. *Free Radical Biology and Medicine* **49**, 919-962.
- Sthijns, M.M., Weseler, A.R., Bast, A., Haenen, G.R., 2016. Time in Redox Adaptation Processes: From Evolution to Hormesis. *International journal of molecular sciences* **17**, 1649.
- Sun, Q., Wang, A., Jin, X., Natanzon, A., Duquaine, D., Brook, R.D., Aguinaldo, J.-G.S., Fayad, Z.A., Fuster, V., Lippmann, M., 2005. Long-term air pollution exposure and acceleration of atherosclerosis and vascular inflammation in an animal model. *Jama* **294**, 3003-3010.

- Sun, Y., Taguchi, K., Sumi, D., Yamano, S., Kumagai, Y., 2006. Inhibition of endothelial nitric oxide synthase activity and suppression of endothelium-dependent vasorelaxation by 1, 2-naphthoquinone, a component of diesel exhaust particles. *Archives of toxicology* **80**, 280-285.
- Swerdlow, R.H., 2016. Bioenergetics and metabolism: a bench to bedside perspective. *Journal of neurochemistry* **139**, 126-135.
- Takanishi, C.L., Ma, L.-H., Wood, M.J., 2007. A genetically encoded probe for cysteine sulfenic acid protein modification in vivo. *Biochemistry* **46**, 14725-14732.
- Tal, T.L., Bromberg, P.A., Kim, Y., Samet, J.M., 2008. Epidermal growth factor receptor activation by diesel particles is mediated by tyrosine phosphatase inhibition. *Toxicology and applied pharmacology* **233**, 382-388.
- Tannahill, G., Curtis, A., Adamik, J., Palsson-McDermott, E., McGettrick, A., Goel, G., Frezza, C., Bernard, N., Kelly, B., Foley, N., 2013. Succinate is an inflammatory signal that induces IL-1 [bgr] through HIF-1 [agr]. *Nature* **496**, 238-242.
- Tao, R., Zhao, Y., Chu, H., Wang, A., Zhu, J., Chen, X., Zou, Y., Shi, M., Liu, R., Su, N., 2017. Genetically encoded fluorescent sensors reveal dynamic regulation of NADPH metabolism. *Nature Methods*.
- Tonks, N.K., 2013. Protein tyrosine phosphatases—from housekeeping enzymes to master regulators of signal transduction. *The FEBS journal* **280**, 346-378.
- Tormos, K.V., Anso, E., Hamanaka, R.B., Eisenbart, J., Joseph, J., Kalyanaraman, B., Chandel, N.S., 2011. Mitochondrial complex III ROS regulate adipocyte differentiation. *Cell metabolism* **14**, 537-544.
- U.S. EPA, 2017. Evolution of the Clean Air Act, pp.
- US EPA, 2004. The Particle Pollution Report: Current Understanding of Air Quality and Emissions Through 2003, pp.
- Valavanidis, A., Fiotakis, K., Bakeas, E., Vlahogianni, T., 2005. Electron paramagnetic resonance study of the generation of reactive oxygen species catalysed by transition metals and quinoid redox cycling by inhalable ambient particulate matter. *Redox Report* **10**, 37-51.
- Van den Bossche, J., Baardman, J., de Winther, M.P., 2015. Metabolic characterization of polarized M1 and M2 bone marrow-derived macrophages using real-time extracellular flux analysis. *JoVE (Journal of Visualized Experiments)*, e53424-e53424.

- Van den Bossche, J., Baardman, J., Otto, N.A., van der Velden, S., Neele, A.E., van den Berg, S.M., Luque-Martin, R., Chen, H.-J., Boshuizen, M.C., Ahmed, M., 2016. Mitochondrial dysfunction prevents repolarization of inflammatory macrophages. *Cell reports* **17**, 684-696.
- Van Laer, K., Hamilton, C.J., Messens, J., 2013. Low-molecular-weight thiols in thiol–disulfide exchange. *Antioxidants & redox signaling* **18**, 1642-1653.
- Vareille, M., Kieninger, E., Edwards, M.R., Regamey, N., 2011. The airway epithelium: soldier in the fight against respiratory viruses. *Clinical microbiology reviews* **24**, 210-229.
- Vats, D., Mukundan, L., Odegaard, J.I., Zhang, L., Smith, K.L., Morel, C.R., Greaves, D.R., Murray, P.J., Chawla, A., 2006. Oxidative metabolism and PGC-1 $\beta$  attenuate macrophage-mediated inflammation. *Cell metabolism* **4**, 13-24.
- Veljkovic, E., Jiricny, J., Menigatti, M., Rehrauer, H., Han, W., 2011. Chronic exposure to cigarette smoke condensate in vitro induces epithelial to mesenchymal transition-like changes in human bronchial epithelial cells, BEAS-2B. *Toxicology in Vitro* **25**, 446-453.
- Wages, P.A., Cheng, W.-Y., Gibbs-Flournoy, E., Samet, J.M., 2016. Live-cell imaging approaches for the investigation of xenobiotic-induced oxidant stress. *Biochimica et Biophysica Acta (BBA)-General Subjects* **1860**, 2802-2815.
- Wages, P.A., Lavrich, K., Zhang, Z., Cheng, W.-Y., Corteselli, E., Gold, A., Bromberg, P., Simmons, S.O.N., Samet, J., 2015. Protein Sulfenylation: A Novel Readout of Environmental Oxidant Stress. *Chemical Research in Toxicology*.
- Wages, P.A., Silbajoris, R., Speen, A., Brighton, L., Henriquez, A., Tong, H., Bromberg, P.A., Simmons, S.O., Samet, J.M., 2014. Role of H<sub>2</sub>O<sub>2</sub> in the oxidative effects of zinc exposure in human airway epithelial cells. *Redox biology* **3**, 47-55.
- Wamelink, M., Struys, E., Jakobs, C., 2008. The biochemistry, metabolism and inherited defects of the pentose phosphate pathway: a review. *Journal of inherited metabolic disease* **31**, 703-717.
- Watanabe, N., Forman, H.J., 2003. Autoxidation of extracellular hydroquinones is a causative event for the cytotoxicity of menadione and DMNQ in A549-S cells. *Archives of Biochemistry and Biophysics* **411**, 145-157.
- Wiegman, C.H., Michaeloudes, C., Haji, G., Narang, P., Clarke, C.J., Russell, K.E., Bao, W., Pavlidis, S., Barnes, P.J., Kanerva, J., 2015. Oxidative stress–induced mitochondrial dysfunction drives inflammation and airway smooth muscle remodeling in patients with chronic obstructive pulmonary disease. *Journal of Allergy and Clinical Immunology* **136**, 769-780.
- Williams, M.C., 2003. Alveolar type I cells: molecular phenotype and development. *Annual review of physiology* **65**, 669-695.

- Wilson, D.F., 2013. Regulation of cellular metabolism: programming and maintaining metabolic homeostasis. *Journal of Applied Physiology* **115**, 1583-1588.
- Winkler-Heil, R., Hofmann, W., 2016. Modeling particle deposition in the Balb/c mouse respiratory tract. *Inhalation toxicology* **28**, 180-191.
- Winterbourn, C.C., Hampton, M.B., 2008. Thiol chemistry and specificity in redox signaling. *Free Radical Biology and Medicine* **45**, 549-561.
- Wong, G.H., Goeddel, D.V., 1988. Induction of manganous superoxide dismutase by tumor necrosis factor: possible protective mechanism. *Science* **242**, 941.
- World Health Organization, 2014. Mortality from household air pollution for 2012, Geneva, pp.
- World Health Organization, UNAIDS, 2006. Air quality guidelines: global update 2005. World Health Organization.
- Wu, M.-L., Layne, M.D., Yet, S.-F., 2012. Heme oxygenase-1 in environmental toxin-induced lung disease. *Toxicology mechanisms and methods* **22**, 323-329.
- Wu, W., Bromberg, P.A., Samet, J.M., 2013. Zinc ions as effectors of environmental oxidative lung injury. *Free Radical Biology and Medicine* **65**, 57-69.
- Xia, T., Korge, P., Weiss, J.N., Li, N., Venkatesen, M.I., Sioutas, C., Nel, A., 2004. Quinones and aromatic chemical compounds in particulate matter induce mitochondrial dysfunction: implications for ultrafine particle toxicity. *Environmental Health Perspectives*, 1347-1358.
- Xu, W., Janocha, A.J., Leahy, R.A., Klatte, R., Dudzinski, D., Mavrakis, L.A., Comhair, S.A., Lauer, M.E., Cotton, C.U., Erzurum, S.C., 2014. A novel method for pulmonary research: Assessment of bioenergetic function at the air-liquid interface. *Redox biology* **2**, 513-519.
- Xue, J., Schmidt, S.V., Sander, J., Draffehn, A., Krebs, W., Quester, I., De Nardo, D., Gohel, T.D., Emde, M., Schmidleithner, L., 2014. Transcriptome-based network analysis reveals a spectrum model of human macrophage activation. *Immunity* **40**, 274-288.
- Yang, I., Fong, K., Zimmerman, P., Holgate, S., Holloway, J., 2009. Genetic susceptibility to the respiratory effects of air pollution. *Postgraduate medical journal* **85**, 428-436.
- Yang, J., Gupta, V., Carroll, K.S., Liebler, D.C., 2014. Site-specific mapping and quantification of protein S-sulfenylation in cells. *Nature communications* **5**, 4776.

- Yang, J., Gupta, V., Tallman, K.A., Porter, N.A., Carroll, K.S., Liebler, D.C., 2015. Global, in situ, site-specific analysis of protein S-sulfenylation. *Nature protocols* **10**, 1022-1037.
- Yang, S., Jan, Y.-H., Gray, J.P., Mishin, V., Heck, D.E., Laskin, D.L., Laskin, J.D., 2013. Sepiapterin reductase mediates chemical redox cycling in lung epithelial cells. *Journal of Biological Chemistry* **288**, 19221-19237.
- Yoon, C.M., Nam, M., Oh, Y.-M., Cruz, C.S.D., Kang, M.-J., 2016. Mitochondrial regulation of inflammasome activation in chronic obstructive pulmonary disease. *Journal of innate immunity* **8**, 121-128.
- Zanobetti, A., Franklin, M., Koutrakis, P., Schwartz, J., 2009. Fine particulate air pollution and its components in association with cause-specific emergency admissions. *Environmental Health* **8**, 58.
- Zheng, J., Cho, M., Jones, A.D., Hammock, B.D., 1997. Evidence of quinone metabolites of naphthalene covalently bound to sulfur nucleophiles of proteins of murine Clara cells after exposure to naphthalene. *Chemical research in toxicology* **10**, 1008-1014.